

Modern Formation Evaluation for Geoscientists:

*Integrated Geological, Petrophysical, Elastic, and Mechanical
Interpretation of Well Logs and Core Measurements*

Carlos Torres-Verdín, PhD, Professor

Brian James Jennings Memorial Endowed Chair in Petroleum Engineering and
Zarrow Centennial Professorship in Petroleum Engineering

Hildebrand Department of Petroleum and Geosystems Engineering
The University of Texas at Austin

cverdin@mail.utexas.edu

January 3, 2023

Copyright © 2023 Carlos Torres-Verdín, PhD, Professor

HILDEBRAND DEPARTMENT OF PETROLEUM AND GEOSYSTEMS ENGINEERING, THE UNIVERSITY OF TEXAS
AT AUSTIN

Austin, TX 78712

Usage and/or extraction of material included in this book without the author's written permission is strictly prohibited and will be subject to legal prosecution according to copyright laws.

This textbook was typed by the author

Fifth draft release, January 2023

About the cover:

background photograph by Julio Torres Juliotorr@gmail.com

and

cover design by Reynaldo Casanova rcasanova@mail.utexas.edu

Preface

...El libro no es un ente incomunicado: es una relación, es un eje de innumerables relaciones...

—Jorge Luis Borges, Otras Inquisiciones: Nota Sobre (Hacia) Bernard Shaw.

This book is intended as a *practical* summary of procedures, methods, assumptions, and equations commonly used in the integrated geological-petrophysical-elastic-mechanical quantification of rock properties based on well logs and core measurements. The objective is to provide a systematic and *example-based* description to serve as reference guide with emphasis on measurement and discipline integration. Furthermore, even though several non-standard applications are considered as discussion examples (e.g., geothermal exploration, methane hydrate assessment, ore mining, and civil and environmental engineering) prominence is given to geohydrology and hydrocarbon reservoir characterization.

Most of existing textbooks on well logging focus their study to either measurement properties and principles (be it instruments or data-acquisition systems) or physical properties that can be used for interpretation. There are also specialized books on well logging entertaining detailed descriptions of a particular subject of interest, e.g., borehole imaging, sonic logging, and nuclear magnetic resonance. On the other hand, there are books on geological processes that make connections with well-log interpretation but which are often misleading and incomplete in their descriptions of borehole measurements. Seldom do well-logging textbooks make an attempt to bridge the gap between borehole measurements and *in situ* storage and flow-related petrophysical properties of rocks. Even more uncommon is to find textbooks on the petrophysical interpretation of well logs that make a serious attempt to include the influence of sedimentary processes and diagenesis on their descriptions of rock properties, especially properties related to multi-phase fluid flow. This book is an attempt to remedy the pervasive disconnect between geology, petrophysics, geomechanics, core data, and borehole geophysical measurements. The author firmly believes that the integration of these five domains of study is the *only* way to interpret well logs and core measurements. Relatively recent work on carbonate formations, tight-gas sandstones, organic shales/mudrocks, and in general, on unconventional hydrocarbon resources, confirms that petrophysical and geomechanical evaluations of spatially complex rocks are reliable only when geology, petrophysics, core data, and borehole measurement properties are simultaneously honored in the analysis. The discipline of *Formation Evaluation* embodies such an endeavor. Furthermore, the adjective “modern” used in the title of the book reflects the design condition that most of the described concepts, examples, and interpretation procedures originate from contemporary practices and measurements. This latter condition becomes glaringly clear in the analysis of unconventional rocks.

Presently, the book reflects work in progress. The author will continue to update the material as time permits based on feedback from interested and motivated readers. More than likely, readers will encounter some typographical errors and rough sentences. However, strong efforts have been made to have the material presented devoid of technical errors. The main disclaimer is that, albeit currently available for distribution to students taking my graduate and undergraduate courses, readers should exercise utmost *patience* when I go through several editorial versions and myriad corrections in the course of one semester. This is especially true concerning the examples and exercises that accompany the book. My apologies in advance! Based on my experience with at least a dozen major revisions thus far, it is very likely that this book will be eventually published in some *live* format (e.g., and e-book format) so that I will have the freedom to continuously update

it with new sections, better descriptions, more examples and exercises, lecture summaries, and accompanying YouTube video lectures. Stay tuned!

The book assumes that readers have a basic conceptual but working understanding on the fundamentals of sedimentary, diagenetic, and tectonic geological processes, that they understand basic petrophysics and basic rock-core laboratory measurements, and that they have a good intuitive and quantitative physics background. I go by the tenets (and biases!) that: (a) Physics is king, (b) Geology is queen, (c) Petrophysics is bishop, and (c) *Integration* is the name of the game (not chess!!) In some subtle ways, the interpretation of borehole measurements is similar to solving a *sudoku* puzzle: the game is over only when vertical lines, horizontal lines, and local squares have been filled out with the proper number set. In close analogy, a formation evaluation project is completed only when geology, petrophysics, and measurement physics have been honored in the analysis and quantification of rock properties. Solving this puzzle requires an integrative mind that is avid for challenge and is willing to accept non-conformal and extraordinary thinking. Petroleum engineering students will find that formation evaluation is in some ways a small, self-contained, and verifiable reservoir description endeavor. I have grown to enjoy this discipline in that every well log embodies a unique confluence of physics, geological, and petrophysical phenomena. No two wells and their measurements are ever alike! Rocks are always more complex than anticipated and one must be flexible to accept the great diversity of geological processes that originate great diversity in rock properties.

It has been said elsewhere that Formation Evaluation is an *art*. I do not agree with such a designation because it implies subjectivity, something which is akin to artistic expression: it suggests that the same set of borehole measurements could be interpreted in many different ways depending on who does the interpretation. Of course, many plausible interpretations are possible for the same data when the measurements are defective and/or incomplete, depending on assumptions and experience. This situation could be disappointing and frustrating to entry-level formation-evaluation practitioners but is also plain wrong! Formation Evaluation, like with any other scientific and engineering discipline, is based on solid physics and mathematical principles that allow *quantification* and are subject to verifiable hypothesis testing. Subjective interpretations are only possible when the available measurements are sparse, inadequate, or noisy, whereby *experiential knowledge* is the only way to fill the measurement gaps in the calculations. Thus, the spirit behind this book is that all the procedures used in the interpretation of borehole measurements should be quantitative and verifiable to be correct, reliable, and accurate.

The book is accompanied by a *Compendium of Formation Evaluation Exercises* which consists of a wide selection of conceptual and practical questions intended to reinforce and *practice* the most important chapters and sections. The vast majority of these exercises are based on actual field examples or computer-generated projects. Readers are encouraged to complete the exercises to verify their learning experience. Passive learning has no place in Formation Evaluation: it does not matter how extensive, complete, and organized this book can be or how many video lectures accompany it, there will always be room for examples and exercises. Verifying the concepts with practice exercises is the only way to cross-validate the learning experience. Indeed, the only effective method to learn Formation Evaluation is to practice concepts and calculations with a wide variety of field examples, and such is the underlying intention of this book. My experience teaching for over 23 years at the University of Texas at Austin has shown me that instruction without doing and without experiential learning is wasted pedagogy; I forcefully want this book to be a paradigm of learning by doing and learning by experimenting!

Acknowledgments

I am humbled to convey my sincere gratitude to my current and former graduate students whose research work and exploratory knowledge have helped to expand the horizons of my own knowledge in many unsuspected directions and greatly in depth. This book has considerably evolved since the first time I taught *Fundamentals of Well Logging* and *Principles of Formation Evaluation* to undergraduate students at the University of Texas at Austin, and has been enriched with my instruction of training courses to oil-company and geohydrology personnel around the world. I am also indebted to many professional colleagues within the SPWLA (Society of

Petrophysicists and Well-Log Analysts), SPE (Society of Petroleum Engineers), SEG (Society of Exploration Geophysicists), EAGE (European Association of Geoscientists and Engineers), SCA (Society of Core Analysts), AGU (American Geophysical Union), and IEEE (Institute of Electrical and Electronic Engineers) communities through whom I have enriched my exposure to new formation evaluation concepts, measurements, and interpretation techniques. In particular, I would like to thank Francis X. Bostick, Jr., E.C. Thomas, Darwin Ellis, David Kennedy, David Herrick, Bill Preeg, Tarek M. Habashy, Stefan Luthi, Mark Proett, Dan Georgi, André Revil, Chris Skelt, Robert Kleinberg, T. S. Ramakrishnan, Fikri Kuchuk, Oliver Mullins, Roberto Suárez-Rivera, Quinn Passey, Larry Lake, Ekwere Peters, Tad Patzek, Martin Blunt, Tom Blasingame, and many others for substantial formative concepts and ideas. Rocks and their myriad properties entertain our brains and guide our engineering instincts in so many interesting directions! And *Formation Evaluation* rocks like the heart of a rock and vibrates with all the profound resonances of these creative friends and colleagues! It has been a great pleasure collaborating/learning with/from all of them over the years!

August 21, 2023

About this Book

The subject of *Formation Evaluation* has been entertained by myriad publications and tens of books since the 1940's, ranging from specialized volumes on borehole-instrument properties, rock-core measurements, and basic interpretation methods to specialized subjects on shaly-sandstone interpretation, saturation-height analysis, geomechanics, and organic-shale interpretation, to name a few. There is no need to write yet another book on the same or similar subjects if the information is already available, albeit fragmented and non-articulated in the copious digital world. At the same time, it is non-trivial to write an all encompassing book because a detailed and comprehensive treatment of *Formation Evaluation* will require multiple volumes, not one. At this crossroads, the only valid excuse to augment the existent digital inventory is to approach the subject with a new, more fertile, and modern multi-disciplinary approach. That is the central idea behind this publication.

Additionally, at the heart of the this book is the inexorable notion that all interpretation methods should be quantitative, hence reproducible and demonstrable. Such a *desideratum* implies that all borehole measurements can be numerically simulated and that it is possible to quantify the error and uncertainty of any estimation of *in situ* rock properties stemming from borehole measurements and/or core laboratory data. There is a world of difference between accepting an interpretation result with, for instance, 20% than 3% inherent error. Some veteran interpreters might say that 20% error is acceptable given the unorthodox interplay between noisy measurements, empirical interpretation models, and paucity of data. Others could argue that achieving interpretation errors below 20% is futile because what one observes in a well is hardly germane to the "geological reality" existing between wells, where rock heterogeneity can be excruciatingly more complex than often observed in wells, which were *ab initio* designed to target "favorable" subsurface regions. But this is hardly an excuse to become sloppy or free-spirited when producing interpretation results. In the end, if one is not able to substantiate and verify the quantitative validity of a calculation then everything else behind and ahead of the calculation becomes moot.

There is great merit in consistently pointing out the ineffable limitations and assumptions of any given calculation method, more so in the discipline of *Formation Evaluation*. And this should be a good starting point to improve and make progress...

August 21, 2023

Contents

1	Introduction	15
1.1	What is Formation Evaluation?	15
1.2	Past and Present of Formation Evaluation: A Brief Historical Perspective	21
1.3	What is a Formation Evaluation Specialist?	22
1.4	Key Properties Required in Aquifer or Hydrocarbon Reservoir Description	23
1.5	Who Uses Well Logs and Why?	24
1.6	Interpretation Method Implemented in this Book	28
1.6.a	Context is everything!	28
1.7	Some Opening Remarks about Well Logs and their Interpretation	30
1.8	Additional Disclaimers (and Warnings!)	33
1.9	Patterns vs. Physics	34
1.10	Estimation of Solid/Fluid Compositions of Rocks From Well Logs	34
1.11	Interpretation Procedures Based on Artificial Intelligence	35
2	Basic Geological Concepts	39
2.1	Basic Concepts on Sedimentary Processes	39
2.2	Clastic vs. Carbonate Formations	42
2.3	Unconventional Rock Formations	44
2.4	Rock Cuttings	46
2.5	Depositional Environment, Architecture, and Spatial Continuity of Flow Units	46
2.6	Concept of Shale Baseline in Siliciclastic Sedimentary Sequences	48
3	Basic Petrophysics Concepts	49
3.1	Petrophysical Properties of Rocks	49
3.2	Estimation of Hydrocarbon Reserves	51
3.2.a	Remarks about the recovery factor	51
3.3	Hydrocarbon Storage and Producibility	52
3.4	Calculation of Porosity	52
3.4.a	Pore volume of rock saturating fluids	53
3.5	Porosity is Over-Rated!	53
3.5.a	The many facets of porosity	53
3.6	Body and Surface Phenomena in Porous Media	56
3.7	Basic Model of a Bundle of Capillary Tubes	57
3.8	Concept of Transport Efficiency of Porous Media	59
3.9	Calculation of Permeability	60
3.9.a	Total porosity	60
3.9.b	Common methods used to calculate rock permeability	61
3.10	Two-Phase Flow Properties	61
3.10.a	Capillary pressure	61

3.10.b Relative permeability	62
3.11 All Petrophysical Properties are Inter-Related!	62
3.11.a The flow of fluids in rocks is similar to that of a shower head!	62
3.12 Size Matters!	63
4 The Fabric of a Well Log	67
4.1 Introduction	67
4.2 The Header of a Well Log	68
4.3 Operational Classification of Well Logs	68
4.4 Measurements of Distance along the Well Trajectory	73
4.5 Borehole Environmental Variables	75
4.6 Processing of “Raw” Borehole Measurements	77
4.7 Essential Suite of Borehole Measurements	77
4.8 Mandrel vs. Pad Measurements	78
4.9 Typical Plotting Scales Used to Display Well Logs	78
4.10 Quality Control of Well Logs	79
4.11 Remarks about the quality and reliability of well logs	79
4.12 Volume of Investigation of Borehole Measurements	80
4.13 Bed-Thickness Effects on Well Logs	82
4.14 Typical Logging Speeds	83
4.15 Well Logs and Signal Processing	85
4.16 Detection of Bed Boundaries with Well Logs	85
4.17 Caliper and Temperature Logs	86
4.18 Geology, Petrophysics, and Well Logs	86
4.19 Corrections Applied to Well Logs Prior to Interpretation	87
4.20 Formation Evaluation Across Multiple Wells	88
4.21 General Guidelines for the Interpretation of Well Logs	89
4.22 The Future of Formation Evaluation Measurements	91
5 “Bistro” or “Quick-Look” Interpretation of Well Logs	93
5.1 “Gluing” Multiple Well Logs	94
5.2 Correlations Between Well Logs	95
5.3 Diagnosis of Lithology	95
5.3.a Some practical pointers for beginners	96
5.3.b Some additional important truisms about formation evaluation	97
5.4 Drill-Stem Testing, DST	98
5.5 <i>In Situ</i> Pressure Measurements	98
6 Common Borehole Instruments and their Measurements	101
6.1 Spontaneous Gamma-Ray Measurements	101
6.1.a Environmental corrections of gamma-ray logs	103
6.1.b Additional applications of spectral gamma-ray logs	103
6.2 Spontaneous Potential (SP) Measurements	104
6.2.a Environmental corrections and possible acquisition problems of SP measurements	107
6.2.b Interpretation corrections of SP measurements	107
6.3 Density Measurements	108
6.3.a Environmental corrections applied to density logs	109
6.3.b Display and interpretation of density logs	109
6.4 Neutron-Porosity Measurements	110
6.4.a Transformation of neutron count rates to apparent, water-filled porosity units	111
6.4.b Effects of fluids lighter than water on apparent, water-filled neutron porosity units	111

6.4.c	Environmental corrections applied to neutron logs	112
6.4.d	Display and interpretation of neutron logs in combination with density logs	112
6.5	Resistivity Measurements	112
6.6	Sonic Measurements	113
6.6.a	Processing of sonic logs	114
6.6.b	Some properties and uses of sonic logs	115
6.7	Magnetic Resonance Measurements	116
6.8	Dielectric Measurements	121
7	The Process of Mud-Filtrate Invasion	123
7.1	Introduction	123
7.2	The Physics of Mud-Filtrate Invasion	124
7.3	Effects of Mud-Filtrate Invasion on Well Logs	126
7.4	Identification of Porous and Permeable Rock Units	129
8	Formation Evaluation of Conventional Clastic Rocks	133
8.1	Clay and Shale	133
8.2	Volumetric Concentration of Shale, C_{sh}	134
8.3	Spatial distribution of shale in the rock volume (shale topology)	135
8.4	Thomas-Stieber diagram	136
8.5	Indirect calculation of C_{sh}	139
8.6	When is C_{sh} not negligible?	141
8.7	Recommended interpretation procedure for siliciclastic sedimentary rocks	141
8.7.a	Effect of clay/shale on density and neutron porosity logs	142
9	Calculation of Porosity	143
9.1	Porosity from Density Logs	143
9.1..1	Derivation	143
9.2	Sensitivity of Calculated Porosity to Errors in Matrix or Fluid Densities	145
9.3	Definition of Density Porosity, ϕ_D	146
9.4	Estimation of Fluid Density via Core Measurements and Density Logs	146
9.5	Porosity From Neutron Logs	146
9.5.a	Correct both ϕ_N and ϕ_D for dominant matrix	147
9.5.b	How many types of solids?	147
9.5.b.1	Derivation	147
9.5.b.2	Quick corrections	147
9.5.b.2.1	Derivation	148
9.5.b.3	Case of a shaly (dispersed shale), water-saturated sandstone	148
9.6	Assessment of Porosity via Density and Neutron Logs	149
9.7	Derivation of Some Important Density/Porosity Formulas	150
9.7.a	Case of laminated shale	150
9.7.b	Case of dispersed shale (grain-coating clay)	151
10	Electrical Resistivity, Porosity, and Water Saturation	155
10.1	Introduction	155
10.2	Assessment of fluid Saturation	156
10.3	Assumptions Implicit in Archie's Equations	158
10.3.a	Iteration between porosity and resistivity to improve the calculation of water saturation	159
10.4	Typical Range of Variation of Archie's Parameters a , m , and n	160
10.5	Mixing Laws for Archie's Porosity Exponent	160
10.6	Some Common Abuses of Archie's Equations	161

10.7 Determination of R_w	162
10.8 Electrical Resistivity of Rocks in the Presence of Invasion	165
10.9 Saturation-Height Analysis: Relationship Between Water Saturation, Capillary Pressure, and Height Above the Free Water-Hydrocarbon Contact	166
10.10 Water Saturation is Typically Not Randomly Distributed in Space	168
10.11 Estimation of Fluid Density From Pore-Pressure Measurements	168
10.12 Bed-Thickness and Invasion Corrections of Electrical Resistivity Measurements	168
10.13 Resistivity Anisotropy and Water Saturation	169
10.14 Some Diagnostic Plots	171
10.14.a Pickett's plot	171
10.14.b Buckle's plot	171
10.14.c Hingle's plot	172
10.15 Interpretation for Sandstones with Grain-Coating Clay	172
10.15.a Physical model	173
10.15.b Waxman-Smits model	174
10.15.c Dual-water model	174
10.15.d Practical implementation of the dual-water model	174
10.15.e More accurate assessment of ϕ_s using equation (10.3.1)	176
10.16 Summary of Resistivity-Porosity-Saturation Formulas for Sandstone with Grain-Coating Clay	176
10.16.a Remark about m and n in shaly-sandstone equations	177
11 Elastic and Mechanical Properties of Rocks	179
11.1 Porosity From Sonic Logs via Wyllie's Equation	179
11.1.1 Using Raymer-Gardner-Hunt's formula	179
11.1.a Usual values used for the assessment of sonic porosity	180
11.2 Biot-Gassmann Fluid Substitution	180
11.2.1 First presentation	180
11.2..1.1 Wood's formula	181
11.2.2 Second presentation	181
11.2.3 Third presentation	182
11.2.4 Reuss presentation	182
11.2.5 Relationship between the velocities	182
11.2.6 Inverse formula	182
11.3 Practical Use of Biot-Gassmann's Equations	183
11.4 Slowness-Time Coherence	183
11.5 Assessment of Volumetric Concentrations of Mineral Constituents: Linear System Approach	183
12 Estimation of Permeability	187
12.1 Rock classification	187
12.2 Pore- and Throat-Size Distributions	187
12.2.a Capillary Pressure	188
12.3 Parallel- and Perpendicular-to-Bedding Plane Permeabilities	189
12.4 Quantification of Uncertainty	189
13 Formation-Tester Measurements	191
14 Rock-Core Measurements	193
14.1 Measurements of Porosity	193
14.2 Measurements of Permeability	193
14.3 Relative Permeability	193
14.4 Measurements of Dispersivity	193

14.5 Measurements of Capillary Pressure	193
15 Numerical Simulation of Well Logs	195
16 Pore-Scale Measurements and Calculations	197
16.1 Other Complementary Field Measurements	197
Bibliography	197
Appendices	209
A Summary of Basic Formulas	211
A.1 Calculation of Temperature Along the Well Trajectory	211
A.2 Correction of Electrical Resistivity for Temperature	211
A.3 Electrical Resistivity of Aqueous Solutions	212
A.3.a From Resistivity to Electrolyte Concentration	212
A.4 Calculation of Shale Index	212
A.4.a Case of a Water-Saturated Sandstone	213
A.5 Spontaneous Electrical Potential (SP) and Water Resistivity	213
A.6 Archie's Equation	214
A.7 Relationship Between Rock Density and Porosity	215
A.8 Rock Density and Porosity of Rocks with Laminated Shale	215
A.9 Rock Density and Porosity of Rocks with Grain-Coating Clay	216
A.10 Fluid Density and Saturations	217
A.11 Density-Neutron Porosity Corrections for Shaly Sandstones	218
A.11.a Case of Sandstone-Shale Laminated Rocks	218
A.11.b Case of Rocks with Grain-Coating Clay Minerals	219
A.11.c Case of Rocks with Laminated Shale and Grain-Coating Clay Minerals	220
A.12 Volumetric Calculation of Shale from Density and Neutron Porosity Logs in a Water-Saturated Sandstone	221
A.13 Electrical Resistivity of Sandstone-Shale Laminated Rocks	221
A.14 Electrical Resistivity of Rocks with Grain-Coating Clay Minerals	223
A.14.a Waxman-Smits Conduction Model	224
A.14.b Juhasz's Modification of the Waxman-Smits Conduction Model	225
A.14.c Dual-Water Approximation of the Electrical Surface Conduction Model	225
A.15 Sonic Porosity	226
A.15.a Sonic Porosity Corrected for Compaction Effects	227
A.16 Calculation of Permeability	227
B Nomenclature	229
C Key to Well-Log Compendium	231
About the Author	231

Chapter 1

Introduction

...C'est véritablement utile puisque c'est joli...

—Antoine de Saint-Exupéry, *Le Petit Prince*.

There are a plethora of books which have been written over the years on topics concerning the acquisition and interpretation of borehole measurements, i.e., well logs. But *Formation Evaluation* is much more than that: it encompasses a much wider and deeper connection of subjects and methods than typically exemplified in standard well-logging books. And it also requires an imbricated interaction of geological, petrophysical, mechanical, and measurement-physics concepts like nowhere else in the Geosciences. I often find myself discussing with my Geosciences colleagues why Formation Evaluation is an undervalued and under appreciated discipline and why it is so unique and exciting! Let me explain why...

1.1 What is Formation Evaluation?

Formation Evaluation is the *engineering discipline* that develops, studies, and implements methods for the measurement and/or estimation of *in situ* properties of rocks penetrated by wells.

Geoscientists routinely invoke Formation Evaluation to analyze and quantify measurements acquired in wells for myriad purposes and objectives. The distinct and unique component of formation evaluation studies is the use of a variety of geophysical measurements which are acquired in a borehole during or after the processes of drilling, completing, and casing the well. Borehole geophysical measurements yield *in situ* rock physical properties and this quality is of utmost importance for their interpretation. Such rock physical properties include, but are not limited to, natural gamma-ray activity, spontaneous electrical potential, electrical resistivity/conductivity, density, neutron migration length, acoustic travel times, nuclear magnetic resonance, etc., which are acquired with instruments that are either stationary or moving along the borehole while the measurements are being acquired.

Figure 1.1.1 illustrates the underlying foundation of the discipline of Formation Evaluation, where *in situ* rock properties are sensed and measured with a variety of active and spontaneous physics principles that are used to “interrogate” rocks surrounding a borehole. Formation Evaluation specialists are constantly exploring/researching new measurements or new implementations of existing borehole geophysical measurements that can provide new, more accurate, and/or higher-resolution *in situ* rock physical properties. However, all borehole measurements have technical constraints and operational limitations stemming from the presence of the borehole and drilling mud, the presence of the instrument itself in the borehole, the distance of penetration away from the wellbore into the surrounding rocks, volume of investigation (or volume of sensitivity), presence of casing, electronic noise, etc., which need to be taken into account for their integration with other

measurements for interpretation purposes. It is important to emphasize that, to this date, there are important rock physics measurements which cannot be measured *in situ* in boreholes, for instance, tensorial permeability, multi-phase fluid pore volumes, capillary pressure, relative permeability, mechanical strength, etc. The latter properties can only be estimated indirectly from the available measurements.

Subsequent processing and interpretation of the acquired *in situ* borehole geophysical measurements, also known as *well logs* is commonly pursued to indirectly estimate other rock properties which cannot or are difficult to measure *in situ* in boreholes, such as rock solid composition, fluid composition, porosity, permeability, elasticity, mechanical strength, etc. The transformation, “translation,” or “mapping” of *in situ* rock physical properties that can be measured in the borehole into compositional, fluid, elastic, and geomechanical rock properties which cannot be measured *in situ* is commonly performed using *effective medium theories* of rocks which are developed based on laboratory and theoretical analyses of rock behavior (Figure 1.1.2). Effective-medium theories of rock physical behavior (e.g., Archie’s equation transforming rock electrical resistivity into water saturation, Biot-Gassmann’s equation transforming compressional- and shear-wave velocities into hydrocarbon saturation, etc.), also generally referred to as *rock physics models*, are the subject of numerous studies by formation evaluation specialists (and, more recently, of machine-learning and artificial-intelligence specialists). Furthermore, effective-medium theories of rock behavior need to be verified, calibrated, complemented and integrated with geological, drilling, and laboratory information and measurements for their reliable and accurate implementation in geophysical, petrophysical, geohydrological, mining, geothermal, and hydrocarbon reservoir studies, among others.

The discipline of Formation Evaluation interacts closely with several other engineering disciplines, especially **Petrophysics**, **Rock Physics**, and **Geomechanics**. Even though there are overlapping domains and very diffuse boundaries among the four disciplines, only Formation Evaluation considers *in situ* borehole geophysical measurements as the centerpiece of its foundational and conceptual objectives. Broadly speaking, *Petrophysics* focuses on the fluid storage and flow properties of rocks, while the term *Rock Physics* is commonly used to designate the study of elastic properties of rocks (even though semantically both nouns, Petrophysics and Rock Physics, are equivalent). *Geomechanics* (also known as *Petromechanics*), on the other hand, centers about the measurement and quantification of mechanical properties of rocks. However, many practitioners do not make a clear distinction among these four disciplines and one term is often used to designate the combination of all of them (e.g., Rock Physics or Petrophysics).

For the purposes of this book, the name *Formation Evaluation* is used to designate the overarching engineering discipline that studies the measurement, quantification, estimation, and interpretation of *in situ* petrophysical, geomechanical, elastic, and compositional properties of rocks and their saturating fluids by making use of borehole geophysical measurements, drilling-related measurements, samples of rocks and fluids acquired and/or originating from the borehole, laboratory measurements performed on those samples, and contextual geological information.

Based on the above definition, the discipline of Formation Evaluation conspicuously resides in the “center of the action” of cross-disciplinary endeavors for, among others, basin analysis, geological and geophysical exploration, drilling and well completion, reservoir/aquifer description and engineering, geomechanics, and fluid production. The greater the complexity of rocks the more important the discipline of Formation Evaluation becomes to explicitly enforce the seamless connection and integration of diverse observations, measurements, and interpretation procedures. Furthermore, the richest and most diverse collection of measurements is typically found in wells, which enhances the role played by Formation Evaluation in the successful completion of cross-disciplinary projects in the geosciences.

Figure 1.1.3 shows an example of some of the typical elements of an integrated formation evaluation project, including (a) contextual geological and geometrical/spatial information, (b) bathymetry data, (c) seismic am-

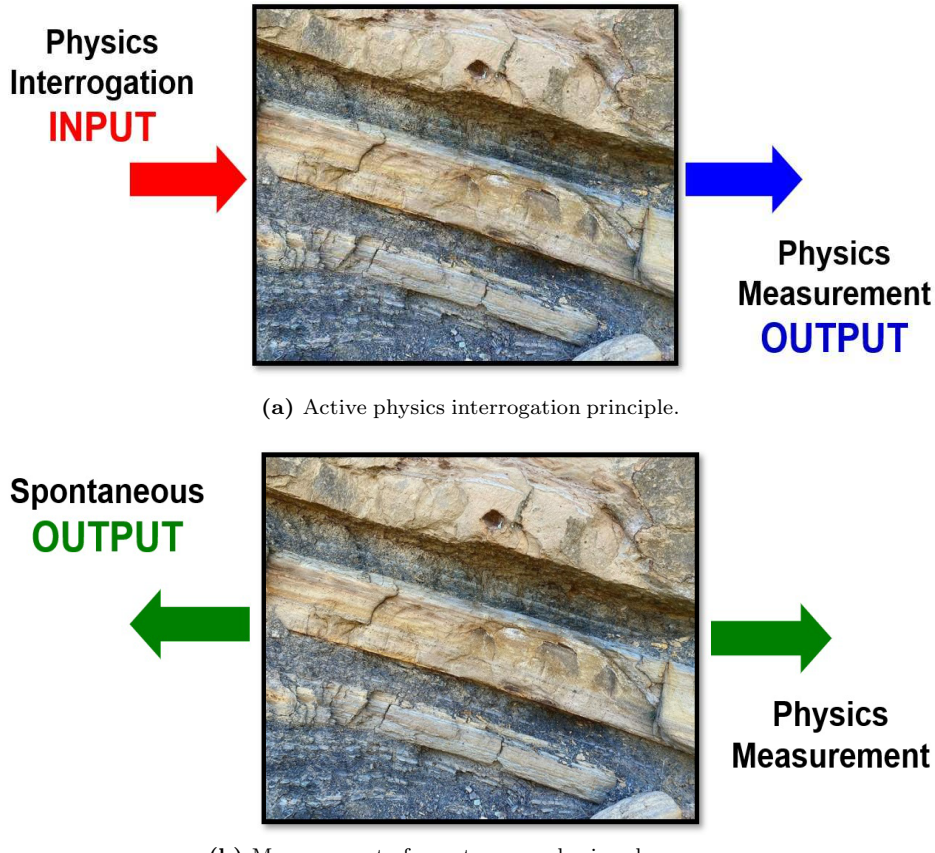


Figure 1.1.1: The discipline of *Formation Evaluation* “sees” rocks with Physics. This is accomplished by either (a) examining physics phenomena in rocks with an outside excitation source and sensing/measuring the corresponding output, or (b) detecting and measuring physics phenomena spontaneously generated by the rock itself. Examples of Panel (a) are electromagnetic and elastic wave propagation, electrical conduction, nuclear radiation, magnetic resonance, fluid pressure pulsing, electrokinetics, and chemical diffusion. Examples of Panel (b) are spontaneous radioactivity by rock-borne radio-isotopes and electric spontaneous potential. The measurements acquired with both physics methods are subsequently transformed into useful rock properties (e.g., compositional, elastic, and fluid-storage and fluid-flow properties) via so-called effective-medium models.

plitude data in the form of time-depth cross-sections and travel-time horizons, (d) whole-core rock samples, and (e) well logs acquired in existing wells. All of these and other elements of analysis are routinely invoked in the quantification of rock properties from well logs for a multitude of engineering objectives, geological and geophysical exploration, geohydrology, hydrocarbon reservoir analysis, geothermal reservoir description, mining, etc. The interpretation of borehole measurements requires the assimilation of all of the above contextual information and measurements.

The detection and quantification of rock properties pursued by Formation Evaluation *explicitly* integrates the following subjects:

- Geological information,
- Borehole geophysical measurements (i.e., well logs),
- Drilling-related measurements,

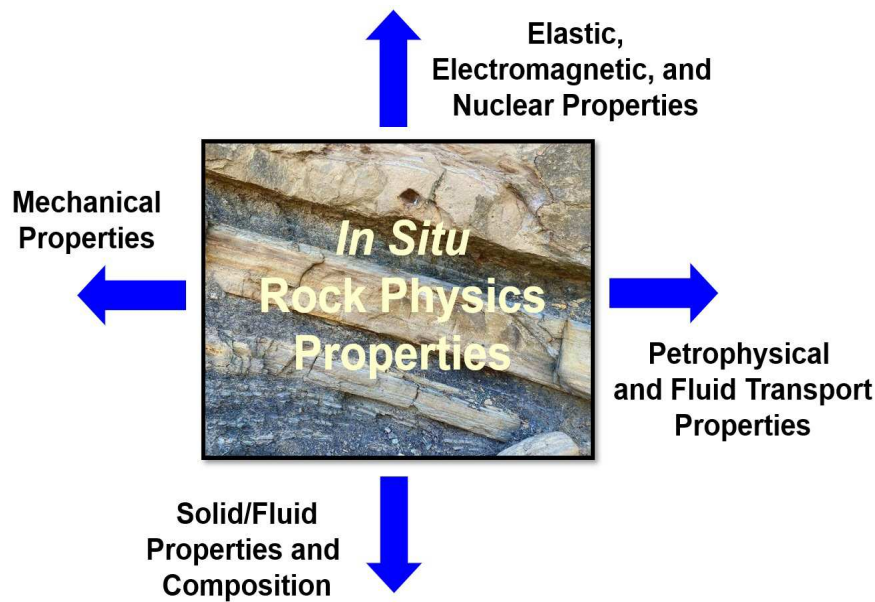


Figure 1.1.2: The discipline of *Formation Evaluation* “transforms” the measured *in situ* rock physics properties (e.g., electrical conductivity/resistivity, elastic properties, nuclear properties, pressure time decays, magnetic time relaxation, etc.) into rock engineering properties such as porosity, fluid/solid properties, fluid and solid concentrations, and elastic and mechanical properties, for instance, using *effective medium* models of rock behavior (e.g., Archie’s equation transforms rock electrical resistivity into water saturation).

- Petrophysics,
- Petrochemistry,
- Geomechanics (Petromechanics),
- Rock elasticity,
- Laboratory measurements of rock samples,
- Fluid properties,
- Temperature, pressure, and stress measurements, and
- Borehole instrumentation and measurement/data processing.

On the other hand, the *in situ* rock properties measured or estimated by the discipline of Formation Evaluation include, but are not limited to:

- Rock mineral (solid) composition and mineral properties,
- Fluid composition and physical/chemical properties of fluids,
- Porosity (pore volume),
- Chemical, physical, and pressure behavior of fluids,
- Interactions between fluid and solid rock components,

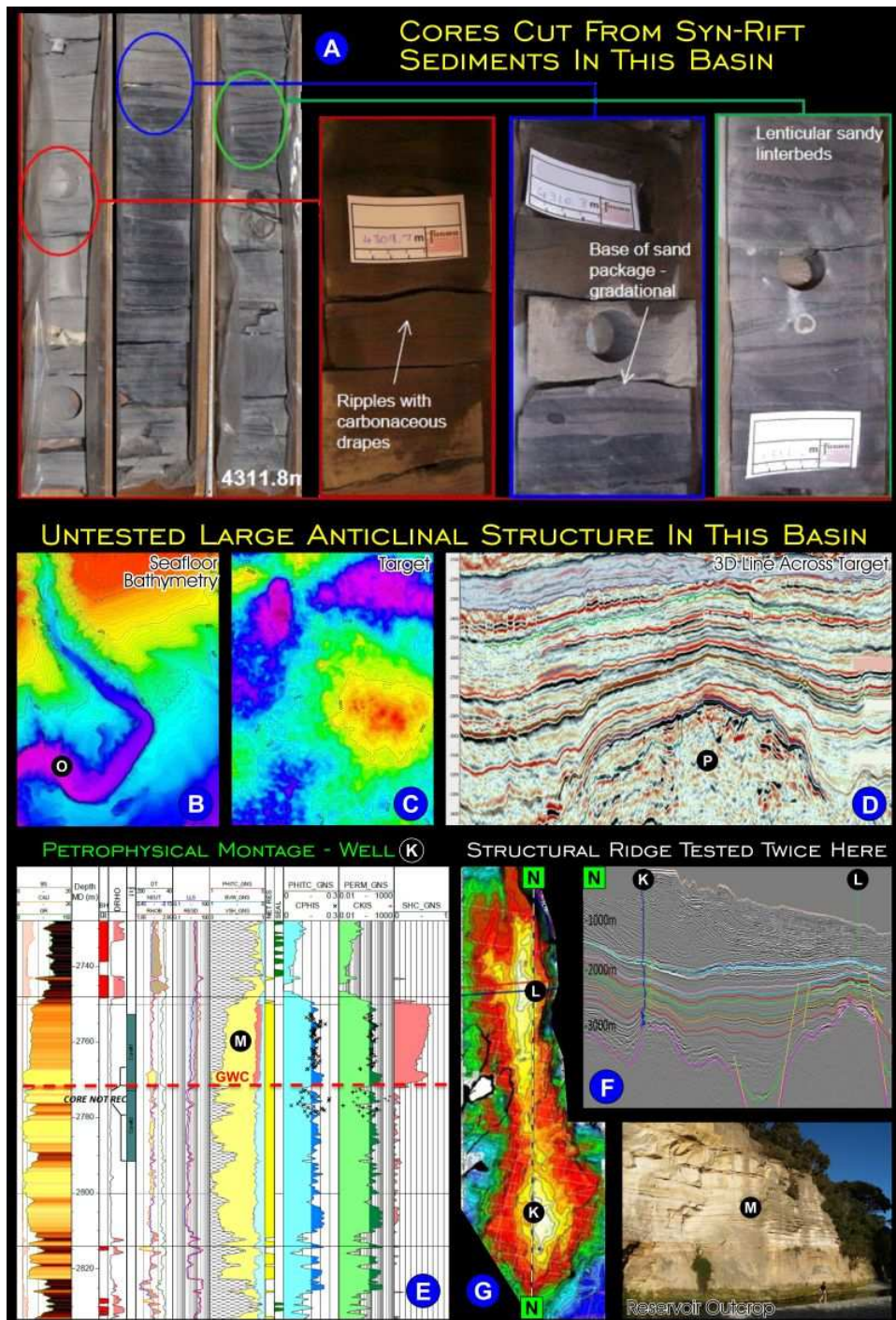


Figure 1.1.3: Example of an integrated formation evaluation project: Canterbury Basin, New Zealand. Image panels A, D, E, and G from [Munday et al. \(2015\)](#), image panels B and C from [Tomlin & Herd \(2015\)](#), and image panels F and G from [Blanke \(2015\)](#). Panel A shows whole-core samples; panels B and C are seafloor bathymetry maps; panel D is a seismic amplitude cross-section; panel E are well logs acquired in well K shown in the F seismic amplitude cross-section; panel G is a seismic travel time map (showing the location of well K) next to a geological outcrop analogue. (Montage courtesy of Steve Walkinshaw).

- Permeability, tensorial permeability,
- Relative permeability,
- Capillary pressure,
- Fracture presence, fracture network, and fracture connectivity,
- Elastic properties,
- Mechanical behavior,
- Pore and overburden pressure, etc.

Formation Evaluation also identifies and quantifies general or composite rock properties in wells such as:

- Geological origin of rocks,
- Layer (bed) boundaries,
- Layer dip and azimuth,
- Internal layering within rocks (e.g., cross-bedding due to grain-size variation or thin sandstone-shale laminations),
- Limits of rock sequences and/or sedimentary unconformities (e.g., formation tops),
- Geological faults,
- Permeability,
- Relative permeability,
- Capillary pressure,
- Fractures,
- Elastic properties,
- Pore and overburden pressure,
- Hydraulic communication between wells,
- Pressure compartments, and
- Pressure seals.

Of special practical importance is the detection and/or estimation of the above properties in multiple neighboring wells penetrating the same or similar rock formations within the same geological structure and sedimentary environment.

The discipline of Formation Evaluation is widely used in the assessment and extraction of subsurface resources such as aquifers, hydrocarbon reservoirs, ore minerals, geothermal reservoirs, and methane hydrates, among others. It is also used in civil and environmental engineering, detection of man-made utilities, and detection of unexploded ordnances. Furthermore, Formation Evaluation complements regional geological studies and geophysical surveillance methods such as seismic amplitude analysis, electromagnetic prospecting, and gravity and magnetic methods, when interpreting geophysical measurements and anomalies in terms of variations of rock properties. Indeed, measurements acquired in wells and laboratory measurements performed on rock samples retrieved from wells provide *ground truth* to a multitude of *regional* geological, geophysical and fluid production measurements and studies.

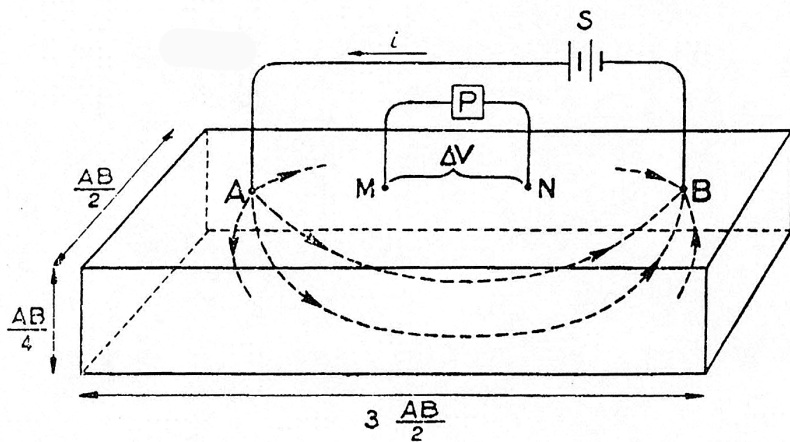


Figure 1.2.1: Schematic of an electrical surface prospecting system: A and B are current injection electrodes while M and N are voltage measuring electrodes (Allaud & Martin, 1977) (Source: Dunstan et al., 1938)

1.2 Past and Present of Formation Evaluation: A Brief Historical Perspective

Formation evaluation is intimately related to the engineering discipline of well drilling. Historically, the oldest wells were drilled to tap fresh-water aquifers and seldom reached more than 60-100 meters in depth. Under such relatively shallow subsurface conditions, the assessment of rock and fluid properties was qualitative in nature and chiefly depended on the visual inspection and analysis of rock samples retrieved from the drilling process itself (Allaud & Martin, 1977; Luthi, 2001). The mining of ore deposits followed a similar trend and so did the much later development of shallow hydrocarbon fields.

However, as wells were drilled deeper and deeper, it was found that retrieving core samples for inspection and analysis was not only very time consuming but also technically challenging and expensive. Furthermore, depending on the mechanical properties of rocks, it was not always possible to retrieve complete rock samples but rather only small and broken fragments, thereby limiting their utility for subsequent qualitative and quantitative analysis. Depending on the drilling method used, only drilling rock cuttings, i.e., rock debris resulting from the drilling process, could be retrieved for subsequent analysis of financial viability. Additionally, it was quickly found that presence of fresh water, hydrocarbon, or valuable mineral ores in a well did not always correlate with financial productivity and viability because what was found in a well often could not be extrapolated far away from it. It was at this very important and transcendental historical juncture that the Schlumberger brothers, Conrad and Marcel, brought to light a technical innovation that forever changed the discipline of Formation Evaluation.

Conrad and Marcel Schlumberger developed some of the earliest surface geophysical prospecting systems intended to locate underground mineral ore deposits based on injecting electrical current into the subsurface and measuring the ensuing voltage differences between two proximal electrodes staked in the ground (Figure 1.2.1) (Schlumberger, 1982; Bowker, 1994). Presence of shallow ore minerals was ascertained by the Schlumberger brothers from abnormally low readings of voltage differences compared to readings made in areas with no such minerals. Parenthetically, very similar surface electrical geophysical systems are still being used today for aquifer and mineral prospection around the world.

Their creativity and very advanced technical knowledge led the Schlumberger brothers to consider the adaptation of a similar geophysical prospecting system in well operations so that the measurements could detect and differentiate presence of fresh water, hydrocarbon, or ore minerals in rocks without the need to rely on rock core samples or drilling cuttings. At the time, Conrad and Marcel Schlumberger knew of the difficulties

being experienced by French hydrocarbon producers to detect and quantify productive hydrocarbon-bearing rocks in wells solely from rock cuttings; they quickly envisioned an electrical detection system that could be engineered for borehole applications. But the successful “adaptation” of their surface electrical detection system turned out to be more difficult than initially thought. Much laboratory and engineering work was needed before the method was verified and deemed practical, repeatable, and reliable. But the Schlumberger brothers had no shortage of knowledge, talent, motivation, and perseverance to make their borehole measurement system an engineering reality (Figure 1.2.2) (Schlumberger, 1982; Oristaglio & Dorozynski, 2009).

In due course, the first successful borehole measurement was acquired by Henri Doll in 1927. Mr. Doll was a young and bright French engineer freshly minted from the *École Polytechnique* and the *École des Mines* in Paris, France, and hired by the Schlumberger brothers to perfect their electrical borehole measurement system (Oristaglio & Dorozynski, 2009). Upon acquiring and hand-plotting the electrical measurements made as a function of depth in the famous Pechelbronn well (located in the province of Alsace, France), Henri Doll found that relatively high values of electrical resistivity successfully correlated with presence of hydrocarbon-bearing sandstones penetrated by the well. It was this correlation (tens of years later scientifically explained and quantified by Gus Archie) that gave rise to the marketing term “electrical coring” (*carottage électrique* in French) to tout the new Schlumberger borehole measurement system as a convenient, reliable, and accurate method to replace cumbersome and expensive rock core retrieving methods to detect hydrocarbon. And this was the memorable beginning of a successful worldwide enterprise tasked with detecting and quantifying *in situ* rock properties from continuous measurements of multiple physical properties acquired in wells, electrical resistivity being only one of them. Eventually, Henri Doll became the most prolific inventor and engineer of a wide variety of successful borehole geophysical measurements beyond electrical resistivity which, to this day, continue to be used around the world (Oristaglio & Dorozynski, 2009). Figure 1.2.3 shows one of the earliest borehole measurement acquisition systems used by Schlumberger around the world (circa 1940), which includes a cable winch, a cable tensiometer, a printer, and two analogue devices used to measure electrical conductivity (Allaud & Martin, 1977). The technology used nowadays for borehole measurements has significantly evolved to also include a wide array of measurements acquired when drilling the well, including deep-sensing electromagnetic systems.

1.3 What is a Formation Evaluation Specialist?

A Formation Evaluation specialist is a technical person who simultaneously masters *Petrophysics*, *Borehole Geophysics and Instrumentation*, *Core Laboratory Measurements*, and *Geology* to make quantitative and qualitative inferences about compositional, petrophysical, mechanical, and elastic properties of rock formations from well logs and core laboratory measurements. This definition is not be confused with that of a *Well-Log Analyst*, who is someone exclusively devoted to the quality control and processing of well logs for calculation of some rock properties, commonly with the intent to assess volumes of fluid in place. While a well-log analyst is skilled at using computer software to transform well logs into some petrophysical properties, a formation evaluation specialist not only can perform calculations from well logs, but is also able to produce quantitative descriptions of rock properties that are consistent with geological knowledge, core laboratory measurements, and fundamental static and flow-related petrophysical properties. A formation evaluation specialist also synthesizes three-dimensional (3D) knowledge to place his/her calculations within the regional context of sedimentary environments, diagenesis, and spatial distribution of fluids.

There are also *Operations Petrophysicists*, who are individuals usually assigned to the supervision of well-logging operations to make on-site decisions about quality of well logs, types of well logs to acquire, depth segments to be analyzed, locations to depths for pore pressure and fluid-sample acquisition, and perforation intervals to be studied based on quick-look calculations.

Formation evaluation specialists have an important role within hydrocarbon-exploration companies because they straddle the geological, geophysical, and reservoir engineering worlds like in no other technical discipline in the Geosciences.

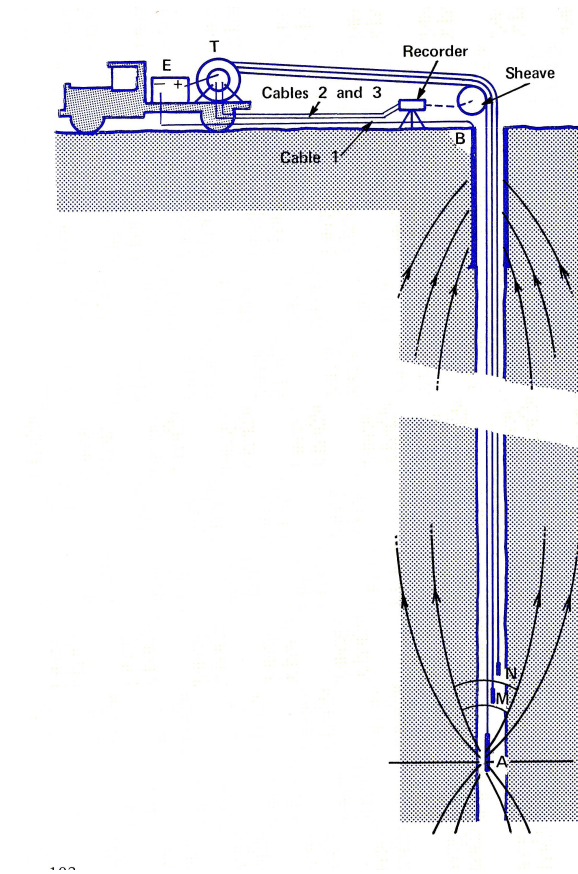


Figure 1.2.2: Schematic of the borehole instrument invented by Conrad and Marcel Schlumberger to measure electrical resistivity of rock formations: A and B are current injection electrodes while M and N are voltage measuring electrodes (Allaud & Martin, 1977) (Source: Allaud & Martin, 1977)

1.4 Key Properties Required in Aquifer or Hydrocarbon Reservoir Description

Formation evaluation specialists working in the hydrogeological and hydrocarbon industries are expected to estimate the following key properties:

1. Hydrocarbon intervals within the well,
2. Porosity, net-to-gross, hydrocarbon volume, reserves,
3. Permeability and anisotropy,
4. Multi-phase flow, associated dynamic properties (e.g. saturation-dependent capillary pressure and relative permeability), and fluid production mechanisms,
5. Recovery factor and ultimate recovery,
6. Production/pressure decline over time,
7. Geomechanical and elastic properties,

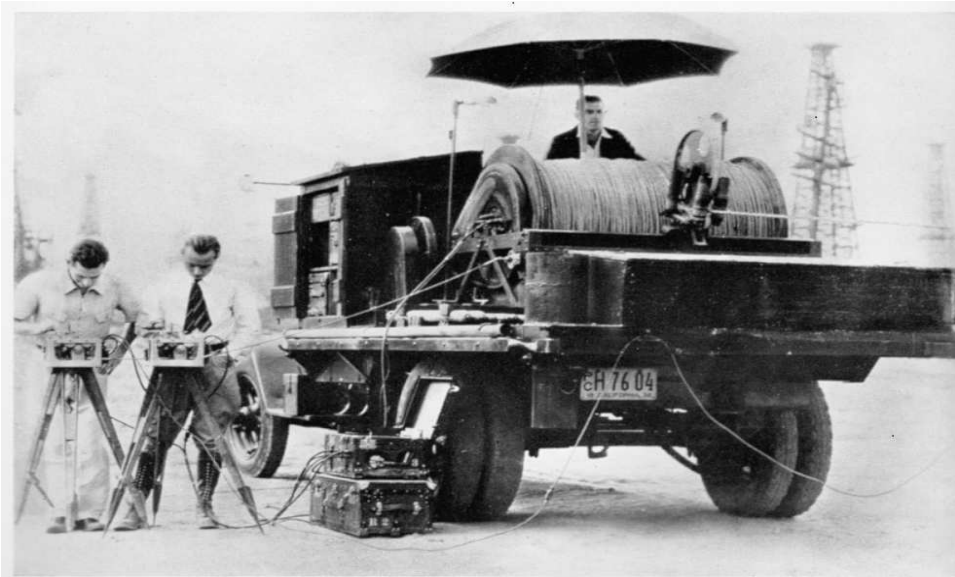


Figure 1.2.3: Photograph of one of the earliest systems used to acquire borehole measurements by Schlumberger. The system includes a winch with cable and tensiometer, a printer, and two electrical analogue systems used to acquire electrical resistivity measurements (Allaud & Martin, 1977) (Source: Allaud & Martin, 1977)

8. Options for well completion and production, and
9. Time-lapse monitoring of rock and fluid properties stemming from production.

1.5 Who Uses Well Logs and Why?

A well log is a measurement of some physical property acquired continuously along the trajectory of a drilled well (a wellbore or borehole), either during drilling, after drilling, or after setting casing and cement (well completion). Measured physical properties include, but are not limited to, natural gamma-ray activity, electrical resistivity/conductivity, spontaneous electrical potential, bulk density, hydrogen index, speed of compressional and shear waves, magnetic resonance time relaxation, pore pressure, temperature, neutron-capture cross-section and gamma-ray spectroscopy, borehole size and shape, and borehole fluid, among others. Well logs are often referred to as *borehole geophysical measurements*. In colloquial terms, well logs “see” rock properties with physics!

Figure 1.5.1 is an example of modern well logs acquired in a vertical well, where the vertical scale is depth and the various plotting *tracks* display well logs acquired separately with different measurement instruments. All these measurements are necessary to estimate rock properties of interest. Figure 1.5.2, on the other hand, shows modern logging-while-drilling (LWD) measurements acquired along a high-angle well, where the horizontal scale is horizontal distance, the lower-most panels shows the well trajectory, and the various plotting tracks display measurements acquired during drilling.

Aside from rock cuttings, whole core, and percussion (rotary) core samples, well logs are the most common and effective means to detect and quantify *in situ* rock and fluid properties penetrated by a well. Prior to the advent of well logs, core samples and rock cuttings were the primary means to assess rock types, rock properties, and saturating fluids.

Even though core samples and their associated laboratory measurements provide *ground truth* about solid and fluid composition, porosity, and pore connectivity, among other important properties, they are not the



Figure 1.4.1: Outcrop of Quaternary alluvial fans showing the spatial complexity and variability of rocks resulting from sedimentary, diagenetic, and tectonic processes. The variability of rocks impacts the spatial distribution of porosity and permeability, for instance; it also affects larger-scale fluid-transport properties such as hydraulic communication, pressure seals, etc. The *contextual* geological information of rocks at all scales needs to be assimilated in the interpretation of well logs and core data (Elephant Trees Formation, California; photograph courtesy of Camilo Gelvez).

most common means to evaluate rock formations because (a) they are expensive to retrieve, (b) they are limited in size and shape, (c) they could be damaged, (d) they are not continuously acquired along the well trajectory, and (e) once brought to the surface they may not be representative of actual *in situ* rock conditions. Coring an entire well is seldom done because of financial, operational, and technical constraints; instead, core samples are commonly acquired along a few sections within the target depth interval. By contrast, well logs can be efficiently acquired in continuous mode along the entire well in a relatively short period of time, regardless of well trajectory, length, or lateral extent. Well logs are the most common measurements used to approach subsurface engineering problems, including the exploration, evaluation, and development of civil engineering, soil, mineral, water, and subsurface energy resources.

In the hydrocarbon industry, well logs are widely used to detect, appraise, and quantify rock properties (including their saturating fluids) along the well trajectory. Examples of application include:

- Drilling engineers use well logs to “navigate” toward and across a reservoir, looking for and remaining within hydrocarbon pay while steering away from water-bearing and shale zones, and to plan coring and fluid-retrieval operations. Drilling cuttings are continuously retrieved and analyzed to reconstruct geological and mechanical properties of rocks penetrated by the drill bit. Fluid analysis systems are also used to detect and quantify fluid properties from the return mud line.
- Geologists use well logs to assess lithology, sedimentary cycles, depositional patterns, weathering surfaces, compaction zones, formation tops, faulting structures, continuity and lateral extent of rock units, etc.

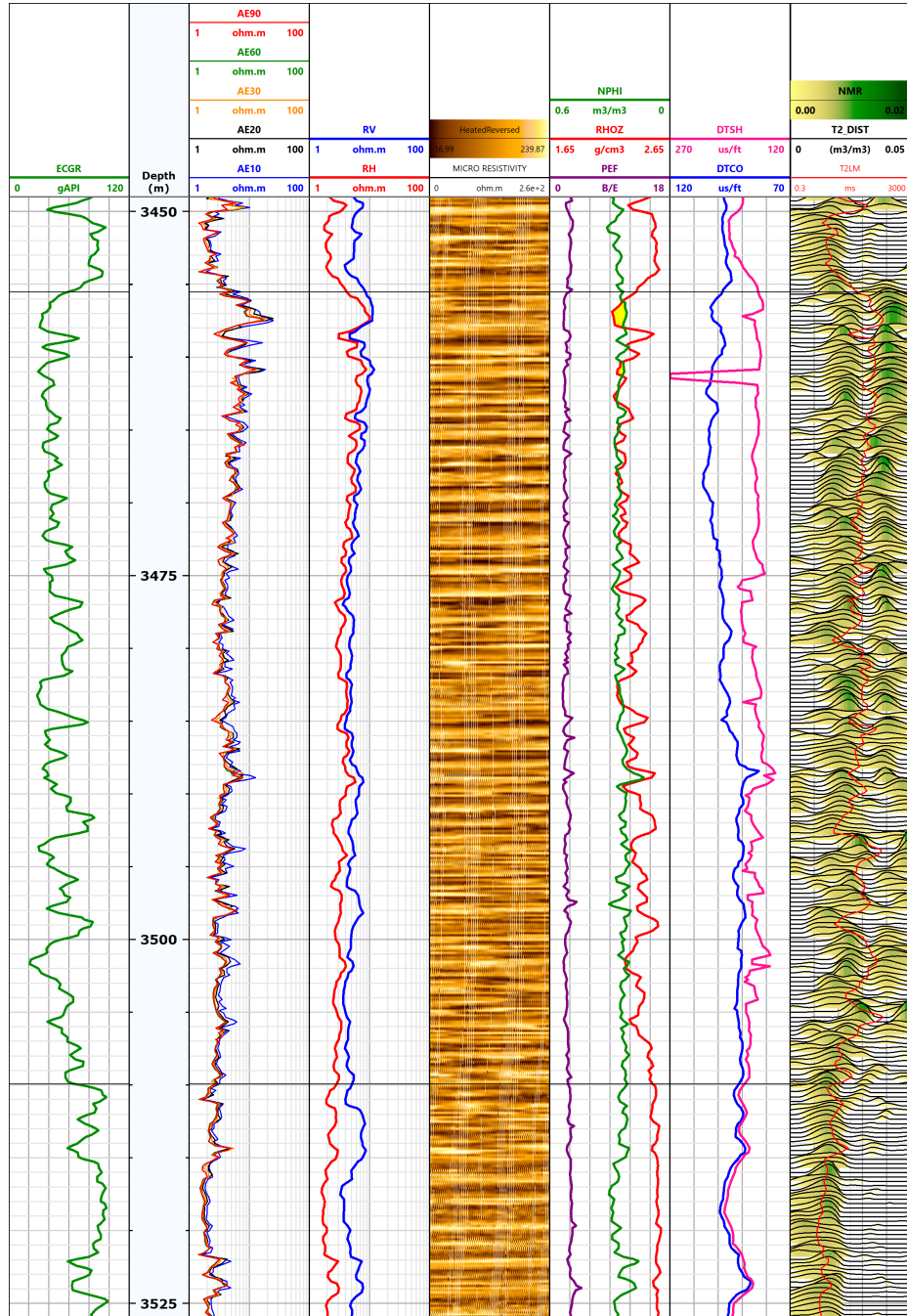


Figure 1.5.1: Example of modern well logs acquired in a vertical well. Track 1 is gamma ray, Track 2 is depth below the KB, Track 3 is electrical resistivity, Track 4 is electrical resistivity parallel and perpendicular to bedding plane, Track 5 is high-resolution borehole resistivity image, Track 6 is apparent density-neutron porosities and PEF, Track 7 is compressional- and shear-wave slownesses, and Track 8 is T_2 magnetic resonance distribution.

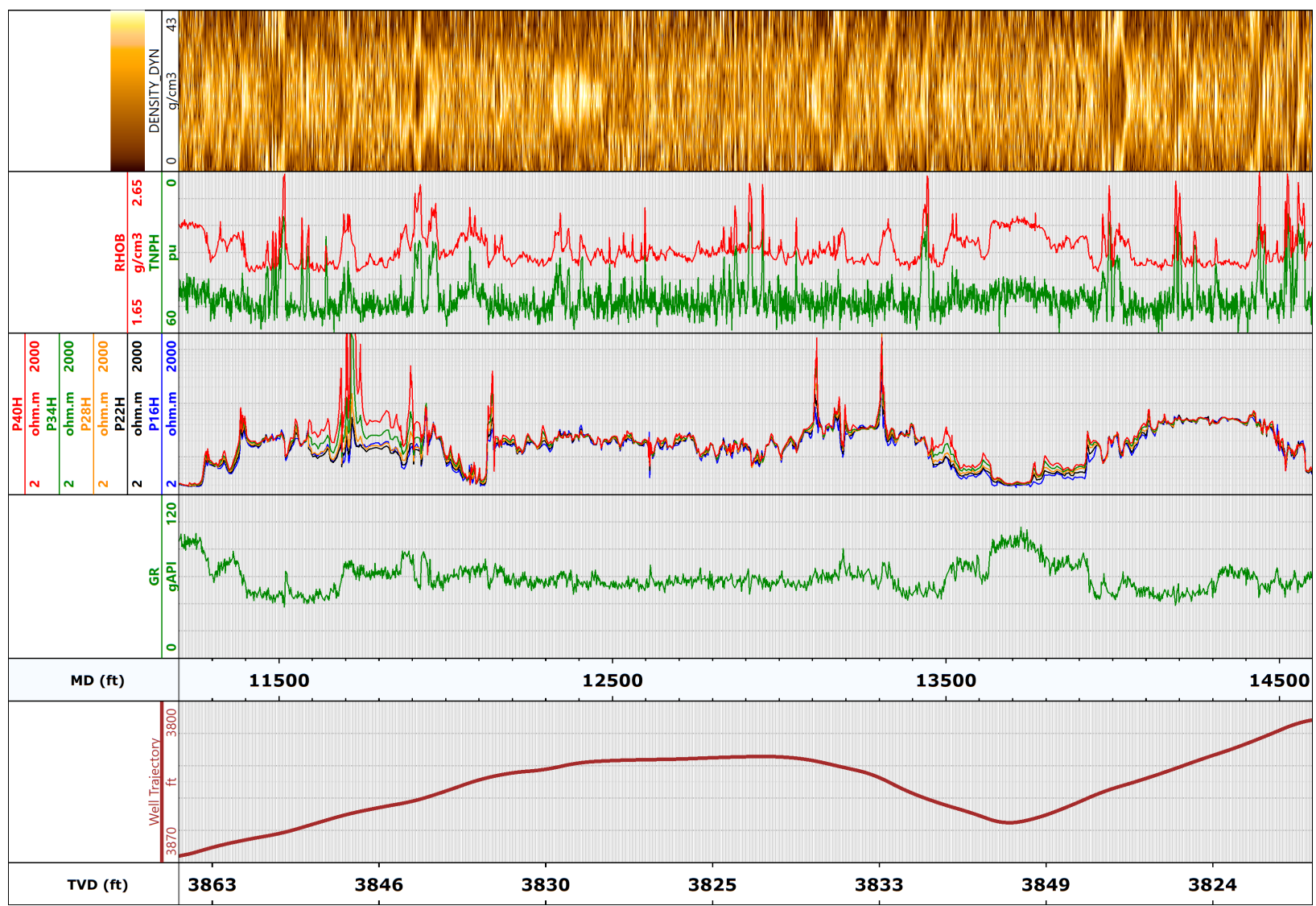


Figure 1.5.2: Example of logging-while-drilling (LWD) measurements acquired in a high-angle well. Track 1 is true vertical depth (TVD), Track 2 is the well trajectory, Track 3 is measured depth(MD), Track 4 is gamma ray, Track 5 is electrical resistivity, Track 6 is apparent density-neutron porosities, and Track 7 is high-resolution borehole density image.

- Petrophysicists use well logs to assess static and dynamic petrophysical properties of rocks, to evaluate pore pressure and pressure seals, to quantify reserves, to assess mechanical/elastic properties, and to quantify fluid properties.
- Reservoir engineers use well logs to assess fluid production mechanisms, to construct reservoir models for numerical simulation, to plan primary and enhanced production strategies, and to forecast aquifer movement and encroachment.
- Geohydrologists use well logs to detect aquifers, to assess their water quality, and to quantify their storage and productivity.
- Completion and well-construction engineers use well logs to assess fluid losses, to quantify borehole size and shape, to plan cementing and casing operations, to plan perforation zones, to design special well completions, to plan and monitor drill-stem and pressure/production testing operations, and to plan hydro-fracturing operations.
- Production engineers use well logs to periodically (time lapse mode) assess the type and volume of fluids produced through perforation intervals, to monitor time variations of pore pressure, fluid type/concentration, and temperature during primary/secondary production or during well-testing operations, to monitor the physical state of casing and cement, and to plan workover and repair operations.
- Geophysicists use well logs to assess *in situ* elastic and mechanical properties of rock formations, to construct seismic velocity models used in reflector migration and imaging, to estimate seismic wavelets, to correlate rock and fluid properties with seismic amplitude variations, and for seismic-time to depth conversions. They also use well logs to design and execute vertical seismic profiling operations.
- Civil and environmental engineers use well logs to assess soil and rock properties for building foundation studies, environmental monitoring, soil contamination and remediation studies, and quality control of buildings/roads infrastructure.

It is therefore clear that well logs provide basic measurements that are necessary for the planning and execution of a multitude of engineering operations.

1.6 Interpretation Method Implemented in this Book

1.6.a Context is everything!

The interpretation method described in this book *integrates* geological information, petrophysics, mechanical properties, core laboratory measurements, well logs, and measurement physics to quantify compositional, elastic, mechanical, storage, and flow properties of rocks.

Well logs should *always* be associated with an outcrop analogue in order to systematically and comprehensively relate rock units to a specific sedimentary environment and its diagenesis. This association provides spatial (geometrical) context and permits the identification of sedimentary cycles, weathering surfaces, etc., and the qualitative assessment of spatial continuity of rock units penetrated by a well (i.e., it provides *geological context*). Figure 1.5.3 best illustrates the important geological and spatial context provided by an outcrop composed of sandstone-shale cycles, where spatial continuity is interrupted by faults with variable slip, heave, and throw. A hypothetical well penetrated this outcrop, be it vertical, inclined, or horizontal, will intersect the various rock layers at variable relative angles (dip) and directions (azimuth). Well logs will detect rock properties in the immediate vicinity of the well. Geological context is necessary to extrapolate those borehole measurements away from the well together with the corresponding petrophysical properties and fluid distributions resulting from capillary equilibrium, for instance.

Another example of the importance of geological and spatial context is shown in Figure 1.6.1, where the gamma-ray log acquired in a vertical well is plotted over the cross-section of the seismic-derived $\lambda\rho$ product



Figure 1.5.3: Photograph of a sandstone-shale clastic sedimentary sequence with faulting blocks (faults in the Honaker Trail Formation, Moab Canyon; photograph courtesy of Peter H. Hennings). Well logs sample but a rather limited spatial segment of the rocks penetrated by a well; it is important to keep the geometrical and geological context in mind when quantifying fluid-transport properties of rocks across large spatial scales.

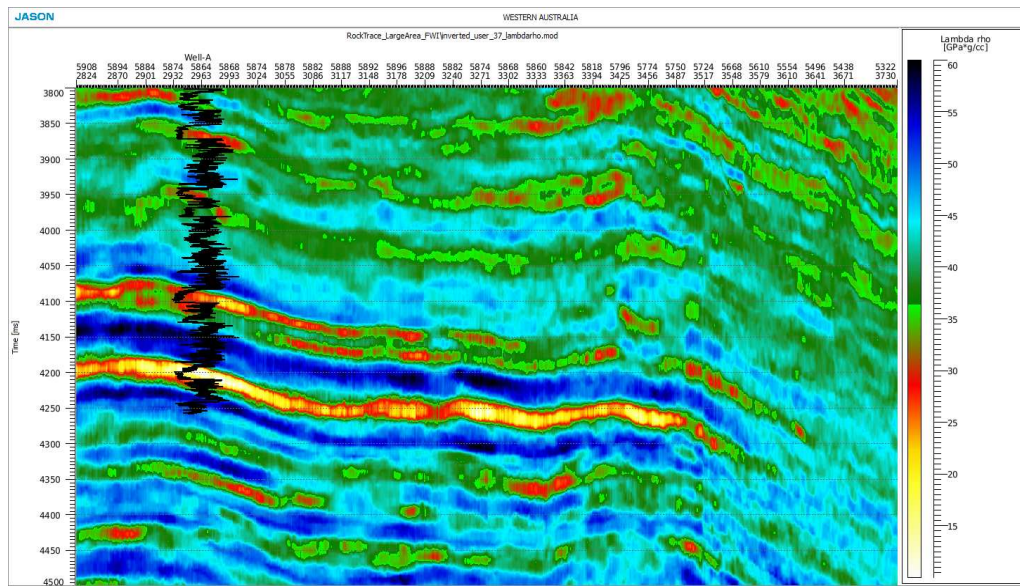


Figure 1.6.1: Gamma-ray log acquired in a vertical well plotted over the cross-section of the seismic-derived $\lambda\rho$ product (vertical scale is two-way seismic travel time, ms). Red- and yellow-colored bands on seismic-derived cross-section correspond to gas-saturated sandstones, thereby evidencing their lateral extent away from the well trajectory. Down-dip, the red-to-yellow colors turn green; this is the location of the free gas-water contact. Offshore Western Australia.

(λ = Lame's elastic constant, and ρ = density). Red- and yellow-colored bands in that seismic cross-section correspond to gas-saturated sandstones, thereby evidencing their lateral extent away from the well trajectory. Down-dip, the red-to-yellow colors turn green; this is the location of the free gas-water contact.

Figure 1.6.2 is an example of 3D geometrical and geological context for two well trajectories and their associated gamma-ray logs provided by 3D seismic amplitude data.

In addition, from the beginning of the interpretation cycle, well-log interpreters should be as familiar as possible with actual rock-core samples, rock cuttings retrieved from mud-logging operations, and rock units identified on an outcrop analogue. Thin sections are essential elements in the interpretation of well logs to quantify type (or types) of grains, makeup (composition) of grains, fine clay laminations, type of cement, grain texture and shape, grain-size distributions, presence and type of clays, and pore connectivity, among others. Quite often, the inexperienced well-log interpreter fails to address these important geological properties and finds him/herself in professional trouble when making interpretations that are inconsistent with the geological framework. It is advisable to look and "touch" rocks as early as possible in the interpretation cycle. Well-log interpretation software should *never* be a substitute for geological understanding.

The "golden rule" of well logging is *a well log is always associated with an outcrop*. This rule is significant in that from the beginning the interpreter is encouraged (and forced!) to associate well logs with a specific sequence of rock units, thereby guaranteeing an interpretation specifically suited to describe the spatial variability of petrophysical properties of those rock types.

Another important element of well-log interpretation is the quantification and detection of *rock classes*. Indeed, rock classification is necessary to assign specific physical properties, storage capacity, and flow capacity, and *interpretation models* to members of the same rock class. The classification of rocks is often performed with emphasis on petrophysical properties. However, quite often, there exists a strong link between sedimentary facies and rock diagenesis *and* the petrophysical classification of rocks. It is also important to emphasize that the definition of rock classes is dictated by the dominant lithology of the rock formations under consideration (i.e., siliciclastic, calcareous, mixtures of both, or mudrocks, for instance). The classification also takes into account the effect of diagenesis on rock storage and production properties.

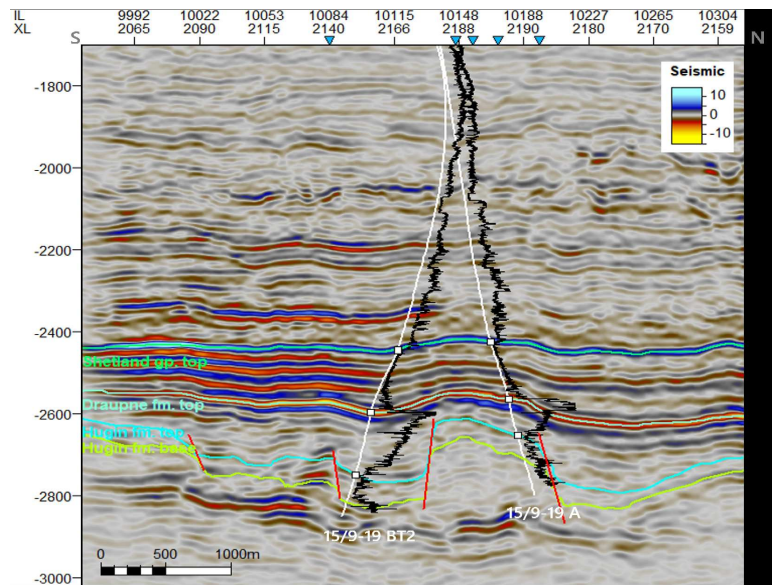
Well-log analysis is but one aspect of the more general discipline of formation evaluation. Traditionally, well-log analysts have been regarded as professionals who can turn a set of well logs into estimates of hydrocarbon reserves, often by means of computer software alone. Formation evaluation experts, however, are professionals who can consistently integrate geology, petrophysics, rock-core data, and borehole measurement physics into the interpretation of well logs, be it for the assessment of hydrocarbon reserves, for geological analysis, for integration with seismic amplitude data, or for the study of dynamic petrophysical properties of rock formations. The spirit of these notes is that of *Formation Evaluation*, which demands a continuous, albeit seamless gravitation between the following inter-related topics:

- (a) Sedimentary processes, rock origin, and diagenesis,
- (b) Petrophysics of immiscible and miscible fluid flow in porous and permeable media,
- (c) Borehole measurement physics, acquisition, and processing, and
- (d) Physics and chemistry of fluids and physics/chemistry of rock-core laboratory measurements.

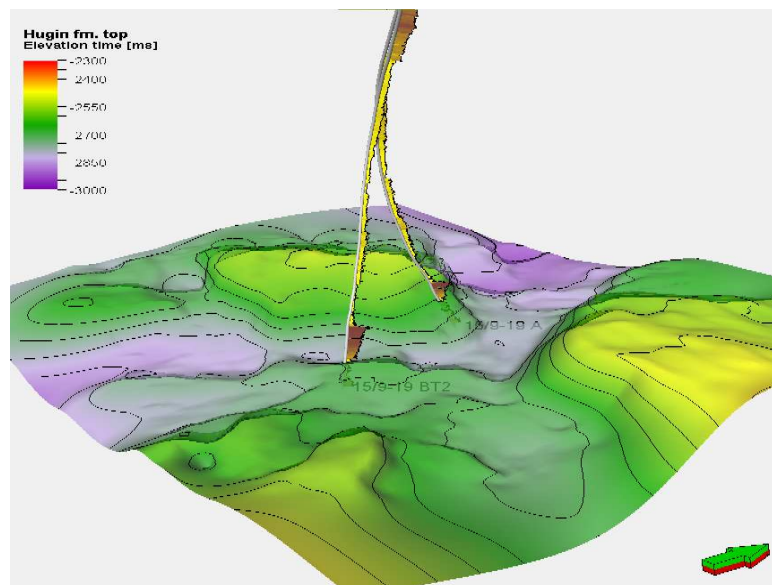
It is hoped that all the interpretation methods described in these notes consistently enforce the above four pillars of formation evaluation.

1.7 Some Opening Remarks about Well Logs and their Interpretation

It is important to emphasize that well logs are not self-sufficient nor are they devoid of imperfections. Interpreting well logs is a *translation* endeavor where the combination of various measured physical properties



(a) Seismic cross-section with two well trajectories.



(b) Three-dimensional view of well trajectories and seismic horizon.

Figure 1.6.2: Well trajectories, seismic amplitude cross-section, and gamma-ray logs acquired along two neighboring wells; vertical scale is two-way seismic travel time (ms). Seismic amplitude data provide 3D geometrical and geological context to the well trajectories and well logs acquired along them. Notice the high degree of correlation between the gamma-ray logs acquired in the two wells. Volve hydrocarbon field, North Sea. (a) Cross-section of post-stack seismic amplitude measurements. (b) Three-dimensional rendering of two well trajectories and seismic reflection surface. (Images courtesy of Valeriia Sobolevskaia).

*is translated into petrophysical, elastic, and/or mechanical rock properties. Accordingly, the translation is performed with a *dictionary* constituted by the pertinent effective-medium properties and rock-physics models.*

The following are important properties and concepts about well logs that need to be assimilated by beginner practitioners of formation evaluation:

- (a) By construction, a well provides a biased line sampling of a usually complex three-dimensional (3D) structure. Therefore, measurements and rock samples acquired along the well trajectory at best represent a statistically biased subset of the global 3D spatial variability of measurements and properties in the reservoir under study. It is also important to recall that most wells are drilled to reach subsurface targets, not for improved or diverse sampling of rock properties; this condition implicitly biases the measurements toward the sampling of target-favorable subsurface regions. Well logs should be considered under their 3D geological context when interpreting them, especially when assessing lateral variability and continuity of rock properties. Seismic amplitude data and well-to-well correlations are often used to provide 3D geometrical and geological context of measurements acquired along well trajectories.
- (b) Not one single well log provides complete information about solid, fluid, petrophysical, and mechanical properties of rock formations. **The magic well log does not exist!** A complete description of rock and fluid properties can only be achieved with the integration of several well logs, core data, and geological information. A formation evaluation specialist is capable of visually, qualitatively, and quantitatively integrating several well logs acquired in the same depth interval and along multiple wells to *estimate* the corresponding rock and fluid properties. One of the most important steps in learning well-log interpretation is how to simultaneously examine several complementary well logs along multiple wells.
- (c) There is not one well log that measures rock porosity. The most common way to estimate porosity is from the bulk density log by making specific assumptions about the densities of solids and fluids present in the rock.
- (d) There is not one well log that measures permeability. The closest way to estimate permeability is from rock mobility (permeability over viscosity) estimated from formation-tester measurements (transient pressure measurements) acquired at discrete well locations. Permeability is usually estimated in an indirect manner using core data and by invoking statistical and/or petrophysical correlations between well logs and laboratory core measurements.
- (e) Most well logs are associated with extremely shallow-sensing measurements; their volume of investigation in most cases does not reach more than one foot away from the wellbore. Electrical resistivity measurements are the deepest sensing, reaching a maximum radial length of investigation of approximately 7 to 8 feet.
- (f) Layers and rock units intersected by a well trajectory can seldom be assumed horizontal and infinite in spatial extent. Most rock units are limited in spatial extent, are spatially asymmetric with respect to the borehole axis, and exhibit non-zero dip and azimuth.
- (g) There is not one single interpretation method or set of specific interpretation procedures that can be uniformly used to evaluate well logs acquired anywhere in the subsurface. In fact, very often there is not one single interpretation method that can be used to interpret well logs along an entire well trajectory. **The magic interpretation button does not exist!** Because of the large diversity of rock composition and pore structure, *in situ* conditions, and fluid properties encountered in the subsurface, the specific method used to interpret well logs needs to be adjusted to face local conditions. A significant component of formation evaluation is the development of interpretation procedures specific to a given set of rocks and/or *in situ* conditions.
- (h) The spatial distribution of fluids and their saturations (or pore volumes) should always be interpreted within the regional fluid context, i.e., in consistency with original fluid saturations, hydrocarbon migration, hydrocarbon re-migration, presence of water-hydrocarbon contacts, presence of pressure seals, capillary equilibrium, PVT properties and phase transitions, and possible influences due to primary hydrocarbon recovery and/or enhanced recovery operations (for instance, water and gas injection).

- (i) Well logs are but one component of formation evaluation. They should never be interpreted without geological knowledge, core measurements, geophysical data (e.g., seismic amplitude data), and petrophysical information.

1.8 Additional Disclaimers (and Warnings!)

It is important to note that not one single well log provides complete and sufficient information about the rocks penetrated by a well; the *magic well log does not exist!* It is imperative to acquire and interpret *several* independent well logs to produce a complete petrophysical and mechanical interpretation of rock formations. In many cases, it is even necessary to acquire core samples to reduce uncertainty and support the interpretation of well logs.

Compared to rock-core laboratory measurements, perhaps the most important feature of well logs is that they measure spatially continuous *in situ* rock properties. However, it is important to emphasize that well logs are neither perfect expressions of rock physical/chemical properties nor direct expressions of petrophysical properties. Without prior experience, it is difficult to attach a measure of reliability and accuracy to well logs. Most of well logs are acquired when the measurement-acquisition instruments are moving in the borehole, either during or after drilling. Only a few measurements are acquired when the instruments are stationary. The speed of logging as well as other borehole environmental conditions could be responsible for various degrees and types of noise, biases, and inconsistencies in the measurements.

In the first place, well logs could be affected by a number of noise and adverse borehole environmental conditions during acquisition. Secondly, most well logs at best provide *spatially smooth* (low spatial resolution) information about physical properties of rock formations. Thirdly, not all the well logs used to estimate petrophysical properties of rocks exhibit the same volume of investigation or the same vertical resolution. Fourthly, most well-logging companies implement a series of post-processing algorithms to the “raw” measurements in order to display them in the form of relatively simple plots for quick-look analysis. All of the above conditions compound to affect the accuracy and reliability of well logs when used for the interpretation of *in situ* petrophysical properties. An example is when a specific type of clay will significantly affect macro-scale petrophysical properties, such as porosity, irreducible water saturation, and permeability. Often, the diagnosis and assessment of type of clay in the pore space requires elaborate laboratory and imaging methods performed at spatial resolutions of the order of several micrometers. None of the commercially available well logs has the spatial resolution necessary to perform these measurements *in situ*. Thus, it is important to complement well-log measurements with both laboratory measurements and direct rock inspection to avoid false (and fatal!) petrophysical interpretations.

Likewise, often the interpretation of well logs leads to non-unique results because of insufficient information and great rock complexity: it is necessary to incorporate external knowledge to select the most geologically and petrophysically plausible interpretation among a few that could be possible. There exist various petrophysical *models* that can be used to indirectly link well logs with petrophysical properties (Archie’s equations being one of them); their selection and the ensuing choice of associated free parameters depends on various factors that are commonly known from information other than well logs themselves.

Beginning formation evaluation practitioners may feel frustrated when finding out that well logs are imperfect or incomplete. It takes a “holistic” petrophysical-geological-geophysical mind to face the corresponding technical challenge and still produce useful interpretations with associated measures of accuracy and reliability. Equally frustrating is the fact that there exist a plethora of interpretation methods to be used for the analysis of well logs acquired in specific classes of rocks (with some variants and exceptions to the rule!) Technical training and interpretation experience are the only safe means to achieve a good level of confidence and practical knowledge in the holistic interpretation of well logs.

1.9 Patterns vs. Physics

Of special significance is the fact that many well-log interpretation procedures are based on *pattern recognition* methods which are the result of years of experience studying, inspecting, and observing well logs acquired across a wide variety of rock types. Even without formal formation-evaluation training, technical personnel can often recognize salient geological and petrophysical features in well logs after having observed many of them in the same field or hydrocarbon play, for instance. Figure 1.9.1 is an example of gamma-ray and resistivity logs acquired in vertical wells located several miles away from each other within the same or in a neighboring hydrocarbon field. The striking resemblance among the logs acquired in the three wells is due to common and spatially continuous stratigraphic/geological features across them despite their relatively long distances. The repetition of “patterns” in well logs, both within the same well or across wells, is what enables the application of similar interpretation procedures for the estimation of petrophysical properties.

Well-log interpretation in siliciclastic rocks can be mastered in a relatively short period of time. However, the interpretation of well logs acquired in carbonate rocks requires sustained experience not only in the analysis of measurements but also in the critical components of rock genesis and diagenesis. At the same time, a good well-log interpreter should have experience with both petrology and the laboratory measurement of petrophysical properties of rock-core samples.

Because of all of the above, it has been stated before that well-log interpretation is an *art*. This is a highly misleading concept that suggests subjectivity, the basic ingredient of artistic creation, and is plain wrong when used to designate well-log interpretation. Even though often one interprets well logs on the basis of insufficient, noisy, and inconsistent data, this does not mean that the underlying principles of formation evaluation, well-log interpretation, and petrophysics are inherently subjective. Contrary to that, most well-log interpretation methods are based on sound physics and mathematics concepts which are *quantitative* by nature and can be rigorously verified in the laboratory and subject to hypothesis testing. However, many of the interpretation methods have a restricted range of applicability and it is important that the well-log interpreter be sufficiently versed on the limitations of a given interpretation method, be it deterministic or statistical. At the same time, it is very important that the well-log interpreter be knowledgeable of the technical limitations, reliability, and accuracy of a given borehole measurement before using it in the calculation of rock properties.

1.10 Estimation of Solid/Fluid Compositions of Rocks From Well Logs

One of the most common uses of well logs is to estimate solid and fluid constituents of rocks and their corresponding concentrations (volume or weight concentrations). This important application of formation evaluation makes use of sophisticated numerical modeling procedures of well logs together with constrained minimization such that the estimated concentrations yield numerically simulated well logs that match the available well logs. All estimated concentrations need to be positive and smaller than one and all the estimated solid/fluid concentrations need to add up to 1. Special conditions arise when some of the available well logs are noisy or there are not sufficient well logs to estimate the concentrations of a large number of constituents (i.e., non-uniqueness).

Figure 1.10.1 shows and example of available well logs and core measurements of porosity, permeability, and water saturation across a mixed carbonate-clastic sedimentary sequence. Of special significance in this plot is the display of solid/fluid constituents and their volumetric concentrations shown in Track No. 5 (colored display of shale, quartz, dolomite, calcite, and fluid concentrations). The concentrations were estimated by iteratively matching the available well logs with their numerical simulations.

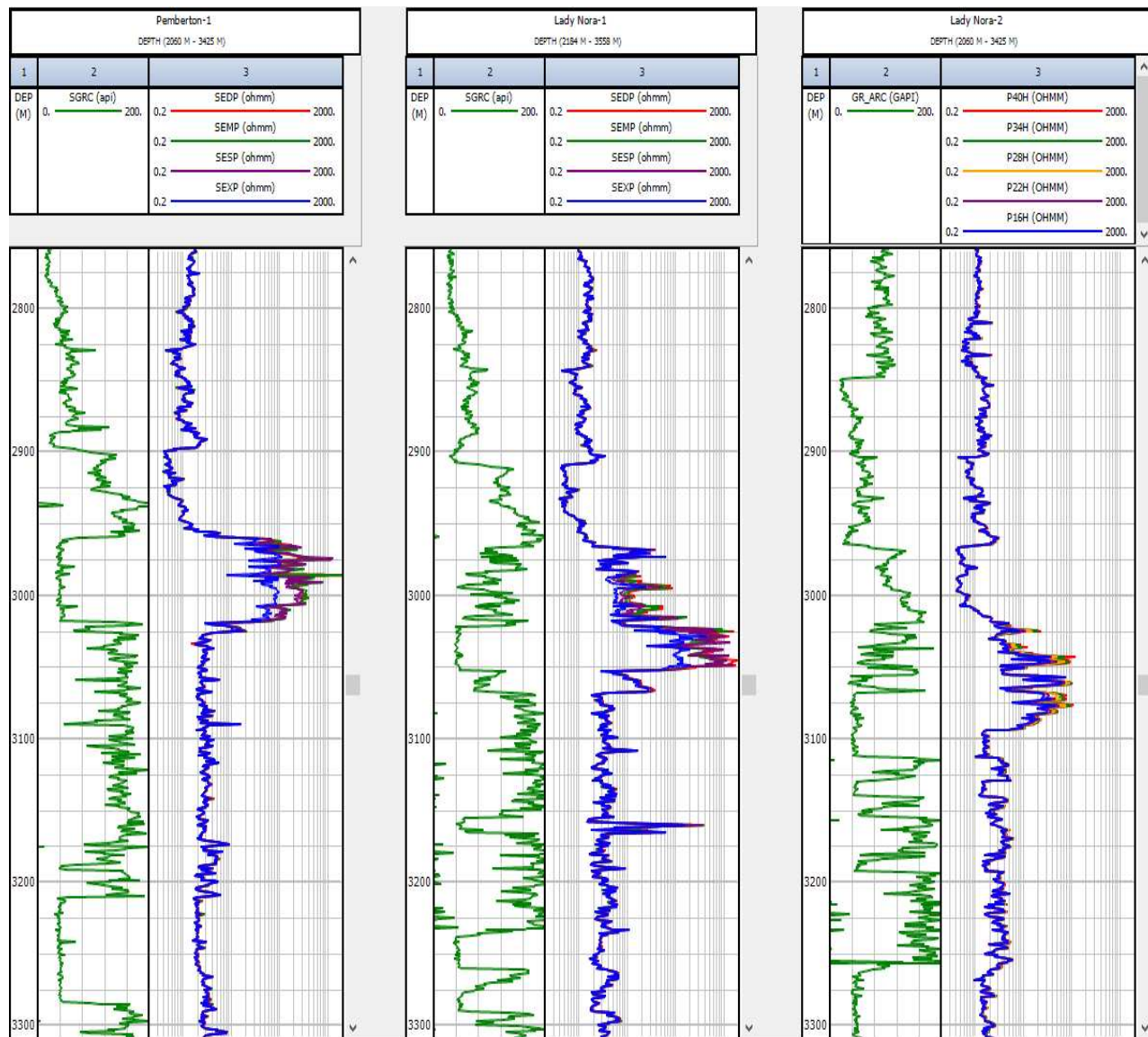


Figure 1.9.1: Plots of gamma-ray (green) and resistivity logs (multiple logs in logarithmic scale with blue being the dominant color) acquired in three vertical wells located in neighboring hydrocarbon fields (Lady Nora and Pemberton fields, offshore Western Australia). The high correlation among gamma-ray logs acquired in the three wells enables the identification of common or similar stratigraphic units bearing different fluids. Well-to-well correlation via well logs is the basis of pattern recognition used to identify repetitive or equivalent stratigraphic units across multiple wells.

1.11 Interpretation Procedures Based on Artificial Intelligence

Because of their continuous nature along well trajectories, well logs have long been a target of interpretation procedures based on artificial intelligence, machine learning, and/or big data. Such procedures require discovery and quantification of deterministic and/or statistical correlations (linear and/or nonlinear) between multiple well logs acquired in multiple wells within the same geological, petrophysical, and fluid contexts. The latter process is typically referred to as *the training step*, and requires that measurements be acquired under varied and

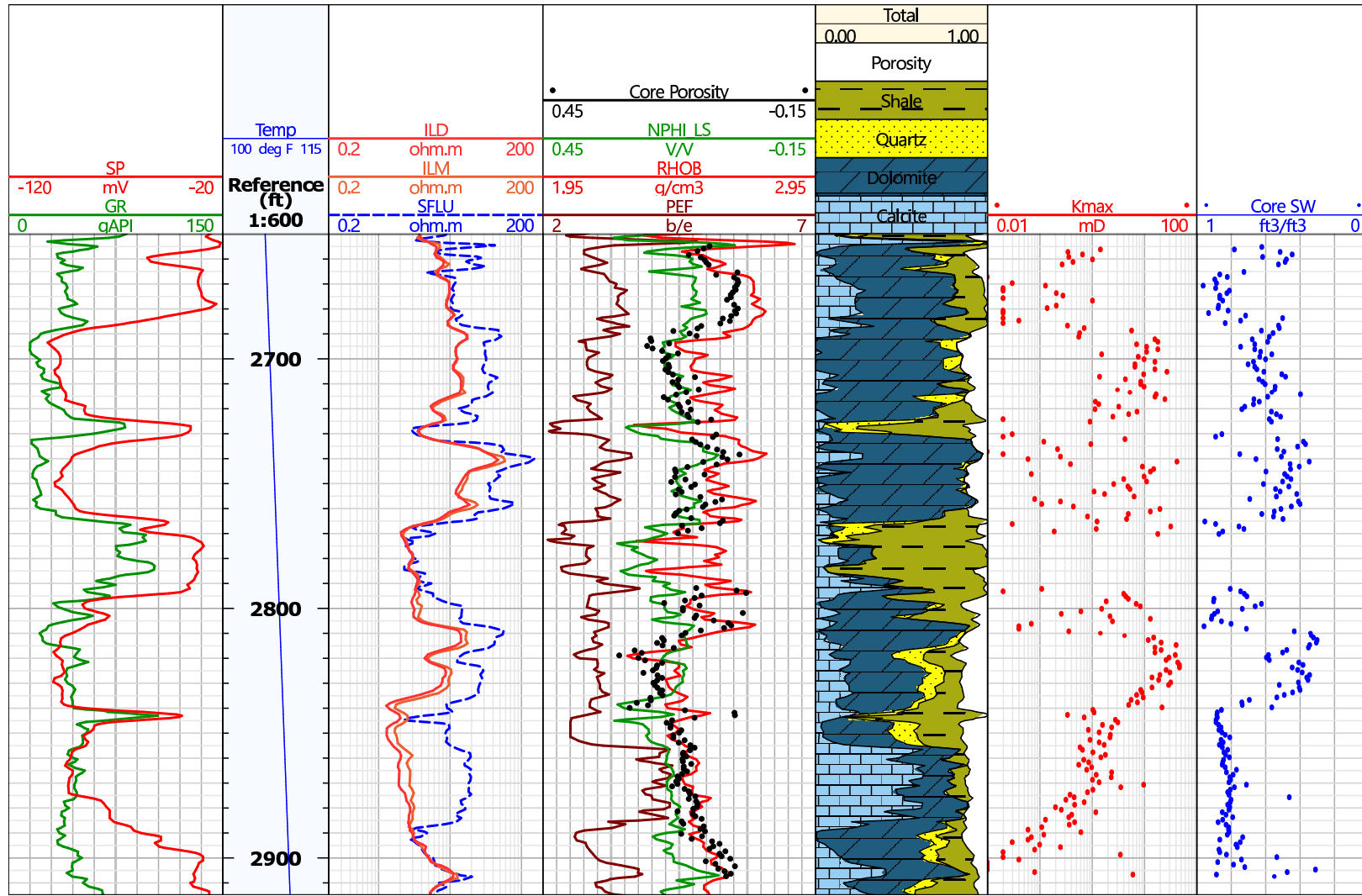


Figure 1.10.1: Example of well logs and core measurements acquired across a mixed carbonate-clastic sedimentary sequence. Track 1 shows gamma-ray and spontaneous potential logs. Track 2 shows depth and formation temperature. Track 3 shows the resistivity logs (shallow-, medium-, and deep-sensing resistivity logs). Track 4 shows the neutron, density, and photo-electric factor (PEF) logs together with core porosity. Track 5 shows the estimated volumetric concentrations of fluid (porosity), shale, quartz, dolomite, and limestone. Tracks 6 and 7 show core permeabilities and core water saturations, respectively.

redundant geological, petrophysical, and fluid conditions. Because some well logs are sensitive to instrumental and borehole conditions (even after they have been corrected for borehole environmental effects), it is also important that the training step be performed with either normalized well logs (i.e., well logs mitigated for instrumental and borehole conditions) or with well logs acquired with multiple instruments and under multiple borehole conditions. This can be typically accomplished in mature hydrocarbon fields that include tens of wells with similar well logs and which have already been subjected to similar interpretation procedures (e.g., well-log interpretations calibrated with core data). After the training step, the detected correlations are expressed as parametric or non-parametric input-output mathematical models which can be used for prediction. Such models are further verified and improved based on blind measurement testing, i.e., by quantifying their prediction errors in wells which include interpretation results but which were not used during the training step to ascertain and quantify correlations.

The mathematical models constructed and calibrated for prediction of interpretation products should also be capable of estimating the uncertainty of their predictions. Examples of such mathematical models include neural networks, deep learning convolutional neural networks, random forest decision trees, and Bayesian connection networks, to name but a few. Thus far, it has been found that the latter models are reliable and accurate for well-log interpretation only in the presence of abundant wells and redundant coverage of geological, petrophysical, and fluid conditions. They are not reliable for interpretation of exploratory wells and should always be subject to verification via blind-well validation. Because of the extreme variability of geological, petrophysical, and fluid conditions encountered in most interpretation projects, to this date there are no general artificial intelligence procedures capable of interpreting wells logs acquired under arbitrary conditions, i.e., the *magic interpretation button* does not yet exist.

Artificial intelligence and machine learning methods have also been used to discover and predict correlations between well logs and core measurements. The discovery (training) of such correlations is performed in wells where there are abundant core measurements and well logs. Subsequently the estimated correlations in the form of deterministic and/or statistical mathematical models is extrapolated to wells which do not include core measurements but include well logs. When estimating and implementing those correlations it is important to take into account the differences in spatial resolution and sampling density between well logs and core measurements.

Chapter 2

Basic Geological Concepts

...Le savant n'étudie pas la nature parce que cela est utile; il l'étudie parce qu'il y prend plaisir et il y prend plaisir parce qu'elle est belle...

—Henri Poincaré, Science et Méthode.

The objective of this Chapter is to briefly describe the salient geological concepts that are required in formation evaluation studies. There are no universal procedures to assess rock properties from well logs and core measurements; every rock is different and so are the methods used for its petrophysical and mechanical evaluation. However, understanding the genesis and diagenesis of rocks helps to elucidate classes of rocks that share common petrophysical and/or mechanical properties, for instance. Understanding the origin of a rock's pore/throat system also helps to evaluate its fluid transport properties at all spatial and time scales.

2.1 Basic Concepts on Sedimentary Processes

Integration of geological concepts on the interpretation of well logs requires basic knowledge about sedimentary processes, diagenesis, tectonic (structural) alteration, and hydrocarbon migration.

For the case of siliciclastic sedimentary sequences, the following is a partial list of depositional environments:

- Alluvial and conglomeratic,
- Fluvial, high and low energy,
- Lacustrian,
- Glacial,
- Deltaic (with its many variants),
- Coastal barriers,
- Estuarine systems,
- Turbiditic,
- Mud systems,
- Etc.



Figure 2.1.1: Example of an outcrop of Cretaceous clastic rocks showing lateral variations of sandstone and shale layers resulting from depositional, diagenetic, and tectonic processes. Well logs sample but a very limited spatial segment of rocks encountered along the well trajectory. Quantifying fluid-transport properties of spatially complex rocks requires additional geometrical, geological, and petrophysical information not provided by well logs (Sun River Canyon, Montana; photograph courtesy of Peter H. Hennings).

More complex depositional systems include mixtures of the above processes. The mechanism of sediment transport has a strong influence on grain size, grain sorting, grain shape, presence of clay minerals, cross-bedding, etc. It also conditions the spatial variability of petrophysical properties, vertically and laterally, and hence the petrophysical quality and spatial extent of hydrocarbon reservoirs. Subsequent alteration of sediments in the form of compaction and diagenesis may give rise to solute precipitation and chemical alteration of original grains, including clay genesis (i.e. authigenic clay, clay alteration, and grain cementation and recrystallization). Likewise, tectonic deformation may give rise to fracturing, enhanced solute transport and solute precipitation, additional rock-fluid chemical alterations, and presence of impermeable flow barriers, among others. Figure 2.1.1 shows an outcrop of a clastic sedimentary sequence characterized by cycles of sandstone and shale layers with variable thicknesses. Diagenesis and tectonic deformation cause spatial variability of fluid-transport properties of sandstones in addition to spatial variability of properties impressed by the original sedimentary processes.

Hydrocarbon migration may originate wettability alterations as well as gradients in the chemical composition of saturating fluids. Drainage and imbibition processes acting over geological time may also have a strong effect on fluid composition and spatial distribution.

Figure 2.1.2 shows an outcrop of a shale, i.e., a clastic rock with negligible permeability. Shales serve as pressure seals above or below aquifers and hydrocarbon reservoirs.

Some features of sedimentary environments have an imprint on well logs. For instance, the concentration of radioactive chemical elements such as K, Th, and U may exhibit vertical variations in response to volumetric concentration of clay minerals associated with grain size variations. Such variations may exhibit distinct patterns that could even repeat themselves in the form of cycles which are often visible along the measured-depth axis of well logs. An alert formation evaluation specialist should pay attention to such patterns and cycles as they could indirectly reveal special features about the underlying sedimentary environment in relation to the geological location of the well, and hence about the associated petrophysical properties and their spatial variability.

Carbonate sedimentary environments are much less amenable to general rock or facies classification than clastic sedimentary environments. The reason is that diagenesis, rock-fluid interactions, and tectonic deformation often place strong constraints on the spatial variability of petrophysical properties. In some cases, the

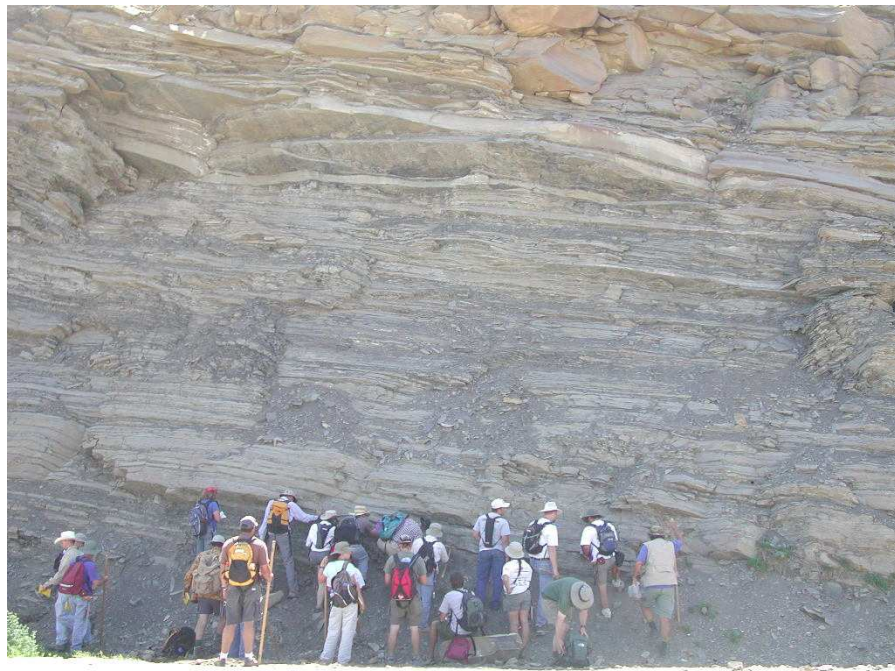


Figure 2.1.2: Photograph of a shale outcrop showing finely laminated cycles of fissile layers (Lewis Shale, Colorado). Shales are very finely laminated clastic rocks with negligible permeability because their average grain diameter is $65 \mu\text{m}$ or smaller. They often serve as pressure seals (fluid flow barriers). Non-fissile shales are often referred to as *mudrocks* (photograph courtesy of Laura Net).

origin and subsequent alteration of the storage and flow properties of carbonate reservoirs becomes independent of the geological origin of the sediments themselves. Clay alteration and calcite/dolomite recrystallization may also have a significant effect on the storage and flow properties of carbonate reservoirs, particularly in the case of grainstones and mudstones. Figure 2.1.3 is an example of deep marine carbonate rocks with depositional (precipitation) cycles (layers) of various thicknesses. Some of these layers exhibit enhanced porosity (and permeability) due to relatively high differential dissolution (due to diagenesis) and abundance of fossils. Vertical fractures are also present originating from tectonic processes.

The petrophysical analysis of carbonate reservoirs, especially of those reservoirs that include touching and non-touching vugs, fractures, and non-connected moldic porosity, can only be performed with the help of specialized core analysis, borehole image logs, and/or magnetic resonance measurements.

One of the first steps of well-log interpretation consists of specifying vertical bounds of sedimentary and/or weathering cycles in measured depth (formation tops and bases). This task is usually performed by an experienced geologist. Rock classification should also be carried out prior to well-log analysis. The specific method used for well-log analysis and interpretation should be adapted to the properties of rock formations elicited by the geologist. It is seldom the case that the same well-log interpretation method can be applied to the entire well (in fact, this is one of the most prevalent mistakes in well-log interpretation) because of variability of rock and fluid complexity .

Unconventional rock formations are those which exhibit negligible permeability and include organic mudrocks (organic shales). Whenever they are saturated with hydrocarbon, their production cannot be carried out with standard primary means; they need to be subject to hydraulic fracturing along extended horizontal wells. The petrophysical analysis of unconventional rock formations is still in development mode because only in the last 5-10 years those formations became financially viable for exploration and development. Their petrophysical assessment is extremely complex because of multiple variables. There are not generalized in-



Figure 2.1.3: Photograph of a carbonate outcrop showing depositional (precipitation) marine cycles with different thicknesses and porosities; vertical fractures are also present in some of the layers (Cretaceous outcrop, Canyon Lake Dam, Texas). The layers with the largest porosity are those subjected to relatively high differential dissolution and abundance of fossils (photograph courtesy of Jerry Lucia).

terpretation methods available to approach their quantification. Every unconventional formation needs to be approached in a unique manner to quantify petrophysical properties, type and concentration of organic matter, and geomechanical properties. Interpreting measurements acquired in unconventional formations requires the highest level of understanding and practical experience with formation evaluation.

2.2 Clastic vs. Carbonate Formations

Siliciclastic (or, in general, clastic or terrigenous) rocks are defined as those formed by the packing of individual grains (i.e., grain packs) and subsequently altered by compaction, diagenesis, solute precipitation, authigenic clay growth, cementation, recrystallization, grain alteration (including the development of grain micro-porosity), and fracturing, among others. Figure 2.2.1 shows a thin section of a cemented aeolian sandstone with variable grain sizes and presence of non-uniform grain cementation.

Even though the adjective “siliciclastic” implies dominant quartz composition, in practice, the chemical/mineralogical makeup of grains in clastic rocks can include feldspars, micas, calcite, dolomite, siderite, pyrite, anhydrite, to name but a few. Examples also abound wherein the chemical/mineralogical composition of cement may be different from that of grains. The porosity of siliciclastic formations originates from the space left between grains and cement, while their permeability originates from the degree and efficiency of inter-communication of the pore space. Gamma-ray logs can exhibit variations from 0 to 300 gAPIs (or larger) in siliciclastic formations depending on grain and clay/shale composition. The nature of the grain pack together with clay/shale topology, composition, and concentration determine the petrophysical properties of siliciclastic formations. Because of this behavior, gamma-ray logs acquired in siliciclastic formations tend to exhibit strong correlations with all other logs. Actually, such a strong correlation is often used to differentiate siliciclastic from

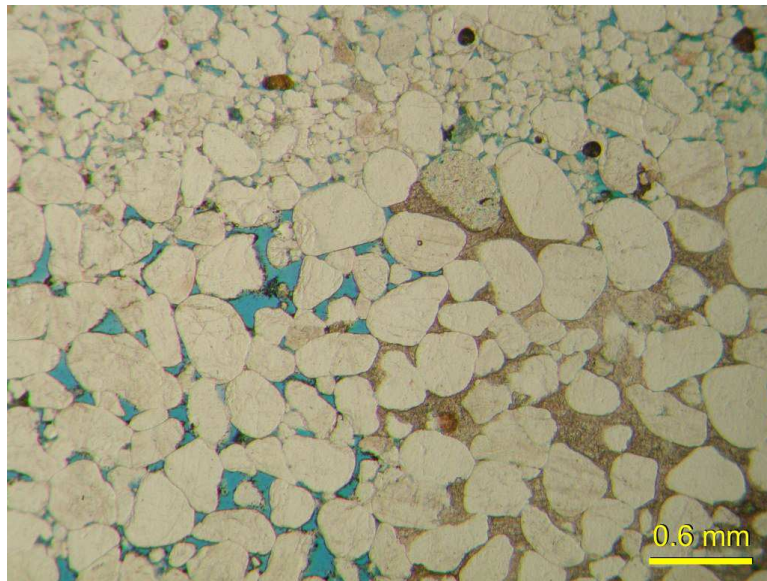


Figure 2.2.1: Thin section of a clastic rock shown variable grain sizes and irregular grain cementation: aeolian sandstone. The storage and fluid-transport properties of clastic rocks are chiefly conditioned by (1) average grain size, (2) grain sorting, (3) grain cementation, (4) grain-size laminations, and (5) presence and concentration of grain-coating or laminated clay/shale. This thin section also includes a few grains with microporosity (photograph courtesy of Laura Net).

carbonate formations based on well logs. **The storage and fluid-flow-related petrophysical properties of clastic rocks are usually controlled by grain size and grain-size uniformity, grain shape and grain-shape uniformity, grain arrangement, and volumetric concentration of clay/shale (be it laminated shale or grain-coating clay).**

Carbonate formations are formed by the spontaneous precipitation and accumulation of calcium and/or magnesium carbonate with and without simultaneous presence of marine organisms (or residues from marine organisms, e.g. shells, coral, algae mounds, etc.) with predominantly calcium carbonate and quartz composition. Occasionally, precipitated carbonates (and residues from living organisms) mixed with very fine terrigenous material originating from marine mud flows (such as in the case of deltaic and turbidite terrigenous mud flows). Because of their genesis, at the outset carbonate rocks exhibit close to null porosity. It is because of **differential dissolution due to diagenesis** (because of compaction, increased pressure and temperature) that pore space begins to open and be filled with fluids. Differential dissolution takes place because of spatial variations of rock composition and mineralogical makeup. An example of this behavior is the accelerated dissolution of animal shells compared to the much slower dissolution of spontaneously precipitated carbonates. Depending on the degree of differential dissolution, the opened pore space may or may not remain topologically inter-connected, whereby total porosity may substantially differ from inter-connected porosity. Accelerated dissolution and fluid circulation in carbonates may also lead to solid precipitation and mineral recrystallization (including the common phenomenon of dolomitization), giving rise to pore textural changes and further constraining pore connectivity (permeability) (Figures 2.2.2 and 2.2.3).

Many carbonate rocks exhibit a significant degree of fracturing due to cycles of tectonic deformation (see Fig. 2.2.4). Accelerated dissolution through fractures may also take place in such rocks. They are usually described as dual-porosity and dual-permeability petrophysical systems, having one type of pore storage and connectivity through the original matrix, and another one through the open fracture network.

Gamma ray logs often exhibit no significant variations in deepwater carbonate sedimentary sequences except in those cases where deepwater turbidites sequentially mix with carbonates giving rise to mudstones. Borehole



Figure 2.2.2: Photograph of a moldic carbonate rock with voids originated from differential rock dissolution of packets originally occupied by fossils: carbonate rock from the Edwards group, Austin, Texas. Differential rock dissolution due to diagenesis gives rise to pore space. Some of the pore space eventually becomes connected (fluid percolation), thereby enabling the transport of fluid. The latter can in turn accelerate solid dissolution and recrystallization, hence give rise to additional modifications to the storage and fluid-transport properties of the rock.

environmentally corrected gamma-ray logs in clay-free carbonates are typically lower than 30-15 gAPI and remain fairly constant with depth. In shallow marine formations, where terrigenous clastics commonly mix with carbonate materials to form rocks referred to as marls, the gamma-ray log can exhibit wide variations, similar to those encountered in siliciclastic sedimentary sequences. Also, abnormally large values of gamma-ray readings can be found across evaporites as the latter commonly exhibit a substantial concentration of potassium.

In the case of clean (clay/shale free) carbonate sedimentary sequences, the gamma-ray log does not tend to correlate with resistivity, density, neutron, and sonic logs (as is generally the case in siliciclastic formations). The underlying property which correlates resistivity, neutron, density, and sonic logs is rock porosity. Petrophysically attractive depth sections in carbonate sedimentary sequences are those with relatively high porosity and exhibiting signs of mud-filtrate invasion. Because porosity is the common denominator among all well logs acquired in a clean carbonate sedimentary sequence, the best petrophysical conditions take place when the electrical resistivity log exhibits the lowest possible values and the sonic log exhibits the largest slownesses. Pore inter-connectivity (permeability) is verified by the presence of mud-filtrate invasion as inferred from the differences between resistivity logs with multiple radial lengths of investigation.

2.3 Unconventional Rock Formations

These formations exhibit negligible permeability and include organic mudrocks. Hydrocarbon-bearing unconventional formations cannot be subject to standard methods of primary production; they require production stimulation via propped hydraulic fracturing along extended horizontal wells. Organic mudrocks are hydrocarbon source rocks, and their financial viability for production is conditioned by their volumetric concentration of organic material, the type and maturity of organic material, presence of natural fractures, *in situ* stresses, pore pressure, and geomechanical properties.

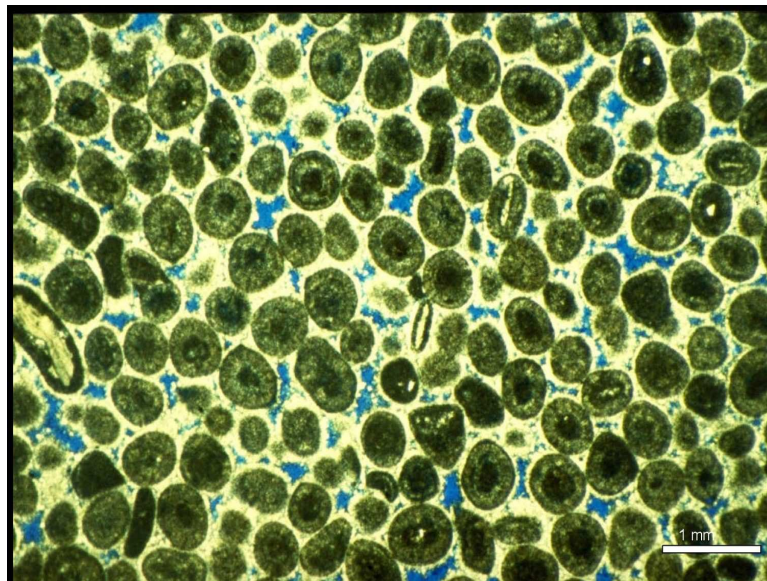


Figure 2.2.3: Photograph of a thin section of oolitic limestone showing the pore space in blue (epoxy) (photograph courtesy of Jerry Lucia).

Figure 2.3.1 shows an example of unconventional rock formation, the Monterey formation at Shell Beach (Pismo Beach) in California, which has given rise the Hondo oil field operated by ExxonMobil. The Monterey formation is composed of chert/porcelenite, occasional dolomite, and organic-rich phosphatic shale. Production from the offshore Monterey formation at the Hondo oil field primarily originates from the fractured chert beds, but some production also comes from the fractured dolomite. Organic richness in the dark shale is 7-10 wt% TOC (total organic content). Cherts (porcellinites) and the dolomites are electrically resistive beds, while the phosphatic/organic-rich siliceous dark mudstones are the recessive (eroded) beds.

The production of fluids from unconventional formations is greatly conditioned by the spatial extent and branching of propped hydraulic fractures away from the borehole, as well as by surface-fluid interactions in both fractures and rock matrix because of the nanometer-meter range of the throat radii involved. Because of this, formation evaluation in unconventional formations requires the joint interpretation of petrophysical, compositional, and mechanical properties of rocks, unlike interpretation procedures undertaken in conventional clastic and/or carbonate rocks. Figure 2.3.2 shows an outcrop of the Eagle Ford formation, an organic-rich mudrock which was the source rock of gas- and oil-saturated clastic reservoirs located higher up in the sedimentary sequence. Dark-colored layers in Figure 2.3.2 include organic material.

Development strategies in unconventional hydrocarbon-bearing formations typically involve one key vertical well and several horizontal wells spudded from it. Diverse and sophisticated well logs are acquired along the vertical well to adequately describe and quantify petrophysical, compositional, and mechanical properties along the depth section that exhibits organic material. The interpretation of well logs requires detailed validation of calculations with core laboratory measurements. Outputs from the interpretation are total porosity, porosity within the organic material, volumetric concentration of organic material, type and maturity of organic material, water saturation, presence and properties of natural fractures, solid composition, presence and volume of adsorbed hydrocarbons, *in situ* stresses, pore pressure, and mechanical properties (e.g. Young's modulus, Poisson's ratio, anisotropy, etc.) among others. Core laboratory measurements include permeability, porosity, solid composition, chemical and geochemical properties of fluids, studies of fluid-solid maturity, and mechanical properties under variable stress conditions. Results obtained from formation evaluation in the vertical well are used to determine locations and orientations of horizontal wells to be spudded from it. Only a few well logs are acquired along horizontal wells (especially LWD measurements, typically only the gamma-ray log) to navigate



Figure 2.2.4: The petrophysical and mechanical properties of carbonate rocks can be substantially affected by diagenesis and tectonic deformation (photograph courtesy of Peter H. Hennings).

the well along the best organic segment of the formation. Geomechanical calculations and interpretations performed in the vertical well are used to designate candidate locations for propped hydraulic fractures along the horizontal well and to optimize the selection of specific engineering parameters needed to generate the hydraulic fractures (water pressure, fluid viscosity, type of proppant, etc.)

Non-organic mudrocks typically exhibit relatively large gamma-ray values and relatively low values of electrical resistivity (because of salty water saturation and non-negligible porosity). Organic mudrocks, on the other hand, tend to exhibit large gamma-ray values and large resistivity values because of their diminished water pore volume occupied by hydrocarbons. Comparison of well logs across inorganic and organic mudrocks is often used to assess organic content in the latter.

2.4 Rock Cuttings

Rock cuttings originate as part of mud-logging operations during drilling. They are retrieved at the shale shaker located immediately adjacent to the mud pit or end of the mud line. Mud logs include detailed rock descriptions that should be used to diagnose and validate the type of sedimentary environment under consideration. The depth uncertainty of rock cuttings is around 5 m. In addition, mud logs should be used to validate the diagnosis of rock types and the corresponding calculation of volumetric concentrations of rock constituents.

2.5 Depositional Environment, Architecture, and Spatial Continuity of Flow Units

Sedimentary depositional environments are associated with specific spatial variations of grain size, porosity, clay content, type of shale/clay distribution, permeability, etc. Likewise, specific sedimentary environments are



Figure 2.3.1: Outcrop of the Monterey formation at Shell Beach (aka Pismo Beach), California. The Monterey formation is composed of chert/porcelenite, occasional dolomite, and organic-rich phosphatic shale. The upper light-colored fractured interval is a dolomitized (carbonate) interval overlying organic-rich siliceous (diatoms) shale. Organic richness in the dark shale is 7-10 wt% TOC (total organic content) (photograph courtesy of Quinn Passey).

associated with ranges of spatial continuity and variability of rock properties along directions perpendicular and parallel to bedding planes.

The study of depositional environments should be based on outcrop analogues, rock-core samples, mud logs, rock cuttings, and thin sections. It is imperative that well logs be associated with a specific sedimentary environment as early as possible in the interpretation cycle. Likewise, wells (and their well logs) should be assigned a specific spatial location within a 3D geological structure and within the spatial limits of a sedimentary environment. This part of the analysis is exceedingly important because well logs sense rock properties within a very short radial distance (typically shorter than 2 m for resistivity logs and less than 1 ft for most other well logs), hence any measure of spatial (lateral) continuity can only be assessed with external geological and/or geophysical information (e.g. seismic amplitude data).

Interpretation of well logs should be preceded by the picking of tops and bases of sedimentary sequences. Each sedimentary sequence is to be treated separately when interpreting well logs and core data into petrophysical and mechanical properties of interest.



Figure 2.3.2: Photograph of the outcrop of an organic shale (organic-rich mudrock) showing presence of finely laminated and very tight layers with abundance of organic material (dark-colored segments; Eagle Ford formation, Del Rio, Texas). These layers are the source rock of clastic gas reservoirs located higher in the sedimentary sequence (photograph courtesy of Rich Aram).

2.6 Concept of Shale Baseline in Siliciclastic Sedimentary Sequences

The interpretation of well logs in siliciclastic rock formations begins with the evaluation of readings across depth intervals of “pure” shale sections. Such readings provide the envelope as a function of depth, or *shale baseline* for each well log. The shale baseline becomes the reference value(s) over which all the logs are considered to quantify petrophysical properties of rocks in a siliciclastic sedimentary sequence. Specifically, the estimation of petrophysical properties of porous and permeable sandstones is performed by first inspecting whether the well logs across sandstones exhibit lower or higher values than across the shale baseline.

For instance, SP measurements above or below the shale baseline will be associated with formation water salinity greater or smaller than that of mud filtrate, respectively. Likewise, resistivity measurements across porous sandstones that are below the shale baseline will be indicative of water-bearing intervals with high porosity and large values of salt concentration.

Shale baseline values of well logs are important because they represent measurements acquired in the *pure shale* end member of the sedimentary sequence. All petrophysical interpretation methods used for the analysis of shaly sandstones rely on well-log values across the *pure shale* member of the sequence. Non-constant shale baselines (with depth) may occur because of depth variations of shale composition and makeup (e.g. shale porosity, type of clays, volumetric concentration of clay, volumetric concentration of silt, and salt concentration of formation water), pressure, and temperature, among others.

Chapter 3

Basic Petrophysics Concepts

...Voici mon secret. Il est très simple: on ne voit bien qu'avec le cœur. L'essentiel est invisible pour les yeux...

—Antoine de Saint-Exupéry, *Le Petit Prince*.

The subject of *Petrophysics* has been treated at great length by many outstanding publications and textbooks (e.g., Peters, 2012; Zinszner & Pellerin, 2007). This chapter includes only descriptions and concepts that are necessary to support subsequent sections focusing on formation evaluation procedures based on well logs and core measurements.

Most petrophysical concepts and *petrophysical models* commonly invoked to calculate the storage and flow properties of rocks implicitly assume that rocks are homogeneous and isotropic within the scale of the measurements. This is hardly the case in the vast majority of contemporary hydrocarbon reservoirs and aquifers. Figure 3.1.1 shows an example of a spatially heterogeneous clastic rock saturated with oil. The high degree of rock variability within relatively short distances causes oil to be present only in short segments with favorable storage and flow properties. Consequently, the rock appears to exhibit “patchy” oil saturation. This behavior brings about multiple technical challenges in reservoir engineering and production, and drastically decreases the recovery factor, thereby making many such hydrocarbon plays financially non-viable. When quantifying the storage and flow properties of rocks, it is very important to keep in mind (1) the spatial scale of the measurements involved (i.e., their volume of investigation) and the effect of time on fluid flow, (2) the degree of spatial variability of rock properties, and (3) the interplay of the two. It is equally important to understand the assumptions and limitations of the equations and methods used in the calculations.

3.1 Petrophysical Properties of Rocks

Petrophysics, a term originally coined by Gus Archie (Archie, 1950), chiefly studies the fluid storage and flow properties of rocks, while the term *Rock Physics* is commonly used (especially among geophysicists) to refer to the study of electrical, elastic, nuclear, mechanical, and other properties of fluid-saturated rocks. Additionally, Petrophysics studies the fluid/solid compositional properties of rocks. Many of these properties are measured in the laboratory using rock samples of various sizes and shapes, in some cases under conditions of pressure, stress, and temperature similar to those encountered in the subsurface.

Petrophysical properties of interest depend on the number and types of fluids (fluid phases) stored and flowing through the rock. Furthermore, the storage and flow properties of rocks are greatly conditioned by the rock’s genesis and diagenesis. It is often necessary to measure or estimate these properties at different scales and to examine their spatial variability in order to quantify their impact on fluid flow at early and late times during primary or secondary production.

Specific petrophysical properties of interest in formation evaluation are the following:



Figure 3.1.1: Photograph of spatially heterogeneous clastic rocks (slabbed whole core segments) saturated with viscous oil. The high degree of spatial variability of rock properties within relatively short distances causes oil to be present only at a few rock sections that exhibit favorable storage and flow properties. Most petrophysical concepts and the so-called *petrophysical models* used to quantify rock properties assume spatially homogeneous rocks.

- Porosity (interconnected, primary, secondary, total, non-shale, effective, non-connected, occluded, etc.),
- Water saturation (mobile, clay-bound, capillary-bound, and irreducible),
- Pore volume of water and hydrocarbon,
- Hydrocarbon saturation (mobile and residual),
- Permeability and anisotropy,
- Relative permeability (saturation-dependent permeability),
- Capillary pressure (imbibition and drainage, wetting-phase saturation cycles),
- *In situ* pressure and temperature,
- PVT properties of fluids and chemical composition, including pH, density, viscosity, electrical resistivity, dielectric constant, miscibility, compressibility, etc.,
- Pore and overburden pressures, and

- Elastic and mechanical properties as a function of *in situ* stress.

It is important to emphasize that some of the above petrophysical properties are interrelated in a deterministic or statistical way or else are simply correlated in a statistical fashion (e.g. porosity, permeability, capillary pressure, and relative permeability).

3.2 Estimation of Hydrocarbon Reserves

One of the central goals of well-log interpretation is to calculate hydrocarbon reserves (hydrocarbon storage capacity). The assessment of hydrocarbon reserves requires layer-by-layer calculations of porosity (non-shale porosity for the case of siliciclastic rocks, and interconnected porosity for the case of carbonates), hydrocarbon saturation, net-to-gross, and recovery factor.

If h is the sampling interval of well logs, one can describe the point-by-point hydrocarbon-reserve contribution as D_i , given by

$$D_i = \phi_i \cdot (1 - S_{wi}) \cdot n_i, \quad (3.2.1)$$

where ϕ_i is porosity (either non-shale or interconnected), S_{wi} is water saturation, and n_i is net-to-gross.

To estimate total hydrocarbon reserves in units of Stock Tank Barrels (STB), one has

$$N_{STB} = 7,758 \cdot \left(\frac{1}{B_0} \right) \cdot \left(\sum_i^N D_i \right) \cdot h \cdot RF \cdot A, \quad (3.2.2)$$

where N is the number of sampling points, h is given in ft, B_0 is oil formation volume factor, RF is recovery factor, and A is the area of the reservoir in acres. The recovery factor is a function of the PVT properties of hydrocarbons but it is also intended to quantify the ability of hydrocarbon-bearing formations to “release” hydrocarbons from their pore space (in this sense, the recovery factor is related to permeability, relative permeability, capillary pressure, and residual hydrocarbon saturation, among other factors). On the other hand, net-to-gross depends on the volumetric concentration of porous rock laminae whose thickness is below the vertical resolution of well logs. In most cases, net-to-gross can only be quantified with rock-core samples (or photographs) or with high-resolution borehole image logs.

Most oil companies enforce specific cut-offs on porosity, net-to-gross, and hydrocarbon saturation to calculate total hydrocarbon pay when booking reserves. Such cut-offs are also specific to a particular basin in the world, to a particular field, and to a given rock formation. Care should be exercised when imposing shale, porosity, and hydrocarbon-saturation cut-offs across highly-laminated siliciclastic sequences.

3.2.a Remarks about the recovery factor

In practice, the hydrocarbon recovery factor of rocks, RF above, is never 100% (the average worldwide hydrocarbon recovery factor is approximately 60% for primary recovery, i.e., without the use of enhanced recovery methods such as water flooding, CO_2 flooding, chemical flooding, thermally assisted flooding, etc.) The recovery factor depends on a multitude of rock and fluid properties as well as on the specific strategy implemented for primary fluid production. In the case of immiscible fluid flow, rock wettability and saturation-dependent rock properties such as capillary pressure and relative permeability and their respective imbibition-drainage cycles play a significant role in hydrocarbon recovery factors. High residual hydrocarbon saturation and abnormally low pore pressures, for instance, are some of the most important properties responsible for low recovery factors in practice. Even in the presence of relatively high hydrocarbon saturation and low water cut of rocks, hydrocarbon production can be negligible because of high residual hydrocarbon saturation and abnormally low relative permeability to hydrocarbon. Formation evaluation specialists are especially concerned with the estimation of hydrocarbon recovery factors.

3.3 Hydrocarbon Storage and Producibility

While hydrocarbon storage (reserves) is controlled by porosity, non-residual hydrocarbon saturation, and thickness, the producibility (flow capacity) of a reservoir is controlled by dynamic petrophysical variables such as permeability, permeability anisotropy, relative permeability, capillary pressure, irreducible water saturation, temperature, pressure, wettability, PVT properties of fluids, etc.

Petrophysical calculations based on well logs yield estimates of porosity and water saturation. In some cases, well logs can help to quantify irreducible water saturation and permeability. Measurements acquired with formation testers *in situ* provide indirect calculations of permeability. Sampling of formation fluids with formation testers allows the measurement of fluid pressure and the calculation of other fluid properties (gas-oil ratio, electrical resistivity, viscosity, density, and optical refraction index, for instance). However, to date the vast majority of flow-related petrophysical properties can at best be estimated via specialized rock-core laboratory measurements. Additional interpretation techniques include the indirect estimation of capillary pressure via saturation-height analysis based on variations of water saturation with TVD above free fluid contacts (e.g. free water-oil contacts).

While hydrocarbon reserves control the “size of the bank account”, it is pertinent to recall that flow-related petrophysical properties such as permeability, relative permeability, and capillary pressure, as well as reservoir production mechanisms such as aquifer pressure, *in situ* fluid pressure, and pressure compartments, control the frequency with which “specific amounts of money can be withdrawn from the bank account.” It is also pertinent to recall that the fluid production of most reservoir includes variable amounts of water whose separation and disposal may have a considerable repercussion on production costs, hence on the financial viability of the reservoir.

3.4 Calculation of Porosity

Contrary to common “wisdom” among many hydrocarbon reservoir description practitioners, *porosity is not measured with logging tools*, but rather *estimated* indirectly from well logs. Moreover, the estimation is based on critical assumptions about the density of the fluid and the density of grains included in the rock. The equation that governs the relationship between rock density and rock porosity is given by

$$\rho_R = \phi \cdot \rho_f + (1 - \phi) \cdot \rho_m ,$$

where ρ_R is rock density (also designated as ρ_b , or bulk density), ρ_m is grain (matrix, solid) density, ρ_f is fluid density, and ϕ is porosity. This equation can be derived from first principles starting from the definition of density and by subsequently enforcing material balance conservation of the mixture. Therefore, the equation is not an empirical formula but rather an exact mixing law. In the above equation, ϕ is *total porosity*; the relationship does not imply knowledge of interconnected porosity (as in the case of Archie’s equation, for instance).

Solving the above equation for porosity requires that ρ_m and ρ_f be known in addition to rock density (which is measured with borehole instruments). Thus, there are three unknowns in the equation whereupon the calculation of porosity requires additional measurements (or external information) in order to reduce the number of degrees of freedom. Such a problem is approached in formation evaluation by (1) making a first approximation to the calculation of porosity with the assumption that the saturating fluid is known (typically, the entry assumption is that the saturating fluid is water), and (2) by diagnosing and quantifying the solid components of the rock. Once the solid (matrix) components of the rock are known, the neutron log is used to assess whether the assumed fluid density is correct or not. If the assumed fluid density is not correct then a correction is made and the corrected fluid density is used to calculate porosity. Subsequently (specifically in the case of carbonate rocks), the sonic log is used to diagnose and quantify presence of heterogeneous (non-uniform) porosity (e.g., in the presence of fractures or vugs). Errors in the calculation of matrix and fluid density will cause errors in the calculation of porosity. Likewise, erroneous (e.g. noisy) measurements of bulk density will cause errors in the calculation of porosity. The length of error bars in the calculation of porosity will depend

on both the range of porosity and the reliability of the measurements. Typically, low-porosity rocks will entail long error bars in the calculation of porosity because of instrumentation noise and because of uncertainty in the grain density of multi-mineral rock compositions.

Accurate calculation and interpretation of porosity, especially for the assessment of permeability (flow capacity) requires that not only total porosity be known but also the pore-size distribution and the portion of the fluid-filled porosity that will not contribute to fluid displacement in the presence of pressure gradients. The latter portion of the pore space includes the component of irreducible water saturation. Magnetic resonance measurements provide information about pore-size distribution and irreducible water saturation which, when combined with density and neutron logs, enable reliable assessments of movable and irreducible fluid saturation.

Assessment of porosity is performed by combining density, neutron, and sonic logs. A more sophisticated assessment of porosity includes the systematic use of density, PEF, neutron, sonic, magnetic resonance (when available) and resistivity logs. It is recommended that the calculation of porosity be validated with core measurements, especially in cases when grain/matrix composition varies widely with depth.

3.4.a Pore volume of rock saturating fluids

In formation evaluation problems, it is often more convenient to calculate **water and hydrocarbon pore volumes**, given

$$\phi \cdot S_w,$$

and

$$\phi \cdot S_{hc},$$

respectively, where ϕ is porosity, S_w is water saturation, and S_{hc} is hydrocarbon saturation [= $(1 - S_w)$], as they are closer to actual fluid volumes.

3.5 Porosity is Over-Rated!

3.5.a The many facets of porosity

Even though porosity is widely used to quantify rock fluid storage, it is not always the most ideal property to describe the relationship between fluid storage and flow capacity of porous media. To begin, porosity is a dimensionless property which does not keep track of pore/throat size (unlike permeability!) because it is defined as the *ratio* of fluid volume over rock volume. Two rocks with different grain sizes can exhibit the same porosity but not the same permeability, for instance. The most appropriate description of the rock's pore space is the rock's **pore-size distribution**, designated by $p(r)$ and which is a density function given by

$$\phi = \int_0^\infty p(r)dr, \quad (3.5.1)$$

where r is pore radius (typically measured in micrometers) and ϕ is *total* porosity. Yet a more practical definition comes from the experimental observation that pore sizes are best described with a logarithmic scale, i.e.,

$$\phi = \int_{-\infty}^{\infty} p(\log r)d\log r, \quad (3.5.2)$$

where $\log r$ is logarithmic pore size.

The ideal situation occurs when $p(\log r) = \delta(\log r)$, where $\delta(\log r)$ is Dirac's delta function, i.e., when the rock has a *unimodal* pore size distribution. In most cases, rocks tend to exhibit quasi Gaussian distributions in the $\log r$ continuum, where the mean and standard deviation of the distribution become measures of the dominant pore size and of the variability of pore sizes, respectively (the larger the standard deviation the larger the degree of variability of pore sizes). Some rocks, especially carbonates, can exhibit bi- and tri-modal distributions in $\log r$, making it very difficult to quantify their pore connectivity, hence efficiency of fluid flow.

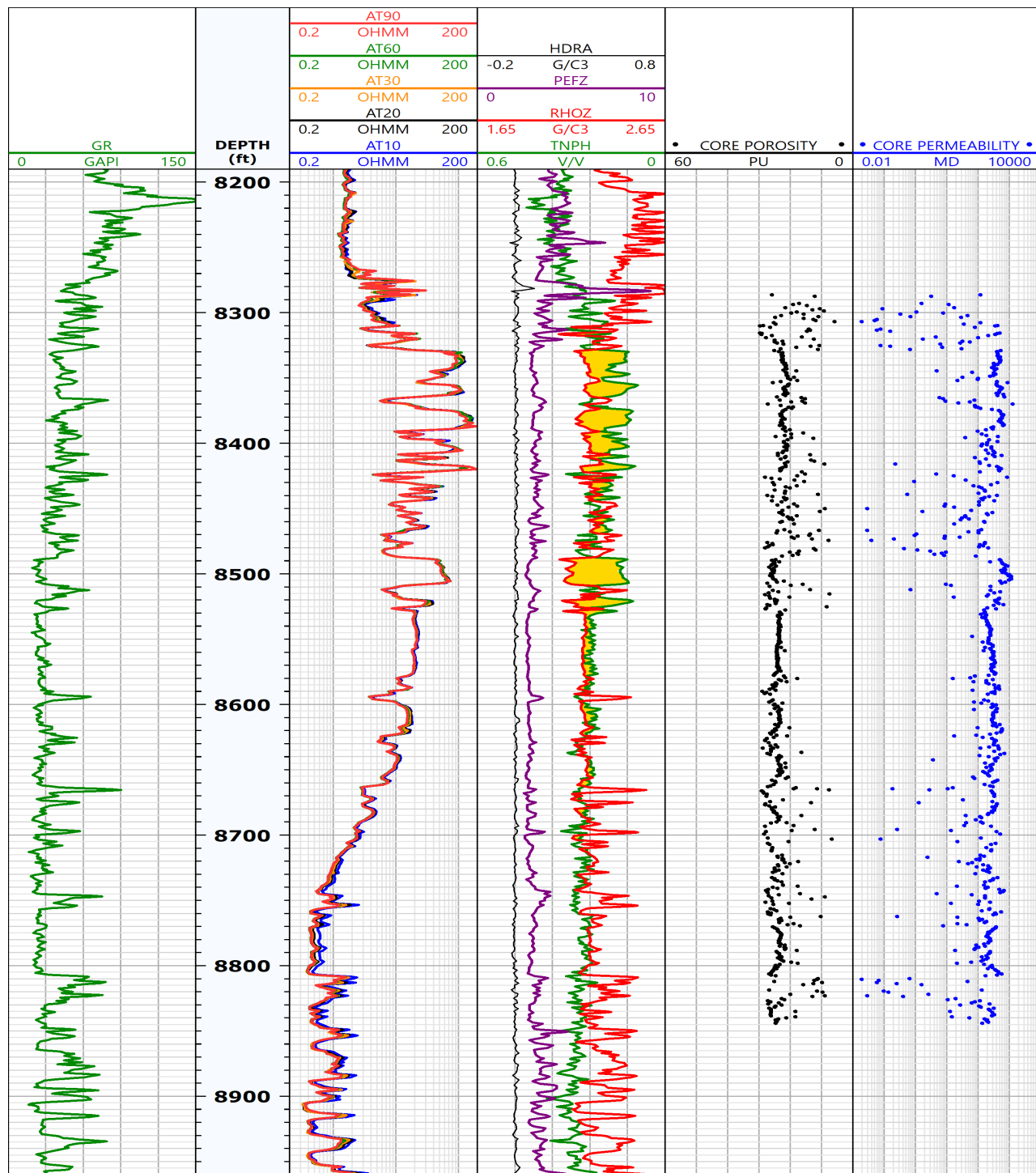


Figure 3.4.1: Example of well logs and core laboratory measurements acquired in a vertical well across an offshore turbidite sedimentary sequence (Andrew Field, North Sea). Track 1 is gamma ray. Track 2 is depth. Track 3 is electrical resistivity (multiple radial lengths of investigation). Track 4 is density, density correction, apparent neutron porosity, and photo-electric factor (PEF) logs. Track 5 is core porosity. Track 6 is core permeability (mD).

However, in general, it is more accurate to predict permeability from the rock's pore-size distribution than from its total porosity (even though, formally permeability is best described with the rock's *throat*-size distribution).

A related point of observation concerns the fact that in water-wet clastic rocks, grains are typically surrounded by a thin film of **immobile** water present because of electro-chemical forces of attraction between the polarity of water (electric dipolar behavior of water molecules) and the non-zero grain's near-surface electric field. The thickness of the thin film of water (hydrated layer) depends on the grain's surface-to-volume ratio and on the strength of the grain's near-surface electric field. An extreme case of large water-film thickness occurs on the surface of clay crystals because of both their large density of negative surface electric charge and their large surface-to-volume ratio. The immobile layer of water is part of the rock's total porosity *but does not contribute to fluid flow*. Consequently, under single-phase fluid flow conditions, the quantity

$$\phi \cdot (1 - S_{wi})$$

is a better descriptor of rock porosity available for the *displacement* of fluids, where S_{wi} is **irreducible water saturation**, defined as the additive component of immobile water saturation in the pore space.

In hydrocarbon-bearing and water-wet rocks, the relative displacement of the water and hydrocarbon phases becomes a function of both capillary pressure and the topology of the surface boundary between the two immiscible fluids. Depending on the cycle of fluid displacement (imbibition or drainage) a fraction of the non-wetting, hydrocarbon phase will remain immobile when the fluids are subject to a pressure gradient. In such a situation, the quantity

$$\phi \cdot (1 - S_{wi} - S_{hr})$$

becomes a better descriptor of the rock porosity available for the displacement of fluids, where S_{hr} is residual hydrocarbon saturation.

The above descriptors become somewhat more complicated when the rock exhibits variable throat-size distributions because every dominant throat size will exhibit its own fractions of irreducible water and residual hydrocarbon saturation. Even if the pore fraction $\phi \cdot (1 - S_{wi} - S_{hr})$ is available for fluid displacement, not all of it will effectively enable fluid displacement because of local variations of capillary pressure due to local variations of throat size (i.e., the applied fluid pressure gradient is not large enough to overcome capillary pressure forces within some of the throats). **Effective porosity**, ϕ_{eff} , is the term usually employed to designate the fraction of the rock's pore space which is available for fluid displacement. It follows that

$$\phi_{eff} \leq \phi(1 - S_{wi} - S_{hr}).$$

This discussion guides one to observe that two given rocks could have the same total porosity but that their corresponding flow pore volume, $\phi(1 - S_{wi} - S_{hr})$ (hence their effective porosity), could be drastically different if their average grain sizes were not the same. The rock with the smaller grains will, in general, exhibit the lowest flow pore volume. A common example of this situation are aeolian sandstones in which total porosity remains approximately constant but where grain sizes can vary across two or three orders of magnitude, hence giving rise to large variations of effective porosity and permeability. This is one of the reasons why, in general, porosity is over-rated and too simplistic (detached of size) of a variable to be useful to quantify the flow capacity of rocks.

Another complication arises in the reconciliation of porosity calculations from multiple well logs or from core measurements. Depending on the physics of the measurements, and their associated calculations, they will be sensitive to total porosity (e.g., bulk density, magnetic resonance, etc.) or to inter-connected porosity (e.g. electrical resistivity), while some other will emphasize the total porosity within the most rigid portion on the rock (e.g. sonic porosity). In the case of shaly sandstones, be them laminated, grain-coating, or structural in the corresponding shale topology, it is often necessary to differentiate between total and non-shale porosity. Similarly, depending on the physics of laboratory core measurements, the latter will yield values of total or inter-connected porosity. However, if porosity is to be used for calculation of permeability it is best to infer pore-size distributions and/or flow pore volumes to guide the assessment.

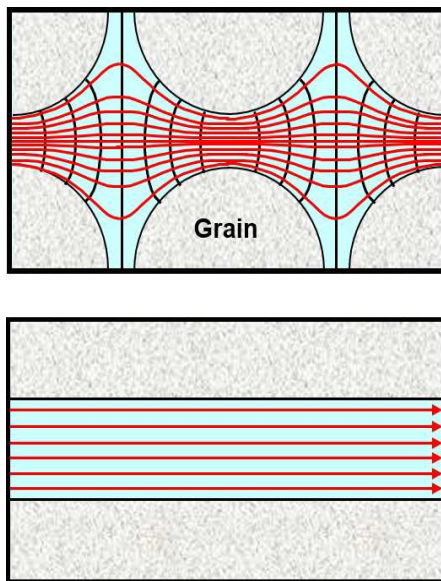


Figure 3.6.1: Cross-section of the spatial distribution of electric lines (red lines) across a pack of spherical grains (top) and a capillary tube of constant cylindrical section (bottom). Rock porosity is the same in the two cases; lines flow from left to right due to the DC (direct current) electrical potential enforced from left (high electrical potential) to right (low electrical potential). Black lines in the top figure are equipotential lines. The density of electric lines across the capillary tube is uniform while it increases and decreases across constrictions and pores, respectively, in the spherical grain pack. Electrical conduction in both cases is entirely due to body forces because of null electrical conduction on the surface of the grains (diagram courtesy of David Herrick).

3.6 Body and Surface Phenomena in Porous Media

The study of physics phenomena taking place in porous media invariably invokes geometrical properties of both solid and fluid components, as well as their spatial continuity and variability. Depending on the physical phenomenon under consideration, e.g., fluid transport, conduction of electricity, propagation of elastic or electromagnetic waves, heat conduction, etc., the effective properties of porous media will depend on either body or surface effects.

For the case of low-frequency electrical conduction in porous media, and assuming that (1) grains are electrically insulating and (2) the pore space is entirely filled with an electrically conductive fluid, the corresponding macroscopic electrical conductivity/resistivity will depend on both the electrical conductivity of the saturating fluid and porosity (Archie's equation), i.e., it does not depend on pore or throat sizes. The latter behavior arises because low-frequency electrical conduction phenomena are insensitive to surface conduction (i.e., electrical conduction taking place near or on the surface of grains), and are solely governed by the continuity and density of electric lines spanning the pore space. In other words, under the assumptions stated above, the electrical conduction of porous media involves only body forces and consequently is not pore/throat-size dependent. The latter condition is illustrated in Fig. 3.6.1 by comparing the spatial distribution of electric lines across rocks with the same porosity constituted by a spherical grain pack and a single cylindrical capillary tube. In the case of the grain pack, the available pore space does not equally contribute to the rock's electrical conductivity, by contrast with the capillary tube, where the available pore space contributes equally to the rock's macroscopic electrical conduction.

The porosity exponent included in Archie's equation, m , is larger or equal to 1, on account of the fact not the entire pore space contributes equally to the macroscopic electrical conduction of porous media. When the porous medium is a collection of straight tubes, $m = 1$ regardless of tube radius or the variability of

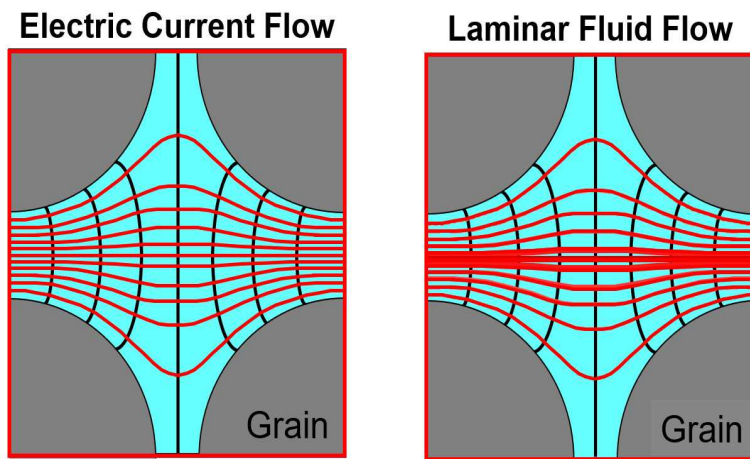


Figure 3.6.2: Cross-section of the spatial distribution of DC electric (left panel) and laminar flow (right panel) lines (red lines) across a pack of spherical grains; lines flow from left to right. Black lines are equipotential lines. The density of flow lines is higher than the density of electric lines at the center of pore/throats because the velocity of flow is null at grain boundaries (no-slip condition) and maximum at the center of throats/pores (diagram courtesy of David Herrick).

tube radii, i.e., the entire pore space contributes equally to the medium's macroscopic electrical conductivity. However, if the tubes are no longer straight and/or their cross-section is not constant, m will be larger than 1, on account of the fact that the density of electric conduction lines will no longer be constant along each tube. A porosity exponent, m , larger than 1 arises because not all the available pore space contributes equally to the macroscopic electrical conductivity/resistivity of the porous medium ($\phi^m < \phi$ when $m > 1$ because $\phi \leq 1$).

In the paradigm of fluid flow in porous media, on the other hand, permeability will depend on the radii of pore throats because the interstitial velocity of fluid across throats is not uniform: on the surface of grains the velocity will be zero because of friction forces (no-slip boundary condition) and will increase to a maximum value at the center of the throat. Capillary pressure and relative permeability are properties of two-phase immiscible fluid flow in porous media which are also governed by surface forces between the solid and the adjacent fluid (wetting fluid) and between the two immiscible fluids (wetting and non-wetting fluids). Any physical phenomenon in porous media that is partially or totally governed by surface forces will cause the corresponding effective macroscopic property to be pore- or throat-size dependent because of its relationship to specific surface (i.e., surface-to-volume ratio).

Figure 3.6.2 compares the spatial distribution of DC electric and laminar-flow lines across a pack of spherical grains. Because of the no-slip flow condition at grain boundaries, the density of flow lines is higher than the density of electric lines at the center of pores/throats.

3.7 Basic Model of a Bundle of Capillary Tubes

Under the assumption of single-phase laminar flow regime, the simplest of Hagen-Poiseuille's equations describes the fluid velocity across a straight capillary tube of circular cross-section, i.e.,

$$v(r) = -\frac{R^2}{4\mu} \left(1 - \frac{r^2}{R^2}\right) \frac{dP}{dx},$$

where v is mass velocity, r is radial location within the circular cross-section measured from the axis of the capillary tube, R is the radius of the capillary tube, μ is the dynamic fluid viscosity, x is axial location along the tube, and dP/dx is the axial pressure gradient (Bird et al., 2002). The above equation disregards tube-end

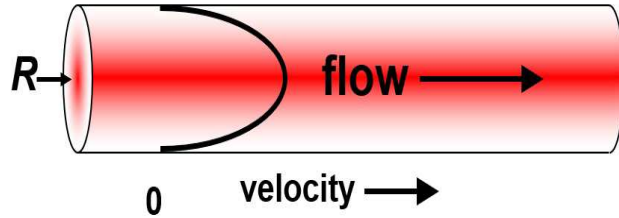


Figure 3.7.1: Velocity of single-phase flow across a straight capillary tube of constant circular cross-section of radius R assuming a viscous fluid. The radial distribution of fluid velocity along the tube's circular cross section is illustrated with red shading and exhibits a parabolic shape with maximum value at the tube's axis, decreasing to zero at the tube's boundary (diagram courtesy of David Herrick).

effects and yields $v = 0$ when $r = R$, i.e., on the surface of the tube (no-slip condition). It then follows that the maximum fluid velocity, v_{max} , takes place at the center of the capillary tube ($r = R$), and is equal to

$$v_{max} = -\frac{R^2}{4\mu} \frac{dP}{dx}.$$

Based on the above equations, the radial variation of fluid velocity from the center of the tube to the tube's boundary exhibits the parabolic shape described in Figure 3.7.1.

The rate of mass flow across the tube's circular cross section, Q , is then given by

$$Q = \int_0^R v(r) 2\pi r dr = -\frac{\pi R^2}{2\mu} \int_0^R \left(r - \frac{r^3}{R^2} \right) \frac{dP}{dx} dr = -\frac{\pi R^4}{8\mu} \frac{dP}{dx}. \quad (3.7.1)$$

On the other hand, Darcy's linear constitutive equation for flow across porous media is given by

$$v = -\frac{k}{\mu} \frac{dP}{dx},$$

where k is permeability (Hubbert, 1956). For a porous medium of cross-sectional area equal to A the corresponding flow rate is given by

$$Q = -\frac{k}{\mu} A \frac{dP}{dx}.$$

When the latter equation is specialized to a straight capillary tube of radius R , it follows that

$$\phi = \frac{\pi R^2}{A} \Rightarrow A = \frac{\pi R^2}{\phi},$$

where ϕ is porosity, whereby

$$Q = -\frac{k}{\mu} \frac{\pi R^2}{\phi} \frac{dP}{dx}. \quad (3.7.2)$$

By equating 3.7.1 and 3.7.2 we obtain

$$k = \frac{\phi}{8} R^2,$$

which remains valid for a single straight capillary tube of cylindrical cross-section and emphasizes the important fact that permeability is size-dependent.

For the case of a bundle of straight capillary tubes of equal cross-section, the above expression can be generalized to

$$k \approx \phi R^2 \Rightarrow \frac{k}{\phi} \approx R^2 \Rightarrow R \approx \sqrt{\frac{k}{\phi}}, \quad (3.7.3)$$

while the corresponding interstitial flow velocity is given by

$$v \approx -\frac{\phi R^2}{\mu} \frac{dP}{dx}.$$

The quantity k/ϕ is an ubiquitous property of porous media that arises in some of the equations used to describe capillary pressure (Leverett, 1941) and relative permeability, and is widely used for rock classification; in that expression, ϕ relates to storage capacity, while k relates to flow capacity. Rocks with similar values of k/ϕ will exhibit similar average throat radii where porosity will decrease only with fewer capillary tubes. In practice, however, the distribution of throat radii in a rock will not be a Dirac δ function but rather a wider function with a mean and a non-negligible standard deviation, or even exhibit a multi-modal distribution, such is commonly the case in carbonate rocks. Realistic cases of approximate capillary tubes in rocks include non-straight tubes, tubes with variable cross-sectional area and shape, and interconnected tubes, among others.

3.8 Concept of Transport Efficiency of Porous Media

Because of the interplay between body and surface forces taking place in the transport of fluid through porous media, not all the available fluid (i.e., the pore volume of fluid) contributes equally to the effective flow rate once a pressure gradient is enforced across it. This behavior is due to the fact that the interstitial fluid velocity in porous media is in general not constant: the velocity is largest at pore constrictions and slower within relatively large pores (Figure 3.6.2). There might also be abnormally tortuous fluid paths or partially occluded pores and/or throats wherein the interstitial velocity is negligible and where the available fluid will “stagnate.”

To account for the latter fluid stagnation effects and for practical purposes, the *transport efficiency* of porous media is typically defined using as reference a bundle of parallel capillary tubes with equal cylindrical cross-section and such that the porosity of the construct with the bundle of capillary tubes is equal to the porosity of the original porous medium. For instance, the electrical conduction efficiency of porous media, E_σ , saturated with electrically conductive water is given by

$$E_\sigma = \frac{\sigma_w \phi^m}{\sigma_w \phi} = \phi^{m-1},$$

where ϕ is porosity and σ_w is the electrical conductivity of water. Clearly, $E_\sigma \leq 1$, and, as expected, the larger the value of Archie's porosity exponent, m the lower the electrical efficiency of porous media.

Figure 3.8.1 illustrates the concept of fluid transport efficiency of porous media, where the x axis is porosity and the y axis is flow efficiency (varying between 0 and 1, where 1 designates maximum efficiency). For a given porosity, the maximum electrical and fluid-transport efficiency occurs when the porous medium consist of a bundle of straight and equal cross-section capillary tubes. The efficiency gradually decreases as the capillary tubes exhibit tortuous paths, non-constant cross-sections, and non-connected segments.

The corresponding single-phase fluid transport efficiency, E_f , of porous media is then calculated from the ratio of the flow rates given by equations 3.7.2 and 3.7.1, i.e.,

$$E_f = \frac{-\frac{k}{\mu} \frac{\pi R^2}{\phi} \frac{dP}{dx}}{-\frac{\pi R^4}{8\mu} \frac{dP}{dx}} = \frac{8}{R^2} \frac{k}{\phi}.$$

To further simplify the latter equation, we note that $\phi = \pi R^2/A$, where A is the cross-sectional area of the rock sample, which implies that $R^2 = A\phi/\pi$, whereupon

$$E_f = \frac{8\pi}{A} \frac{k}{\phi^2}.$$

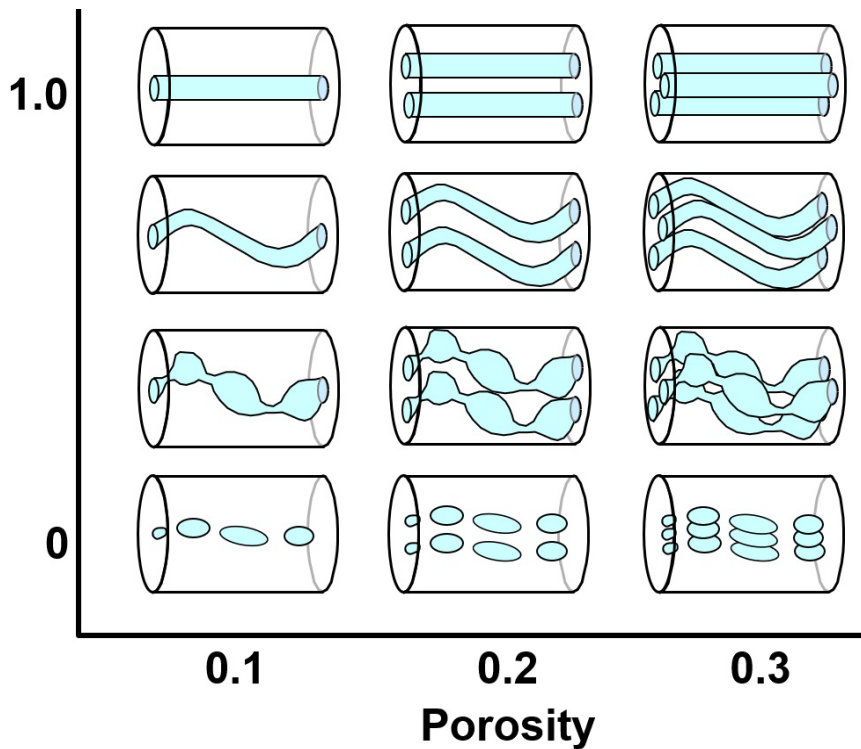


Figure 3.8.1: Graphical description of the concept of fluid *transport efficiency* of porous media. The x and y axes describe porosity and transport efficiency, respectively, both varying between 0 and 1. For a given porosity, the most efficient porous media are those constructed with straight capillary tubes of equal-radius circular cross-sections. Transport efficiency decreases as the capillary tubes become tortuous, exhibit non-constant cross-sections, and include non-connected segments (diagram courtesy of David Herrick).

For instance, for a rock with $\phi=25\%$, $k=0.5D$ ($1D = 9.86923310^{-9} \text{ cm}^2$), and $A=9 \text{ cm}^2$, one has $E_f=2.2048\times10^{-7}$, indicating that the pore space in this 0.5D rock is approximately 22 million times less hydraulically efficient than a medium with the same porosity but constructed with straight capillary tubes!

3.9 Calculation of Permeability

3.9.a Total porosity

It is important to note that practically all the methods and equations used to calculate transport properties of rocks invoke *total porosity*, rather than a specific fraction of the available rock porosity (e.g., the fraction of porosity containing non-movable fluid). The use of total rock porosity is necessary to explicitly honor material balance in the calculation of properties, regardless of the laboratory procedure used to measure the same properties, and such the calculated properties are inter- and self-consistent (e.g., permeability, capillary pressure, and relative permeability).

3.9.b Common methods used to calculate rock permeability

The Kozeny-Carman equation is one of the most popular ways to calculate the permeability of clastic rocks, given by

$$k = a D^2 \frac{\phi^3}{(1 - \phi^2)},$$

where a is a constant, D is median grain diameter in micrometers, ϕ is porosity, and k is given in millidarcies (mD) (Kruczek, 2015). It was derived assuming that the fluid-transport properties of the clastic rock can be approximated with a bundle of capillary tubes. The applicability of the equation depends on availability of grain-size measurements.

A more widely used method to calculate permeability in formation evaluation stems from the use of the Timur-Tixier formula, given by

$$k = \alpha \phi^\beta \left(\frac{1 - S_{wi}}{S_{wi}} \right)^\gamma, \quad (3.9.1)$$

where α , β , and γ are constant values for rocks within the same storage/fluid-transport class. This formula emphasizes the role played by irreducible water saturation (hence effective porosity) in permeability. The larger irreducible water saturation, the lower the rock's permeability; conversely, the lower irreducible water saturation, the larger permeability. In a way, the fraction

$$\frac{1 - S_{wi}}{S_{wi}}$$

included in the above equation represents an adjustment of the total porosity to account for only the mobile component of porosity in the calculation of permeability. In shales, for instance, $S_{wi} \approx 1$, whereby $k \approx 0$.

Figure 3.4.1 is an example combination of well logs and core laboratory measurements of porosity and permeability. This is an offshore vertical well penetrating a turbidite sedimentary sequence in the North Sea (Andrew field). While porosity is relatively constant across sandstones, permeability exhibits significant variations (plotting scale is logarithmic) because of the wide variations of irreducible water saturation in eq. (3.9.1) due to grain-size variations and presence of laminated shale.

3.10 Two-Phase Flow Properties

The fluid transport properties of rocks depend on whether one or more fluids are flowing through them. For the case of immiscible fluids, capillary pressure and relative permeability (both saturation dependent) are needed to describe the relative differences in the velocity of each of the fluid phases. Their definition, measurement, and/or calculation is given in terms of the fluid phase wetting the solid components of the rock. In the case of water-wet rocks, water saturation (S_w) is used to describe saturation-dependent capillary pressure and relative permeability. Both properties are governed by surface forces: (1) surface forces (friction forces) between the solid and fluid components of the rocks and (2) surface forces (interfacial tension forces) between the immiscible fluid phases themselves. Additionally, both capillary pressure and relative permeability depend on whether the immiscible fluid moves through the rocks by way of imbibition or drainage.

The flow of immiscible fluids through porous media is governed by both capillary and viscous drag forces, where the interplay or dominance between the two forces is a function of the effective throat radius.

3.10.a Capillary pressure

Capillary pressure is the result of the interfacial tension between two immiscible fluids stored or flowing through a finite-size tube (also known as capillary tube). The equilibrium condition is to minimize the surface area of the interfacial tension. Capillary pressure is typically measured as a function of the saturation of the fluid phase which wets the solid surface of the rock pores/throats.

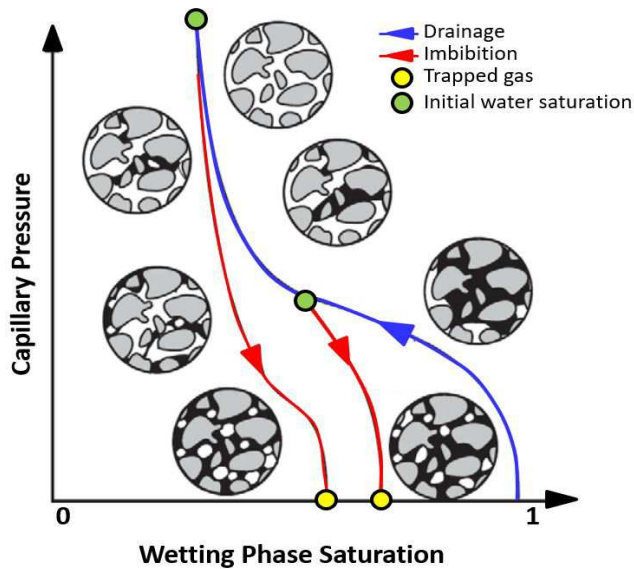


Figure 3.10.1: Schematic of the gas-water capillary pressure of a water-wet rock as function of wetting-phase saturation for both imbibition and drainage cycles of fluid displacement (graphic courtesy of Germán Merletti).

Figure 3.10.1 shows a schematic of the general behavior of capillary pressure of gas-saturated rocks as a function of wetting-phase saturation (water saturation in this case) for both imbibition and drainage cycles of fluid displacement.

3.10.b Relative permeability

Relative permeability quantifies the relative differences of velocity between two immiscible fluids flowing through porous rocks under quasi-stationary conditions. Those differences are governed by the difference in saturation between the two phases, their interfacial tension, the wetting phase, and the geometrical properties of the rock's pore space. By definition, relative permeability varies between 0 and 1, because it represents a dimensionless reduction factor with respect to the rock's single-phase permeability.

3.11 All Petrophysical Properties are Inter-Related!

It is exceptionally important to remark that in practice all petrophysical properties of a given rock, be them associated with storage or fluid flow, are inter-related. In other words, these properties should never be considered independent from each other or in isolation. For instance, irreducible water saturation impacts effective porosity, permeability, capillary pressure and relative permeability. Likewise, an increase of capillary pressure causes a decrease of permeability. Following important laboratory studies of rock properties, Leverett found that the ratio k/ϕ could be used to normalize the saturation-dependent capillary pressure of rocks belonging to the same “fabric” class (Leverett, 1941).

3.11.a The flow of fluids in rocks is similar to that of a shower head!

Conceptually, the efficiency of fluid flow taking place in rocks can be considered analogous to that of a shower head. Even though this is a rather simplistic representation, it provides valuable physical insights to understanding the co-dependency of multiple petrophysical properties and their combined effects on flow properties. Modern shower heads include a distribution of orifices with various diameters. The diameter of one such orifice



Figure 3.11.1: The transport of fluids in rocks is in some ways analogous to the passage of water through a shower head. Hole sizes in a shower head are analogous to throat sizes in rocks. The efficiency of water flow through a shower head is dictated by the velocity and volume of water per unit time transported through the set holes, both of which depend on the applied pressure gradient, the size of holes, and the distribution of hole sizes. Assuming that the total cross section of the shower holes is the same for all the shower heads shown (equal porosity), the most efficient shower head is the one that has the largest and most uniform hole sizes.

is akin to the diameter of a capillary tube. All orifices are subject to the same pressure gradient. The normalized sum of diameters is equal to porosity. For an idealized set of rocks whose porosity is constant, the most efficient rocks (efficiency, of course, in the context of fluid flow) in the set are those whose orifice diameter is constant and the largest possible (the velocity of flow is the same across all the shower orifices). The velocity of flow will not be uniform across all the orifices when the orifice diameter is not constant (i.e., the interstitial velocity will exhibit dispersion) and this will decrease the efficiency of flow. One can conclude that porosity and permeability are not the only variables that are needed to reliably describe the efficiency of flow of rocks, even in the presence of only one fluid phase. Figure 3.11.1 shows 4 different types of commercial shower heads with different distributions of hole size.

In the case of two-phase fluid flow, the velocity across each orifice will be further “slowed down” by capillary forces; irreducible water saturation will increase across the smallest orifices. Because of this, differences in velocity across the orifices will be enhanced in the case of two-phase fluid flow, given rise non-piston like displacement of the original fluid phase(s) by the invading fluid phase. In turn, this will decrease the recovery factor.

3.12 Size Matters!

The calculation and measurement of rock properties, be them petrophysical, mechanical, or of any other physical nature (e.g., electrical resistivity and P- and S-wave velocities), typically makes the assumption that the rock sample remains identical regardless of size. Seldom, however, do rocks remain identical over large volumes of investigation (see, for instance Fig. 3.1.1). While sample size is a typical constraint in most

specialized systems used for laboratory analysis of rocks (e.g., laboratory samples are typically cylindrical, ranging in diameter anywhere from a fraction of an inch to a couple of inches), thin sections, SEM's, whole-core samples, and well logs do not probe the rock's spatial variability with the same standardized volume. Furthermore, when investigating rock properties between wells, the volume of investigation of measurements such as pressure-transient testing, tracer arrival times, and cross-well seismic tomography, for instance, can be of the order of the existing separation between wells. Fluid-flow barriers and abnormal flow-enhancing zones which were not sampled/detected by the measurements may exist between wells which can drastically dominate inter-well connectivity, production/pressure decline, seismic travel times, and amplitudes, electrical resistivity, etc.

The acronym **REV**, or *Representative Elementary Volume* is typically used to designate the volume of the rock sampled (or investigated) by a given measurement. Depending on the rock's spatial variability and the associated REV of the measurement, the corresponding calculated rock property may or may not remain constant. For instance, the estimated/measured permeability of a rock will change with respect to the REV of the measurement when the rock exhibits grain-size laminations or fractures which were not properly captured in the rock sample because of its location, size, and orientation. Being a direction-dependent flow property, permeability will also exhibit different degrees of anisotropy depending on the size and orientation of the rock sample. In spatially variable rocks, it is found that the corresponding rock property (e.g., porosity, permeability, electrical resistivity, and P- and S-wave velocities) will rapidly change as the corresponding REV decreases, while it tends to reach a constant value as the REV increases. Figure 3.12.1 shows the typical behavior of rock petrophysical property vs. REV for unconventional rocks. The figure shows a collage of rock images anywhere from pore-scale FIB-SEM (Focused Ion Beam Scanning Electron Microscopy) SEM, and BIB-SEM (Broad Ion Beam Scanning Electron Microscopy) images to thin sections, micrographs, micro-CT (Computerized Tomography) scans, and whole-core photographs, emphasizing the large variability of rock properties with scale. An insert in the same figure illustrates the expected behavior a generic petrophysical property as a function of sample volume/surface, identifying the location of the various rock images. While the oscillatory behavior of the plot decreased with an increase in volume/surface, the expected asymptotic behavior still depends on the rock's variability (in the case of permeability, for instance, the asymptotic behavior of the plot will be determined by the rock's intrinsic large-scale anisotropy).

Figure 3.12.1 also emphasizes that the calculated/measured petrophysical property needs to be associated with the formation-evaluation objective, whether it is to predict flow behavior at the pore scale, at the scale of whole core or core samples, at the scale of well logs, or at the scale of well-to-well separations. Therefore, the volume of investigation/measurement needs to capture all the relevant rock properties that influence fluid flow behavior at the pre-specified scale of interest by taking into account the relevant rock spatial variability at that scale. It is important to know *ab initio* what that fundamental spatial scale is in a given formation evaluation project so that all measurements, analyses, and calculations thereof are geared toward satisfying the ultimate objective, winnowing those details which have no impact in the final estimations. The term "upscaling" is usually invoked to designate the process whereby high-resolution details about rock properties are converted (i.e., *averaged*) into corresponding larger-scale properties for purposes as diverse as computer modeling under memory and CPU time constraints, comparison of measurements originating from diverse physical principles, reconciliation of rock physics models, etc.

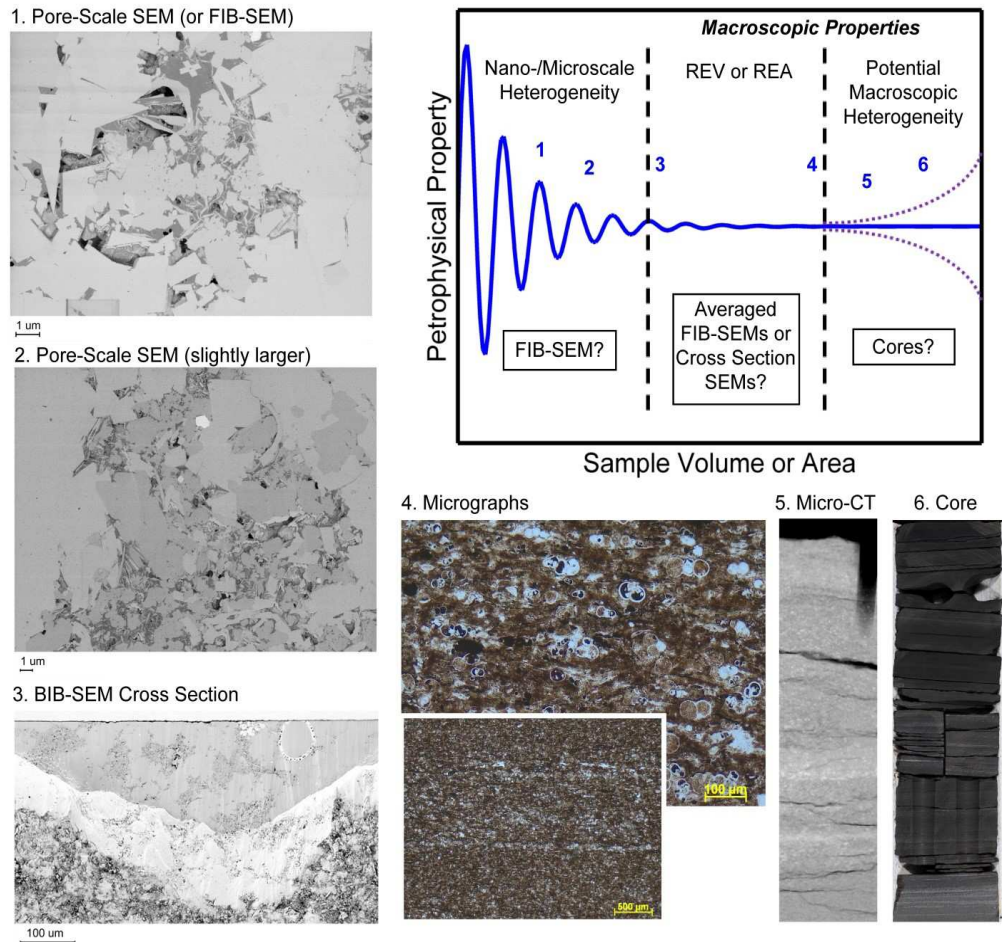


Figure 3.12.1: Example of spatial scales of analysis, measurement, and quantification of petrophysical properties. The collage of images/photographs illustrates the paradigm a rock sample from an unconventional formation, and emphasizes how the measured/calculated petrophysical property is intimately related to the representative elementary volume (REV). REV diagram adapted from Bear (1993) and VandenBygaart & Protz (1999). Micro-CT images are 11 μm /voxel and the width of the presented image is approximately 11 mm. The core sample is on the order of centimeters (adapted from Figure 10 of Kelly et al. (2016)).

Chapter 4

The Fabric of a Well Log

... You can know the name of a bird in all the languages of the world, but when you're finished, you'll know absolutely nothing whatever about the bird... So let's look at the bird and see what it's doing that's what counts. I learned very early the difference between knowing the name of something and knowing something...

—Richard P. Feynman, *What Do You Care What Other People Think?: Further Adventures of a Curious Character.*

As employed in geological studies, the term *fabric* is typically used to describe the geometrical/spatial distribution of a rock's constitutive elements. Specifically, the term describes the spatial and geometrical configuration of a rock's solid and fluid constituents, including its pore space. In close analogy and affectionate parabole, the *fabric of a well log* concerns the origin, format, and graphical display of the multiple components of a well log. Such is the conventional way to report the borehole geophysical measurements acquired during or after drilling a well.

4.1 Introduction

Well-log descriptions are commonly given/reported as long printouts as a function of depth (or distance along the well trajectory). Modern well-log descriptions are provided by logging companies as digital files organized in a systematic manner to include borehole environmental variables and measurements. The standard digital format is referred to as **LAS**, or Log-ASCII Standard, while some logging companies make use of more descriptive and general digital binary formats such as **LIS** or **DLIS** (Schlumberger). Log displays can also be given in digital format for efficient exchange and distribution (e.g. Schlumberger's **PDS** format). Digital formats of log measurements are nowadays widely accepted by oil companies for easy access and distribution through internal data bases.

The functional structure of a well-log (either digital or graphical) consists of the following components:

- Header,
- Description of data acquisition and processing conventions,
- Description of the tool string used to log the well and its components,
- Additional operator's comments,
- Log displays and/or digital measurements using tracks,
- Repeat runs (if any),

- Report of tool calibrations,
- Report of quality control of measurements,
- Nomenclature of measurements, and
- Record of implemented borehole environmental corrections.

4.2 The Header of a Well Log

The header of a well log contains an itemized description of geographical, procedural, and borehole environmental variables associated with the acquisition of well logs. Descriptions include:

- American Petroleum Institute (API) number, name of field, date of acquisition, geographical location, oil company, well-logging company, etc.
- Type of mud (oil-base, water-base, or synthetic), mud weight, mud viscosity, mud salinity, electrical resistivity of mud, electrical resistivity of mud filtrate, etc.,
- Type of lithology and type of fluid assumed for the display of density and neutron porosity logs,
- Reference depth for drilling, casing, and logging operations, vertical location of Kelly bushing (KB), ground level (GL), Derrick floor (DF), etc.,
- Surface and bottom-hole temperature, and
- Special remarks or comments included by the field engineer who acquired the measurements.

Figure 4.2.1 shows an example of log header for modern triple-combo well logs acquired in a vertical well reaching the deepwater Gulf of Mexico. The well was drilled with oil-base mud and the maximum depth reached below the sea floor was over 18,000 ft with a recorded bottom-hole temperature of 228 °F. On the other hand, Figure 4.2.2 shows the log header for an onshore well which was drilled with water-base mud; the log header describes measurements of electrical resistivity performed on drilling-mud components.

The “Bronze Rule” of well logging is *a well-log is always associated with a header*. A strong suggestion in well logging is that one should never interpret well logs without having looked at the log header. Such a simple precaution will guard well-log practitioners against the application of non-suitable petrophysical models to the interpretation of measurements.

4.3 Operational Classification of Well Logs

Well logs can be acquired during drilling operation, after drilling but before setting casing (or completions), or after setting casing and cement. The standard nomenclature is as follows:

- **Mud logging:** It comprises geological, petrological, and fluid descriptions of rock cuttings retrieved uphole from the shale shaker at the end of the mud flow line. Time of drilling and rate of penetration (ROP) are transformed into measured depth to properly display the description of rock cuttings as a function of location in the well trajectory. Fluid descriptions are performed by either visual inspection or with a chromatographic unit. The depth uncertainty of rock cuttings is typically larger than 5 m.
- **Measurements-while-drilling (MWD):** This designation comprises continuous drilling-specific measurements such as rate of penetration (ROP), weight-on-bit, time of drilling, torque motion, torque-on-bit, mud weight, etc. Some of these measurements are used to assess rock mechanical properties and pore pressure, for instance.



Company: BP Exploration & Production, Inc.

Well: OCS-G 32306 001 ST00BP01
 Field: Mississippi Canyon 252
 Waters: Gulf of Mexico State: Louisiana

LOCATION			
Gulf of Mexico	Mississippi Canyon 252		
Field:	Surf Loc. X=1202798.33 & Y=1043		
Location:	OCS G 32306 001 ST00BP01		
Waters:	API Serial No.	Latitude:	Longitude:
Field:	608174118901	28 44' 17.304" N	88 21' 57.403" W
Location:		Rig:	DWHorizon
Well:			
Company:			
Logging Data			
Logging Date	10-Apr-2010		
Run Number	R1D1		
Depth Driller	18360 ft		
Schlumberger Depth	18280 ft		
Bottom Log Interval	18270 ft		
Top Log Interval	17157 ft		
Casing Driller Size @ Depth	9.875 in	@ 17165 ft	@
Casing Schlumberger	17157 ft		
Bit Size	9.875 in		
Type Fluid In Hole	Rheoliant - Synthetic Based Mud		
MUD	Density	14 lbm/gal	103 s
	Viscosity		
	Fluid Loss	0 cm ³	0
	PH		
	Source Of Sample	N/A	
	RM @ Measured Temperature		@
	RMF @ Measured Temperature		@
	RMC @ Measured Temperature		@
	Source RMF	RMC	N/A
	RM @ MRT	RMF @ MRT	@ 225 @ 228
	Maximum Recorded Temperatures	228 degF	228
	Circulation Stopped	Time	10-Apr-2010 5:00
	Logger On Bottom	Time	11-Apr-2010 2:19
	Unit Number	Location	2082 Larose, Louisiana
	Recorded By	Victor Emmanuel / Ryan O'Toole	
	Witnessed By	Gaina Skripnikova / Stuart Lacy	

Figure 4.2.1: Example of well-log header for a well that was drilled with oil-base mud in the deepwater Gulf of Mexico. The header indicates that the well was logged with a modern triple-combo set of measurements (Schlumberger). Note the maximum depth and temperature reached at the bottom of the well.

- **Logging-while-drilling (LWD):** It comprises log measurements acquired concomitantly with the drilling process some distance away from the drill bit. This includes images of several physical properties acquired as the drill bit rotates around the perimeter of the wellbore. LWD measurements can also be acquired when the drill pipe and bit are being brought back to the surface for measurement verification and time-lapse analysis (e.g., mud-filtrate invasion), for instance.
- **Open-hole logging (wireline logging):** It comprises well logs acquired after the drilling process has been completed but before the setting of cement and steel casing (or of any other completion process).
- **Production logging and behind-casing logging:** It comprises well logs acquired behind casing or during fluid production. The main objective of these measurements is to monitor time lapse variations of fluid and rock properties after the onset of production, e.g. types of flowing fluids inside the tubing, fluid speed, water cut, carbon/oxygen ratios, thermal neutron capture cross-section (Sigma), etc.

Company: BURK ROYALTY CO. LTD							
Well: JETT #1		State: TEXAS					
Field: Wildcat		Rig Name: BASIN 103					
County: Madison		Date: 09-Nov-2014					
Service Company: Halliburton							
ACRt Tool, Spectral Density Tool, Compensated Spectral Natural Gamma Ray Tool.							
Location	Surf Loc: X= xxx xxxx & Y = xxx xxxx		Elev:	K.B. 174 ft G.L. 148 ft D.F. 173 ft			
	Permanent Datum: G.L. Log Measured From: K.B. Drilling Measured From: K.B.		Elev: 148 ft 0 ft above Permanent Datum				
	Job Number 901796673	API Serial No. 42313312290000	Latitude xxx xxxx xx N	Longitude xxx xxxx xx W			
				Rig Basin 103			
	Run Number						
	R1D1						
	Top Log Interval						
	2559.5 ft						
	Bottom Log Interval						
	10317.0 ft						
	Casing Driller Size @ Depth						
	9.625 in @ 2805 ft						
	Bit Size						
	8.75 in						
	Type of Fluid in Hole						
	WTR						
MUD	Density		Viscosity	9.4 ppg 57 s/qt			
	Fluid Loss		pH	N/A 9.9			
	Source of Sample						
	MUD TANK						
	RM @ Measured Temperature						
	0.29 OHMM @ 225 degF						
	RMF @ Measured Temperature						
	0.95 OHMM @ 57 degF						
	RMC @ Measured Temperature						
	1.31 OHMM @ 57 degF						
	Maximum Recorded Temperature						
	270 degF						
	Circulation Stopped	Time	09-Nov-14	12:55			
	Logger On Bottom	Time	09-Nov-14	12:55			
	Unit Number	Location	10760375	Kilgore, TX			
	Witnessed By		R. Hyde				
	Recorded By		W. Warren				

Figure 4.2.2: Example of well-log header for a well that was drilled with water-base mud. The header indicates that the well is located onshore and was logged with a modern triple-combo set of measurements (Halliburton). Note the (1) maximum depth and temperature reached at the bottom of the well, and (2) measurements of electrical resistivity of drilling mud components.

Figure 4.3.1 is an example of mud log, which displays (1) descriptions of rock cuttings (predominantly geological descriptions) acquired at the surface on the shale shaker while the drilling process is taking place, (2) chromatographic and chemical measurements performed on fluid samples taken at the surface from the drilling-mud line, and (3) basic drilling measurements such as rate of penetration. Rock cuttings and chromatographic/chemical measurements are transformed from time-of-drilling to depth using the drilling rate of penetration. Chromatographic measurements differentiate between biogenic and thermogenic gas, among other things. The uncertainty of depth location for mud logs can be anywhere from a few feet to tens of feet depending on several factors such as variations in the density of rock cuttings, angle of well deviation, flow rate of mud, etc. Even though, in many cases, mud logs lack accuracy for petrophysical evaluations, they provide context and ground truth to verify the calculations performed with well logs and core measurements.

The interpretation procedures described in these notes are mainly concerned with wireline and LWD measurements. Figure 4.3.2 shows an example of LWD resistivity tool (toroidal antenna used as transmitter) where the transmitters, receivers, electronics, and telemetry are located within the thickness of the drill pipe while drilling mud is flowing toward the drill bit. The LWD measurement acquisition environment presents multiple

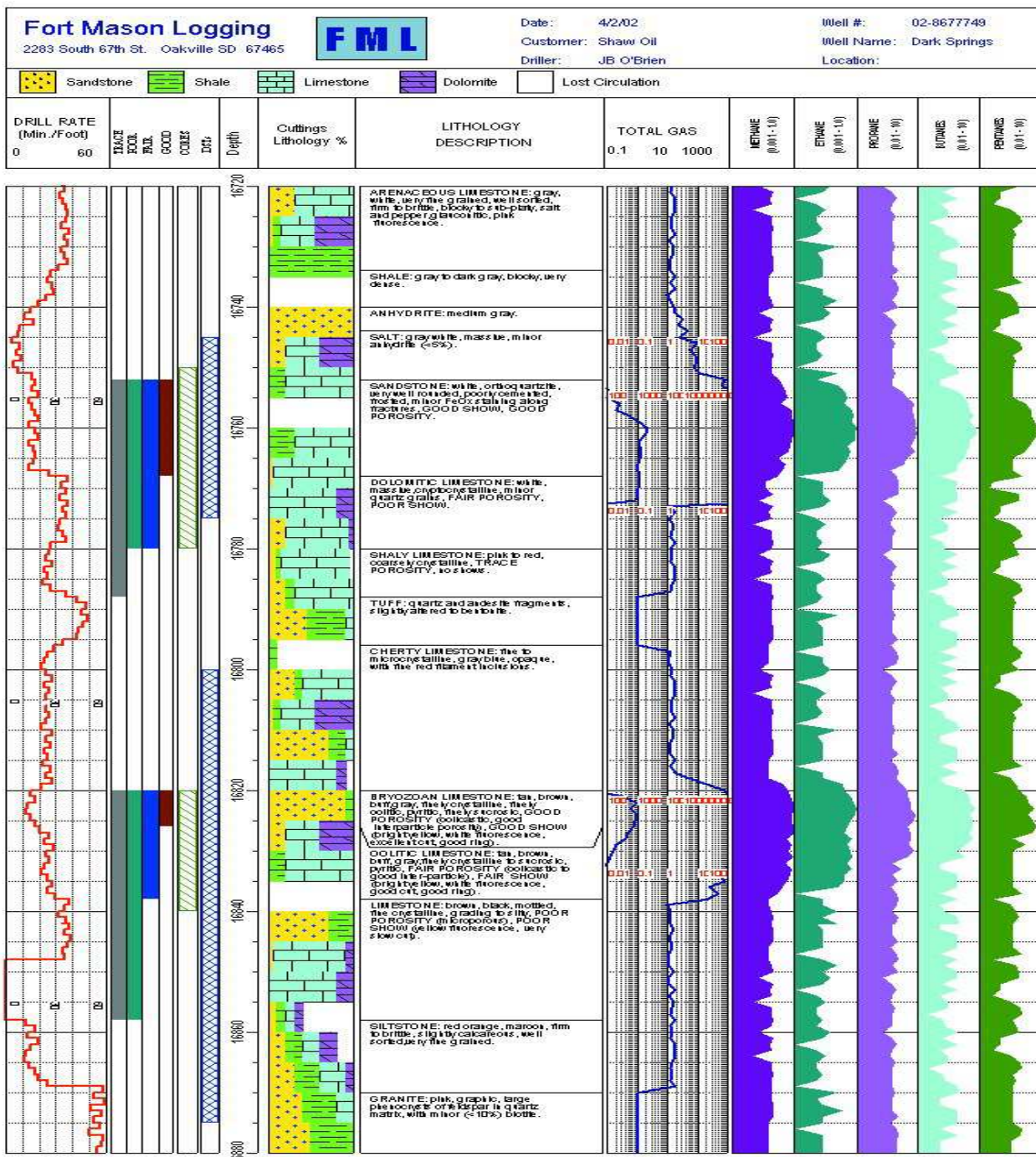


Figure 4.3.1: Example of mud log comprising rock cuttings descriptions and chromatographic-chemical analyses performed on fluid samples acquired at the surface from the drilling-mud line. The mud log also includes basic drilling measurements which are used to transform the rock cuttings and mud-line measurements from time-of-drilling to depth. Chromatographic measurements can differentiate between thermogenic and biogenic gas (image courtesy of RockWare.)

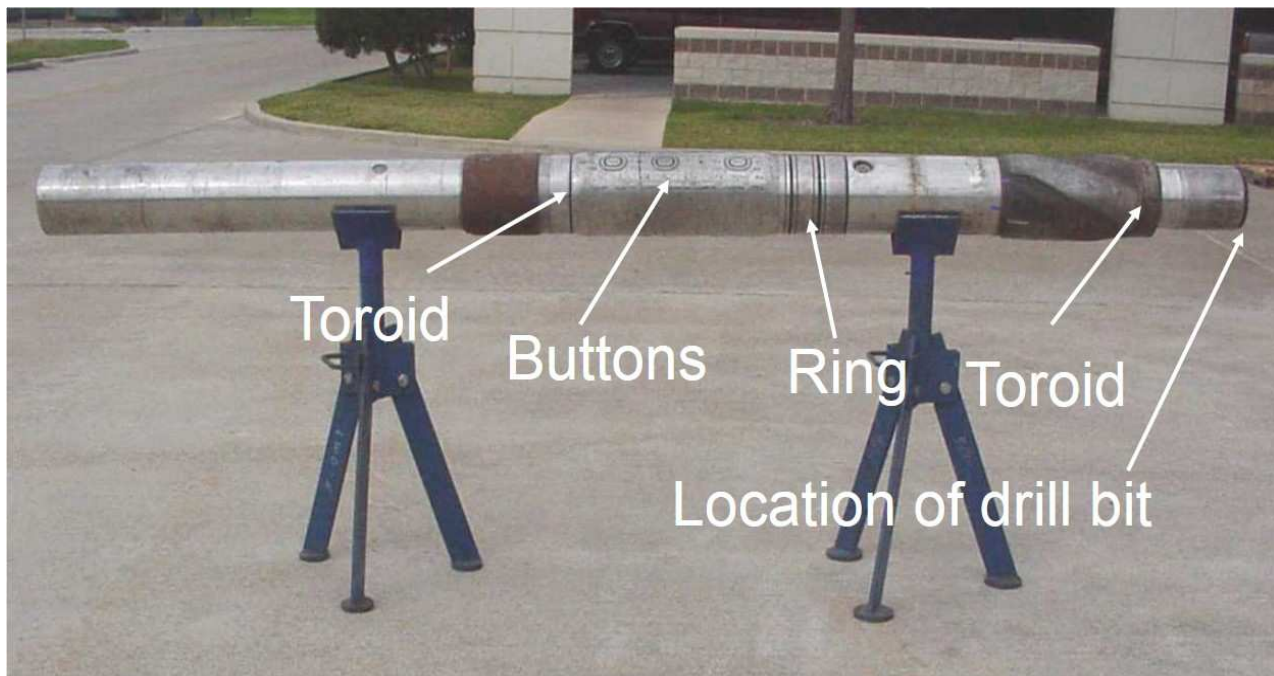


Figure 4.3.2: Example of LWD resistivity tool (toroid-based electromagnetic instrument) showing how the transmitter, receivers, electronics, and telemetry are located within the drill pipe while drilling mud flows toward the bit through the center of the pipe. Measurements are acquired in the presence of electrically conductive drill pipe, while the pipe is moving forward and rotating around the wellbore, and when the drill bit is subject to strong vibrations (photograph courtesy of Brian Clark, Schlumberger).

technical challenges to the design of instruments, including an electrically conductive drill pipe itself, a moving and rotating pipe, drilling mud flowing inside the pipe, real-time measurement telemetry to the surface based on mud pressure pulsing, and harsh noise conditions due to drill-bit vibrational modes. By comparison, Figure 4.3.3 shows several wireline logging tools. Some of the wireline tools are designed to work centralized with the borehole, while others require to be pressed against the borehole wall when operating them. Their diameter determines the minimum borehole size in which they can acquire measurements. Different instruments are assembled along a continuous tool string which is pulled by the wireline cable from the bottom/end of the well at a constant speed dictated by the instrument themselves. Further, the length of the cable corrected for tension effects is used to measure distance along the well. All measurements are depth matched at the end of the logging run using the cable speed and tension and different tool-string locations, as though all measurements were simultaneously acquired at the same location along the well.

Figure 4.3.4 compares resistivity measurements acquired in the same depth interval of a vertical well with both LWD and wireline instruments. LWD resistivity logs sense a shallower volume of the rock adjacent to the borehole than wireline logs and they are often shown in amplitude and phase versions. Likewise, the effect of mud-filtrate invasion on resistivity logs increases with time of invasion. LWD resistivity logs are less affected by mud-filtrate invasion than wireline resistivity logs. Finally, the logging instrument used to acquire the measurements may also influence the displayed resistivity logs. It is necessary to mitigate instrument and mud-filtrate invasion effects on resistivity logs before using them for calculation of hydrocarbon saturation, for instance.

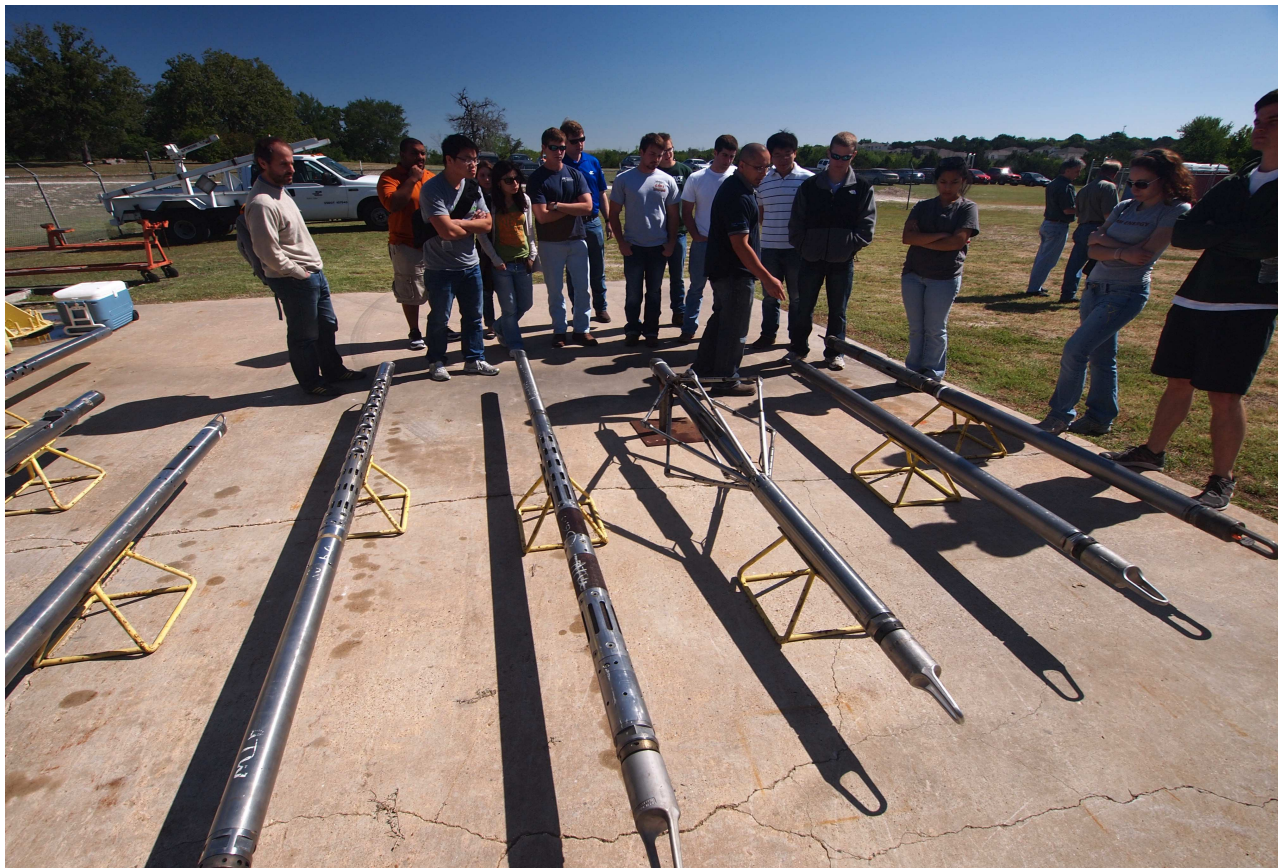


Figure 4.3.3: Example of wireline logging tools. Some of these tools are designed to work centralized with the borehole and some others require to be pressed against the borehole wall when acquiring measurements. The diameter of the tool determines the maximum size of borehole in which they can operate. Various tools are assembled into a long tool string which is pulled by the wireline cable out of the borehole starting from the bottom (end) of the well. Power and telemetry are delivered/implemented with the wireline cable itself. The cable pulls the tool string at a speed which depends on the type of instruments included in it. Likewise, the cable serves to measure distance along the well trajectory after implementing corrections for cable tension.

4.4 Measurements of Distance along the Well Trajectory

Distances and measurement locations along the trajectory of the well are quantified either as measured depth (MD) or true vertical depth (TVD). The two options are equivalent in a vertical well. However, along highly-deviated and horizontal wells, the location of a particular logging point requires a three-dimensional description. In those cases, logging companies prepare a so-called survey-trajectory file, which describes the location of a set of points along the well trajectory. *Measured Depth* is defined as the continuous distance measured from a reference point to a given point in the well following the well trajectory. On the other hand, *True Vertical Depth* is defined as the true vertical distance (dictated by gravity) measured between the reference point and any given point along the trajectory of the well. The reference point (zero measured or true vertical depth) could be the Kelly bushing (KB), the derrick floor (DF), or the ground level (GL).

The length of the logging cable (with calibration corrections due to exerted tension) is used in most cases to measure distance along the trajectory of the well in wireline operations. Special conveyance devices are used to transport logging tools in highly-deviated and horizontal wells without the assistance of gravity. In

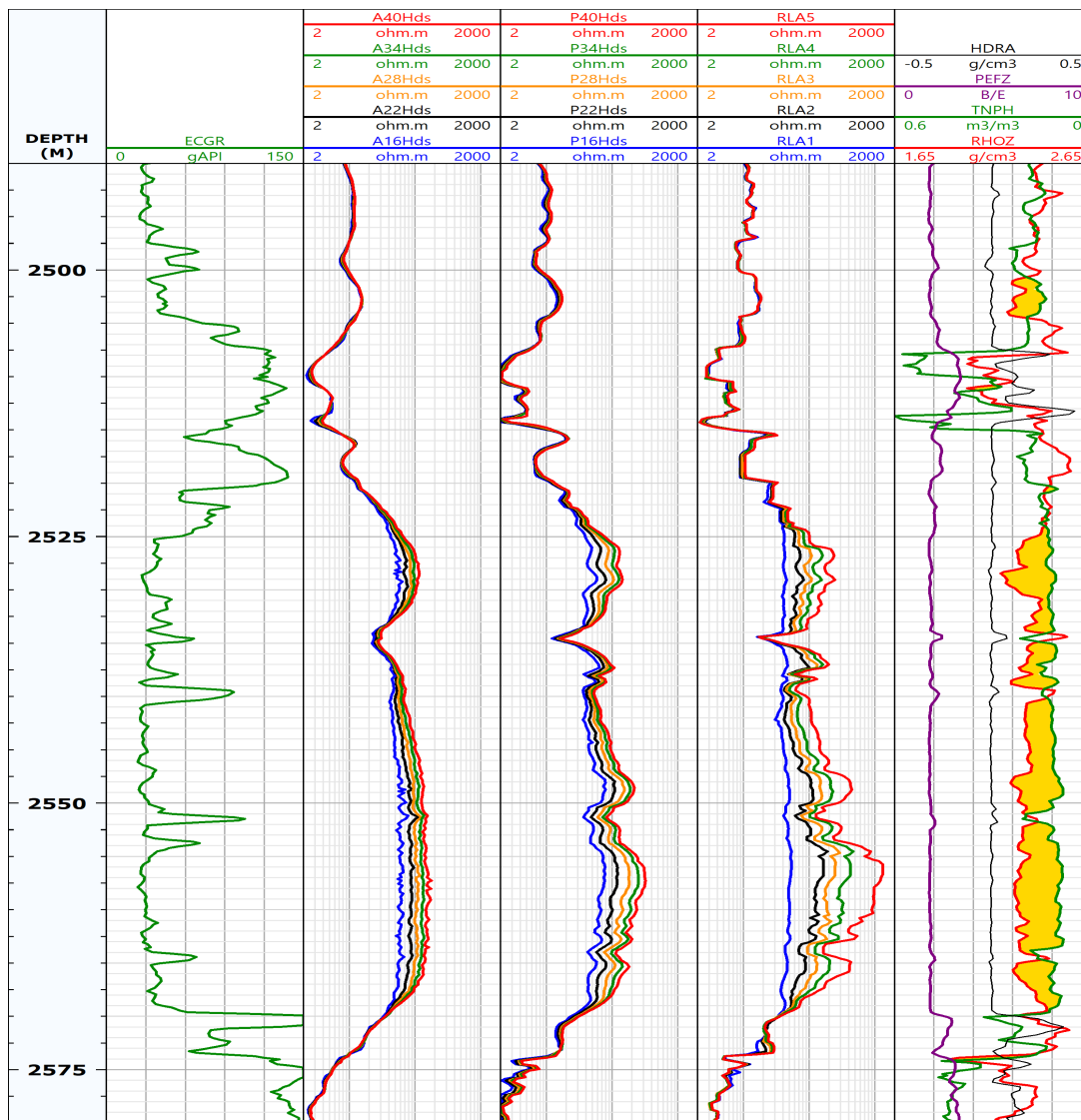


Figure 4.3.4: Comparison of LWD and wireline logs acquired along the same depth interval of a vertical well. LWD logs were acquired during drilling whereas wireline logs were acquired 10 days after drilling. Track 1 is gamma-ray, Track 2 is LWD amplitude resistivities, Track 3 is LWD phase resistivities, Track 4 is wireline Laterolog resistivities, and Track 5 is wireline rock density, apparent neutron porosity, photo-electric factor(PEF), and density correction. Resistivity values are not equal because of (1) mud-filtrate invasion, and (2) instrument used to acquire the measurements. Gas-saturated aeolian sedimentary sequence.

the case of LWD operations, distance along the trajectory of the well is measured by taking note of the number of drilling-casing segments and the length of an individual drilling-casing segment with pertinent corrections for longitudinal deformation due to compression. Discrepancies between LWD and wireline location are common and tend to increase with measured depth. Depth-matching of the two sets of measurements should be performed prior to performing well-log interpretation.

One needs a reference point (and depth) to transform measured or true-vertical depths to absolute vertical depth. This requires that the logging reference depth be properly stated in the header of the log. Well logs are

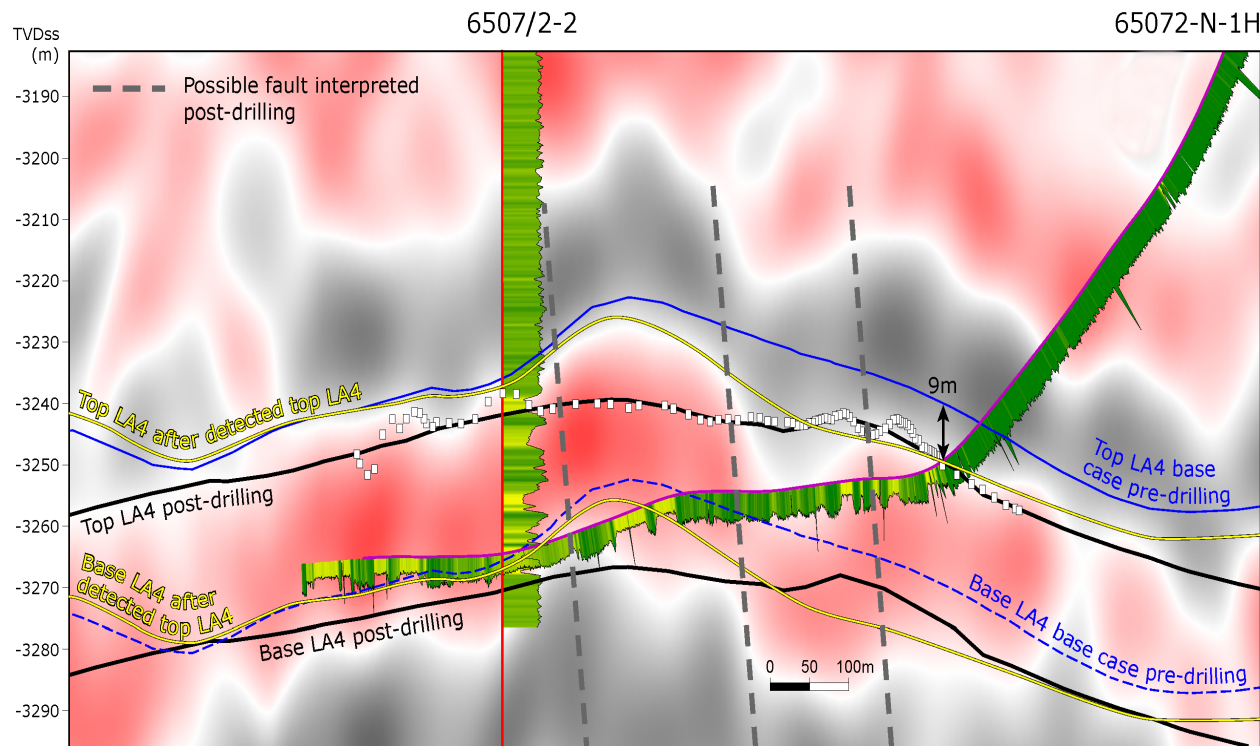


Figure 4.4.1: Example of two well trajectories, one vertical and one undulated, and their corresponding gamma-ray logs plotted over a cross-section of seismic amplitude data (two-way time converted to depth, m below the bottom of the sea) with formation boundaries and faults. The two well trajectories almost intersect. Well logs are commonly plotted with respect to distance along the well trajectory (measured depth, MD) or true vertical depth(TVD).

usually acquired when moving the tool string from the bottom of the well upward. Figure 4.4.1 is an example of two well trajectories, one vertical and one undulated, targeting the same clastic hydrocarbon reservoir, and plotted over a cross-section of seismic amplitude data (two-way travel time converted to depth) with formation boundaries and faults included for spatial reference. The figure also displays the color-coded gamma-ray logs acquired along the two well trajectories. Measurements of relative/absolute distance and location along well trajectories are exceedingly important to overlap data sets with different properties.

Figure 4.4.2 shows photographs of the logging truck and logging cabin used for onshore and offshore wireline logging operations, respectively. The wireline logging acquisition systems include a winch to spool and retrieve cable, a cable-length meter, and a tensiometer to measure cable tension.

4.5 Borehole Environmental Variables

Knowledge of borehole environmental variables is necessary to apply environmental corrections to most of well logs. Environmental corrections are necessary to put on equal footing all measurements acquired in a multitude of wells within the same hydrocarbon field. Wells in one hydrocarbon field are not always logged by the same company or even logged with the same tools. In addition, some wells within the same field could have been drilled with oil-base mud and others with water-base mud; bit sizes could also vary significantly from well to well. Variable volumetric concentrations of barite in the mud (used to control mud weight) can also significantly affect nuclear logs. Because of these differences in borehole environmental conditions across



(a) Logging truck, winch, and cable for onshore wireline logging.



(b) Cabin, winch, and cable for offshore wireline logging.

Figure 4.4.2: Photographs of logging truck (or cabin), winch, and cable for onshore (a) and offshore (b) wireline logging operations. The winch includes a cable-length meter and a tensiometer to measure cable tension.

the same field, it is imperative that environmental corrections be applied to all log measurements before using them for consistent calculations of petrophysical properties and/or well-to-well correlations.

The following is a summary of key borehole environmental variables to pay attention to when interpreting well logs:

1. Mud properties (oil base, invert emulsion, water base, synthetic base, density (weight), viscosity, PH, salt concentration, potassium concentration, electrical resistivity of mud filtrate, presence of barite, paper-filter press measurements, etc.)
2. Temperature (surface, bottom-hole, continuous with depth).
3. Depth of the well and depth interval for the acquisition of borehole measurements, drilling vs. logging depth, casing depth.
4. Drilling variables, e.g. bit size, rate of mud circulation, trip-out schedules, etc.
5. Bit size and caliper.
6. Time during which the well was exposed to mud-filtrate invasion.
7. Chemical composition of mud (especially for the case of oil-base and synthetic muds).
8. Types of tools that were used to log the well.
9. Variables needed for borehole environmental corrections.

In addition, knowledge of borehole environmental variables is necessary to assess whether a particular well-logging tool is appropriate and/or reliable for a given environmental condition. For instance, not all the logging tools can be lowered into narrow boreholes, while some tools work reliably only within strict physical bounds of temperature and pressure.

One cannot assume that well logs are free of measurement errors. Consequently, it is important to (a) acquire logs that could diagnose anomalous acquisition conditions and (b) to make redundancy checks and repeated passes through one or more depth segments.

It is also common that not all the well logs be acquired with the same tool string. Different depth and tool-string runs are subsequently “spliced” into one single run using, most commonly, the gamma-ray log for depth-matching purposes. An alert well-log interpreter should always verify that all well logs are properly depth matched before performing interpretations.

4.6 Processing of “Raw” Borehole Measurements

Most service (well-logging) companies apply special processing techniques to calculate the readings typically displayed on well-log printouts. The trained well-log interpreter is always aware of potential biases caused by pre-processing techniques that could result in inaccurate assessments of petrophysical properties. Examples are apparent resistivity curves calculated under the assumption of no invasion, no shoulder beds, no dip, and no electrical anisotropy. Likewise, density and neutron curves are often calculated from raw near- and far-sensor measurements using depth and resolution-matching processing methods exclusively designed to work in vertical wells penetrating horizontal layers. Operating companies should request a complete list and description of processing methods applied to raw measurements when displaying them on printouts or when included in digital files. The petrophysical analysis of rock formations subject to extreme 3D geological conditions could require raw measurements instead of processed measurements.

4.7 Essential Suite of Borehole Measurements

The following list briefly describes the most common well logs used for the assessment of lithology and petrophysical properties of rock formations:

- Caliper [inches]: measures the equivalent diameter of the borehole,
- Bit Size [inches]: reports the intended size of the drill bit,
- Differential caliper [inches]: measures the difference between caliper and bit size [inches]. Indicates presence of washouts or mudcake,
- Cable Speed [ft/hour] and Cable Tension [pounds force], necessary to assess the accuracy and reliability of other well logs,
- Temperature [$^{\circ}\text{C}$ or $^{\circ}\text{F}$]: measures the temperature of mud,
- Gamma ray [gAPI]: measures the natural (spontaneous) combined radioactivity of Th, U, and K emanated by rocks. Spectral gamma-ray logs separately measure the radioactivity of Th, U, and K emanated by rocks,
- SP (spontaneous potential) [mV]: due to ion and cation mobility in the aqueous phase between the borehole and the pore space of permeable rocks. It measures the difference in static (DC) electric potential between a reference electrode and an electrode placed in the borehole. Spontaneous potential measurements originate from the difference in electrolyte concentration between drilling mud and formation water. Presence of either oil-base mud or hydrocarbon-bearing formations suppresses SP measurements,
- Electrical resistivity (induction or laterolog) [Ohm-m, or $\Omega\text{-m}$]: measures the electrical resistivity of rock formations penetrated by the well by “activating” electrical currents inside rocks surrounding the borehole. Electrical resistivity instruments are designed to probe rock formations at multiple radial lengths of investigation. Micro-log resistivity measurements, for instance, are designed to probe the mudcake

and the flushed zone, whereas deep resistivity measurements are designed to probe the intermediate and virgin (uninvaded) zones,

- Density [gm/cc]: measures the electron density of a rock, which is converted to rock (bulk) density,
- Photoelectric factor (PEF) [$barns/cm^2$]: measures the photoelectric cross-section and primarily responds to the solid components of a rock,
- Neutron [apparent water-filled porosity units]: measures the hydrogen index (number of hydrogen atoms per unit volume) contained in rocks,
- Sonic [$\mu\text{sec}/\text{ft}$]: measures the slowness (inverse of speed) of P-wave (compressional) waves propagating in rock formations,
- Pressure [psi]: *In situ* fluid pressure is measured with a formation tester,
- Magnetic resonance: measures the magnetic time relaxation of rocks due to proton diffusion, and
- Sigma [capture units, cu]: measures the thermal neutron capture cross-section of rocks.

In addition to the above basic suite of borehole measurements, modern logging operations include the measurement of S-wave slowness, Stoneley-wave velocity, dielectric properties of rocks, and formation testing, among others. Well logs can be acquired with either wireline (open hole) or LWD (logging-while-drilling) tools.

There are several classifications of well logs, depending on the type of petrophysical estimation that can be made from them. Some logs measurements are exclusively sensitive of the solid component of the rock, while others are exclusively sensitive to the fluid components of the rock. However, the vast majority of well logs are sensitive to both solid and fluid components of the rock.

4.8 Mandrel vs. Pad Measurements

Depending on the physics of a particular measurements and associated practical engineering limitations, borehole measurements are acquired with either mandrel or pad tools.

Mandrel tools are cylindrical devices that are often centralized with the borehole. Sources and/or sensors are included within the diameter of the cylinder and are connected to other cylindrical sections in the tool string which house electronic and telemetry systems. Examples of mandrel tools are induction resistivity, laterolog resistivity, and sonic, among others. There are also mandrel tools that are pressed against the borehole wall for measurement acquisition. This operation reduces borehole effects. Examples are the gamma-ray and neutron tools. Most LWD tools operate in mandrel mode.

Pad (or skid) tools consist of sources and/or sensors located along the surface of a mechanical arm which is extended from the center of the mandrel toward the borehole wall. These tools perform measurements as closely as possible to the borehole wall in an attempt to reduce influence of borehole environmental conditions. Examples of pad tools are density, electrical microlog, and dipmeter, among others. Pad tools can also measure caliper.

Typically, mandrel tools are affected by variations of borehole size and borehole fluid, as well as tool eccentricity, while pad tools are highly sensitive to rugose conditions on the borehole wall, including abrupt variations of borehole size. The difference of operation also causes differences in vertical resolution. The vertical resolution of pad-type tools is normally higher than that of mandrel-type tools.

4.9 Typical Plotting Scales Used to Display Well Logs

Well logs are graphically displayed as measurements with respect to either measured depth (MD), true vertical depth (TVD), or horizontal/curtain distance (in the case of horizontal and high-angle wells). Measurements

scales and order of values (minimum vs. maximum values to the left or right of the plot) depends on convention and ease of calculation.

Resistivity logs are typically plotted with a logarithmic scale because of their wide range of values.

4.10 Quality Control of Well Logs

It is exceedingly important to assess the quality of borehole measurements before using them for petrophysical calculations. For instance, rapid depth fluctuations in the diameter of the borehole could significantly affect measurements acquired with pad tools (e.g. bulk density logs). On the other hand, large borehole diameters could impair the ability of mandrel-type tools to reliably sense formations properties. The following is a list of quality-control variables and logs used to assess the reliability of borehole measurements:

1. Calibration record of measurements (e.g. yellow flags for quality control, multiple (repeated) runs),
2. Caliper, differential caliper,
3. Cable tension and cable speed (used to diagnose tool sticking and yo-yo effects, for instance),
4. Delta density ($\Delta\rho$),
5. Temperature,
6. Repeated runs on a specific depth segment,
7. Log splicing methods,
8. Assumptions made in the acquisition and processing of measurements, including depth-matching procedures, and
9. Depth-matching of well logs acquired in the same or during different tool runs.

Interpretation of well logs can only proceed after verifying that their quality is acceptable. In practical applications, it is possible that bad-quality measurements occur only along depth interval of no commercial interest, such as shale sections, which will have negligible consequences on the assessment of hydrocarbon reserves, for instance.

4.11 Remarks about the quality and reliability of well logs

- You won't understand the reliability and accuracy of the calculations made and obtained from well logs without first understanding how the measurement/instrument works.
- It is paramount to be able to recognize when a measurement is faulty, i.e., when a given well log is not a complete expression of rock properties.
- It is very important to verify and reality-check all calculations performed with well logs; core measurements and mud logs can often be used for this purpose.
- If the interpreter does not know how to perform calculations, then he/she does not understand the physics of the measurements.
- All measurements have practical limitations and all calculations have implicit assumptions; a formation evaluation specialist should be familiar with them.

4.12 Volume of Investigation of Borehole Measurements

All well logs are associated with a specific volume of investigation (also known as *volume of sensitivity*) that describes the spatial zone of response within the rock which gives rise to the measurement. Shallow-sensing measurements are associated with a small volume of investigation, whereas deep-sensing measurements are associated with a larger volume of investigation. The volume of investigation defines the vertical resolution and radial length of investigation of well logs.

Vertical resolution is defined as the thickness of the thinnest bed that can be resolved with a given tool. The larger the resolution of the measurements, the thinner the bed that can be detected and quantified with them. This is an important concern when using two or more types of logs that exhibit different vertical resolutions and depths of investigation to perform calculations of petrophysical properties (e.g. the density log used to calculate porosity, the neutron log used to diagnose light fluids, and resistivity logs used to calculate hydrocarbon saturation). Equally important is the case of highly laminated siliciclastic sequences in which the individual laminae are much thinner than the vertical resolution of the logging instrument. Both sampling interval (measured depth between two adjacent measurements) and speed of logging may also have an effect on the vertical resolution of well logs. Insufficiently sampled beds cannot be differentiated from their shouldering layers. Likewise, because well logs are acquired at the same time the tool string is moving along the trajectory of the well (usually starting from the bottom of the well toward the surface), a fast moving tool will not permit sufficient measurement redundancy, thereby potentially masking with noise otherwise useful signals. In deviated wells, depending on the angle between well trajectory and formation dip, the resolution of the measurements will increase compared to that of a well which is perpendicular to formation layering because more sampling points are included within one bed (recall that measurement sampling is performed along the well trajectory).

It is also important to note that well logs are extremely localized measurements: the rock volume of investigation of most well logs is within one foot of the borehole wall. Commonly, LWD measurements are associated with a smaller volume of investigation than wireline measurements. The longest radial distance away from the borehole wall that can be sensed with well logs is no more than 10 ft (deep resistivity induction logs or laterologs exhibit the longest possible radial length of investigation). Because of this limitation, well logs by themselves cannot indicate the lateral extent of beds penetrated by the well. There is also a possibility that nearby hydrocarbon-bearing beds exist which were by-passed because the well trajectory did not intersect them (e.g. beds pinching out such as those of fluvial sedimentary environments).

The radial length of investigation is also referred to as “depth of investigation.” In general, high vertical-resolution measurements exhibit a short radial length of investigation. Radial length of investigation is also important because of the phenomenon of mud-filtrate invasion and because of possible formation damage due to drilling. Depending on their radial length of investigation, some measurements will be sensitive to the invaded zone, some to the virgin (uninvaded) zone, and some to the transition zone. Sonic logs, for instance, may also be influenced by drilling damage in the near-wellbore region, thereby impairing their ability to probe radially deeper into the rock.

Effective medium theories are typically used to interpret well logs acquired in thinly bedded and highly-laminated siliciclastic sequences. In addition, electrical and elastic anisotropy is often used to diagnose presence of highly-laminated siliciclastic sequences, and to quantify the petrophysical properties of individual sandstone laminae from the degree of anisotropy.

Figure 4.12.1 is an example of high-resolution ultrasonic image. The radial length of investigation of this image is close to zero (less than 1/10 of one inch) but its extremely high vertical resolution captures very thin open and closed fractures as well as voids due to rock collapse along the complete borehole surface, which is not possible with standard sonic logs, for instance. Ultrasonic images describe the reflectivity and travel time of an ultrasonic pulse emitted toward and reflected from the borehole wall. In this example, the well penetrates fractured carbonates in the Edwards formation (Austin, Texas) which serve as aquifer.

Figure 4.12.2 compares the vertical resolution and radial length of investigation (also known as *depth of investigation*) of several commercially available wireline logs. In the presence of spatially heterogeneous rocks surrounding the borehole, different volumes of investigation associated with the different wireline logs will give

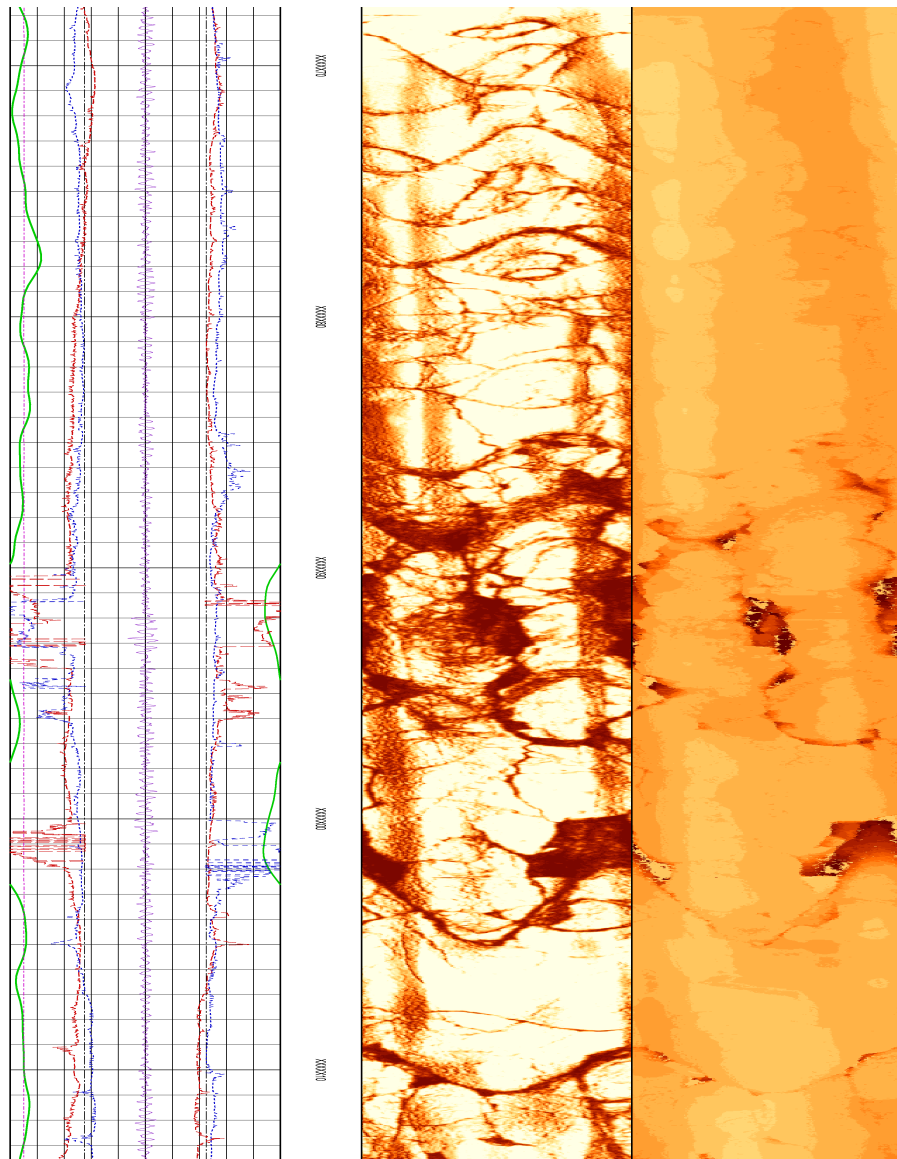


Figure 4.12.1: Example of ultrasonic borehole image acquired in a vertical well penetrating the Edwards carbonate formation (Austin, Texas). Track 1 is standard well logs. Track 2 is depth. Track 3 is ultrasonic reflectivity image (light and dark red colors identify high and low ultrasonic reflectivities, respectively). Track 4 is ultrasonic travel time image (dark red color identifies long travel times). Ultrasonic images provide high-resolution descriptions of reflectivity and travel time along the complete borehole surface. This image shows open and closed fractures, and voids resulting from rock collapse, all part of the flow system in the Edwards aquifer.

rise to different spatial averages of rock properties. It is important to take into account these differences in volume of investigation when calculating petrophysical properties from well logs. Figure 4.12.2 also compares the different volumes of investigation of wireline logging instruments to whole-core sizes and typical sizes of core samples used in laboratory measurements. One must also take the differences in sample size and volume of investigation into account when reconciling core laboratory measurements and petrophysical calculations performed with well logs.

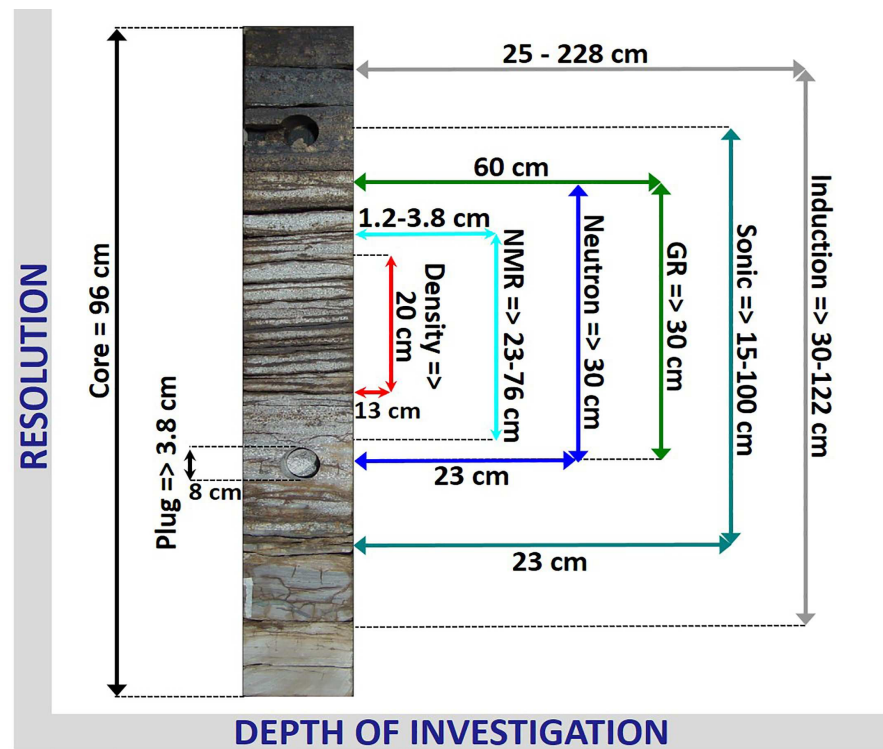


Figure 4.12.2: Comparison of the resolution and radial distance of investigation (aka depth of investigation) of the various commercially available wireline logs. Well-log resolution is a measure of the minimum bed thickness that can be detected with a given logging instrument. Notice that in the context of spatially heterogeneous whole core (as the carbonate whole core shown in the figure), different well logs inherently implement different volumetric averages of the rocks surrounding the well. The figure also shows the typical size of core samples used in laboratory measurements and studies.

4.13 Bed-Thickness Effects on Well Logs

Because of the finite volume of investigation associated with all well logs, an otherwise sharp transition between two adjacent beds appears as a smooth transition in a well-log display. Usually, the boundary between two adjacent beds is recognized as the inflection point in the log. The larger the volume of investigation of the well log, the longer the depth transition observed in the log between two adjacent beds. This transition effect is often referred to as “shoulder-bed effect” in well-log interpretation. Because of such an effect, petrophysical calculations performed with logs could be biased in the vicinity of bed boundaries. Along thin beds, it is recommended that the center point of the bed be used for calculation of petrophysical properties from well logs. However, even the well logs acquired in the midpoint of very thin beds could be biased because of shoulder-bed effects. Corrections to well logs are necessary in these extreme conditions of bed thickness.

Formation evaluation practitioners often group bed-thickness effects on well logs into two categories:

- **Thinly bedded formations**, where the vertical resolution of well logs is close to the average bed thickness. In this case it is possible to “sharpen” the well logs to improve bed-property resolution (hence improve rock-property interpretations) via post-processing deconvolution procedures and numerical simulation of well logs.

- **Laminated formations**, where the vertical resolution of well logs is much greater than the average bed thickness. The interpretation of well logs in this case requires the use of *effective medium theories* which, depending on the specific rock physical property sensed by the well logs (e.g. electrical resistivity), may also need to account for anisotropy.

It is important to keep in mind that the acquired and displayed well logs could have some remnant effects of the instrument itself used to acquire the measurements. Service (logging) companies try to mitigate all pertinent instrument and borehole effects (i.e., environmental effects) on the delivered measurements so that their measurements can promptly be used to perform calculations of rock properties. But the truth is that different instruments do not sample the same volume of rock adjacent to the borehole because they work with different physical principles, especially in the presence of thin beds, mud-filtrate invasion, and deviated wells (or, equivalently, dipping layers), for instance. Typically, and because of engineering design considerations, the same logging instrument cannot work for all possible rock/fluid conditions with the same accuracy and reliability. For instance, some logging instruments are designed to deliver the maximum bed resolution possible, while others are designed to deliver the maximum distance of penetration possible; not often it is impossible to combine the two designs in the same instrument. Also, some instruments are more reliable in the presence of oil-base mud while others perform better in the presence of water-base mud. A good formation evaluation specialist is aware of potential instrument-related effects on well logs that could explain discrepancies between calculations and core laboratory measurements, for instance. Correction charts or numerical modeling are sometimes used to mitigate those effects on well logs.

As an example, Figure 4.13.1 shows how different resistivity instruments could give rise to different resistivity logs for the same earth model of electrical resistivity. The original earth model considered in this example is a synthetic model of a mud-filtrate-invaded vertical well with multiple horizontal layers designed to replicate common field conditions. Accurate numerical calculations were performed on a computer to obtain the corresponding resistivity logs. The figure shows both LWD and wireline resistivity logs with multiple radial lengths of investigation; it also shows the original earth-model resistivities. It is found that different instruments give rise to different degrees of “smoothness” of resistivity logs. Furthermore, not all the deepest-sensing resistivity logs for the different instruments give rise to the same resistivity or/and they are different from the expected layer resistivities (recall that resistivities are plotted with a logarithmic scale). It is exceedingly important to reconcile these differences before using resistivity logs to calculate hydrocarbon saturation, for instance.

4.14 Typical Logging Speeds

The sampling interval along the trajectory of the well is conditioned by the specific type of measurement and by the logging speed. Some log measurements are acquired every inch or centimeter, while others are acquired every one or two feet. In general, the smaller the sampling interval, the slower the speed of logging. Likewise, presence of biasing noise in the measurements can sometimes be reduced with slower logging speeds that lend themselves to measurement redundancy and averaging.

Logging speeds can vary greatly, usually (with some exceptions) between 600 ft/h and 4,000 ft/h . Here are some examples:

- DSI[®] sonic tool by Schlumberger[®]:
 - All six modes simultaneously, with 6 – in Δt : $v = 900 \text{ ft/h}$.
 - All six modes simultaneously, without 6 – in Δt : $v = 1,000 \text{ ft/h}$.
 - One 8-waveform set (single mode) : $v = 3,600 \text{ ft/h}$.
- Dual Induction-spherically focused resistivity Tool (DIT): $v = 10,000 \text{ ft/h}$.
- Accelerator Porosity Sonde (APS): $v = 1,800 \text{ ft/h}$.
- Hostile Environment Gamma Ray Sonde (HNGS): $v = 3,600 \text{ ft/h}$.

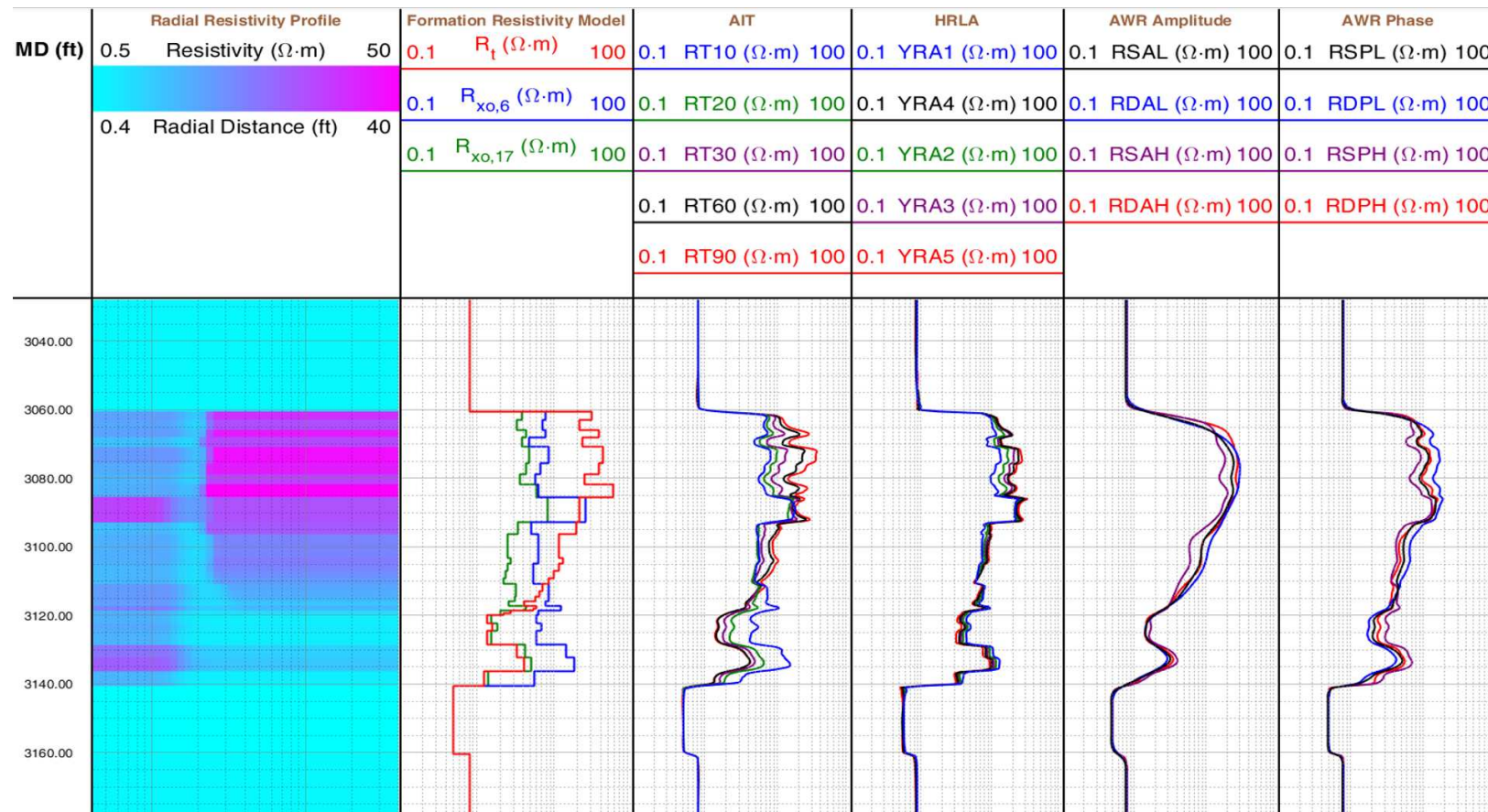


Figure 4.13.1: Example of resistivity logs numerically calculated to replicate actual field conditions of a vertical well penetrating multiple horizontal layers of various thicknesses and invaded with mud filtrate. Track 1 is depth. Track 2 shows the synthetic earth model (color-coded spatial distribution of electrical resistivity in the vertical and radial directions). Track 3 shows the actual values of electrical resistivity as a function of distance away from the wellbore. Track 4 is wireline induction resistivity. Track 5 is wireline laterolog resistivity. Track 6 is LWD amplitude resistivity. Track 7 is LWD phase resistivity. The deepest- and shallowest-sensing resistivity logs are plotted with red and blue/black lines in each case. Note the difference in “smoothness” between some of the resistivity logs and the original earth-model resistivities. Also note that not all the deepest-sending resistivity logs are equal among themselves or to the original earth-model resistivities. Discrepancies between actual earth-model resistivities and resistivity logs give rise to errors in the calculation of hydrocarbon saturation, for instance. Numerical simulations performed with **UTAPWeLS**.

- Hostile Environment Litho-Density Sonde (HLGS): $v = 1,800 \text{ ft/h}$.

In general, the faster the logging speed, the poorer the quality of the corresponding measurement. This property is to be remembered when logging sedimentary sequences with thin reservoir units, where the assessment of petrophysical properties requires robust statistical averages in the face of instrumental noise and other adverse borehole environmental conditions.

It is also important to emphasize that well logs are acquired with a rigid tool string, where sensors for the different measurements are distributed along its nominal length. Measurements performed at different tool locations along the trajectory of the well are then used to re-locate, in almost real time, all the different sensor measurements as though they were acquired at the same location along the well trajectory (collocated measurements). This standard operation for re-collocation of measurements, which is often referred to as *depth matching*, is performed based on both tool speed and sampling interval. If the tool string did not move evenly (at constant speed) during the acquisition process, then corrections for location are performed based on the tool speed and acceleration, and cable tension. In the case of dipmeters, multi-arm caliper, borehole images or, in general, measurements acquired with reference to location along the perimeter of the wellbore, additional corrections are performed for cable rotation and orientation to display all measurements as though they were acquired with respect to a fixed direction (e.g. true magnetic north). The tool string is equipped with a set of magnetometers and inclinometers to enable the assessment of its position as it moves along the trajectory of the well. In the case of ultra-precise operations, the tool string will include a set of gyroscopes for accurate positioning with respect to true geographic coordinates.

One of the first steps of well-log interpretation is the verification of accurate *depth matching* of all measurements (and implementation of corrections if necessary), including those which were acquired during different runs and with different tools (e.g. logging-while-drilling, open hole, and cased hole measurements), or in cases where the cable tension and speed were uneven. It is also the case that core data need to be depth-matched with well logs because the former are usually located with the same depth-measurement system used in drilling operations (which may not be same measurement system implemented by logging companies).

4.15 Well Logs and Signal Processing

In some respects, well logs can be examined and quantified with the same procedures used to analyze and quantify general time- or space-domain signals. Signal processing concepts such as energy, correlation, auto-correlation, cross-correlation, low- and high-frequency components, filtering, etc., can be readily adapted for processing and interpretation of well logs. Along these lines, 3 key elements of well logs are:

- The *energy* of a well log is a measure of the number and relative amplitude of oscillations per unit distance along the well trajectory. This metric can be associated with, for instance, number of beds per unit length and variability of bed properties per unit length.
- The *average* value of a well log is a measure of the most dominant bed property per unit length; it is indicative of the average property of a sequence of beds per unit length.
- The *drift* of a well log is a measure of the average slope of a well log along a given depth segment; it is indicative of varying average bed properties per unit length.

4.16 Detection of Bed Boundaries with Well Logs

Well logs are *smooth* representations of actual physical properties of beds penetrated by the well. Because of this, well logs will not exhibit sharp (discontinuous) transitions between adjacent beds. At bed boundaries, well logs are depth averages of the actual physical properties of beds located above and below them. Deep-sensing well logs will be smoother across a bed boundary than those that are shallow sensing.

The detection of bed boundaries is usually performed with the log that exhibits the largest vertical resolution. Inflection points in this log are good detectors of bed boundaries. Density and micro-resistivity logs are commonly used to detect bed boundaries. It is also desirable that the well log used to detect bed boundaries be mostly affected by the solid component of the rock so that it can be consistently used across all the wells located within the same hydrocarbon field.

Because of the smoothness of logs across bed boundaries, log values across thin beds (beds thinner than the vertical resolution of the log) could be biased downward or upward with respect to true physical properties. Therefore, it is recommended that the petrophysical assessment of thin beds be performed with well-log values acquired at the center of the bed.

4.17 Caliper and Temperature Logs

Caliper logs measure the size (diameter) and shape of the borehole along the well trajectory. Measurements of caliper can be made with one or more mechanical arms. Multiple-arm caliper logs are preferred in those cases where the shape of the borehole is highly irregular. Two-arm caliper logs are sufficient to diagnose and quantify ovalized boreholes. The shape of the borehole is conditioned by the interplay between drilling forces, *in situ* stress, mechanical properties of the rock, and chemical alterations due to temperature and chemical reactions between drilling mud and rocks and their saturating fluids. Often, caliper measurements are displayed as *differential caliper*, which is the difference between the diameter of the borehole and the diameter of the drill bit. Positive differential caliper values are indicative of borehole washouts (common in shale sections), whereas negative differential caliper values could be due to presence of mudcake (common in porous and permeable rocks). Presence of open fractures can sometimes cause erratic variations of caliper.

Quantifying the size and shape of the borehole is of great importance in drilling and completion operations because it permits the calculation and verification of mud losses and volume of cement needed to properly bond the casing with the surrounding rock formations. Mud losses need to be accounted for by the volume of the well, thus why it is important to accurately and continuously measure the borehole diameter and shape.

Temperature affects a multitude of well logs, including resistivity, PEF, density, and neutron. Moreover, the electrical resistivity of formation water is a function of temperature. It is necessary that temperature be measured along the trajectory of the well to accurately perform the corresponding measurement corrections. Temperatures are often assumed to vary linearly with vertical distance. In those cases where such an assumption is correct, it suffices to measure temperature at two points along the well trajectory. The common procedure is to measure temperature at the surface and at the bottom of the well. Surface and bottom-hole temperatures are usually measured with a mercury thermometer. Some logging tools (e.g. resistivity tools) include a thermistor, which can provide continuous temperature measurements along the well trajectory. Modern production logs could also include continuous depth measurements of temperature acquired with a fiber-optic cable.

The equation used to describe linear variations of temperature as a function of depth is given by

$$T(z) = T(z_1) + G \cdot (z - z_1) , \quad (4.17.1)$$

where z is *true vertical depth*, TVD, measured with respect to the logging reference point,

$$G = \frac{T(z_2) - T(z_1)}{z_2 - z_1}$$

is the geothermal gradient [*temperature/length*], T is temperature, and z_1 and z_2 are the two TVDs at which temperatures were recorded during logging acquisition (most commonly at the KB and at the bottom of the well). The bottom-hole temperature is commonly identified with the acronym **BHT**.

4.18 Geology, Petrophysics, and Well Logs

Well logs sense *bulk*, or *effective* physical properties of rocks, such as electrical conductivity (electrical resistivity), spontaneous electric potential, volumetric concentration of radioactive isotopes (thorium, uranium, and

potassium), density, hydrogen index, velocity of propagation of compressional and shear waves, magnetic time relaxation, and fluid pressure, among others. These effective properties are not infinitesimal expressions of rock behavior but rather a spatial average performed over the volume of investigation of the corresponding measurement. In other words, well logs “see” rocks with continuous measurements of multi-physics properties. It is up to the Formation Evaluation specialist to transform those properties into geological, petrophysical, elastic, and mechanical descriptions of rocks.

Petrophysicists are obviously interested in transforming effective physical properties of rocks measured by well logs into petrophysical properties such as grain composition and size, porosity, clay (shale) content, hydrocarbon saturation, and permeability, to mention but a few possibilities. Owing to the ample variations of rock composition and pore distributions encountered in nature, it is impossible to precisely (and deterministically) quantify the relationship that exists between *effective* physical properties of rocks and *petrophysical properties*. Some of these relationships are statistical in nature on account of rock heterogeneity and spatial variability. In addition, well logs exhibit a specific *volume of investigation* that effectively averages the physical properties of rocks over that volume.

Formation evaluation specialists are interested in measuring physical properties of rocks that can provide the maximum measurement contrast possible between two or more alternative conditions of pore-saturating fluids, and/or solid composition, for instance (e.g., to better distinguish between presence of oil and water, presence of gas and oil, quartz or limestone solid composition, etc.) Quite often, however, the unique and precise differentiation of alternative states of rock fluid/solid composition requires simultaneous measurements of *multiple* physical properties of rocks. Time-lapse measurements can also be invoked to improve the accuracy of the above assessment and to secure information about dynamic rock properties, such as permeability. Rock physicists are always in search of new and alternative physical properties of rocks to assess additional details about pore and fluid properties, among others.

One specific example is the simplest possible calculation of porosity from density logs via the equation

$$\rho_R = \phi \cdot \rho_f + (1 - \phi) \cdot \rho_m , \quad (4.18.1)$$

where ρ_R is rock density (bulk density), ϕ is total rock porosity, ρ_f is fluid density, and ρ_m is matrix (grain) density. As emphasized in a subsequent section of these notes, the above equation can be derived from first principles subject to the assumption of a rock composed of *only* one type of grain chemical composition and *only* one type of saturating fluid. Presence of more than one type of grain composition (in variable volumetric proportions) plus more than one type of saturating fluid (e.g. irreducible water saturation, gas, oil, and mud filtrate) would transform the simple form of the above equation into a complex nonlinear system of equations involving volumetric proportions of grain constituents and electrical resistivity measurements whose solution will require multiple iterations to arrive at a petrophysically plausible result.

One of the central objectives of well logging is to develop *rock models* that “transform” effective physical rock properties intrinsically sensed by the measurements into petrophysical properties for specific types of rocks. These models will be discussed in subsequent sections.

4.19 Corrections Applied to Well Logs Prior to Interpretation

Because of multiple assumptions made in the acquisition and processing of well logs by service companies, “as-received” well logs can be affected by several geometrical and borehole effects that need to be mitigated before performing interpretations of rock/fluid properties with them. Some of these effects can be neglected but others can be significant, for instance in the case of highly-deviated and horizontal wells (most well-logging instruments currently in operation were designed for the case of vertical wells penetrating horizontal layers). Service companies provide well-log interpreters with correction tables for some of those effects but it is often necessary to perform numerical modeling to implement general corrections. Yet some service companies can implement the corrections as part of a post-processing step, which can be time consuming and expensive.

The following is a list of borehole and geometrical effects on well logs that need to be accounted for before performing rock-property interpretations with them:

- **Borehole Effects.** Most well logs are affected by the borehole and the instrument (tool) used to acquire the well logs. Factors include borehole diameter (caliper), borehole rugosity (variability of borehole caliper within the volume of investigation of a given measurement), mud type (e.g. mud salinity), mud weight (e.g. presence of barite), and temperature. Most of these factors are normally corrected for in modern logging operations when service companies deliver their measurements to clients, but it is still important to routinely verify them.
- **Mud-Filtrate Invasion Effects.** Except when well logs include measurement subsets with different radial lengths of investigation (e.g. resistivity logs), well logs can be greatly affected by mud-filtration effects depending on type of mud (e.g., oil- vs. water-based mud, mud salinity, special mud chemistry, etc.), overbalance pressure, time of acquisition after drilling, formation permeability, etc. Corrections for mud-filtration effects are typically not performed by well-logging companies before delivering measurements to clients. Some corrections can be performed with tables prepared by service companies but it is often necessary to invoke numerical simulation methods for that purpose.
- **Bed Thickness and Bed Boundary Effects.** Depending on their volume of investigation (especially vertical resolution) in relation to bed thickness, bed thickness and bed boundary effects on well logs can be significant. Corrections are not typically implemented by service companies before delivering their measurements to clients. Some corrections can be performed with tables prepared by service companies but it is often necessary to invoke numerical simulation methods to reliably implement the corrections.
- **Well-Deviation Angle and Formation Dip Effects.** These are some of the most conspicuous effects observed in well logs acquired across highly-dipping formations or highly-deviated wells. Their magnitude depends on the relative angle between the well trajectory and the formation dip and azimuth, volume of investigation of the measurement, and presence of rock anisotropy (e.g, in the case of resistivity and sonic logs). They include the so-called “horn” effects on resistivity logs acquired across boundaries between beds with large resistivity contrasts. Corrections of these effects on well logs are typically not performed by service companies before delivering their measurements to clients; they require sophisticated numerical simulation methods.
- **Combined Effects.** Complex situations may involve the combined effects of mud-filtrate invasion, bed thickness, and well-deviation/formation-dip effects on well logs. Corrections of well logs are necessary in these cases and require sophisticated numerical simulation methods. The most adverse situations occur in cases of non-symmetric mud-filtrate invasion around the borehole in highly-deviated wells.

4.20 Formation Evaluation Across Multiple Wells

When performing petrophysical interpretations across multiple nearby wells, it is very important to verify that all the available well logs were corrected for borehole environmental effects.

It is commonly the case that not all wells are drilled with the same drilling mud or with the same bit size even across a common subsurface target zone. Some drilling muds could also include different concentrations of barite or bentonite. Yet another possibility is that well logs were not acquired with the same instruments or by the same logging company in all the wells (especially in reservoirs with a long history of exploration and development). A nowadays more common situation arises when some of the wells are highly deviated or horizontal.

Whenever reliable borehole environmental corrections for the available well logs (e.g., gamma ray, neutron, density, etc.) are uncertain or non-existent (the best option is always to request that the well-logging company provide the operator with sets of well logs with and without borehole environmental corrections), the interpreter needs to verify the range and distribution of values across a common formation or geological zone penetrated by all of the wells and preferably across similar saturating fluids (in the case of fluid-sensitive well logs such as density, neutron, resistivity, etc.) Furthermore, this verification is typically carried out in vertical wells with slightly dipping beds to minimize asymmetric effects on the weighted volume of investigation of the various

instruments. Under similar geological and petrophysical conditions, the well logs acquired in multiple wells should exhibit similar histograms and value ranges. If that is not the case, the interpreter needs to choose one of the wells as key, or reference well, and use its corresponding well-log histograms to perform either average-value corrections or value-range corrections, or both (histogram-semblance correction), in all of the remaining wells, one correction per type of well log.

In the case of different instruments used to acquire the corresponding well logs in different wells (e.g., laterolog vs. induction resistivity, array induction vs. dual induction resistivity, spectral gamma ray vs. high-resolution gamma ray, etc.), the normalization of well logs should be carried out in strict compliance with the corresponding differences in vertical resolution and depth of investigation.

Normalization of well logs along highly-deviated and horizontal wells cannot be accomplished with basic histogram-semblance corrections; well logs acquired in highly-deviated and horizontal wells can be greatly affected by borehole geometrical effects, formation dip, anisotropy (in the case of resistivity and sonic logs), and general 3D formation/borehole property variations within the volume of investigation of the instrument. Numerical modeling is usually required in the latter situations to assess well-log variability.

4.21 General Guidelines for the Interpretation of Well Logs

Even though there is not a general and universal procedure to interpret well logs, the following are practical guidelines to carry out rock evaluations from well logs:

1. Inspect the header of the logs to assess well trajectory, type of mud, depth range, pressure and temperature range, presence of barite in the mud, zones of abnormal pore pressure, and in general any extraordinary environmental variable that could have a measurable impact on well logs.
2. Inspect and study the mud logs (geological-control logs) to assess general lithology and types of fluids. Assess whether gas present in rock formations is biogenic or thermogenic; examine all geochemical footprints of fluids. Inspect all drilling variables contained in mud logs to ascertain variations in rock mechanical properties, pore pressure, etc.
3. Determine well-log acquisition systems and become familiar with the tool string(s) and specific modular components used to acquire the measurements. Assess whether multiple passes and runs were used to acquire the measurements.
4. Assess all borehole environmental properties, including size and borehole shape, variability of borehole fluids, abnormal cable tension and speed (e.g. stick-and-pull effects), and determine locations where well logs could be compromised because of abnormal caliper or cable speed/tension variations, or incorrect depth matching. Determine depth segments where core samples are available.
5. Become familiar with the global geological properties of rocks penetrated by the well, including geological age, depositional systems, tectonic processes, compaction, and diagenesis. Study outcrop analogs and evaluate formation tops. Inspect core samples if available. It is important to construct a mental image of the rocks and their geological background as early as possible in the interpretation of well logs.
6. Inspect available seismic amplitude measurements to appraise local structural features, tectonic embedding, presence of faults, strong seismic reflecting surfaces, and (whenever possible!) sedimentary structures and fluids.
7. Depth match all available logs and depth match core measurements with well logs. Correct defective well logs whenever possible and reliable. Determine and correct depth locations of available pore-pressure and fluid measurements.
8. Inspect well logs along the entire well trajectory to assess compaction zones, abnormal pore pressures, formation tops, etc., and in general to examine target reservoir intervals. Match formation tops and compaction zones with strong seismic reflectors.

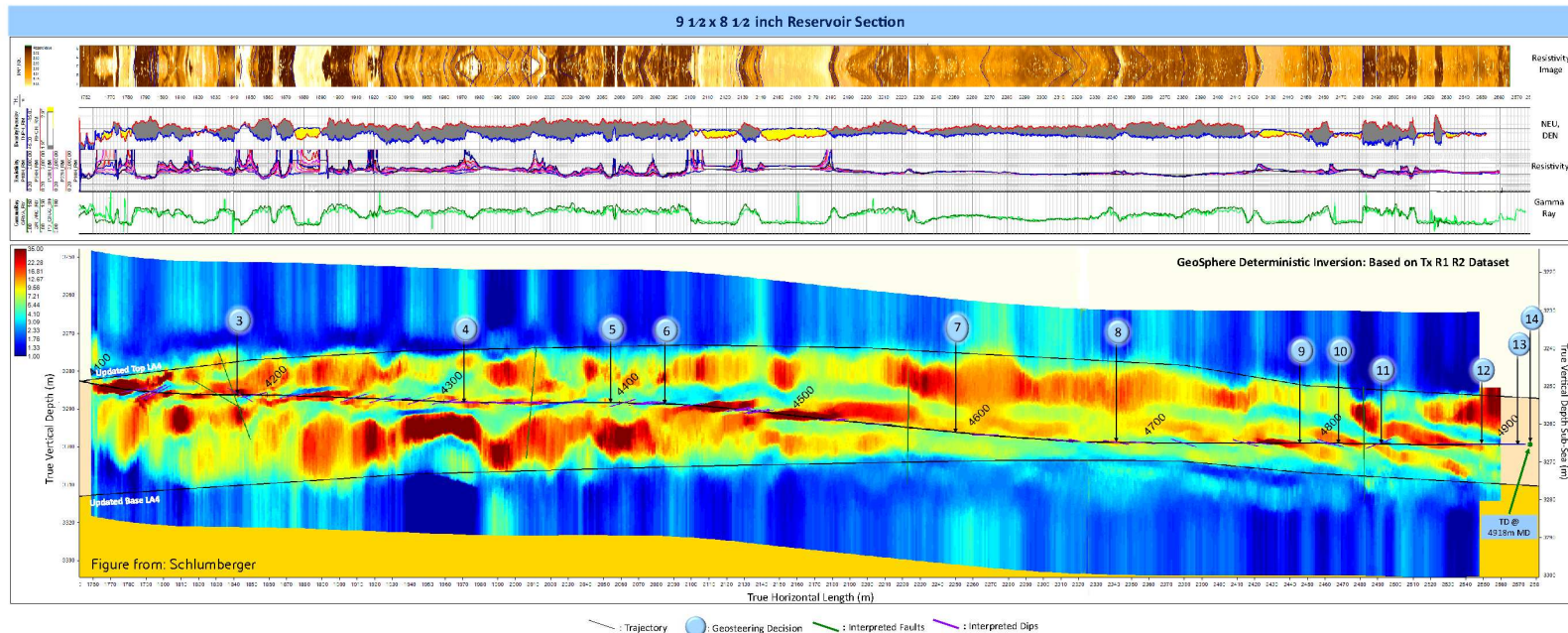
9. Determine possible reservoir units, shale sections, and pressure seals. In the case of siliciclastic sequences, determine and evaluate shale baselines and their affinity with shale present in sandstone units. In the case of carbonate or mixed (carbonate/siliciclastic) sequences, determine presence of likely pressure seals such as anhydrites, salt, low-porosity limestones, etc.
10. Assess the dip and azimuth of possible reservoir units and compare to outcrop analogs. Associate true dips and azimuths with sequence stratigraphy, sedimentary environments, and local tectonic embedding.
11. Determine types of fluids present in reservoir units and examine mud-filtrate invasion effects on well logs. Locate all water-bearing zones. Detect and examine permeable zones based on the effect of mud-filtrate invasion on well logs. Study fluid zones based on pore-pressure gradients, capillary pressure, and likely free water-hydrocarbon contacts.
12. Assess predominant mineral compositions of reservoir units. In the case of siliciclastic sequences, locate *pure shale* and *clean sandstone* end members of sedimentary sequences within formation tops. In the case of carbonate or mixed sequences, determine shale intervals and predominant carbonate/siliciclastic mineral composition. Verify and support the analysis of mineral compositions with mud logs and core data.
13. In multi-well development projects, perform well-to-well correlations to assess lateral extent and continuity of flow units.
14. Classify rock types based on their storage and flow capacities. Support the classification with core data, well logs, and geological footprint. If available, verify the classification with capillary transitions of water saturation, mud logs, and core data. Identified rock types will be treated separately when performing calculations of porosity, water saturation, and permeability (each rock type will be associated with a specific rock-physics model to transform well logs into petrophysical properties.)
15. Assess lateral extent of reservoir units and fluid zones (hydraulic communication) based on geological footprint, true dips and azimuths, well-to-well correlations, seismic amplitude data, pore-pressure gradients, well testing, and geochemical analyses of fluid samples.
16. Verify pressure seals and hydraulic compartments based on pore-pressure measurements, capillary pressure, and TVD variations of water saturation in the presence of active aquifers.
17. Evaluate elastic and mechanical rock properties based on sonic and density logs, and core data. Perform *in situ*/near-borehole stress, compaction, and pore-pressure analyses. Assess presence of anisotropy in elastic/mechanical properties and potential rock failure mechanisms during hydro-fracturing operations. Perform seismic-tie analysis (e.g. synthetic seismograms or detailed correlations with vertical seismic profiles) to verify estimated elastic properties.
18. Select locations to retrieve additional core plugs for laboratory measurements. Determine whether additional well logs and/or borehole measurements are needed for rock evaluation.
19. Rank all hydrocarbon units based on their storage and flow capacities, effective volume, production mechanism, and expected time depletion. This ranking will be used to plan and design perforation zones for further production testing. Convey this information to reservoir engineers for effective planning of production methods and facilities.
20. Plan completion and production methods and facilities, including the selection of hydro-fracturing intervals. Determine cemented and cased depth intervals. Quantify cement volumes. Assess perforation intervals and methods.
21. Plan and execute drill-stem and production tests. Verify results with prior assessments of fluid content, storage/flow capacities, effective volumes, and lateral hydraulic continuity.

22. Plan final production and workover operations and production facilities.
23. Plan future well interventions for time-lapse production monitoring and cleanup.
24. On to the next well/field!

4.22 The Future of Formation Evaluation Measurements

We have witnessed a rapid advance of borehole technology in the last few years. New and more compact instruments are now available to rapidly acquire relevant measurements in high-angle and horizontal wells to diagnose and quantify rock solid and fluid composition. Similarly, new and more reliable laboratory measurements of rock samples are possible to quantify petrophysical and mechanical properties under variable conditions of *in situ* stress and pore pressure. The rapid, almost exponential evolution of sensor and computer technology in the last decade has brought about new ideas for sorely-needed measurements and interpretation methods that can process millions of measurements in real time. Hopefully some of these developments will enable the direct and continuous measurement of flow-related properties such as permeability, capillary pressure, and relative permeability, i.e., *production-oriented formation evaluation* for both conventional and unconventional reservoirs.

One of the most exciting and interesting recent technological developments in formation evaluation is the acquisition of deep-sensing electromagnetic (EM) measurements while drilling. These measurements enable the detection of rock features (both petrophysical and geometrical) about and ahead of the drill bit anywhere between 10 to 50 ft, compared to 1 to 2 ft with LWD resistivity measurements. Figure 4.22.1 is an example of LWD and deep-sending EM measurements acquired along an undulated horizontal well in the North Sea. The original 3D well trajectory was planned based on available information (including seismic amplitude data) but adjusted in real-time with the influx of LWD and deep EM measurements to target relatively thin hydrocarbon-bearing layers along a spatially heterogeneous and faulted turbidite sedimentary sequence. The upper panel of Figure 4.22.1 shows the conventional LWD logs, which include a borehole image emphasizing the great variability of sandstone/shale layer thicknesses and associated relative dips. Deep-sensing resistivity values shown in the lower panel of the same figure with a color-coded scale (red and blue colors denote high and low values of electrical resistivity, respectively) indicate with unprecedented spatial resolution the vertical and lateral extent of those layers, presence of faults (and potential reservoir compartments across them), additional hydrocarbon-bearing sandstones, bounding shales, and hydrocarbon-water contacts. The combination of deep-sensing borehole EM measurements and seismic amplitude data enable the construction and/or verification of high-resolution reservoir models for improved prognoses of production via reservoir history matching. In other words, deep borehole EM measurements promote a better and closer connection between formation evaluation and reservoir engineering because of their common rock volume of investigation. Deep borehole EM measurements also foster production-oriented drilling practices which target reservoir zones with a well trajectory that is optimal for completions and production.



Chapter 5

“Bistro” or “Quick-Look” Interpretation of Well Logs

...To produce a mighty book, you must choose a mighty theme. No great and enduring volume can ever be written on the flea, though many there be who have tried it...
—Herman Melville, Moby-Dick; or, The Whale.

The word *bistro* in Russian (быстро) means *quick* and is here used to refer to the “first pass” commonly performed to interpret well log on site. As much as possible, procedures for well-log interpretation should include verification against rock properties measured in the laboratory, core measurements, mud logs, thin sections, outcrop analogues, and any other contextual information associated with the geological depositional environment and rock fabric under consideration.

There are several procedures published in the well-logging literature that attempt to provide a “cook-book” recipe approach to the interpretation of well logs using over-simplified petrophysical response models. Even though these methods provide a “bistro” or “quick-look” analysis for initial entry into a more formal petrophysical assessment, attention should be paid to potentially damaging mistakes that could condemn the viability of the reservoir because of erroneous conclusions about, for instance, marginal hydrocarbon reserves (net pay).

The standard sequence of interpretation procedures for “bistro” log interpretation is as follows:

1. Flagging of depth segments along the well where measurements could be inaccurate and/or unreliable,
2. Calculation of a temperature log,
3. Diagnosis of whether one is dealing with a siliciclastic or a carbonate rock sequence,
4. Calculation of volumetric concentration of shale if one is dealing with a siliciclastic sedimentary sequence.
Diagnosis of elemental grain constituents and quantification of their volumetric concentrations for the case of complex carbonate sequences,
5. Calculation of total porosity assuming one type of fluid (one fluid density) and one type of grain composition (one grain density),
6. Assumption of null residual hydrocarbon saturation and calculation of formation water resistivity within a water-saturated zone; extrapolation to all depths in the well (temperature extrapolation), and
7. Assumption of constant values of Archie’s parameters and calculation of hydrocarbon saturation in porous and permeable zones. In siliciclastic sedimentary sequences, winnowing out of shale sections in the calculation based on a pre-specified cut-off applied to volumetric concentration of shale.

Subsequently, it will be explained why the above method, albeit simple, can often get a naïve petrophysicist into deep technical trouble. As emphasized earlier, it is imperative that interpretation methods be specialized to specific formations with prior picking of formation tops. Archie's parameters, for instance, should be measured and implemented for specific rock types. Estimation of electrical resistivity of formation water should be performed separately for fluid zones that are hydraulically connected. Moreover, the calculation of hydrocarbon saturation and fluid densities should be consistent with measured *in situ* fluid pressures.

5.1 “Gluing” Multiple Well Logs

As emphasized earlier, not one single well log bears all the information needed to assess rock properties. It is necessary to combine all the available logs, core data, and geological information to quantify petrophysical and geomechanical properties, and saturating fluids. Likewise, **it is important to recall that not all the information necessary for well-log interpretation is usually found at one single measurement point**. The analysis requires that measurements acquired at different points be compared to diagnose variations of shale concentration, porosity, and saturating fluids. An effective way to perform the qualitative inspection is to bear in mind two very simple equations. One is the relationship between bulk density, ρ_R , and porosity, ϕ given by

$$\rho_R = \phi \rho_f + (1 - \phi) \rho_m, \quad (5.1.1)$$

where ρ_f and ρ_m are fluid density and matrix density, respectively, whereupon,

$$\phi = \frac{\rho_m - \rho_R}{\rho_m - \rho_f}. \quad (5.1.2)$$

The latter relationship implies that **an increase in rock density causes a decrease of porosity and vice versa**, provided that both fluid density and matrix density remain constant.

Archie's equation (Archie, 1942) is the second important relationship, given by

$$R_t \approx R_w \frac{a}{\phi^m} \frac{1}{S_w^n}, \quad (5.1.3)$$

where R_t is the rock's electrical resistivity, R_w is the electrical resistivity of formation water (which depends on electrolyte concentration and temperature), S_w is water saturation, and a , m , and n are fitting constants usually inferred from core data but which remain unchanged with equal rock texture. It follows that

$$S_w \approx \left(\frac{R_w}{R_t} \frac{a}{\phi^m} \right)^{\frac{1}{n}}. \quad (5.1.4)$$

This last set of equations imply that an increase of rock's electrical resistivity could be due to a decrease of porosity or a decrease of water saturation (i.e., an increase of hydrocarbon saturation), under the assumption that R_w and rock texture do not appreciably change. Similarly, they indicate that a decrease of rock's electrical resistivity could be due to an increase of porosity or an increase of water saturation (i.e., a decrease of hydrocarbon saturation). It is necessary to simultaneously inspect the gamma-ray, density, and resistivity logs to ascertain whether the change of electrical resistivity was due to either a change of porosity or a change of water saturation. This is done by selecting two measurement points for inspection, one of them used as reference. What the two relationships above imply is the following:

1. If the gamma-ray and density logs remain constant but the rock's electrical resistivity increases with respect to that at the reference point, then most likely S_w has decreased, i.e., hydrocarbon saturation has increased at the latter point.
2. If the gamma-ray and density logs remain constant but the rock's electrical resistivity decreases with respect to that at the reference point, then most likely S_w has increased, i.e., hydrocarbon saturation has decreased at the latter point.

3. If the gamma-ray log remains constant but the rock's electrical resistivity increases, this behavior could be due to a decrease of porosity, i.e., an increase of rock density. It is necessary to verify that the increase is not due to a decrease of porosity (an increase of density) before concluding that the increase of electrical resistivity is due to an increase of hydrocarbon saturation.
4. If the gamma-ray log remains constant but the rock's electrical resistivity decreases, this behavior could be due to an increase of porosity, i.e., a decrease of rock density. Before concluding that the decrease of electrical resistivity is due to a decrease of hydrocarbon saturation it is necessary to verify that the decrease is not due to an increase of porosity (a decrease of density).
5. A decrease of rock porosity can be usually verified with a decrease of sonic slowness (the rock becomes more rigid); conversely, an increase of rock porosity can be usually verified with an increase of sonic slowness (the rock becomes less rigid).
6. Changes of fluid density can be usually verified with the combined behavior of density and neutron logs; for instance, with no variations in matrix density, it is usually the case that the neutron-density crossover increases with a decrease of fluid density.
7. It is important to always compare points to equal values of gamma ray because some of the changes in rock density, rock's electrical resistivity, neutron porosity, and sonic slowness could be due to variations of shale concentration.

5.2 Correlations Between Well Logs

Because of the rock property relationships described in the previous section, it is usually the case that well logs exhibit a certain type of point-by-point correlation among them, which is chiefly governed by shale concentration, porosity, and water saturation. In siliciclastic sequences, for instance, relative (local) minima and maxima of gamma-ray logs are indicative of presence of sandstone and shale layers, respectively. Within sandstone layers, the minima of gamma-ray logs could be positively or negatively correlated with resistivity logs.

A **positive correlation** between two given well logs occurs when their local minima and maxima are aligned, i.e., when their minima and maxima are *depth matched*, minima with minima and maxima with maxima. Conversely, a **negative**, or **mirror-image** correlation between two well logs takes place when the local minima (maxima) of one of the logs are depth matched with the local maxima (minima) of the other log. The correlation between gamma-ray and electrical resistivity logs is often positive in high-porosity sandstones with 100% saturation of salty formation water. However, the correlation between the two logs becomes negative in cases of fresh formation-water saturation or low-porosity sandstones. Changes in correlation between gamma-ray and resistivity logs often take place between water and hydrocarbon saturated sandstones. In fact, very often, the point where the change in correlation takes place is used to locate the free hydrocarbon-water contact.

5.3 Diagnosis of Lithology

One of the first steps of log interpretation consists of identifying types of rocks. Specific procedures for the interpretation of well logs depend on whether one is dealing with clastic, carbonate, mixed rock sequences, or unconventional hydrocarbon-bearing formations. More detailed descriptions of rocks include presence of fractures, diagenetic alterations, and presence of volcanic matter, coal, etc., to name a few.

The following is a list of possible lithology types:

1. Clastic depositional sequences: require the quantification of clay/shale volumetric concentration and/or detection and quantification of types of clays/shale and of their spatial distribution in the pore space (e.g. dispersed, structural, or laminated),

2. Carbonates: require the calculation of volumetric concentrations of limestone, dolomite, anhydrite, halite, quartz, shale, etc., as well as of the quantification of connected and non-connected porosity,
3. For mixed lithologies: a possible method used to assess volumetric concentrations of rock constituents is described in section 11.5, and
4. For shales: assess whether they are laminated, dispersed, or structural, using a Thomas-Stieber diagram.
5. Unconventional hydrocarbon-bearing formations: they exhibit negligible permeability and require the assessment of volumetric concentration of organic content, type and maturity or organic content, *in situ* stresses, pore pressures, and geomechanical properties.

5.3.a Some practical pointers for beginners

Even though well-log interpretation can, at times, be exceedingly complex, to the point of requiring sophisticated modeling software and diverse core measurements for accurate assessment of petrophysical properties, there are simple steps to follow to detect interesting reservoir units and to quantitatively assess their porosity and hydrocarbon saturation. A basic set of guidelines for beginners is as follows:

1. Determine the type of drilling mud and well trajectory (e.g. vertical, deviated, or horizontal well) and assess possible abnormal borehole conditions based on maximum logging depth, maximum recorded temperature, and maximum mud weight. Evaluate the caliper log to detect locations where well logs could be compromised in quality and reliability.
2. Examine the gamma-ray log and determine whether it reliably responds to presence of shale. Within the depth zone of interest, determine specific minimum and maximum gamma-ray values and search for patterns of variability and repetition that could be indicative of sedimentary features and depositional environments. Look for “pure” shale end members in the sedimentary sequence. Graphically (or mentally!) trace the shale baseline along the different log tracks.
3. Based on the gamma-ray log and the shale baseline for the different logs, detect possible reservoir units and qualitatively determine their degree of “shaliness.” Assess whether some of these sandstone units could be water saturated based on the shale baseline on the deep apparent resistivity log (this step is not trivial in the case of fresh formation water).
4. Inspect the available apparent resistivity logs (shallow-, medium-, and deep-sensing) across the detected reservoir units to recognize signs of mud-filtrate invasion. Pay special attention to the specific values and differences between apparent resistivity logs across the various previously detected reservoir units.
5. Concomitantly with the previous two steps, inspect the density log to *qualitatively* assess and rank the porosity of the various reservoir units detected with the gamma-ray log. Recall that bulk density and total porosity are linearly related but vary inversely with respect to each other, i.e. bulk density increases when total porosity decreases, and bulk density decreases when total porosity increases. This step makes the tacit assumption that the densities of fluid and solid constituents remain constant when making the comparison. Pay special attention to both density and deep apparent resistivity logs acquired in water-saturated sandstone units.
6. Making *qualitative* use of Archie’s equation (Archie, 1942), determine whether an increase of apparent electrical resistivity in existing reservoir units was due to a decrease of porosity or a decrease of water saturation. Assuming that the electrical resistivity of formation water remains constant in the comparison (constant electrolyte type and concentration, and constant temperature), Archie’s equation states that the electrical resistivity of a rock increases with either a decrease of (inter-connected) porosity or a decrease of water saturation. Conversely, the electrical resistivity of a rock decreases with an increase of (inter-connected) porosity or an increase of water saturation. To separate the effects of porosity and

water saturation on electrical resistivity, select two or more reservoir units that exhibit approximately the same gamma-ray and density values and then inspect their apparent electrical resistivities. If there are differences between the apparent electrical resistivities of the selected reservoir units, most likely, those differences will be due to differences in water saturation. Determine which of the selected reservoir units exhibit the largest water saturation based on their differences in apparent electrical resistivity.

7. Making *qualitative* use of Archie’s equation, reconcile the variations of shallow-, medium-, and deep-sensing apparent resistivity in reservoir units with porosity, presence of invasion, type of mud filtrate (oil- or water-based mud filtrate) and pre-invasion water saturation.
8. Determine possible free water-hydrocarbon contacts and assess whether the variations of apparent electrical resistivity across reservoir units located above the contacts could be due to capillary transitions.
9. In the presence of reservoir units encountered at a state of irreducible water saturation, permeability is inversely related to irreducible water saturation and directly related to porosity. Therefore, under the very restrictive assumption of a state of irreducible water saturation, when two reservoir units exhibit the same porosity (and the same degree of shaliness) but different deep apparent resistivities, the reservoir unit that exhibits the largest apparent electrical resistivity will exhibit the lowest irreducible water saturation and, consequently, the largest permeability. Use this very simple interpretation principle to rank the detected reservoir units in the hydrocarbon zone and *qualitatively* compare their permeabilities.

5.3.b Some additional important truisms about formation evaluation

- In formation evaluation, not all the answers/data are found at the same depth. The estimation of rocks properties from well logs at any given depth often requires the analysis and/or comparison of well logs acquired along other depth segments and/or in other neighboring wells. For instance, the evaluation of hydrocarbon-bearing rocks from well logs is usually supported by the evaluation of well logs across water-bearing depth segments.
- All calculations performed from well logs need to be verified with core measurements or other alternative sources of information (e.g., mud logs, drilling measurements, etc.), especially in key wells.
- All calculations need to be consistent with both the 3D geological context (i.e., location of the well in the 3D geological structure, sedimentary environment, diagenetic and tectonic imprint, etc.) and the fluid context (i.e., the effect of gravity and capillary pressure and imbibition-drainage on the spatial distribution of fluids, PVT fluid properties, temperature, pressure, pressure gradients, presence of pressure seals, etc.)
- The variability of well logs with respect to either time (e.g., LWD vs. wireline) or radial length of sensitivity (e.g., shallow- vs. deep-sensing electrical resistivity) provides an indirect means to diagnose or assess flow-related petrophysical properties such as permeability, and saturation-dependent capillary pressure/relative permeability.
- The acquisition of borehole measurements should be planned not only to assess storage properties of rocks but also their dynamic properties with the intent to assess the rock’s production potential under primary or enhanced recovery conditions.
- The interpretation of well logs and core measurements should be performed with some notion of the reservoir production mechanism (i.e., aquifer drive, gas solution drive, etc.) in mind. This condition helps the interpreter to focus and adapt the target and ultimate use of his/her calculations and assessments performed from well logs, core data, pressure and fluid measurements, etc.

5.4 Drill-Stem Testing, DST

Drill-stem testers (DSTs) are used to assess initial flow and fluid conditions of rocks along short segments of the drilled well. This test is performed after the well is cased and/or completed. To that effect, a short segment of the well (usually a few feet long) is hydraulically isolated from the rest of the well with inflatable packers. The same segment has been previously perforated to ensure hydraulic communication between the well and the adjacent rocks. Those segments along the well selected for DSTs have been previously designated as promising reservoir segments based on mud logs, rock cutting, well logs and core samples (when available). The objective of DSTs is to verify and quantify initial flow conditions. After the segment of the well has been hydraulically isolated from the rest of the well, a pump is used to withdraw fluids from the rocks into the well under variable operational conditions of pressure and/or flow rate. The collected fluids are brought to the surface with a dedicated small pipeline to detect type of fluids and their volumetric concentrations as a function of time after the inception of pumping.

Even when hydrocarbons are detected via mud logs and/or well logs, there is no guarantee that they will flow at economically viable rates and volumes when commercial production begins, especially when (a) the rocks are pressure depleted, or (b) the rock-fluid conditions are close to residual hydrocarbon saturation, and/or (c) rock permeability is low. Low flow rates and volumes detected by DSTs may also indicate that commercial fluid production can only be achieved with stimulation techniques such as hydraulic fracturing and/or acidification, for instance. Furthermore, DSTs are valuable to verify zonal isolation and wellbore integrity (resulting from proper well-completion practices, i.e. well casing and cementing).

When flow rates, volumes, and stimulation techniques quantified with DSTs are found not commercially viable, the tested well segment is plugged to re-establish hydraulic isolation with the rest of the well.

5.5 *In Situ* Pressure Measurements

One of the most important borehole measurements is the assessment of *in situ* pore (fluid) pressure. There are two pressure measurements necessary for practical engineering consideration: *overburden pressure*, i.e., the pressure resulting from the weight of the sedimentary column and lateral stresses, and *pore pressure*. A rock is in pressure equilibrium when the overburden pressure is equal to the pore pressure. An over-pressure condition arises when the pore pressure is higher than the overburden pressure, while an under-pressure (depletion) condition arises when the pore pressure is lower than the overburden pressure. Over- and under-pressure regimes are the result of temporal (transitional) or permanent non-equilibrium conditions due to either lack of pressure communication (hydraulic communication), and/or non-negligible solid/fluid compressibility.

Measurements of pore pressure are typically performed with a **Formation Tester**, which is a mini-DST equipped with a small-volume pump and fluid pressure sensors. They are commonly acquired before the well is cased and completed (either during or after drilling), although there are sophisticated instrumentation versions capable of drilling a hole through casing and cement to establish hydraulic communication with rocks in cased/completed wells. Formation testers perform stationary measurements wherein the tool is positioned at a predefined borehole location and a mechanical arm is extended to establish hydraulic communication with the formation via a small orifice (typically less than half-an-inch in diameter). A pump then begins to withdraw fluids from the rocks at a pre-specified flow rate and the collected fluids brought through a small pipe to the inside of the tool where a pressure sensor measures the total fluid pressure as a function of time from the inception of pumping (pressure draw-down regime). Next, the pump stops its action and the fluid inside the small pipe is allowed to pressure equilibrate with the fluid in the rock (pressure buildup regime). This operation is repeated a few times (a few repeat cycles of pressure draw-down and pressure buildup) until the pressure measured at equilibrium conditions (at the end of the pressure buildup cycle) no longer changes. Because of the relatively small volumes of fluid involved in the operation of formation testers (typically a fraction of a cubic centimeter) the measurement can be completed anywhere from a few minutes to a few hours depending on the rock permeability (short and long pressure buildup times are necessary to achieve pressure equilibrium conditions in high- and low-permeability rocks, respectively). In fact, the time evolution of pressure draw-

down/buildup measurements is often used to estimate rock mobility. Measurement cost increases with time of acquisition for obvious reasons. Figure 5.5.1 is a photograph of a modern wireline formation tester showing the clamping pistons used to position the tester in contact with the borehole wall, and the small orifice used to withdraw small volumes of fluid from the formation.

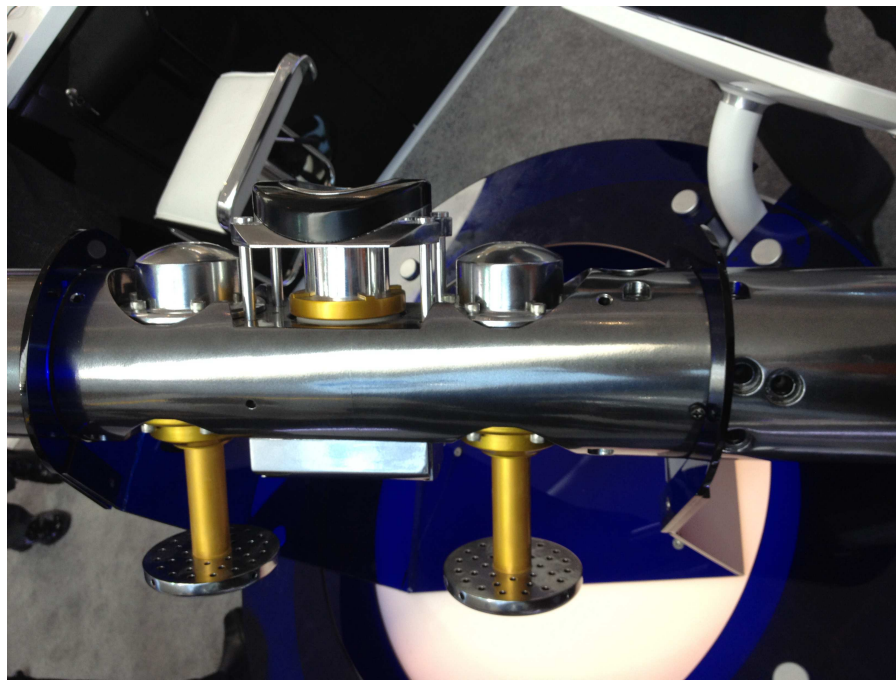


Figure 5.5.1: Photograph of a wireline formation tester. One of the primary functions of formation testers is to measure pore pressure based on draw-down and build-up pressure transients established with a pump drawing small volumes of fluid from rocks adjacent to the borehole. Formation testers include a pump, a fluid receptacle, and small orifice pressed against the borehole wall through which the pump establishes hydraulic communication with the fluids in the rocks.

Some formation testers can also measure the type(s) of fluids entering the tool via optical and other physical principles in real time as fluid pumping takes place. At the beginning of pumping, most of the fluid entering the tool is mud filtrate. With time of pumping, the relative concentration of pre-drill (*in situ*) fluid increases. When fluid sensors indicate that the degree of fluid contamination (i.e. the relative concentration of mud filtrate) is negligible, then the tool proceeds to acquire fluid samples which are stored in special containers designed to maintain *in situ* pressure and temperature conditions for further laboratory analysis uphole (e.g., measurements of composition, density, viscosity, PVT phase transitions, miscibility, etc.) Depending on permeability and relative permeability (fractional flow rates), the acquisition of clean (non-mud-filtrate contaminated) fluid samples may take anywhere from a few minutes to a few hours.

Figure 5.5.2 shows an example of tens of pore pressure measurements acquired with a formation tester in an offshore vertical well penetrating a turbidite sedimentary sequence (Andrew field, North Sea). There are three distinct pore-pressure gradients indicated by the pressure measurements and corresponding to water, oil, and gas depth zones from the bottom to the top of the well, respectively.

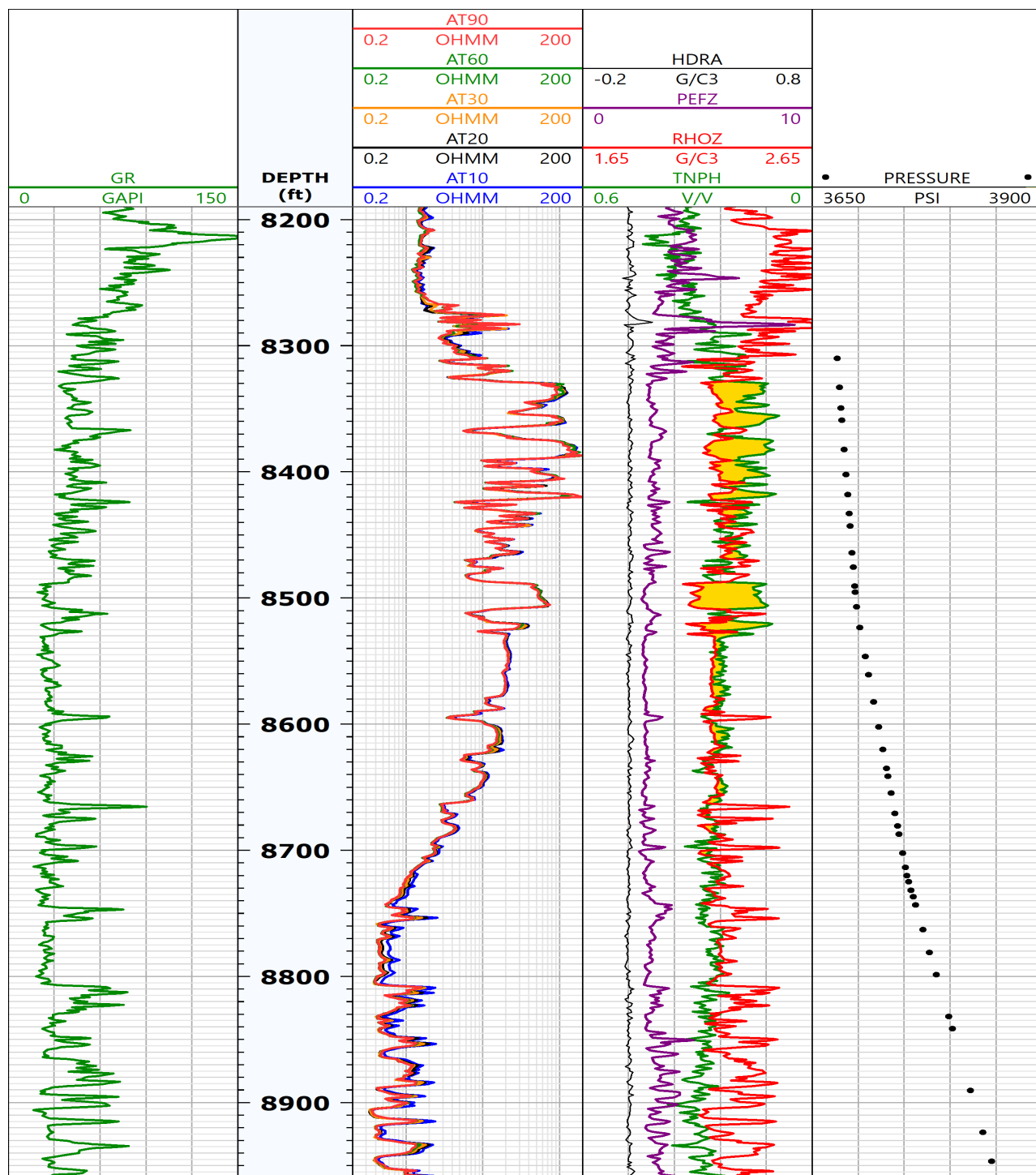


Figure 5.5.2: Example of well logs and pore pressure measurements acquired in a vertical well across an offshore turbidite sedimentary sequence (Andrew Field, North Sea). Track 1 is gamma ray. Track 2 is depth. Track 3 is electrical resistivity (multiple radial lengths of investigation). Track 4 is density, density correction, apparent neutron porosity, and photo-electric factor (PEF) logs. Track 5 is pore pressure (psi). Pore pressure gradients indicate the presence of water, oil, and gas depth zones from the bottom to the top of the well, respectively.

Chapter 6

Common Borehole Instruments and their Measurements

...A man of genius makes no mistakes. His errors are volitional and are the portals of discovery...

– James Joyce, Ulysses.

Excellent books abound concerning detailed engineering descriptions of instruments (tools) used for the acquisition of borehole geophysical measurements. The intention of this chapter is to provide the minimum information about borehole instruments and their principles necessary for measurement interpretation. In addition to knowing about the physical principle of operation, it is important to know when the instrument delivers reliable, accurate, and useful measurements, and when it does not.

6.1 Spontaneous Gamma-Ray Measurements

One of the main applications of spontaneous gamma-ray borehole measurements is to diagnose and quantify presence of clay/shale in rocks.

Rock formations may contain radioactive elements within their solid and fluid components. In addition to α particles, β particles, and neutrinos, gamma rays are spontaneously released by radioactive earthen materials. The detection of gamma rays is preferred in borehole operations over the detection of α and β particles and neutrinos to diagnose and quantify radioactive elements because of their null electric charge, hence deeper radial length of investigation compared to α and β particles.

Gamma rays are photons, which have no mass and no electric charge; they are pure energy carriers. Their intrinsic energy, E is given by Planck's equation,

$$E = \hbar \cdot \nu ,$$

where \hbar is Planck's constant and ν is frequency. Thus, gamma rays originate in a wide spectrum of are defined by energy (or, equivalently, frequency). A typical “burst” of gamma rays will include a *spectrum*, or range of energies/frequencies. The specific spectrum (energies/frequencies and their relative count rates) will depend on the radioactive element from which they emanate.

Well-logging operations measure gamma-ray activity specifically within the energy spectra of thorium (Th), uranium (U) and potassium (K). Detectors consist of light-sensing scintillators (photo multipliers included) that “count” the number of gamma rays per unit time for a specific energy “window” (or energy/frequency range, or band). The count of gamma rays impinging upon the detector per unit time is referred to as *count rate*. There are two possibilities for measurement acquisition: one is to measure the gamma-ray count rate for the combined spectrum of Th, U, and K, which gives rise to the standard gamma-ray log. The second possibility is to measure gamma-ray count rates *separately* for the energy spectra of Th, U, and K, thereby

giving rise to three separate well logs which are often referred to as *spectral gamma-ray logs*. While gamma-ray scintillators sense gamma rays reaching them from all azimuthal directions, gamma-ray tools are designed to operate in contact with the borehole wall for maximum formation sensitivity in the presence of large boreholes and heavy mud weight.

Gamma-ray count rates are transformed to normalized units, designated gAPI units (standard of the American Petroleum Institute) that span the interval between 0 and no more than 250 in most practical situations. In addition, sensors are calibrated against standard artificial rock formations located at the University of Houston to transform gamma-ray counts into universal gAPI values.

One important consideration in gamma-ray acquisition is the speed of logging. The probability of a given number of gamma rays to be spontaneously released by a radioactive element during a given period of time is governed by Poisson's probability distribution. Because of instrumental considerations, gamma-ray count rates need to exceed a measurement noise threshold for reliable acquisition. Both Poisson's probability distribution and the size of the detector determine the time necessary for such a count rate to be reached during logging. The time of count-rate acquisition will limit the speed of logging. Excessive logging speeds will cause gamma-ray logs to exhibit abnormally low values and abnormal transitions between adjacent beds.

The reason why gamma-ray count rates are acquired specifically within the energy spectra of Th, U, and K to produce the standard gamma-ray log is because the half life of these naturally-occurring radioactive elements is close to the age of the earth. Such elements exist as impurities in the crystalline structure of most clays in such a manner that gamma-ray count rates can be correlated with the rock's volumetric concentration of clay. This explanation does not mean that sandstones are free of Th, U, and K. Spectral gamma-ray logs acquired across clay-free sandstones are seldom zero. The important fact to emphasize here is that the volumetric concentration of these three elements is normally larger in clays/shales than in clean (clay-free) sandstones.

Clays are the result of prolonged periods of chemical weathering, mechanical weathering, and diagenesis of rocks, usually spanning time cycles of millions of years. The chemical composition and crystalline structure of clays is adapted to endure the large chemical and physical variations associated with chemical and mechanical weathering and diagenesis. It is often said that a recently created rock will eventually "metamorphose" into clay when subject to long periods of diagenesis and/or weathering (some layman explanations for the existence of clays use the analogy of Darwinian adaptation of rocks when subject to weathering and diagenesis, whereby clays are the ultimate result of the adaptation and hence are better fitted to withstand further weathering and diagenesis). If at the onset of this long process the rock contains volumetric concentrations of several radioactive elements, as time progresses only those radioactive elements with long half lives will remain in the rock. Radioactive elements with relatively short half lives will be transformed into other residual elements stemming from radioactive decay. The *only* original radioactive elements which endure the long time cycles of weathering and diagenesis undergone by rocks are the ones whose half lives are comparable to the duration of those time cycles. Radioactive elements with the longest half lives are precisely Th, U, and K, thereby explaining why the gamma-ray energy spectra of these three elements are the ones used in well-logging operations to diagnose and assess volumetric concentration of clay/shale in rocks.

The chemical composition of clays is chiefly aluminum (Al), oxygen (O), and silicon (Si). Coincidentally, these are the most abundant elements in the Earth's crust. Clays are minerals with a very stable, organized, and repetitive crystalline structure consisting of individual tetrahedra and octahedra. The "stacking" of individual clay units creates repetitive growth patterns akin to the stacking of bricks to construct a wall. In close analogy, the "mortar" between bricks in the wall may consist of water layers, specific chemical elements, and even impurities. Clays may appear in the pore space of rocks because of "mixing" of clay and grains that accompanies the process of sedimentation itself. The name *exogenic clays* is normally used to designate this type of clay minerals. However, clays can also originate *in situ* when the rock is subject to gradual increases of temperature and pressure because of burial and weight of overlying sediments (diagenesis). In such cases, rock grains may transform into clays, either partially or completely. Clay minerals which originate *in situ* are usually referred to as *authigenic clays*. Chlorite is one common example of the transformation of feldspathic grains into grain-coating clay. In addition, diagenesis may also "metamorphose" one type of clay into another type of clay which is more stable under the new conditions of pressure, temperature, and ambient chemical

composition. For instance, increase of both pressure and temperature may cause chlorite to transform into kaolinite and subsequently into illite.

Interpretation problems arise when naturally occurring rock grain minerals which are not clays comprise relatively large volumetric concentrations of either Th, U, or K. The case of arkose sandstones is an example where their feldspathic composition includes abnormally large concentrations of K because of the rapid deposition and burial of rocks in close proximity to the igneous rock source. Some evaporites may include abnormally large concentrations of K. There are also cases of thorium-rich grains in sandstones originated from batholithes and deposited and buried closed to the source rock. Uranium-rich sandstones may also occur in the presence of coal or other organic material. The only way to avert these abnormal and potentially damaging conditions in the interpretation of gamma-ray logs is to acquire spectral gamma-ray logs instead of standard gamma-ray logs.

Geologists make use of the gamma-ray log to diagnose grain size and variations of grain size across rock units. This is a widely used method to study some of the depositional characteristics of sedimentary rock units, including coarsening-up and coarsening-down sequences that mark the spatial evolution, migration, and accommodation of sediment deposition. While it is true that in most cases the gamma-ray log correlates with grain size (the larger the value of gamma-ray reading the smaller the particle size), attention should be exercised to avert pathological cases in which large grain sizes could have large amounts of clay.

6.1.a Environmental corrections of gamma-ray logs

Borehole environmental corrections of gamma-ray logs are important when comparing measurements acquired in several wells within the same hydrocarbon field. If environmental corrections are not applied, variations of gamma-ray readings across wells could be wrongly interpreted as due to variations of clay content when in fact they are due to variations of borehole size, mud weight, etc. Often, well-log analysts transform gamma-ray readings into a so-called *shale index* in an effort to reduce the effect of environmental corrections. This latter approach is only a partial remedy. An alert well-log analyst would calculate histograms of gamma-ray readings for individual wells and would compare the histograms of all the wells involved in the analysis. Large variations in the properties of histograms (mean, standard deviation, skewness, long non-symmetric tails, etc.) not due to clay-content variations between wells will be diagnostic of variable borehole environmental conditions.

The following is a list of environmental corrections applied to gamma-ray logs:

- Borehole size,
- Tool standoff,
- Mud weight (especially with the presence of barite),
- Temperature, and
- Presence of potassium in the mud.

6.1.b Additional applications of spectral gamma-ray logs

Spectral gamma-ray logs can be used to diagnose the specific group of clay minerals contained in shale. This diagnosis is performed with cross-plots of the three spectral gamma-ray logs (Th, U, and K). Depending on the relative values of the three logs, logging companies prepare and distribute charts that describe zones in the cross-plots pertaining to specific groups of clay minerals, or combinations of clay minerals, as well as grain compositions with abnormal concentrations of the three radioactive elements. The diagnosis of specific groups of clay minerals on occasion permits one to draw conclusions about the history of sedimentation and diagenesis undergone by the rock.

Another important cross-plot used for clay-mineral identification (and possibly grain composition) is the one constructed with PEF (photoelectric factor) and spectral gamma-ray logs.

Spontaneous potential is a DC (zero frequency) electrical potential (customarily expressed in the units of mV) that is measured along the trajectory of the well and that originates from differences in salt concentration between mud filtrate and formation water. Presence of oil-base mud (which does not have the ability to dissolve salt) completely suppresses and hence renders SP measurements useless. Likewise, presence of hydrocarbon in rock formations suppresses SP measurements. Spontaneous potentials can be either positive, negative, or zero.

SP measurements are acquired with a voltmeter that connects two contact electrodes. One of these electrodes is located at the end of the tool string while the other is grounded at the surface. As the tool string moves through the well and across rock units, the voltmeter records the potential difference between the ground electrode and the electrode located at the end of the tool string. These electric potential differences are due to the presence of spatial distributions of surface electric charge along the borehole wall.

Logging companies do not charge for the acquisition of SP measurements given their often low reliability (for instance, the placement of an “electrically stable” contact electrode on the ground could be impaired by steel pipes, electric generators, etc., and could be nearly impossible to secure in offshore or lake operations). However, in the past, SP measurements were routinely employed to detect and quantify porous and permeable beds. In combination with gamma-ray measurements, SP measurements diagnose the mobility of ions contained in the aqueous phase of porous and permeable beds. Ion mobility is affected by presence of clay and hydrocarbon, thereby providing an alternative way to diagnose shaly and hydrocarbon-bearing rock units.

The mobility of ions contained in the aqueous phase of porous and permeable rocks is governed by temperature, salt concentration, and pore connectivity. Spontaneous potentials arise when two aqueous solutions with different ionic concentrations (e.g. NaCl) are placed in contact through a porous, ion-selective membrane (also called semi-permeable membrane). The natural tendency of ions is to “migrate” from the solution with large ionic concentration to the solution with low ionic concentration. This behavior is the underlying “engine” of the ion migration system. Even though positive charge is always balanced with negative charge, the selectivity of ions by the membrane (the semi-permeability of the membrane) will give rise to a spatial separation of electric charge. In turn, such a separation of electrical charge will give rise to a net non-zero electric field which will be sensed by the SP downhole electrode. In the borehole, the regions of separated electrical charge will occur at or near the borehole wall.

One of the main uses of SP measurements in well logging is the calculation of the electrical resistivity of formation water. As described below, the latter quantity is one of the crucial parameters required for the calculation of water saturation from electrical resistivity measurements.

In saturated porous media, there are three mechanisms whereby ions can selectively migrate from one aqueous solution to another:

- Ion diffusion potential,
- Membrane potential, and
- Electrokinetic (streaming) potential.

Diffusion potentials arise because the porous medium that connects the two aqueous ion solutions (mud filtrate and formation water) offers a preferential path to the smallest of the two hydrated ions in solution (for the case of NaCl aqueous solution, hydrated chlorine has the smaller molecular radius). This ion-selection mechanism (ion-size selection) causes a spatial separation of negative and positive charges whereby there is accumulation of non-zero net electrical charge on the boundaries between porous media and ion solutions.

For the case of membrane potential, clay/shale plays the role of an ion-selective membrane when placed between the two aqueous solutions with different ionic concentrations. Dry clay exhibits a net negative electric charge because of (a) irregular terminations of its crystal lattices that permit steady-state, spontaneous ion passage in one preferential direction, and (b) spontaneous replacements of Al, Si, and Mg atoms in the lattice. When placed in contact with NaCl solutions, water molecules will be attracted to the surface of dry clay because of the interaction between the dipolar Van der Walls forces of water and the net negative electric charge of

clay. Water dipoles will orient themselves with the electric field imposed by the “stack” of negative electric charge surrounding dry clay and will bind to it. Such phenomenon creates a mono-layer of water around clay crystals and is responsible for clay-bound water saturation.

Solute Na ions in water exist in hydrated form wherein six molecules of water surround one single Na molecule. A similar situation occurs with Cl ions. The hydration of ions explains why water can only dissolve a maximum amount of NaCl at given pressure-temperature conditions. Hydrated Na ions will be attracted to the surface of clay because of the affinity of their positive electric charge with the negative electric charge of dry clay. Thus, hydrated Na ions will “stack” over water molecules already attached to dry clay, thereby creating a diffuse, mobile “cloud” of net positive electric charge. Often, the combination of the spatial distribution of net negative electric charge on the boundary of hydrated clay and the cloud of positive electric charge of hydrated Na ions within the aqueous phase surrounding dry clay is referred to as “double layer” (the term “double layer” is intended to designate the close proximity of individual, separate layers of negative and electric charge; however, the term is not precise because it implies discontinuous thin surfaces of opposite electric charge separated by a finite distance; in reality, the spatial distribution of hydrated Na ions in constant motion because of continuous ionic exchange between the aqueous phase and dry clay, even the picture of a “cloud” of Na ions surrounding dry clay is but a time snapshot of a constantly changing spatial distribution).

The size of the cloud of positive electric charge (hydrated Na ions) and its average density of charge are governed by temperature, ion concentration in water, and the surface-to-volume and net negative electric charge of clay. The combined effect of these variables on the size and density of the spatial distribution of hydrated Na ions is quantified as the *Cation Exchange Capacity* of clay, or **CEC**. The CEC of a specific combination of clay and ion-saturated water has a significant influence on the electrical resistivity of shaly fluid-saturated rocks, as will be explained later. Under the same temperature-pressure and ion-concentration conditions, the CEC of smectite is larger than the CEC of kaolinite, illite, or chlorite, mainly because of differences in surface-to-volume ratio (specific surface) and growth pattern. The CEC value also has a direct influence on clay-bound water saturation or clay/shale microporosity.

What is important to emphasize here is that the density of hydrated Na ions within the diffuse ion cloud surrounding dry clay is larger than the average density of hydrated Na ions in free water. The abnormally high, spatial concentration of hydrated Na ions in the vicinity of dry clay provides a preferential path of ions when an electrical current is established in porous media, thereby increasing the rock’s electrical conductivity with respect to the electrical conductivity of the same rock without clay. The spatial region occupied by the cloud of abnormally-high hydrated Na ions is often referred to as Stern, Chapman, or Gouy layer. It is found that the enhancement of electrical conduction of rocks in the presence of clay is a function of both the relative pore volume of the cloud and the density of hydrated Na ions within the cloud. Within porous media, the size of the cloud is restricted by average pore and throat size. In the presence of partially hydrocarbon-saturated porous media, the size of the cloud is also restricted by the average thickness of the continuous aqueous phase. Abnormal conditions may exist in oil-wet rocks.

When two aqueous solutions with different NaCl concentrations are placed in contact through a shale membrane, the movement of hydrated Na and Cl ions (from the solution with the higher ionic concentration to the solution with the lower ionic concentration) will interact with the abnormally high concentration of hydrated Na ions near dry clay. Because of the net negative electric charge of clay, the movement of hydrated Na ions through shale will be favored over the movement of hydrated Cl ions. This ion “selectivity” (or semi-permeability) of the shale membrane to the passage of hydrated Na ions over hydrated Cl ions will result in spatial separation of electrical charge within each of the solutions, thereby causing a net non-zero electric field, hence an electric potential difference. Such is the origin of the membrane SP potential.

Because of their physical/chemical nature, diffusion and membrane DC (steady-state) electric potentials have opposite signs. The superposition of diffusion and membrane potentials is usually referred to as *static spontaneous potential*, or SSP. One of the main applications of SSP measurements is the assessment of the electrical resistivity of formation water, R_w (Ohm-m). Such an assessment is performed based on experimental equations developed by Nernst, which describe the relationship between SSP, temperature, NaCl ion mobility, and the difference of volumetric concentration of NaCl between the two solutions placed in contact through porous media and/or an ion-selective shale membrane.

The experimental equation that describes the relationship between SSP, temperature, concentration of NaCl in mud filtrate, and concentration of NaCl in formation water is given by

$$SSP \approx -K_{SP} \cdot \log_{10} \left(\frac{C_w}{C_{mf}} \right),$$

where K_{SP} is a constant that depends on temperature and ion mobility (≈ 71 mV), C_w is the concentration of NaCl in formation water, and C_{mf} is the concentration of NaCl in mud filtrate. The above equation assumes that neighboring shales behave as perfect semi-permeable membranes. When $C_w > C_{mf}$ (salt concentration of formation water is larger than salt concentration of mud filtrate) the above formula correctly predicts a negative SSP (vice versa, if $C_w < C_{mf}$ then the formula correctly predicts a positive SSP); if $C_w = C_{mf}$ then the SSP is null. In terms of electrical resistivity, the above expression can be written as

$$SSP \approx -K \cdot \log_{10} \left(\frac{R_{mfe}}{R_{we}} \right),$$

where K is a temperature-dependent constant, equal to $61 + 0.133 \cdot T$ and $65 + 0.24 \cdot T$ when temperature (T) is given in degrees Fahrenheit or Centigrades, respectively. In the above expression, R_{mfe} and R_{we} are *equivalent* electrical resistivities of mud filtrate and formation water, respectively, where the adjective “equivalent” is used to designate values of electrical resistivity for the two solutions measured at the same temperature and assuming that both liquids include concentrations of NaCl only.

From the above equations it follows that

$$C_w \approx C_{mf} 10^{-SSP/K_{SP}}.$$

The above equations are used to calculate the electrical resistivity of formation water from SSP measurements. This is done as follows:

1. Measure the electrical resistivity of mud filtrate at surface conditions. Determine the type of ions contained in the solution (e.g. NaCl, KCl, etc.)
2. Identify a depth point on the log that corresponds to a porous and permeable formation fully saturated with water (or else at residual hydrocarbon saturation). Determine the ionic components contained in the solution (NaCl, KCl, etc.) Draw the shale baseline on the SP log and measure the difference between the SP reading across the water-saturated sandstone and the SP shale baseline; note the sign of the deflection as well. This difference is the SSP (sign included). Determine the temperature of the formation at this point.
3. Convert the measured electrical resistivity of mud filtrate to the temperature of the formation calculated in the previous item. Convert to equivalent electrical resistivity for an aqueous solution with NaCl. This calculation will yield R_{mfe} .
4. Calculate the constant K with the previously calculated formation temperature.
5. Solve the equation of SSP for the unknown value of R_{we} at formation temperature. This value will have to be corrected for temperature variations when extrapolated to other depths (temperatures) in the well.

The above procedure for the calculation of formation-water resistivity (R_w) is one of the several methods available to well-log analysts to estimate this important parameter (which is necessary for the calculation of hydrocarbon saturation). There are several technical issues concerning the reliability of that calculation, especially in light of the often poor quality of SP measurements (see the sections below). An alternative method (the most widely used method) is to calculate R_w directly from electrical resistivity measurements. Differences between values of R_w calculated separately with SP and resistivity measurements can sometimes be used to diagnose presence of clay/shale in the water-saturated formation.

In theory, SP measurements across hydrocarbon-saturated rock formations should be zero because of the absence of ions in solution to enforce ionic exchange with mud filtrate. The reason why often SP measurements across hydrocarbon-saturated sandstones are not zero is because of ion mobility that takes place through irreducible water. Thus, SP measurements can be used to diagnose and quantify inter-connected irreducible water saturation. Presence of clay/shale in porous and permeable formations decreases SP deflections about the shale baseline with respect to deflections across clean (shale free) formations. The reason for this behavior is that clay-bearing rocks will inhibit ion movement due to a decrease of the efficiency of membrane potential against shouldering shales. Gamma-ray measurements can be used to ascertain whether the reduction of SP deflections across porous and permeable rocks is due to presence of hydrocarbons or presence of clay/shale, or both.

Care should be exercised when interpreting SP measurements in sedimentary basins with large variations of NaCl concentration of formation water (percolation of meteoric water being one possible mechanism for such irregular occurrence of depth variation of NaCl concentration of formation water). Likewise, presence of deep invasion will tend to suppress diffusion potentials because of the longer distance between the ion “wall” and the borehole wall.

On occasion, kinetic (streaming) potentials will be of consideration in the presence of active invasion but will tend to substantially decrease when the rate of mud-filtrate invasion reaches its late-time steady-state behavior. Streaming potentials arise when ions of opposite charge are spatially separated as the aqueous phase “streams” through a constrained throat in porous media. Compared to diffusion and membrane potentials, streaming SP potential tend to be significant only in cases of high permeability formations. It is often said that SP potentials are a qualitative indicator of permeability. This statement is strictly true only if the measured SP is governed by streaming potentials.

Diffusion and membrane potentials are also frequency dependent. The time-variable equivalent of SP measurements corresponds to induced polarization (IP) measurements.

6.2.a Environmental corrections and possible acquisition problems of SP measurements

Spontaneous potential measurements are borehole-centralized measurements. Variations of borehole size as well as tool eccentricity could cause variations of SP in addition to those due to presence of porous formations and shales. Another important concern for measurement acquisition is the proper grounding of the reference electrode uphole. Presence of electrically charged pipes, DC rectifiers, and even variations of the free water table in the vadose zone during acquisition could cause significant variations of SP measurements downhole. Acquisition of SP measurements at offshore platforms requires electrically isolated grounding, which is often difficult to secure. Because of the above, nowadays most oil and well-logging companies neglect the quality of SP measurements, even though they are normally free of monetary charge and routinely acquired in most wells.

6.2.b Interpretation corrections of SP measurements

The estimation of electrical resistivity of formation water from SP measurements requires differential (sign included) readings of SP with respect to the shale baseline. To that end, it is necessary that SP measurements be corrected for acquisition drift due to variations of both temperature and membrane potential (variations in the chemical composition of shales). This acquisition drift mainly affects the shale baseline. Upon correction for shale-baseline drift, the differential SP (SSP) could be affected by presence of shoulder beds. Shoulder-bed effects consist of a smooth transition of SP measurements between adjacent shales and porous and permeable formations. For thin beds (beds thinner than 2 ft in this case), SP measurements across permeable beds will not reach the value of SP that would be reached for an equivalent, infinite bed. Therefore, in addition to measuring SP in the center of beds to reduce bed-thickness (shoulder-bed) effects, it is necessary to correct SP readings for bed thickness. Logging companies provide charts to perform such a correction.

6.3 Density Measurements

Borehole density measurements are acquired with a radioactive source, Cs¹³⁷, that emits a “burst” of gamma rays in a narrow energy band around 0.66 MeV. The gamma ray are “collimated” toward rock formations surrounding the borehole, and directed toward a pair of NaI scintillators (and photo multipliers) that function as detectors and are separated by a distance of less than one foot away from the source. The source and the detectors are mounted on a rigid pad that is pressed against the borehole wall by means of a mechanical arm (which is also used to measure caliper). The NaI scintillators and associated photo multipliers count the number of gamma rays per unit time that impact them (gamma-ray count rate) shortly after being released by the Cs¹³⁷ radioactive source. At the time of detection, the count rate of gamma rays at the scintillators is lower than that released by the Cs¹³⁷ radioactive source and their energy is much lower than their initial energy of 0.66 Mev. The count rate of gamma rays at the NaI detectors is used to quantify bulk density and photoelectric factor (PEF). Another important feature of the Cs¹³⁷ radioactive source is that its half life is approximately 30 years. This property makes it possible to secure a stable “stream” of gamma rays over relatively long periods of time for reliable logging operations.

Detectors are labeled short- and long-spaced (SS and LS, respectively) depending on their distance from the radioactive source on the tool pad. The gamma-ray count rate measured by the detectors depends on the energy absorption properties of the rocks through which gamma rays are “streamed.” For the specific case of a Cs¹³⁷ radioactive source, gamma rays interact with electrons by way of Compton scattering and photoelectric absorption (pair production is negligible here because of the relatively low energy of the gamma rays emitted by the source). When the energy of the incoming gamma ray is larger than the atomic binding energy of the electrons then the interaction of the incoming gamma ray with the electron results in both loss of energy and deflection of the impacting gamma ray together with ejection of the electron outside its orbit. This gamma-ray interaction is referred to as *Compton scattering*. On the other hand, when the energy of the incoming gamma ray is equal or lower than the binding atomic energy of the electron then the gamma ray will be completely absorbed by the electron thereby resulting in extra electron energy. The latter gamma-ray interaction is referred to as *photoelectric absorption*. Every interaction of gamma rays with a “cloud” of electrons by way of Compton scattering results in the differential loss of energy borne by the gamma rays. The reduction in count rate is due to the absorption of some of the original gamma rays emitted by the Cs¹³⁷ source when they are subject to photoelectric effects.

Gamma rays detected by the density tool bear energies within both the Compton-scattering and photoelectric energy bands. The gamma-ray count rate in the Compton energy scattering range is used to calculate electron density, while the gamma-ray count rate in the photoelectric energy range is used to calculate the photoelectric factor (PEF, measured in the units of barns/electron, or b/e). Compton energy absorption depends on the number of electrons per unit volume (electron density, ρ_e) of the impacting atoms, whereas photoelectric absorption depends solely on the number of electrons (atomic number, Z). The relationship between electron density and bulk density is given by

$$\rho_e = 2 \cdot \frac{Z}{A} \cdot \rho,$$

where A is atomic mass number and ρ is bulk density. For common rocks, the ratio $\frac{Z}{A}$ is nearly constant and equal to 0.5, whereupon electron density becomes a very good approximation to bulk density. For general cases, the following empirical formula is used to relate electron density and bulk density (in the units of gm/cm³):

$$\rho = 1.0704 \cdot \rho_e - 0.1883$$

Even though the calculation of electron density and PEF is possible with one single detector, the reliability and accuracy of such an acquisition system is often poor in the presence of mudcake, barite in the mud, and borehole rugosity. A two-detector system is preferred to compensate for the effects of mudcake and borehole rugosity in the acquisition of gamma-ray count rates. In such a system, the value of electron density is calculated from the two individual SS and LS gamma-ray counts via a calibration “spine.” The value of PEF is calculated solely from the gamma-ray count measured at the SS detector. Compensation for presence of

mudcake is performed with the so-called “spine-and-rib” charts thereby yielding the compensated value of density, ρ reported by the logging company, and the size of density compensation, $\Delta\rho$.

The count rate follows an exponential law given by

$$N_\gamma = N_{\gamma_0} \cdot \exp [-\alpha (\nu) \cdot L] ,$$

where N_γ is gamma-ray count per unit time, N_{γ_0} is the gamma-ray count per unit time emanating from the radioactive source, L is the effective distance from the radioactive source to the sensor, and α is a constant that depends on the gamma-ray absorption capacity of the medium, and it is referred to as *energy cross-section* to indicate the dependency of this function on energy, ν . The energy cross-section is a function specific to the medium through which the emitted gamma rays travel through and eventually become absorbed. Specifically, the energy absorption of the medium is a function of the number of electrons per unit volume (Compton scattering) and the number of electrons (photoelectric absorption).

The probability of having N_γ rays reach the detector during a period of time, Δt , follows a Poisson distribution where the standard deviation of the distribution is determined by N_γ . This distribution of probabilities places the most important constraint on the speed of the tool as it moves in the borehole while acquiring the measurements. The higher the density of the medium the lower the count rate of gamma rays detected by the sensors and hence the slower the speed of the tool required to secure a reliable measurement.

6.3.a Environmental corrections applied to density logs

Environmental corrections of density logs are necessary because of the presence of mudcake (mudcake thickness and mudcake weight), which is commonplace in porous and permeable formations. These corrections are performed in real time with the use of “spine and rib” corrections charts (new correction systems are based on inverse estimation procedures that rely on measurement charts). The specific corrections are:

- Mudcake thickness,
- Mudcake weight (density), and
- Temperature.

Upon performing the environmental corrections, logging companies report both the corrected density measurement and the size and sign of the correction, both in the units of gm/cm^3 . A log is output, referred to as $\Delta\rho$, and plotted alongside the density log. It is important to inspect the $\Delta\rho$ log before performing calculations of porosity with the density log because the size of the correction could have an adverse effect on the calculated porosity.

6.3.b Display and interpretation of density logs

The interpretation of density measurements is based on the study of caliper, $\Delta\rho$, density, and PEF logs. Because density logs are acquired with a pad tool it is imperative that the shape of the wellbore be sufficiently constant through the length of the pad. Rapid variations of caliper (within the length of the pad) will render the density log unreliable. Moreover, it is imperative that attention be paid to the specific value of $\Delta\rho$ reported by the logging company to assess the size of the correction applied to the reported density measurement and the corresponding effect on the calculated porosity.

Proper acquisition of density logs requires that the speed of logging be adequate for the range of expected values of porosity. Low-porosity rocks exhibit relatively large values of density. For this type of rocks, the gamma-ray count rate will tend to be relatively low. Thus, acceptable signal-to-noise ratios for reliable and accurate density measurements will require a relatively low speed of logging.

PEF measurements become unreliable in the presence of barite in the mud. However, when barite is not present in the mud, PEF logs are extremely useful to diagnose type of solid components in the rock. The diagnostic of solid components of the rock is performed in combination with the density log using response guides, or “spines” for pure quartz, calcite, and dolomite lithologies of variable water-filled porosity.

6.4 Neutron-Porosity Measurements

Neutron-porosity logs are acquired with an active neutron source. This source can be either chemical or based on a miniature particle accelerator. Americium-Beryllium (AmBe) Chemical sources are the most widely used method to acquire neutron-porosity logs. The AmBe neutron source produces a “burst” of neutrons with energies in a wide band centered about 4.5 MeV. On the other hand, miniature accelerator neutron sources, also referred to as *minitrons*, accelerate hydrogen atoms with a variable magnetic field until they reach high velocities and are subsequently impacted to a target of hydrogen atoms. A byproduct of the impact is a “burst of neutrons” with energies in a very narrow band centered at 14 MeV. In both cases, the “burst” of neutrons is omnidirectional when directed toward rock formations (collimation of neutrons is not possible). Because of their relatively high energy, minitron sources are commonly used in through-casing operations for fluid-production monitoring. The interaction of neutrons with rock formations will result in their loss of initial energy and, eventually, in their complete absorption.

In addition to the neutron source, borehole neutron tools include a group of helium detectors (usually two detectors) that count the neutrons impacting them per unit time (neutron count rate) after being released from the source. Detectors have the ability to count neutrons in separate energy bands for subsequent analysis. Usually, there are two bands of neutron energy considered by neutron tools, a low or *thermal energy* band, and a high or *epithermal energy* band. Thermal neutron counts are used to assess the hydrogen index of rock formations.

Neutrons “bombarded” into rock formations lose their initial kinetic energy by way of elastic and inelastic collisions. Elastic collisions are governed by laws similar to those of mechanical collisions of particles. Part of the kinetic energy borne by the incoming neutron is transformed into kinetic energy of the impacted particle. Because of their size, neutrons do not interact with electrons but rather with the nuclei of atoms. Owing to the principles of conservation of momentum and energy, the total energy and momentum before and after collision should be equal. Therefore, the maximum transfer of kinetic energy from the incoming neutron to the impacted nucleus will take place when both the neutron and the impacted nucleus have similar masses. The mass of a neutron and a hydrogen atom are almost equivalent, whereupon the maximum loss of energy of the impacting neutron will take place when the impact is against a hydrogen nucleus (presence of other light element is uncommon in rocks). Thus, the larger the volumetric concentration of hydrogen nuclei the larger the loss of energy of the impacting neutrons. When the energy of the impacting neutron reaches the so-called thermal level, instead of sustaining a collision, the neutron is completely absorbed by the nucleus of the impacted atom. This phenomenon is referred to as *neutron capture*. In such a situation, the absorption of an additional neutron by the impacted atom renders the latter radioactive. Upon becoming radioactive, the atom will release alpha and beta particles and gamma rays. The specific energy of the emitted gamma rays will be determined by the atom which originated them. Advanced nuclear logging devices measure count rates of these gamma rays and are used for precise lithology typing. The acquisition and interpretation of gamma rays released by atoms which absorbed neutrons is referred to as *neutron-capture gamma-ray spectroscopy*. It is also the basis of the so-called Σ logs, which measured the rate of time decay of the neutron population, and are widely used for the assessment of water saturation behind steel casing.

Even though, light elements will cause neutrons to lose their energy more rapidly than heavy elements, it is hydrogen atoms that cause the largest loss of neutron energy. The loss of energy of neutrons per unit length is a property of the medium and is usually referred to as *mean-free path or migration length*. The migration length of a rock is determined by its *hydrogen index*, which is defined as the number of hydrogen atoms per unit volume. Hydrogen in rocks occurs mostly in the form of fluids. However, the chemical composition of some rocks also includes hydrogen atoms in the form of hydroxyls, or OH radicals, most notably in the case of clays. Thus, the loss of neutron energy (reflected in their count rates at detectors) cannot always be associated with the fluid component of the rock.

Hydrated chlorine atoms present in aqueous solution are good thermal neutron absorbers. Because of this behavior, detector neutron count rates acquired by logging tools need to be corrected for presence of NaCl in both borehole and rock formations.

6.4.a Transformation of neutron count rates to apparent, water-filled porosity units

As explained above, measured neutron count rates are governed by the hydrogen index of the formation (which is related to the so-called migration length). Rather than transforming the measured neutron count rates to equivalent values of hydrogen index, logging companies transform them to equivalent values of water-filled porosity units of ideal rocks. To that end, calibration models are constructed for three types of ideal (pure) lithologies: sandstone (quartz), limestone (calcite), and dolomite. In the three cases, calibration models includes a range of porosity values where the pores are completely filled with fresh water at ambient conditions of pressure and temperature (recall that hydrogen index depends on pressure and temperature). Neutron count rates for standard source-detector conditions are measured for all the ideal water-filled porosity models. When a neutron count rate is measured in the borehole, the operator first decides which one of the three ideal rock models to use and then pairs the measured neutron count rate to the corresponding water-filled porosity value associated with the chosen lithology.

For compensated measurement systems, neutron count rates are acquired separately for both short- and long-spaced detectors (SS and LS, respectively). The transformation from individual sensor count rates to equivalent water-filled porosity units can be done either with spine-and-rib calibration charts, or else from the ratio of the two-sensor count rates. The most commonly used method is to transform the ratio of the short- to long-sensor count neutron count rates (larger than 1) to water-filled porosity units of the specified lithology.

The above description indicates that neutron log readings across water-filled pure lithologies should be equal to actual porosity values. Similarly, when density logs are transformed to water-filled porosity units with the correct (ideal) matrix assumption, both density and neutron porosity logs should overlap across water-saturated rocks. If the lithology is accurately defined for the neutron and density logs, and both logs are defined for water-filled porosity units, then a discrepancy between the two logs is an indication that the saturating fluid is not water. Most often, if the two logs do not agree when the matrix is accurately defined then the neutron porosity is lower than the density porosity. The difference between density and neutron porosity values depends on the density of the fluid and the pore-volume of the saturating fluid; the lower the density of the fluid and the larger its pore volume the larger the difference between matrix-corrected, water-filled density and porosity logs. The reason for this discrepancy is explained below.

6.4.b Effects of fluids lighter than water on apparent, water-filled neutron porosity units

Under the same conditions of pressure, volume, and temperature, water exhibits more hydrogen molecules per unit volume than gas (e.g. methane). Thus, when gas fills the pores of any of the three ideal lithologies, regardless of porosity, the hydrogen index of the formation is lower than when the same pores are filled with water. Because of this, the neutron count rate is higher for the case of gas than for the case of water filling the same pore volume. This behavior causes the equivalent water-filled porosity units to be lower in the presence of gas than in the presence of water for equivalent values of pore volume. Thus, the effect of gas saturation on neutron logs is neutron porosity values lower than those calculated with density porosity for equal matrix conditions (assuming, of course, that the corresponding matrix has been properly diagnosed and quantified). Because of their relatively shallow radial length of investigation, neutron and density logs are only sensitive to presence of gas in the cases of (a) shallow invasion when the rock's porosity is relatively high, and (b) high values of residual gas saturation regardless of porosity. There are a number of practical cases in which the invasion of mud filtrate is so radially deep that neither the density nor the neutron logs exhibit sensitivity to gas even though gas is present at *in situ* (pre-drilling, pre-invasion) conditions. The reason for this anomalous behavior is that the rock's residual gas saturation is low and mud-filtrate has completely displaced the gas originally filling the pore space. Attention should be paid to resistivity logs to avert the possibility of by-passing such gas zones.

6.4.c Environmental corrections applied to neutron logs

Neutron logs require a significant number of environmental corrections for proper accuracy and reliability, these are:

- Borehole size,
- Hydrogen index of borehole fluid,
- Temperature,
- Pressure, mudcake thickness and mudcake density,
- Salt concentration in the borehole,
- Salt concentration in the formation, and
- Tool standoff.

Some of these corrections have opposite signs and hence tend to balance one to another. For high-porosity, water-saturated rocks, the largest environmental correction corresponds to borehole size.

6.4.d Display and interpretation of neutron logs in combination with density logs

Density and neutron logs are most commonly displayed on the same graphical track. In addition, most logging displays assume the same solid matrix and saturating fluid (water) for the two logs and show them in porosity units for quick comparison and assessment. The combination of the two logs is one of the most commonly used methods to diagnose lithology and to assess the respective proportions of volumetric concentrations.

The first step of the combined interpretation of density and neutron porosity logs consists of determining the underlying lithology. This is done with specialized charts prepared by logging companies (the charts are tool dependent) which include the ideal spines of sandstone, limestone, and dolomite.

Both density and neutron porosity logs should be calculated using the same solid matrix that corresponds to the type of lithology previously diagnosed with the density-neutron chart (or cross-plot). For the case of siliciclastic sedimentary units, it is common practice to assume quartz as the basic solid component of the matrix, calculate the corresponding water-filled porosity units for both density and neutron logs, and then make a correction for presence of shale using the previously calculated value of volumetric shale concentration (C_{sh}). If the matrix was correctly calculated, then both density and neutron porosity logs should be identical across water-filled rock units, especially when the drilling mud is water based. If the matrix is correct but the two logs are not equivalent this condition is clear indication that the saturating fluid is not water. In such a case, neutron porosity log should be lower than density porosity, thereby indicating that the saturating fluid is lighter than water. The difference between density and neutron porosity is thereafter used to assess the density of the saturating fluid and its pore volume. In so doing, attention should be paid to the presence of invasion because part of the saturating fluid sensed by density and neutron logs could be mud filtrate.

6.5 Resistivity Measurements

Laterolog measurements are acquired with galvanic tools that enforce a direct electrical conduction path through the borehole between the electrical current source and the formation. Induction tools, on the other hand, introduce electrical currents in rock formations by magnetic induction, i.e. using time-varying magnetic fields which in turn generate time-varying electric fields, thereby giving rise to closed loop currents in rock formations. Therefore, electrical induction systems do not require that electrical currents traverse the borehole to reach rock formations. The magnitude of the induced electric currents in rock formations is marginal when the electrical conductivity of mud is large or when the borehole is large, or both. Thus, laterolog tools are

preferred over induction tools when the ratio of electrical resistivity of the formation to electrical resistivity of mud is large. Induction tools are preferred when that ratio is low. Because of the same reasons, induction tools are the only way to measure electrical resistivity of rock formations in the presence of oil-base mud. Induction tools become inappropriate when the resistivity of rocks is larger than approximately 600 Ohm-m (this number depends on the specific type of induction tool) because at those resistivities the effect of rock-induced currents becomes negligible.

Induction resistivity tools typically consist of a set of co-axial transmitter-receiver coils operating in the frequency range from 10 to 200 kHz for wireline systems and above 1 MHz for LWD systems. Each sensor consists of two closely spaced coils wound in opposition to decrease voltages induced by the primary coil (transmitter coil) and hence to enhance the voltage induced by co-axial secondary currents taking place in rock formations that surround the borehole. Transmitter-receiver spacing and frequency of operation are varied to increase the radial length of investigation within the probed rock formations. Short transmitter-receiver spacings and high operating frequencies are used to probe shallow radial zones, whereas large transmitter-receiver spacings and low frequencies are used to probe deep radial zones. Because of their principle of operation, induction tools require that the electrical resistivity of the borehole be a few times larger than that of the surrounding formations.

Laterolog tools are galvanic devices that consist of an electric source with end contact electrodes located on the mandrel itself. Electrical conduction is enforced between these two electrodes by imposing a voltage difference between them. Accordingly, electric lines emanating from the mandrel electrode pass through the borehole and into the formation to close the electrical circuit at the second (reference) electrode. Focusing electrodes are included on the tool mandrel to direct electric lines perpendicular to the mandrel into the formation and to reduce electrical conduction through the borehole. Various spacings between focusing electrodes are included in the tool to provide multiple radial lengths of investigation into the probed rock formations. Because of their principle of operation, laterolog devices require that the electrical resistivity of the borehole be a few times lower than that of the surrounding rock formations. Thus, laterolog tools are not intended for operation in the presence of oil-base muds.

Microlog resistivity tools are miniature versions of laterolog tools mounted on a pad and pressed against the borehole wall. These tools include the spherical focused log (SFL) and the micro-spherical focused log (MSFL), among others. They are intended to probe the resistivity of both mudcake and flushed zone and are designed to operate in conductive muds. Only until recently logging companies developed similar microlog resistivity tools for operation in the presence of oil-base muds.

The frequency of operation of wireline resistivity tools is below 200 kHz, with laterolog devices operating below 10 KHz. For the case of LWD resistivity tools, the frequency of operation is above 1 MHz. Such frequency is necessary for proper enforcement of electrical conduction in the surrounding formations in the presence of conductive drill pipe. At those relatively large frequency, electromagnetic excitation of rock formations is enforced partly by propagation (displacement currents) and partly by conduction (conduction currents).

6.6 Sonic Measurements

Borehole sonic measurements are used to assess elastic and mechanical properties of rock formations. In some instances, sonic measurements are also used to quantify interconnected porosity, presence of vugs, or presence of fractures, diagnosis of unconsolidation, etc., in combination with density-neutron porosity logs.

Measurement of elastic and mechanical properties of rocks is best performed at static laboratory conditions. In so doing, differential stresses are applied to the rocks and the corresponding differential deformation is measured under conditions of reversible deformation (elastic behavior). In well-logging operations, however, it is impractical to perform *in situ* static tests of elastic deformation. Instead, sonic tools excite an acoustic wave in the borehole which propagates into the surrounding rocks as both compressional (P) and shear (S) waves. This excitation is also responsible for fluid waves that propagate in the borehole through fluid-solid interactions. Elastic and mechanical properties of rock formations are estimated *indirectly* from the measured velocities of propagation of compressional, shear, and borehole waves. Because of the dynamic nature of sonic

measurements, it is important to assess the dependence of elastic properties of rocks on the frequency of the propagation (or wavelength). Seismic measurements are performed in the range from 2 to 150 Hz, sonic measurements in range from 1 to 20 KHz, and ultrasonic measurements in the MHz range. The difference in frequency (or wavelength) will cause differences in the volume of investigation sensed by dynamic propagation measurements.

Compressional (acoustic) waves travel through rocks by way of dilation and compressional stresses longitudinal to the direction of propagation. On the other hand, shear waves propagate by shear-stress deformation perpendicular to the direction of propagation. Solids can support the propagation of both compressional and shear waves, whereas fluids can only support the propagation of compressional waves. It is the combination of compressional- and shear-wave velocities that allows interpreters to diagnose and quantify the effect of solid and fluid components of the rocks on bulk elastic properties.

Traditional sonic logging tools only measure the time of arrival of the fastest mode of wave propagation between the source to the sensors. These tools consist of an omnidirectional acoustic (vibrating) source immersed in the borehole fluid and an array of piezo-electric sensors (sonic receivers) located along the axis the tool some distance away from the source. The fastest mode of propagation is the one that travels as a head (evanescent) wave on the borehole wall. This wave emanates as compressional wave in the borehole, reaches the borehole wall at an incidence angle larger than the critical angle, travels on the borehole wall with the velocity of the formation, and leaves the borehole wall to reach the sensors through borehole propagation. Tools measure the time of arrival of this wave by synchronizing the source with the start of the timing clock. Results are displayed in the form of slowness, which is the inverse of speed and is given in the units of $\mu\text{s}/\text{ft}$. Slowness is calculated by dividing the time of flight of the fastest wave by the distance between source and receiver.

Because of the physics involved in the propagation of the fastest sonic wave, the latter senses a very thin radial segment of the formation and hence is very sensitive to borehole rugosity and presence of mudcake. Excessive borehole rugosity causes the sonic tool to measure longer than actual times of flight. To reduce this problem, modern sonic logging tool make use of an array of sources and receivers whereby the time of flight is calculated from the arrival times detected at neighboring receivers. These acquisition method is referred to as *sonic compensated acquisition* and drastically decreases the deleterious influence on the measured time of flight due to borehole rugosity and presence of mudcake.

Modern acquisition systems include dipolar sources in addition to monopole (omni-directional) sources. Moreover, modern sonic logging tools include an array of receivers with capabilities to detect and quantify not only the head wave but also compressional, shear, flexural (in the case of dipole excitation), and Stoneley waves associated with the presence of the borehole. The array of sources and receivers enables the acquisition of continuous time waveforms in similar fashion to surface seismic acquisition systems. The relative orientation of the sensors and dipolar sources permits to diagnose presence of anisotropic elastic properties.

The time of flight of the fastest wave (head wave) is often used to assess porosity. Such a procedure is based on empirical models developed by Wyllie which are strictly valid for the case of low-porosity, cemented, and well consolidated rocks. The so-called sonic porosity is used in combination with density-neutron porosity to assess the degree of consolidation and cementation of the rock. In other instances, particularly in the case of carbonate formations, discrepancies between sonic and density-neutron porosity are used to assess presence of secondary porosity. Accordingly, in pore systems composed of a main, primary interconnected pore system plus a secondary (often non-connected) pore system, the shortest time of flight takes place through the stiffest part of the rock. Thus, the sonic porosity will mainly respond to the porosity of stiffest (most rigid) part of the rock.

6.6.a Processing of sonic logs

Usual formulae:

Velocity of compressional waves :

$$V_P = \sqrt{\frac{\lambda + 2\mu}{\rho}} \quad (6.6.1)$$

Velocity of shear waves :

$$V_S = \sqrt{\frac{\mu}{\rho}} \quad (6.6.2)$$

where λ and μ are called the Lamé coefficients (S.I. Units : $kg \cdot m^{-1} \cdot s^{-4}$ or $Pa \cdot s^{-2}$); μ depends on the solid properties of the rock and skeleton, whereas λ depends on the solid properties of the rock, skeleton, and fluids. Acoustic and shear impedances (S.I. Unit : $kg \cdot m^{-2} \cdot s^{-1}$) :

$$Z_P = \rho \cdot V_P \text{ and } Z_S = \rho \cdot V_S \quad (6.6.3)$$

The reflection coefficient at the interface between two layers is defined by :

$$R = \frac{A_{reflected}}{A_{incident}} \quad (6.6.4)$$

So that the reflection coefficient between layer 1 and layer 2 for normal incidence is :

$$R = \frac{Z_2 - Z_1}{Z_2 + Z_1} \quad (6.6.5)$$

Bulk modulus :

$$k = \lambda + \frac{2}{3} \cdot \mu \quad (6.6.6)$$

The bulk modulus is experimentally defined by applying a hydrostatic pressure to a cylindrical piece of rock, with the assumptions that there is no fluid drag and that both skeleton and fluid are being deformed at the same time (assumption of low frequency). If ΔP is the difference between the applied pressure and the original pressure, and ΔV the difference between the volume of the rock under pressure and the original volume, then :

$$\frac{\Delta V}{V} = -k \cdot \Delta P \quad (6.6.7)$$

6.6.b Some properties and uses of sonic logs

- Comparison of ϕ_S and ϕ_e : this can help to verify that the assessed fluids are the correct ones ($\phi_S > \phi_e \Rightarrow$ fluid lighter than water) and confirm that nothing affects the type of porosity (primary / secondary).
- There is practically no frequency dispersion¹ in the head wave.
- V_P , V_S and ρ depend on ϕ , S_w , C_{sh} and the type of fluid.
- Multipole tools improve the P-S coupling but decrease the frequency (and therefore the vertical resolution) and increase the dispersion.
- The S-waves have a longer depth of investigation than the P-waves. Therefore invasion has to be taken into account. Moreover, the density tool has a depth of investigation of a few inches, whereas the depth of investigation of the P-waves is deeper (except in shales). Therefore, the vertical resolution of the densities is higher than the one of the P-velocity log, and thus the density has to be averaged over a depth window (cf Backus average).
- S-waves are sensitive to the rugosity of the borehole and to the problem of skip cycles.
- The $\frac{V_P}{V_S}$ ratio is small in gas. Therefore, if there is some gas, this ratio is not sensitive to S_w .
- An increase of porosity implies a decrease in the rigidity of the skeleton and therefore a decrease in V_S , whereas shales typically increase the rigidity of the skeleton and therefore increase V_S .
- The *lambda* coefficient remains almost the same in sandstones when the fluid changes, but this is not true in carbonates.
- V_P and V_S decrease when hydrocarbon saturation increases.

¹Dispersion comes from an inelastic behavior, this is, energy is lost through the medium

6.7 Magnetic Resonance Measurements

Nuclear magnetic resonance (NMR) measures the time diffusion of proton (hydrogen nuclei) magnetization contained in the fluid filling the rock's pore space. Protons involved in this measurement are only those present in the hydrogen component of pore-saturating fluids. Therefore, as long as the pore-saturating fluid includes hydrogen in its composition it can be sensed with NMR measurements. Furthermore, because of the time-diffusion principle underlying magnetic resonance, the measurement is only sensitive to hydrogen nuclei included in fluids. By comparison, neutron measurements are sensitive to hydrogen nuclei contained in both fluids and solids.

Owing to its time-diffusion principle, NMR is the only borehole measurement that remains sensitive to rock pore sizes. Differential sensitivity to pore sizes is important because two rocks can exhibit the same total porosity but very different permeabilities due to differences in dominant throat sizes. However, because NMR measurements are also sensitive to fluid properties, the measured time diffusion of proton magnetization is affected by both pore sizes and fluid properties when the rock pore space is partially saturated with more than one immiscible fluid. Only when the rock's pore space is saturated with a single fluid can NMR measurements can be uniquely associated with a distribution of pore sizes.

Protons exhibit an intrinsic quantum mechanical property referred to as "spin." This property causes protons to behave as magnets (magnetic dipoles), with the spin of a proton given by $\pm 1/2$. Chemical elements whose nucleus includes an even number of protons do not exhibit net spin, while chemical elements whose nucleus includes an odd number of protons do exhibit non-zero net spin. When an external DC (time constant) magnetic field is applied to protons they align in the direction of the applied magnetic field in a non-instantaneous manner and begin to precess around that direction with an angular Larmour frequency, f , given by

$$f = \Gamma B_0$$

where Γ is an intrinsic physical property called the *gyromagnetic ratio* and B_0 is the intensity of the applied DC magnetic field. The time of alignment of protons in the presence of a external DC magnetic field is referred to as **longitudinal magnetic relaxation** and symbolized as T_1 , i.e.,

$$M(t) = M_0 \left(1 - e^{-t/T_1}\right), \quad (6.7.1)$$

where M is proton longitudinal magnetization, t is time, and M_0 is maximum magnetization. As reference, it takes approximately 3 seconds for a water sample at ambient conditions to align all of its protons (hydrogen nuclei) along the direction of the applied DC magnetic field. It takes several more seconds than with water to align protons included in methane (CH_4), while the time of alignment is faster for heavy fluids such as honey or heavy oil, for instance. The time of longitudinal alignment, T_1 , is inversely proportional to the hydrogen index of the fluid involved. In the case of saturated rocks, T_1 is a function of both the saturating fluids *and* the distribution of pore sizes included in the rock. The constant M_0 included in eq. (6.7.1) is the volumetric concentration of mobile protons included in the rock, i.e. it depends on the porosity of the rock and the hydrogen index of the rock's saturating fluids; it is customarily normalized with respect to the hydrogen index of water at ambient conditions, whereby M_0 equals the product of porosity times the net hydrogen index of the saturating fluids.

A second and crucial step in the acquisition of magnetic resonance measurements follows the longitudinal proton alignment: it consists of subjecting the aligned protons to a time-varying magnetic field of frequency equal to their Larmour frequency and oriented perpendicular to the direction of the external DC magnetic field. This time-varying magnetic field causes the aligned protons to rotate along a Euclidean plane perpendicular to the direction of the DC magnetic field. Next, the time-varying magnetic field is turned off, causing the protons to diffuse, i.e. causing all the protons to perform random walks while aligned and preceding at their Larmour frequency. Because of proton-proton magnetic interactions (dipole-dipole interactions), proton-solid magnetic interactions, and spatial gradients in the DC magnetic field taking place during random walks, protons begin to lose perpendicular alignment and will eventually return to their original alignment along the direction of the external DC magnetic field; when that happens, the net time-varying magnetic field perpendicular to

the applied DC magnetic field becomes null. *Transverse magnetic relaxation* is the name given to the latter phenomenon and is given by

$$M(t) = M_0 e^{-t/T_2}, \quad (6.7.2)$$

where T_2 is the characteristic time of the exponential time decay of transverse magnetic relaxation, referred to as *transverse relaxation time*. The latter characteristic time is the net diffusion time of transverse proton magnetization due to fluid, space-restricted, and magnetic field-accelerated diffusion effects. In the fast diffusion limit, T_2 is given by

$$\frac{1}{T_2} = \frac{1}{T_{2B}} + \frac{1}{T_{2S}} + \frac{1}{T_{2G}}, \quad (6.7.3)$$

where:

T_{2B} is bulk fluid diffusion time of transverse proton magnetization due to fluid-fluid magnetic interactions,

T_{2S} is the restricted diffusion time of transverse proton magnetization due to fluid-solid magnetic interactions, and

T_{2G} is the gradient-accelerated diffusion time of transverse proton magnetization due to fluid-fluid magnetic interactions in the presence of spatial gradients of the external DC magnetic field.

While T_{2B} and T_{2G} are fluid-related properties, T_{2S} is governed by the specific surface (surface-to-volume ratio) of solid boundaries and the surface density of paramagnetic materials (i.e., surface relaxivity) present on solid boundaries, i.e.,

$$\frac{1}{T_{2S}} = \rho_s \frac{S}{V},$$

where ρ_s is surface relaxivity (typically expressed in $\mu\text{m}/\text{s}$) due to paramagnetic materials, S is surface area, and V is volume, i.e., T_{2S} is governed by pore radius (recall that for a spherical pore, $S/V = 3/R$, where R is the sphere radius).

Realistic and practical examples of porous rocks, however, may include a variety of fluids and pore sizes, whereupon, by invoking the superposition principle one can write

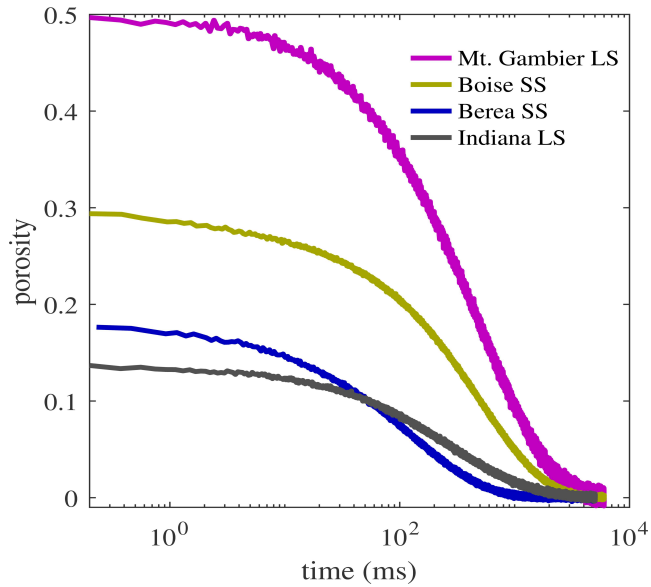
$$M(t) = \sum_{i=1}^N M_{0i} e^{-t/T_{2i}},$$

where N is the total number of pore sizes, M_{0i} is the volumetric concentration of protons within the i -th pore, and T_{2i} is the effective transverse proton magnetization time within the i -th pore.

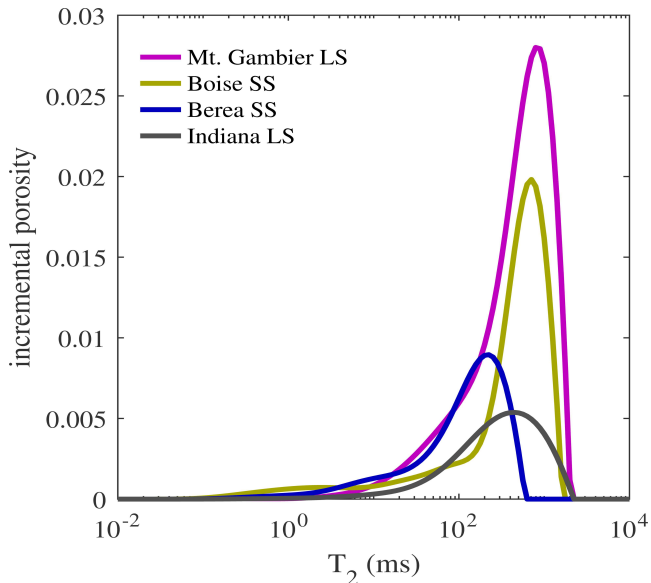
In the presence of only one type of fluid and a constant value of surface relaxivity for all pores, the characteristic time T_{2i} in the above expression becomes an exclusive function of pore size. Therefore, if the time-decay measurements of transverse proton magnetization, $M(t)$ are inverted into a set of N characteristic pores together with their respective radii and relative porosity, one can infer the *pore size distribution of the porous medium*, which in turn can be used to estimate permeability under some assumptions. The latter is one of the most important applications of transverse NMR measurements of rocks.

Figure 6.7.1 compares NMR laboratory measurements of transverse proton relaxation acquired from several clastic and carbonate rock samples fully saturated with water and their corresponding T_2 distributions. All measurements were acquired with the same top bench NMR laboratory measurement system and were calibrated with a water sample. Because of the latter calibration, the $t \rightarrow 0$ asymptote of the NMR time decays is equal to the rock's porosity, while the time necessary to reach zero proton magnetization is proportional to the average pore size; the longer the time needed for proton magnetization to reach zero the larger the pore size. Also, by construction, the area under a given T_2 distribution is equal to the corresponding rock porosity and this determines the average amplitude of the T_2 distribution; the larger the amplitude the larger the rock porosity.

One of the most important NMR laboratory experiments conducted on saturated rocks consists of acquiring transverse-relaxation measurements both before and after centrifuging a sample which is fully saturated with



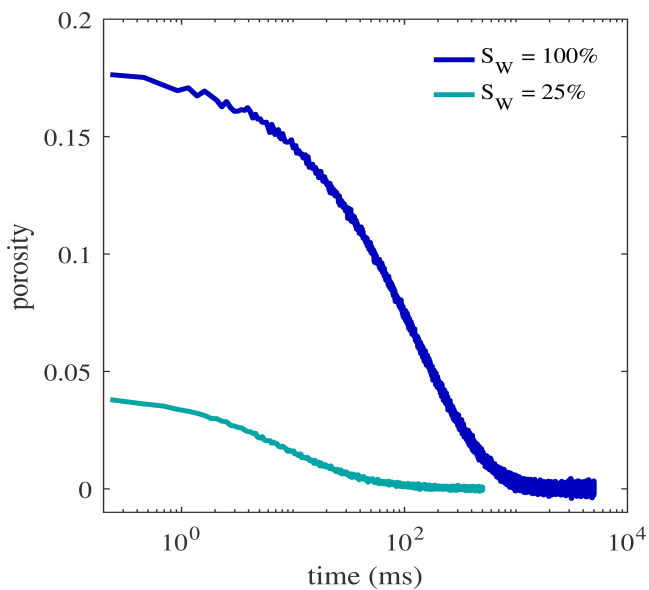
(a) Time decay of proton magnetization (transverse relaxation) for various rock samples fully saturated with water.



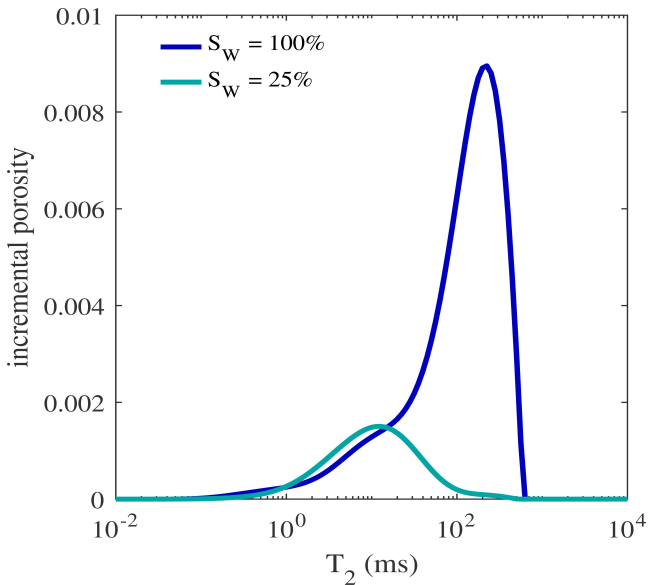
(b) T_2 distributions estimated from the time decays of proton magnetization shown above.

Figure 6.7.1: (a) Comparison of time decays of NMR transverse relaxation magnetization and (b) their corresponding T_2 distributions for various rock samples (clastics and carbonates) fully saturated with water. All measurements were acquired with a top bench laboratory NMR measurement system (images courtesy of David Medellín).

water. Assuming that the maximum centrifuging pressure reaches the capillary pressure of the sample close to irreducible water saturation then the NMR T_2 distribution acquired after centrifuging provides a suitable approximation for the pore volume of irreducible water. The latter pore volume can then be used to calculate the permeability of the rock sample via eq. (A.16.2), for instance. Figure 6.7.2 shows an example of NMR

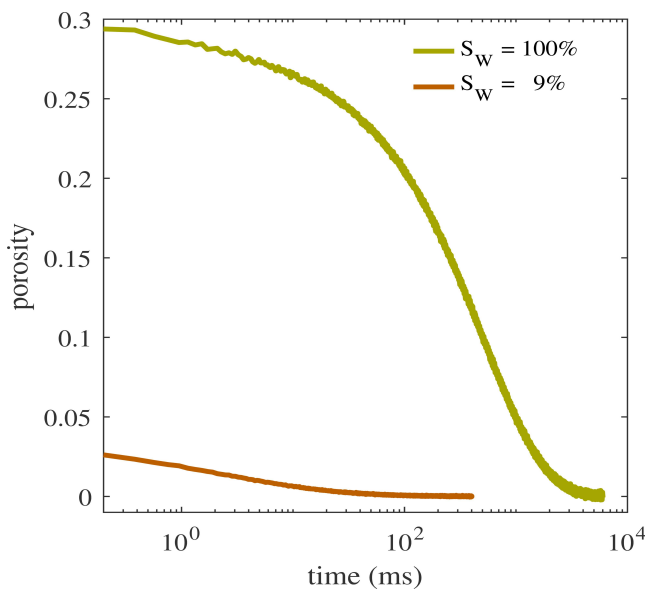


(a) Time decay of proton magnetization (transverse relaxation) for a Berea sandstone before ($S_w = 100\%$) and after centrifuging the sample.

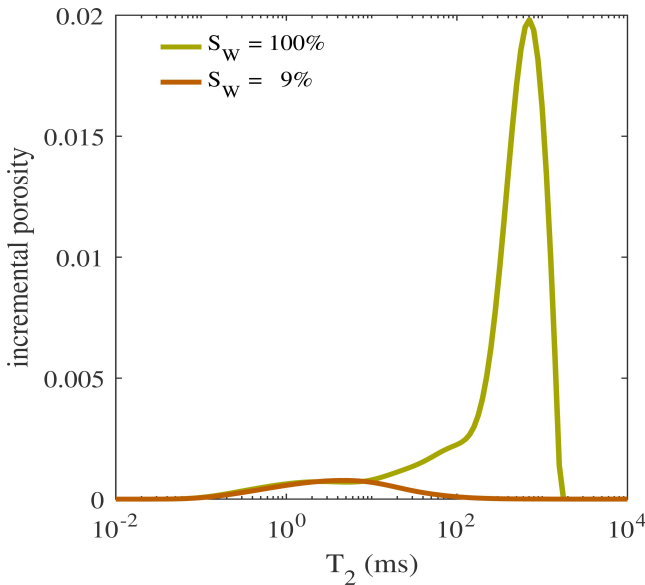


(b) T_2 distributions estimated from the time decays of proton magnetization shown above.

Figure 6.7.2: Comparison of time decays of NMR transverse relaxation magnetization and their corresponding T_2 distributions for a **Berea sandstone** sample before ($S_w = 100\%$) and after centrifuging the sample. The fraction of remnant water after centrifuging the rock sample corresponds to grain- and capillary-bound water, i.e., an approximation of irreducible water saturation. Permeability can be estimated from the difference between the NMR T_2 distributions acquired before and after centrifuging the rock sample. All measurements were acquired with a top bench laboratory NMR measurement system (images courtesy of David Medellín).



(a) Time decay of proton magnetization (transverse relaxation) for a Boise sandstone before ($S_w = 100\%$) and after centrifuging the sample.



(b) T_2 distributions estimated from the time decays of proton magnetization shown above.

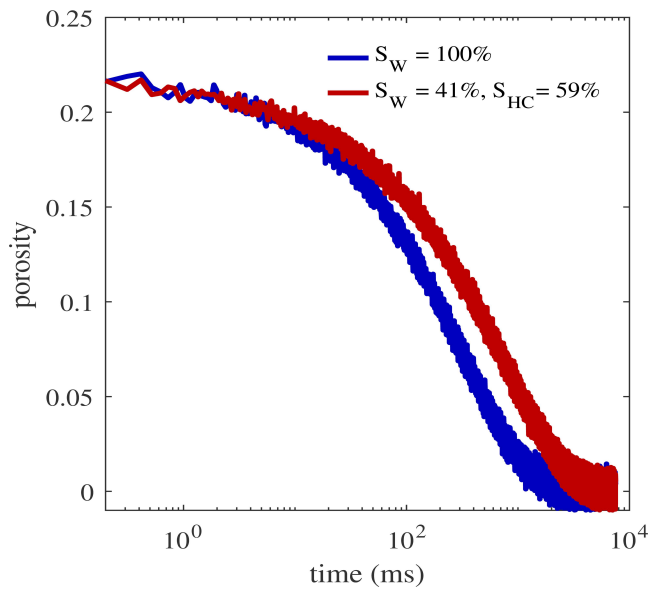
Figure 6.7.3: Comparison of (a) time decays of NMR transverse relaxation magnetization and (b) their corresponding T_2 distributions for a **Boise sandstone** sample before ($S_w = 100\%$) and after centrifuging the sample. The fraction of remnant water after centrifuging the rock sample corresponds to grain- and capillary-bound water, i.e., an approximation of irreducible water saturation. Permeability can be estimated from the difference between the NMR T_2 distributions acquired before and after centrifuging the rock sample. All measurements were acquired with a top bench laboratory NMR measurement system (images courtesy of David Medellín).

transverse relaxation measurements acquired before and after centrifuging a sample of Berea sandstone. By comparison, Figure 6.7.3 shows the corresponding NMR transverse relaxation measurements acquired for a Boise sandstone sample. The fraction of pore volume of irreducible water saturation is larger for the Berea sandstone sample than for the Boise sandstone sample (note, however, that the porosity of the two samples is not the same).

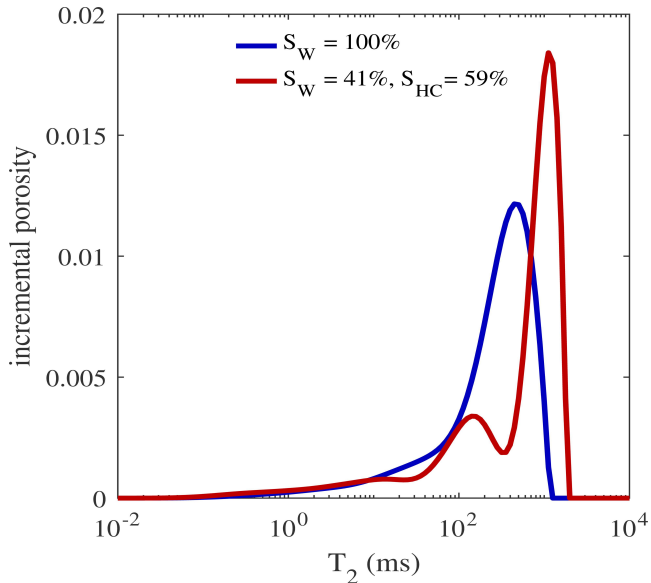
Figure 6.7.4 shows another important property of NMR transverse relaxation measurements of rocks. When two immiscible fluids occupy the pore space of the rock and both include hydrogen in their composition (which in the case of air the relative concentration of hydrogen is negligible for all practical purposes, as in a centrifuge experiment), then depending on the relative saturation of the two fluids the acquired NMR transverse relaxation measurements will exhibit non-negligible superimposed effects due to both dominant pore size(s) and fluid type(s). Consequently, the NMR T_2 distribution of Figure 6.7.4 shows two dominant peaks when partially hydrocarbon saturated compared to one dominant peak when fully water saturated. Bulk hydrocarbon exhibits a slower time decay of transverse proton relaxation than water (i.e., the T_{2B} of hydrocarbon is greater than that of water), whereby one of the two dominant peaks of the T_2 distribution in the presence of partial hydrocarbon saturation will take place later (greater T_2) than the expected peak for water at $S_w = 100\%$. Care must be exercised when interpreting T_2 distributions acquired in the presence of partial hydrocarbon saturation not to confuse the measurements as dominantly influenced by pore size, for instance, when estimating permeability via eq. (A.16.2).

6.8 Dielectric Measurements

These are electrical measurements of saturated rocks performed from the KHz to the GHz range. They include measurements of the real and imaginary components of electrical conductivity (electric conductivity and dielectric permittivity). Different components and features of the rock respond differently depending on frequency.



(a) Time decay of proton magnetization (transverse relaxation) for a Berea sandstone sample at full water saturation and partial water/oil saturation.



(b) T_2 distributions estimated from the time decays of proton magnetization shown above.

Figure 6.7.4: Comparison of (a) time decays of NMR transverse relaxation magnetization and (b) their corresponding T_2 distributions for a **Berea sandstone** sample at full water saturation $S_w = 100\%$) and partial water/oil saturation ($S_w = 41\%$ and $S_{HC} = 59\%$). Partial hydrocarbon saturation causes the NMR transverse relaxation to exhibit superimposed effects due to dominant pore size(s) and fluid type(s). All measurements were acquired with a top bench laboratory NMR measurement system (images courtesy of David Medellín).

Chapter 7

The Process of Mud-Filtrate Invasion

All sorts of things can happen when you are open to new ideas and playing around with things.

– Stephanie Kwolek, Kevlar inventor.

Wells are drilled using mud whose weight is controlled so that the pressure within the borehole is higher than the pore pressure of the surrounding formations in order to prevent wellbore collapse. While the mud pressure cannot be too high to avoid mechanical failure of the surrounding rocks, it originates fluid transport from the borehole into the surrounding permeable rocks, thereby displacing original rock fluids away from the wellbore's immediate proximity. This phenomenon is often a nuisance because the original rock fluid near the wellbore will be masked by a non-negligible fraction of mud filtrate. However, when properly understood and quantified, the process of mud-filtrate invasion into permeable rocks can be used to indirectly assess several important fluid transport properties.

7.1 Introduction

Wells are drilled with either water-base, oil-base, or synthetic-base muds (there are unique cases where the mud is made with foam too!) Water-base mud may include variable concentrations of NaCl as well as KCl. Oil-base muds, on the other hand, in addition to including light oil (or diesel), contain variable amounts of water maintained in solution within the oil phase with the use of chemical emulsifiers.

In overbalanced wells, the pressure of drilling mud is higher than that of formation pore fluids to provide mechanical stability and hence avoid mechanical collapse (failure) of the well when penetrating soft (non-rigid) rock formations. the overbalance pressure between drilling mud and pore pressure may range from a few psi to 600-3000 psi in most cases. Drilling mud also provides lubrication and temperature control for the drill bit as it penetrates rock formations. Moreover, the relatively high density of drilling mud permits the floating (buoyancy) of rock cuttings and hence their transport up-hole by the column of circulating mud.

Depending on their composition, drilling muds can interact chemically and mechanically with the rocks penetrated by the well over short or long periods of time, thereby giving rise to potentially damaging alterations of original (*in situ*) rock conditions (formation damage). Excessive mud pressures can also result in the mechanical failure of rocks (e.g., borehole-induced fractures). Of particular interest to well-log practitioners is the fact that hydraulically overbalanced mud can invade porous and permeable rock formations surrounding the borehole.

Muds are composed of both fluids and solid particles which remain in fluid suspension. Bentonite and barite are the common composition of solid particles. Typical solid particles range from 0.01 to 100 μm in size; particle sizes are distributed according to a histogram of sizes wherein particle-size modes are centered about 0.4 μm for bentonite and about 20 μm for barite. The fluid component of mud is usually referred to as *mud filtrate*.

Mud properties are routinely sampled at the well site with a standard API static paper-filter test. During such test, a sample of mud taken from the mud flow line is placed in a small container which includes a permeable paper filter on one open end. Mud is placed above the filter and sedimented by the action of gravity. The time of complete sedimentation is referred to as the viscosity of mud. At the end of this process, the solid components of the mud separate from mud filtrate and the operator measures the thickness and porosity of mudcake left on the filter as well as the chemical and electrical properties of mud filtrate left in the container (e.g. salt concentration, electrical resistivity, pH, etc.)

7.2 The Physics of Mud-Filtrate Invasion

At the onset of the invasion process, mud filtrate flows into the formation almost unimpeded. The process of fluid invasion during this relatively brief period of time is usually referred to as “spurt” fluid loss. Subsequently, solid particles contained in the mud will be “retained” by pore throats when the particle radius is larger than the throat radius. Some of these particles may be transported a short distance into the formation before they are finally blocked by a pore throat. The “filtered” mud filtrate which flows through pore throats will displace original fluids radially away from the borehole wall. Such fluid displacement process is governed by the same physics laws that govern miscible/immiscible fluid displacement in porous media (e.g. Buckley-Leverett theory of immiscible fluid displacement in porous media).

Deposition of solids on the borehole wall will create a thin film of solid materials that is usually referred to as *mudcake*. This deposition will only take place on the borehole wall of porous and permeable rocks. By contrast, mudcake will not be formed along impermeable shale segments. Mudcake itself becomes a porous medium with its own porosity and permeability which serves as a *filter* to additional mud-filtrate invasion. As time progresses, the thickness of mudcake will increase and its permeability will decrease because of the retention of small particles. Mudcake will also exhibit a characteristic porosity which is time dependent, hence it will exhibit storage and flow capacities that will vary with time of invasion. Flow capacity of mudcake will be different from the flow capacity of the invaded rock formation. Figure 7.2.1 is a photograph of mudcake remaining at the boundary of a cylindrical borehole drilled into a large block of Navajo sandstone. The invasion experiment was performed in the laboratory to quantify the effects of water-base drilling mud into permeable rocks.

The volumetric rate of mud filtrate displacing original fluids will decrease toward a usually small steady-state value. The time necessary for mud filtrate to reach its steady-state value of invasion will depend on the interplay between the properties of the mud (average particle size and particle-size distribution, viscosity, and other rheological properties) and the petrophysical properties of the invaded formation, including porosity, permeability (throat-size distribution and pore interconnectivity), capillary pressure, relative permeability, and fluid viscosity. Typical values of mudcake thickness will be anywhere between a fraction of a millimeter to a centimeter. The efficiency of displacement of original fluid by mud filtrate will also be conditioned by capillary pressure and relative permeability. Likewise, an internal filter cake will be formed by the “stacking” of solid particles in the throats of the invaded rock. Such an internal filter cake may affect the production efficiency of the formation at the onset of hydrocarbon production.

Deeply invaded formations will cause well logs to sense petrophysical properties of formations saturated with a mixture of mud filtrate and original fluids and this can cause serious interpretation problems to inexperienced well-log analysts. As emphasized in a subsequent section of these notes, the radial length of invasion is primarily controlled by porosity and, to some extent, by time of invasion, permeability, relative permeability, viscosity, and capillary pressure. Typical radial lengths of invasion will fluctuate anywhere between one or two inches to up to 10 or 15 ft. In the case of invasion of hydrocarbon-bearing formations with oil-base mud, the radial length of invasion will be ill-defined given the partial miscibility of oil-base mud and native oil.

The time the well is exposed to invasion may range from a minutes to hours and days depending on the difficulty of the drilling environment, logging time, and type of well completion. Even though LWD measurements are acquired shortly after drilling, in practice these measurements will also be affected by



Figure 7.2.1: Photograph of mudcake remaining at the boundary of a cylindrical borehole after several hours of invasion into Navajo sandstone. Invasion experiment conducted with a large block of rock in the laboratory to quantify the effects of water-base drilling mud.

invasion because of spurt fluid loss. However, invasion effects on LWD measurements will, in general, be less significant than for the case of wireline logs.

Figure 7.2.2 shows X-ray images of Berea sandstone samples subject to the same controlled conditions of mud-filtrate invasion (injection) in the laboratory; the accompanying color scale describes time after the onset of invasion. Notice that even with the same conditions of overbalance pressure, water-base mud gives rise to thicker mudcake than oil-base mud, while the displacement of original fluid (in this case, air) is faster for the case of water-base mud-filtrate invasion.

Figures 7.2.3 and 7.2.4 show X-ray cross-sections acquired before and after the onset of mud-filtrate invasion into Berea sandstone and Edwards limestone samples, respectively. The physics of invasion was replicated under laboratory conditions using small rock samples so that they can be imaged with high-resolution X-ray machines during the process of invasion. Both samples were initially saturated with air and subject to water-base mud-filtrate invasion through their cylindrical center using a common preparation of drilling mud which included both bentonite and barite. The imposed overbalanced pressure was approximately 100 psi between the center of the samples and their outer boundaries. Both figures show the formation of mudcake after the onset of invasion (deposition of solids contained in the drilling mud along the inner cylindrical hole) and the displacement of original saturating fluid (air) by mud filtrate. However, after the onset of invasion, Figure 7.2.3 shows an almost piston-like fluid-displacement front while Figure 7.2.4 shows a highly irregular fluid displacement front. The differences between the two invasion fronts are due to differences between the petrophysical properties of the two rock samples: Berea sandstone exhibits an approximate unimodal pore/throat size distribution, while Edwards limestone exhibits a non-unimodal and irregular pore/throat size distribution which includes vuggy porosity. The differences in the spatial distribution of fluids into the invaded rock samples causes important differences in their electrical, density, neutron, magnetic resonance properties, for instance, that need to be taken into account when interpreting well logs. Likewise, the spatial distributions of fluids resulting from invasion will depend on the time of invasion (early times for LWD measurements and late times for wireline measurements).

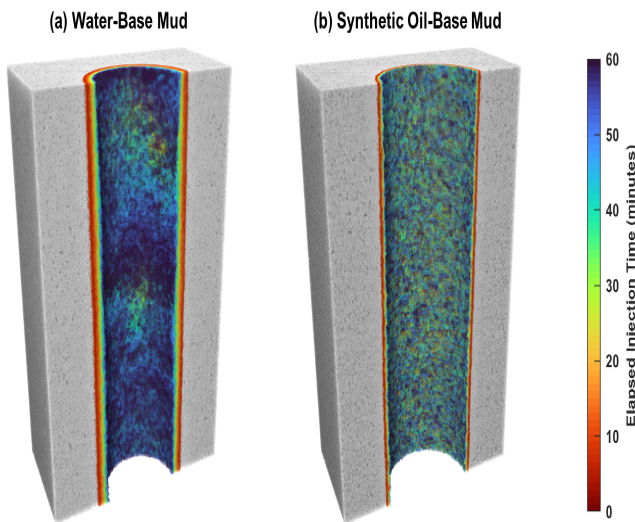


Figure 7.2.2: X-ray images of Berea sandstone invaded with water- and oil-base drilling mud. Panels a and b correspond to the cases of water- and synthetic oil-base drilling mud, respectively. The color scale describes time after the onset of mud-filtrate invasion. Cylindrical samples of Berea sandstones were subject to injection of drilling mud in the laboratory under the same controlled conditions to compare the relative effects of water- and oil-based mud-filtrate invasion; time-lapse X-ray images were acquired during the process to assess the evolution of mudcake thickness and fluid displacement. Notice that mudcake thickness is larger for the case of water- than oil-base mud-filtrate invasion (images courtesy of Colin Schroeder).

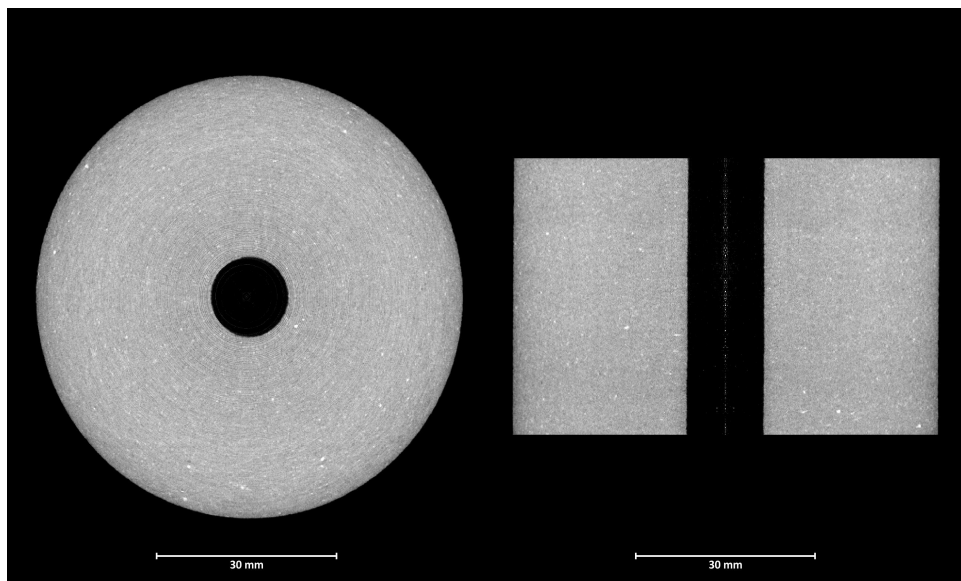
7.3 Effects of Mud-Filtrate Invasion on Well Logs

When interpreting apparent resistivity logs in the presence of invasion, it is important to invoke the shape and length (front location) of the radial profile of fluid saturation resulting from invasion. This shape will be determined by both capillary pressure and relative permeability, which in most cases are correlated with porosity and permeability. There will also be fluid pressure variations in the radial direction, starting with the mud pressure at the borehole wall and ending with the original fluid pressure of the formation radially away from the wellbore. When the overbalance pressure is not large enough to overcome capillary pressure and hence displace original fluid with mud filtrate, then the process of invasion will naturally come to a halt. Thus, both formation of mudcake and capillary pressure forces are responsible for slowing down and eventually halting the process of mud-filtrate invasion.

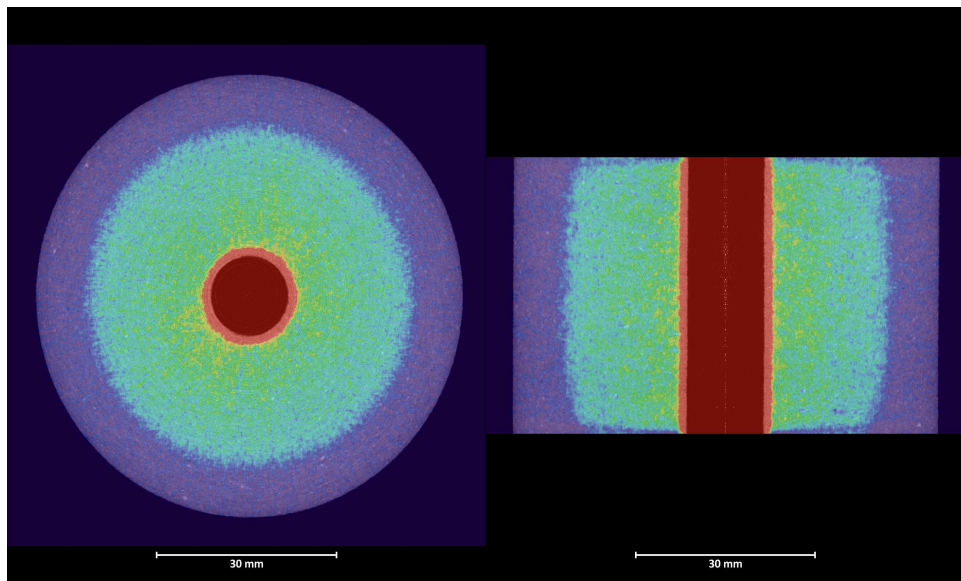
Invasion with water-base muds will also cause salt exchange between mud filtrate and formation water, depending on the difference of salt concentration between the two solutions. If formation water is saltier than mud filtrate, then the exchange of salt will be exactly in the opposite direction as that of fluid displacement. At the same time, the temperature of mud filtrate will be slightly lower than that of *in situ* fluids and this difference during mud circulation will cause a radial temperature transition between the borehole wall and the formation.

Invasion of oil-base mud into hydrocarbon-bearing formations will cause partial compositional mixing between the two fluids. On occasion, presence of surfactants in oil-base mud (included in the mud to keep a small amount of water under emulsified conditions, such as in the case of invert mud emulsions), will cause changes in the surface tension of the rock, thereby releasing water previously retained on grain/clay surfaces by electrochemical forces. Presence of emulsifier in the mud will also affect the growth rate and final thickness of mudcake, which will be conditioned by droplet size.

Presence of invasion will affect the extraction of native fluid samples with either formation testers or through a drill-stem test (DST). At the beginning of fluid extraction, samples will be almost completely contaminated

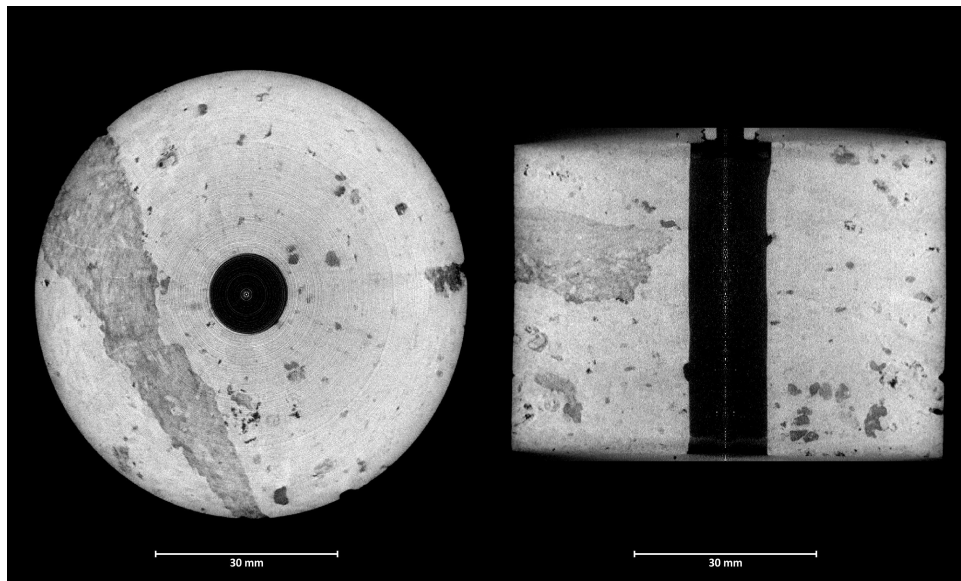


(a) X-ray cross-sections of a Berea sandstone sample before invasion.

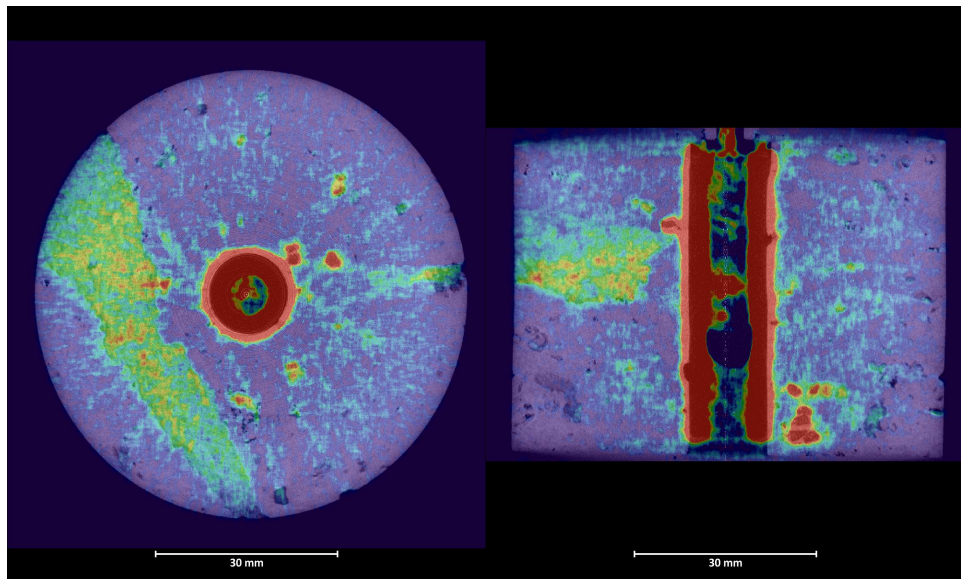


(b) X-ray cross-sections of a Berea sandstone sample after invasion.

Figure 7.2.3: Areal and vertical X-ray cross-sections of a Berea sandstone sample (a) before and (b) after water-base mud-filtrate invasion performed in the laboratory. The center of the images is a replica of the borehole and the sample is originally saturated with air. Notice in (b) the formation of mudcake after the onset of invasion and the advancement of the mud-filtrate invasion front into the sample (color-coded density). Because of the petrophysical properties of Berea sandstone (almost unimodal pore/throat size distribution), the fluid-displacement front resulting from invasion (air being displaced by water-base mud filtrate) exhibits a quasi-piston-like behavior (images courtesy of Colin Schroeder).



(a) X-ray cross-sections of an Edwards limestone sample before invasion.



(b) X-ray cross-sections of an Edwards limestone sample after invasion.

Figure 7.2.4: Areal and vertical X-ray cross-sections of a Edwards limestone sample (a) before and (b) after water-base mud-filtrate invasion performed in the laboratory. The center of the images is a replica of the borehole and the sample is originally saturated with air. Notice in (b) the formation of mudcake after the onset of invasion and the advancement of the mud-filtrate invasion front into the sample (color-coded density). Because of the petrophysical properties of the Edwards limestone (non-unimodal and irregular pore/throat size distribution, including vuggy porosity), the fluid-displacement front resulting from invasion (air being displaced by water-base mud filtrate) exhibits an irregular (non-uniform) behavior (images courtesy of Colin Schroeder).

with mud filtrate, with the degree of contamination decreasing with time as the fluid-extraction process takes place. The time necessary to recover uncontaminated (pristine) fluid samples will depend on a multitude of fluid and petrophysical properties such as viscosity, density, porosity, permeability, relative permeability, capillary pressure, and radial length of invasion, among others.

The process of mud-filtrate invasion gives rise to three radial saturation zones:

- Mudcake: comprised of a consolidated aggregate of small solids originally included in the mud as particles in suspension. At the onset of invasion, the thickness of mudcake is negligible and its permeability is infinite. As time progresses, mudcake thickness increases and its permeability decreases to a point that eventually it effectively seals the invaded formation against further displacement by mud filtrate.
- Flushed Zone: characterized by a high percentage of mud-filtrate saturation, irreducible water saturation, and a relatively small percentage of original-fluid saturation (e.g. residual hydrocarbon saturation).
- Intermediate (Transition) Zone: characterized by non-complete saturation of both mud filtrate and original fluids, in addition to irreducible water saturation.
- Virgin (or Uninvaded) Zone: characterized by a large percentage of original fluid saturation plus irreducible water saturation and a negligible percentage of mud-filtrate saturation.

Because of the process of mud-filtrate invasion, some well logs are designed to exhibit variable radial lengths of investigation. A subset of these measurements will sense the fully invaded (flushed) zone while others will sense both the invaded and virgin (uninvaded) radial segments of porous and permeable rocks.

Presence of invasion is undoubtedly an indication that the invaded rock is porous and permeable. Even though this process might be considered a nuisance by some log analysts, it is actually one of the few ways whereby petrophysicists have access to indirect information about the *dynamic* petrophysical properties of rock formations otherwise unavailable through standard borehole measurements. In some ways, the process of mud-filtrate invasion is analogous to enhanced oil recovery (EOR) operations where water or other fluids are injected into reservoirs to improve the “sweep” efficiency of *in situ* hydrocarbons. Exactly the same static and dynamic petrophysical properties that control EOR processes govern the process of invasion. An alert petrophysicist could positively collaborate with reservoir engineers in their design of flooding operations, for instance, by quantifying the sensitivity of rock formations to the process of invasion. The “Silver Rule” of well logging is *a well log is always associated with the process of mud-filtrate invasion*. This is one of most important rules in well-log interpretation.

It is also important that well-log analysts take into account the mobility of the various fluid phases in the rock formations as well as the effect that mud filtrate has on displacing those phases. Irreducible water saturation, for instance, will affect the electrical resistivity of the formation and the measured SP, but will have no effect on fluid displacement by mud filtrate. Along a capillary transition zone, free water will be displaced by mud filtrate and this process could have a measurable impact on most well logs. Residual hydrocarbon saturation, on the other hand, because of its null displacement by mud filtrate, may have a measurable effect on well logs but could be mistakenly assumed as free hydrocarbon fluid.

7.4 Identification of Porous and Permeable Rock Units

The identification of porous and permeable rock formations is performed after the assessment of lithology (e.g. sandstone, shale, limestone, dolomite, anhydrite, mixed composition, etc.) Porous and permeable rock formations will be subject to mud-filtrate invasion while impermeable formations will not (e.g. shales and anhydrites). On occasion, presence of invasion (hence permeability) can be diagnosed by inspection of the differential caliper because invaded formations enable the formation of mudcake, which in turn decreases the original borehole caliper.

Presence of mud-filtrate invasion is usually diagnosed with the separation of resistivity curves that exhibit multiple radial lengths of investigation. However, in hydrocarbon-bearing zones invaded with oil-base mud, the

separation of resistivity curves could be zero in the absence of free water (the resistivity curves will “stack”). Attention should be paid to situations in which the separation of resistivity curves may also be due to electrical anisotropy in deviated wells or across dipping beds.

The shape of the radial distribution of fluid saturation within invaded rocks depends on the interplay between overbalance pressure, permeability, porosity, relative permeability, and capillary pressure. If we assume piston-like invasion (i.e. if we neglect capillary-pressure effects, such as assumed by Buckley-Leverett's theory of immiscible fluid displacement in porous media), negligible irreducible water saturation, and negligible residual hydrocarbon saturation, the radial length of invasion will be inversely proportional to the square root of porosity. The demonstration is as follows: assume a porous and permeable formation of porosity equal to ϕ invaded with mud filtrate at a constant rate per unit vertical length. Let us designate the borehole radius as R_b , the radial length of invasion measured from the center of the well as r , and the thickness of the invaded formation as h . Likewise, let V be the volume of mud filtrate invading the formation during the duration of invasion. Because of the above assumptions, the ratio

$$\frac{V}{h} \quad (7.4.1)$$

becomes a constant. When the invasion process comes to an end (either when (a) mudcake hardens and seals the formation, (b) capillary pressure impedes further fluid displacement, or (c) casing is set), because of mass balance, the volume of displaced original fluid is equal to the volume of injected fluid, i.e.

$$\frac{V}{h} = \pi \cdot (r^2 - R_b^2) \cdot \phi = \text{constant} = c. \quad (7.4.2)$$

For $r^2 \gg R_b^2$ one has

$$r^2 \approx \frac{c}{\pi \cdot \phi},$$

whereupon

$$r \approx \underbrace{\sqrt{\frac{c}{\pi}}}_{\text{Constant}} \cdot \sqrt{\frac{1}{\phi}} \Rightarrow r \propto \frac{1}{\sqrt{\phi}}. \quad (7.4.3)$$

This result indicates that the radius of invasion will increase with decreasing values of porosity. Thus, porosity has a leading effect on the radial length of invasion because of mass balance. High values of permeability will accelerate the displacement of the volume of fluid available during the duration of invasion. At the same time, the thickening (and hardening) of mud cake as well as capillary pressure forces will slow down (and halt!) the process of invasion. Hence, even though because of mass balance low-porosity formations tend to exhibit relatively deep invasion, their permeability tends to be low, whereby more time is required to reach their full length of invasion than for the case of high-permeability formations. If mudcake fully forms before that time, then invasion will be halted and the radial length of invasion will be shorter than the length predicted by porosity alone.

In the presence of non-negligible irreducible water saturation, the corresponding analysis indicates that the radial length of invasion will be inversely proportional to

$$\phi \cdot (1 - S_{wi}), \quad (7.4.4)$$

where S_{wi} is irreducible water saturation. Lastly, in the case of non-negligible residual hydrocarbon saturation, the radial length of invasion will be inversely proportional to

$$\phi \cdot (1 - S_{wi} - S_{hr}), \quad (7.4.5)$$

where S_{hr} is residual hydrocarbon saturation. An important consequence of these last two equations is the following: in the case of two invaded formations exhibiting the same porosity but different values of irreducible water saturation, the formation with the lowest permeability will exhibit the largest irreducible water saturation, therefore the deepest invasion.

It is also noted that low-porosity formations will cause the radial profile of fluid saturation to exhibit a smooth transition zone between the invaded and virgin zones. This is due to the interplay between capillary-pressure and relative permeability. Low-porosity formations are commonly associated with variable pore-size distributions, thereby resulting in fluid dispersivity (variable fluid velocity across different pores and capillary tubes). Such a behavior will cause smooth radial variations of water saturation from the borehole wall to the virgin zone (some pores and throats will be filled with mud filtrate while others will be filled with original fluid at the same radial distance from the wellbore). By contrast, high-porosity formations will tend to exhibit uniform pore-size distributions with large individual pore sizes and throats, in which case the velocity of flow will be uniform across all pores and hence the radial distribution of water saturation will exhibit a piston-like (shock-front) behavior (as predicted by Buckley-Leverett theory).

Salt concentration, on the other hand, will only be exchanged between mud filtrate and formation water through the spatially continuous aqueous phase, and hence will not be conditioned by capillary forces. Convection and diffusion govern the exchange of salt through the aqueous phase. When the aqueous phase is in movement, convection of salt will dominate over diffusion. For the case of water-base muds, large differences of salt concentration between mud filtrate and formation water will cause the separation of resistivity curves to strongly respond to the process of salt mixing rather than to immiscible fluid displacement. The interplay between relative permeability and the efficiency of salt mixing can cause “dephasing” of the radial salt concentration front with respect to the radial fluid-saturation front. As shown in a subsequent section of these notes, such front-dephasing effect may result in an abnormal annulus in the radial profile of electrical resistivity. However, existence of a resistivity annulus with water-base mud-filtrate invasion is, in most cases, a good surprise as it unequivocally implies presence of movable hydrocarbons, hence ability of rock formations to radially displace immiscible fluids.

When diagnosing presence of invasion in permeable rocks, it is imperative to understand which fluids are involved in the process, whether the fluids are immiscible or partially miscible, and whether the fluids are mobile. Water will be immobile if it is present in the pore space as irreducible water saturation. Some of the water and hydrocarbons held within pores and throats by capillary forces will be immobile if the overbalance pressure is not high enough to overcome capillary pressure. Hydrocarbons, on the other hand, will be immobile if they are present in the pore space as residual hydrocarbon saturation.

For instance, oil-base mud (OBM) invading a hydrocarbon-bearing formation at irreducible water conditions will result in no radial variations of either salt concentration or water saturation. Resistivity measurements acquired with multiple radial lengths of investigation will “stack” (the curves will not exhibit separation among themselves) in this case because water saturation and salt concentration are constant in the radial direction. It is necessary that a fraction of water held in pores and throats be mobile to be radially displaced by OBM, hence cause a separation of electrical resistivity curves. However, if OBM invades a rock formation fully saturated with water, OBM will radially displace movable water while the radial concentration of salt will remain unchanged. Radial variations of water saturation will cause the electrical resistivity curves to separate. The separation of resistivity curves is governed by overbalance pressure, time of invasion, porosity, permeability, capillary pressure, and relative permeability. On occasion, the separation between resistivity curves could be used to estimate permeability.

Conversely, if water-base mud (WBM) invades a hydrocarbon-bearing formation, the invasion process will include immiscible radial displacement of hydrocarbon by WBM, radial displacement of mobile water by WBM, and salt mixing between WBM and formation water. Depending on whether salt concentration of formation water is greater than salt concentration of WBM or vice versa, the radial movement of salt in the aqueous phase will be opposite to radial displacement or not, respectively. In this case the separation of electrical resistivity curves will be jointly governed by the radial distributions of water saturation and salt concentration. It is in this specific case that the radial distribution of electrical resistivity could exhibit an annulus. Depending on whether salt concentration of mud filtrate is lower or higher than salt concentration of formation water, the radial profile of electrical resistivity could “ramp” down or up, respectively.

Chapter 8

Formation Evaluation of Conventional Clastic Rocks

...Als Gregor Samsa eines Morgens aus unruhigen Träumen erwachte, fand er sich in seinem Bett zu einem ungeheuren Ungeziefer verwandelt...

– Franz Kafka, Die Verwandlung.

Clastic rocks originate from grain packs which are subsequently compressed and cemented due to overburden pressure and diagenetic processes. The petrophysical and mechanical properties of clastic rocks chiefly depend on grain sorting (variability of grain sizes), degree of grain/fluid compression, degree and type of grain cementation, and type, volumetric concentration, and spatial distribution of clay minerals and shale in the pore space. Clay minerals in rocks arise because of exogenic and authigenic processes and are often *metamorphosed* as a consequence of diagenesis, giving rise to substantial variations of the rock's pre-burial properties. Therefore, it is important to diagnose and quantify the type and amount of clay minerals and their spatial distribution in the pore space to estimate the corresponding rock's petrophysical and mechanical properties regardless of the engineering application.

8.1 Clay and Shale

Siliciclastic sedimentary environments commonly include variable volumetric concentrations of clay (dry clay) and shale. Clay is a mineral as well as a rock made of clay minerals. Non-organic shale is a combination of small-size particles (whose mineral composition does not need to be quartz in general), clay minerals, and clay-bound (immobile) water. The diameter of grains contained in shale is, by definition, between 4 and 63 μm (micrometers), which is the diameter range associated with *silt*. Within such a diameter range, particles do not sediment when immersed in still or slightly-moving water but rather remain in suspension because buoyancy forces dominate over gravity forces. The distinction between clay and shale is confusing in most well-loggin books, where one often finds the same terms used to designate either one of the two components, the two, and/or the two components including the volume of irreducible water associated with them. Such mixtures may include Th, U, and K in the form of impurities or detrital matter. In practice, shale could be composed exclusively of single-mineral grains, hence be associated with negligible values of spontaneous gamma-ray activity that could be mistaken as originating from permeable sandstone.

The precise description of shale is that of a chemically and mechanically stable mixture of silt, water, and clay. In this definition, water is included not only in irreducible form between quartz grains but also on the surface of clay crystals and between clay crystals. Perhaps the most practical and intuitive description of a shale is **mudrock** because of its genesis. Other names often used to describe similar rocks are *siltstone* and *mudstone*. The total porosity of shale is seldom zero **but its permeability is negligible**.

Presence of shale in an otherwise clean rock can affect porosity, irreducible water saturation, permeability, relative permeability, residual hydrocarbon saturation, capillary pressure, etc. Quantification of the effect of shale on well logs requires knowledge of their specific spatial distribution (topology) in the rock, volumetric concentration, and composition. Concerning spatial distribution (topology) in the rock volume, it is necessary to diagnose and quantify whether shale is distributed in laminar form, or else contained in the pore space in dispersed form (grain-coating clay), or in structural form by way of grain replacement. Specific methods used to calculate porosity, water saturation, and permeability in siliciclastic sequences from well logs require the quantification of type of clay, its volumetric concentration, and its type of distribution in the pore space of the rock. Often clays are classified as either authigenic or exogenic depending on their origin, before, during, and after the sedimentary process that gave rise to the rock in question. Clay minerals also may transform from one to another because of changing temperature and pressure (depth of burial) conditions (compaction and diagenesis).

Clay/shale concentration in a rock can often be indirectly quantified from well logs or combinations of well logs. The most commonly used method to quantify volumetric concentration of shale is based on the gamma-ray log.

8.2 Volumetric Concentration of Shale, C_{sh} .

Volumetric concentration of clay/shale is defined as

$$C_{sh} = \frac{\text{partial volume of clay/shale contained in a rock sample}}{\text{volume of the rock sample}}.$$

It is emphasized that, in the above definition, the volume of shale includes both the volume of solids associated with silt and clay, the volume of pore space associated with their component of irreducible water (which is often designated as *microporosity*), and the volume of water included between clay crystals.

In most siliciclastic systems, all the available porosity is interconnected by the aqueous phase but only a fraction of it is available for fluid displacement in the presence of pressure gradients. *Effective porosity*, ϕ_{eff} (also known as *flowing porosity*) is the term usually employed to designate the porosity which contributes to fluid flow in the presence of pressure gradients (e.g. when centrifuging a saturated fluid sample). Typically, $\phi_{eff} \leq \phi_t$. When performing laboratory measurements of porosity based on rock-core samples, it is important to understand the physical principles of the measurements to assess whether the measured core porosity includes the non-shale porosity or the shale porosity (microporosity), or both. Discrepancies between calculated values of porosity from well logs and core porosity may arise when the two values are not consistent with the definition assumed in the calculations performed with well logs.

Accurate calculations of volumetric concentration of clay/shale can only be performed on rock-core samples in the laboratory with infrared spectroscopy methods or with laser spectroscopy, or else from well logs with specialized mineral analysis based on neutron-capture gamma-ray spectroscopy. Indirect procedures used to calculate volumetric shale concentration are based on linearly normalized gamma-ray values, typically referred to as “shale index.”

Classical textbooks on well-log interpretation describe the volumetric concentration of shale as “volume of shale” which is obviously a misnomer (volume of shale should be measured in cubic units of length and hence should not be dimensionless!) The common symbol is V_{sh} . However, in these notes the use of the symbol C_{sh} is enforced in an effort to correct the misnomer.

From a practical viewpoint, the evaluation of siliciclastic rock formations requires the separate petrophysical assessment of the two end members of the sequence: **clean sandstone** and “**pure**” shale. It is relatively simple to recognize the “pure” shale end member of the sequence within specific formation tops and in sufficiently thick and representative layers. Conversely, it is rather difficult to detect a representative clean sandstone, especially across old rocks which have been subjected to non-negligible diagenesis. In siliciclastic sequences which lack a clean sandstone member it is customary to resort to water-saturated sandstones to quantify their volumetric concentration of shale in lieu of that of a clean sandstone. Any rock within the two end members

of the siliciclastic sequence is then conceived of as a transitional “hybrid” (or mixture) between them. In other words, **any transitional rock within the same formation is assumed to exhibit shale properties equal to those of the “pure” shale end member of the formation.** This is one of the strongest assumptions made in the petrophysical interpretation of siliciclastic rocks from well logs. The Thomas-Stieber diagram detailed below is often used to diagnose the type of existing end-members mixtures within a siliciclastic sequence as well as to calculate the corresponding effects on total porosity and volumetric concentration of shale.

8.3 Spatial distribution of shale in the rock volume (shale topology)

Shale is found to be spatially distributed in clastic rocks according to three main possibilities (or topologies): laminated, grain-coating (dispersed), and structural.

Shale-laminated systems consist of stacked alternations of layers of pure sandstone and pure shale. Individual layers can be anywhere between tens of feet to a few μm in thickness. There could be clay present in the pore space of pure-sandstone layers. However, clay mostly occurs within shale laminae. These systems are typically associated with relatively young and unconsolidated siliciclastic rocks that have undergone a minor amount of diagenesis subsequent to sedimentation and burial. Examples are Tertiary turbidite deposits as well as distal portions of pro-delta sedimentary systems. This is perhaps the most common spatial distribution of clay/shale in the pore space of clastic rocks. Figure 8.3.1 is a white- and ultraviolet-light photograph of whole core retrieved from a Miocene turbidite sedimentary system in the deepwater Gulf of Mexico. It shows a typical sandstone-shale laminated system where the sandstone layers are saturated with hydrocarbon (based on the ultraviolet-light photograph). Volumetric concentration of shale is approximately 45% while sandstone porosity is approximately 32%. The rock sample is intrinsically anisotropic concerning direction-dependent physical properties such as permeability, electrical conductivity, compressional- and shear-wave velocities, etc. However, despite its relatively large concentration of shale it is still a financially viable rock for hydrocarbon recovery.

In *dispersed shale systems* clay/shale is located within the pore space of an otherwise clean sandstone in the form of grain-coating clay minerals (in fact, the proper name for dispersed shale should be grain-coating clay); clay/shale comprises its own microporosity and does not occupy the space of the rock taken by grains. This is second most common spatial distribution of clay/shale in the pore space of clastic rocks, especially in those rocks that have undergone diagenesis and cementation. Clays can be allocated in the pore space either by surrounding existing grains (e.g. chlorite) or else by “bridging” grains (e.g. illite and kaolinite). Clays can also be transformed from one type to another depending on the depth of burial (formation pressure) and temperature. Because of this, clay minerals present in dispersed systems can originate from both exogenic (mixing of clean grains with clay during sediment transport) and authigenic (after sedimentation) processes. In all cases, the petrophysicist should inspect thin sections and images acquired with scanning-electron microscopes (SEM) to determine the type of clay and its specific spatial distribution in the pore space with respect to grains. Diagnostics of the type of clay can provide valuable information about the diagenetic processes undergone by the rock after sedimentation and hence indirectly yield information about producibility of pore fluids. Figure 8.3.2 shows an example of fibrous illite coating the surface of Rotliegend sandstone grains, North Sea. The presence of grain-coating clay minerals increases the surface-to-volume ratio (specific surface) of the original sandstone grains, increases microporosity and irreducible water saturation, thereby decreasing effective porosity and permeability.

Dispersed clay/shale systems seldom exhibit null values of volumetric clay/shale concentration. The cleanest possible sandstone in these systems is rarely as clean as the clean sandstone of a laminated system. Likewise, compared to sandstone-shale laminated systems, the porosity of clay/shale in dispersed systems tends to be much lower because of solution precipitation and sedimentation.

In the case of *structural clay/shale systems*, entire original sandstone grains have been transformed into shale via the generation of authigenic clay and due to prolonged exposure of the rock to diagenesis, chemical

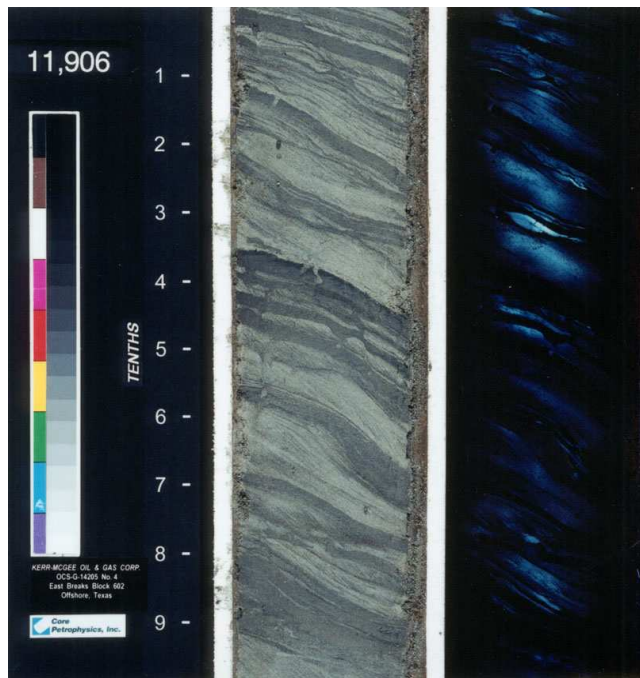


Figure 8.3.1: White- and ultraviolet-light photographs of whole core of a sandstone-shale laminated rock. Core retrieved from a Miocene turbidite sedimentary system in the deepwater Gulf of Mexico. The ultraviolet-light photograph indicates the sandstone layers in the rock sample are saturated with hydrocarbon.

precipitation, and/or extreme conditions of pressure and temperature. The case of structural clay/shale is the most uncommon among the three possible types of shale topology.

8.4 Thomas-Stieber diagram

The Thomas-Stieber diagram is used to diagnose presence of laminar, dispersed, or structural clay/shale in rocks originating from clastic depositional systems. It is based on simple principles that govern the mixing of volumetric proportions of clay/shale and sandstone to determine effective values of volumetric shale concentration and total porosity. A Thomas-Stieber diagram can be constructed either with rock-core measurements or with well logs.

The most important conceptual elements of the Thomas-Stieber diagram comprise the limiting cases of a “pure sandstone” and a “pure shale.” These limiting components are associated with their respective values of total porosity (clean-sandstone porosity, ϕ_s , and shale porosity, ϕ_{sh} , respectively). When plotted on a volumetric-shale-concentration C_{sh} vs. total porosity (ϕ_t) graph, the two points for the two end members describe the “extremal” points of the Thomas-Stieber diagram.

The corresponding volumetric concentration of shale in laminated systems is equal to the volumetric concentration of shale laminae in the mixture, C_{sh-lam} . Accordingly, the corresponding total porosity of the mixture is given by

$$\phi_t = C_{sh-lam} \cdot \phi_{sh} + (1 - C_{sh-lam}) \cdot \phi_s .$$

The straight line that connects the end-member points of a pure sandstone and a pure shale defines the locus of all possible (C_{sh}, ϕ_t) variations of the mixture. In this particular case, sandstone porosity is given by

$$\phi_s = \frac{\phi_t - C_{sh-lam} \cdot \phi_{sh}}{1 - C_{sh-lam}} .$$

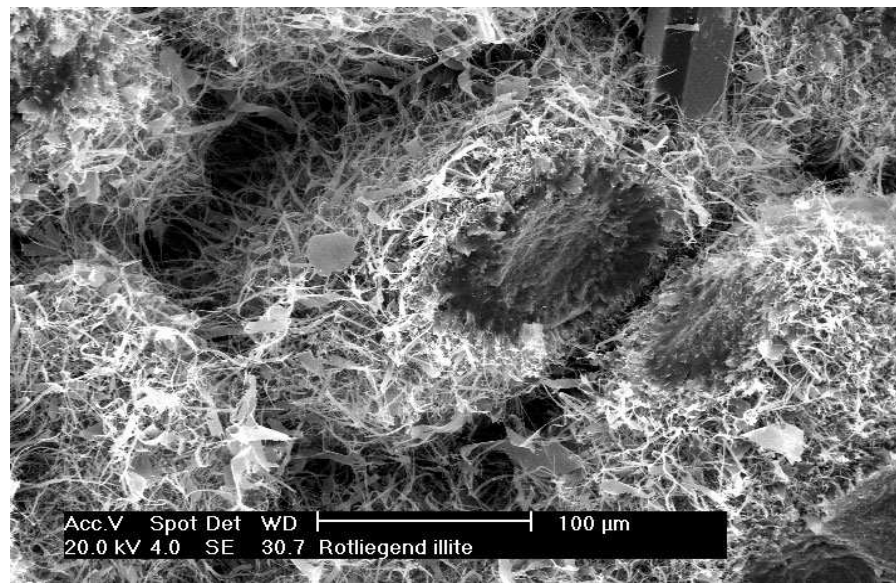


Figure 8.3.2: Example of fibrous illite coating the surface of Rotliegend sandstone grains, North Sea (Sample Ill-34: Macaulay Collection; field of view $\approx 30 \mu\text{m}$ wide). Presence of grain-coating clay increases the original surface-to-volume ratio of grains, increases microporosity and irreducible water saturation, thereby decreasing effective porosity and permeability (photograph courtesy of M. Roe, Macaulay Institute).

This last equation is used to infer the porosity of pure sandstones contained in the sequence from measurements of total porosity and C_{sh} , and assuming that one knows the porosity (microporosity) of the pure-shale end member of the sequence. In the sandstone-shale laminated systems described above C_{sh} should be interpreted in terms of the *net-to-gross* ratio of the sequence. Specifically, when $C_{sh} = 1$ the net-to-gross ratio of the sequence is zero, while the net-to-gross ratio of the sequence is 100% when $C_{sh} = 0$. The link between gamma-ray values and C_{sh} is the simplest possible for the case of sandstone-shale laminated systems, and is given by

$$\gamma = C_{sh-lam} \cdot \gamma_{sh} + (1 - C_{sh-lam}) \cdot \gamma_s ,$$

where γ is gamma-ray log value, and γ_{sand} and γ_{shale} are the gamma-ray log values measured across the pure-sandstone and pure-shale end members of the sequence, respectively. It then follows that

$$C_{sh} = I_{sh} = \frac{\gamma - \gamma_{sand}}{\gamma_{shale} - \gamma_{sand}} ,$$

where I_{sh} is defined as *shale index*.

Now consider the case of *dispersed clay/shale systems*. Typically $C_{sh} \leq \phi_s$. Because clay/shale exists *only* with the pore space of an otherwise clean sandstone, the maximum possible value of C_{sh} in a dispersed clay/shale system is equal to ϕ_s , with the corresponding value of total porosity equal to $\phi_s \cdot \phi_{sh}$. Thus, the total porosity of a dispersed clay/shale system is given by

$$\phi_t = (\phi_{sh} - 1) \cdot C_{sh} + \phi_s ,$$

with

$$0 \leq C_{sh} \leq \phi_s ,$$

and

$$\phi_s \cdot \phi_{sh} \leq \phi_t \leq \phi_s .$$

When plotted on a Thomas-Stieber diagram, the locus of (C_{sh}, ϕ_t) points included in a dispersed clay/shale system describes a finite-length line (equal to 1) connecting the end points $(0, \phi_s)$ and $(\phi_s, \phi_{sh}\phi_s)$. The slope of the latter line is lower than the slope traced by the locus of sandstone-shale laminated systems. In dispersed clay/shale systems the equality $C_{sh} = I_{sh}$ does not hold. A different formulation is needed to transform gamma-ray log values into values of volumetric concentration of clay/shale (to be discussed later).

When the shale-sandstone system is laminar but individual sandstone laminae contain clay/shale in their pore space (e.g. because of diagenesis undergone by originally pure-sandstone, pure-shale laminated systems), the corresponding locus of points in the Thomas-Stieber plot will be a straight line contained between the lower straight line of dispersed clay/shale and laminated clay/shale.

Note that when $C_{sh} > \phi_s$ the shale contained in the rock cannot be solely of dispersed type, it needs to include some volume fraction of laminated shale. The case of dispersed shale can only take place if $C_{sh} \leq \phi_s$.

In the case of *structural clay/shale systems*, because clay/shale exists *only* as replacement of otherwise clean sandstone grains, the maximum possible value of C_{sh} in a structural clay/shale system is equal to $1 - \phi_s$, with the corresponding maximum value of total porosity equal to $\phi_s + (1 - \phi_s) \cdot \phi_{sh}$. Thus, the total porosity of a structural clay/shale system is given by

$$\phi_t = \phi_s + \phi_{sh} \cdot C_{sh},$$

with

$$0 \leq C_{sh} \leq 1 - \phi_s,$$

and

$$\phi_s \leq \phi_t \leq \phi_s + (1 - \phi_s) \cdot \phi_{sh}.$$

When plotted on a Thomas-Stieber diagram, the locus of (C_{sh}, ϕ_t) points included in a structural clay/shale system describes a finite-length line connecting the end points $(0, \phi_s)$ and $(1 - \phi_s, (1 - \phi_s)\phi_{sh})$. The slope of the latter line has the opposite sign to that of sandstone-shale laminated systems. As in the case of dispersed clay/shale systems the equality $C_{sh} = I_{sh}$ does not hold in structural clay/shale systems. A different formulation is needed to transform gamma-ray log values into values of volumetric concentration of clay/shale (to be discussed later).

The three line segments described by the above equations define the fundamental limiting boundaries of the Thomas-Stieber diagram. These boundaries serve as guideline to diagnose variations of clay/shale concentration that are linear combinations (superposition) of the three basic modalities of clay/shale concentration. General clay/shale systems will include the three fundamental modalities of clay/shale systems, whereby their corresponding locus in (C_{sh}, ϕ_t) space (which could result in scattered points) will be contained within the boundaries imposed by fundamental systems.

It is advised that the Thomas-Stieber diagram be constructed as early as possible in the well-log interpretation cycle. A diagram should be constructed separately for each formation unit to avoid the mixing of local trends. One of the common mistakes in the construction of Thomas-Stieber diagrams occurs when the interpreter includes points for an excessively long depth interval. In such cases the diagram will result in a diffuse cloud of points with no evident linear trends. Linear trends often emerge when the diagram is constructed only with points that are included in the same sedimentary cycle, and which have also undergone the same diagenesis.

Thomas-Stieber diagrams are easily constructed with rock-core measurements. Alternatively, they can be constructed with gamma-ray log values instead of calculated values of volumetric concentration of clay/shale, and density log values instead of calculated values of total porosity as long as only one saturating fluid is involved (preferably water). Quite often, Thomas-Stieber diagrams constructed with well logs will clearly indicate the “location” of pure-shale end members. The corresponding linear trends can then be used to infer (extrapolate) the corresponding location of the hypothetical pure-sandstone member of the diagram.

The Thomas-Stieber diagram underlies a method to perform rock classification in siliciclastic sedimentary sequences. According to this method of rock classification, shale-sandstone laminated systems constitute a specific type wherein calculations of porosity, hydrocarbon saturation, and permeability should be performed with parameters (and models) specific to that system. Other systems included in the Thomas-Stieber diagram

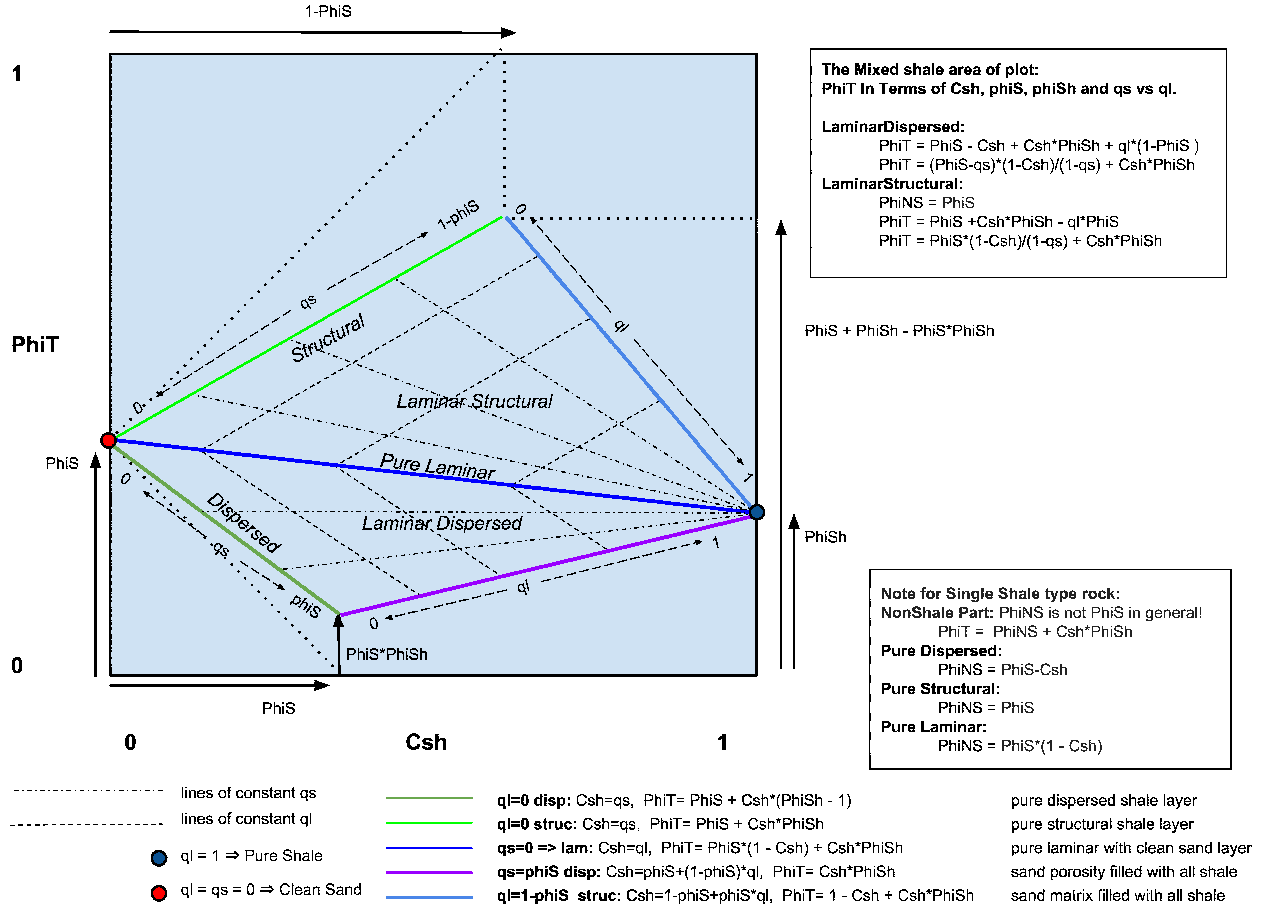


Figure 8.4.1: General description of the Thomas-Stieber diagram.

should be treated and quantified with interpretation models specifically suited for them. Figure 8.4.1 shows a general description of the Thomas-Stieber diagram.

8.5 Indirect calculation of C_{sh}

The procedure for indirect calculation of volumetric concentration of shale from well logs is based on the previous calculation of shale index, I_{sh} , which is often based on the gamma-ray log but on occasion can also be calculated from SP and neutron/density logs. The procedure is to be implemented separately for each sedimentary sequence, and is as follows:

First, the shale index I_{sh} is calculated using the gamma-ray log:

- The gamma-ray log across a pure (clay-free) sandstone corresponds to $I_{sh} = 0$.
- The gamma-ray log across a pure shale corresponds to $I_{sh} = 1$.

- If the well log did not penetrate a pure shale or a pure sandstone, then the density and neutron logs acquired across a water-saturated sandstone are used to determine the value of I_{sh} associated with that specific sandstone.

Then compute C_{sh} as a function of I_{sh} using one of the following formulas:

- Linear: $C_{sh} = I_{sh}$. This calculation is reliable and accurate *exclusively* for the case of sandstone-shale laminated systems consisting of alternations of layers of pure sandstone and pure shale.
- Larionov I: $C_{sh} = 0.083 (2^{3.7 \cdot I_{sh}} - 1)$ for Tertiary clastics.
- Larionov II: $C_{sh} = 0.33 (2^{2 \cdot I_{sh}} - 1)$ for Mesozoic and older rocks.
- Clavier: $C_{sh} = 1.7 - \sqrt{3.38 - (I_{sh} + 0.7)^2}$.
- Stieber:
 - Main formula for South Louisiana Miocene and Pliocene: $C_{sh} = \frac{I_{sh}}{3 - 2 \cdot I_{sh}}$.
 - Variation 1: $C_{sh} = \frac{I_{sh}}{2 - I_{sh}}$.
 - Variation 2: $C_{sh} = \frac{I_{sh}}{4 - 3 \cdot I_{sh}}$
- Histogram-cumulative density function (CDF) approach. This procedure is based on the construction of a histogram of gamma-ray values acquired within the depth interval of interest. The histogram is then transformed into normalized cumulative values which, by definition, vary between zero and one. These normalized cumulative values are then used to define the relationship between C_{sh} and I_{sh} (histogram equalization).
- Construct a specific relationship between I_{sh} and C_{sh} based on rock-core measurements of C_{sh} and gamma-ray log values. This procedure requires that rock-core samples be acquired across a wide range of C_{sh} values.

In all cases, it is extremely important to verify the accuracy and reliability of the transformation using rock-core measurements of C_{sh} . To that end, one constructs a $C_{sh,core}$ vs. $C_{sh,log}$ plot. If points do not correlate, then one modifies either the values of γ_{sand} , γ_{shale} , or the relationship between I_{sh} and C_{sh} ¹ until securing an acceptable correlation. In all cases, the correlation should be consistent with the clay/shale diagnosis elicited from a Thomas-Stieber diagram.

A cross-validation procedure for the calculation of I_{sh} consists of correcting the density porosity and neutron porosity logs for presence of shale within a water-saturated sandstone. The correction is based on readings of density and neutron porosity logs across a pure shale, and is given by

$$\frac{\phi_N - \phi_D}{\phi_{(N,shale)} - \phi_{(D,shale)}},$$

where ϕ_N and ϕ_D are neutron and density porosity logs, respectively, expressed in water-filled sandstone porosity units, and $\phi_{(N,shale)}$ and $\phi_{(D,shale)}$ are readings of the neutron and density porosity logs (water-filled sandstone porosity units), respectively, across a pure shale. After performing the shale correction, both density porosity and neutron porosity logs should overlap (“stack”) along a water-saturated sandstone. Thus, the value of I_{sh} necessary for both logs to stack within a water-saturated provides an excellent calibration in the calculation of I_{sh} via gamma-ray logs. This procedure is *only* applicable across water-saturated sandstones.

¹There is also a possibility to use a relationship such as $I_{sh} = a_0 + a_1\gamma + a_2\gamma^2$ so that $\sum_{i=1}^n (V_{sh,i} - I_{sh,i})^2$ is minimized.

8.6 When is C_{sh} not negligible?

Even though the effect of shale/clay on the petrophysical, flow, electrical, nuclear, elastic, mechanical, etc. properties of clastic rocks can sometimes be neglected when C_{sh} is low, it is important to have a reliable point of quantitative reference for that purpose. As described above, the effect of shale/clay on rock properties depends on the distribution of shale/clay in the pore space, i.e., grain-coating, laminated, or structural shale/clay, as well as on (a) shale porosity, (b) shale composition, (c) types of clay minerals, and (d) shale saturating fluids. As a rule-of-thumb, experience shows that, in general, shale/clay presence in clastic rocks cannot be neglected in the quantification of rock properties when C_{sh} is higher than 10% of the rock's total porosity. This nominal value (10%) may vary slightly according to the specific application but it should always be implemented in reference to the rock's total porosity (e.g., for very low-porosity rocks C_{sh} does not have to be significantly large before shale/clay effects on rock properties become appreciable).

8.7 Recommended interpretation procedure for siliciclastic sedimentary rocks

To assess type, distribution, and volumetric concentration of clay/shale in siliciclastic sedimentary rocks, the following procedures are recommended when evaluating well logs acquired in several wells within the same hydrocarbon field:

1. Verify that gamma-ray logs truly respond to clay/shale content (as opposed to abnormal grain composition, e.g. in the case of arkose sandstones, volcanic sandstones, tuffs, coal seams, etc.)
2. Assess whether gamma-ray logs were corrected for borehole environmental effects. This could be done by constructing a histogram of gamma-ray log values for each of the wells and by quantifying the degree of compatibility (overlapping) among them. If well logs do not exhibit compatible histograms (ranges, modes, means, standard deviations, skewness, asymmetric tails, etc.) then it will be necessary to “balance” all well logs prior to performing the analysis.
3. Partition well logs into depth segments corresponding to tops and bases of rock formations or sedimentary cycles as described by a local geologist. This segmentation will permit one to specialize the analysis and interpretation of well logs to the specific depth segments in the various wells that share the same conditions of sedimentation, diagenesis, and clay alteration. Shale composition and makeup may vary from sedimentary cycle to sedimentary cycle, hence the importance of performing separate analyses for each sedimentary cycle.
4. Construct a histogram of gamma-ray log within a given rock formation and compare it among the corresponding histograms for all the available wells. This histogram comparison will allow the interpreter to assess the presence of distinct sandstone and clay/shale populations (two modes in the histogram), as well as the presence of transitional variations between the two populations. The degree of mixing between the two populations should be associated with the sedimentary environment under consideration, the spatial location of the wells within that sedimentary environment, and the degree of diagenesis and clay alteration.
5. Calculate the shale index, I_{sh} based on global minimum and maximum values of gamma-ray logs acquired in the various wells and across the same formation. Verify the consistency between I_{sh} and the values of C_{sh} measured on rock-core samples (if available). Also verify that C_{sh} is indeed zero when $\gamma = \gamma_{sand}$, which can be done across a water-saturated sandstone. If C_{sh} and I_{sh} are zero across a water-saturated sandstone then both density and neutron porosity logs (expressed in water-filled sandstone porosity units) should be equal (they should “stack”) to each other.

6. Calculate total porosity and construct the Thomas-Stieber diagram. Assess the types of clay distribution included in the rock formation and differentiate the depth segments in the well that exhibit laminar, dispersed, and/or structural clay/shale distribution. Verify this assessment with available geological studies of sedimentary origin and diagenesis. Recall that the equality $C_{sh} = I_{sh}$ only holds true in sandstone-shale laminated systems.
7. Assess type or types of clay within each clay/shale distribution diagnosed in the previous item. Complement the analysis with inspection of thin sections and SEM photographs.
8. Determine the extremal points (vertex) of the Thomas-Stieber diagram with the properties of pure-sandstone and pure-shale end members.
9. Specialize the petrophysical calculations based on the specific distribution of clay/shale. For laminar shale/sandstone systems, consider the effects of measurement anisotropy whenever applicable.

8.7.a Effect of clay/shale on density and neutron porosity logs

It is common to assume a quartz matrix for the calculation of density and neutron porosity logs across siliciclastic rock formations. Along a clean (clay/shale free) sandstone which is fully saturated with water, both neutron and density porosity logs expressed in sandstone porosity units should be the same. In the presence of clay/shale, the neutron log will tend to exhibit higher porosity values than those of the density log even when the sandstone unit is exclusively saturated with water. This behavior is due to both presence of a matrix other than quartz (specifically clay), and presence of hydroxyls in the chemical composition of clay. In such a case, one proceeds to correct the two logs (density and porosity) for the presence of clay/shale such that the corrected logs are indicative of only non-shale porosity. After performing the latter correction both logs should be equivalent across water-saturated sandstones. The shale correction requires knowledge of two parameters: volumetric shale concentration (C_{sh}) and the corresponding value of both porosity logs across a “pure” shale, ϕ_D^{sh} and ϕ_N^{sh} for density and neutron porosity logs, respectively. After performing the shale correction, the corrected logs should be equal to zero across “pure” shales, thereby reflecting the fact that non-shale porosity is null in pure shales.

Shale corrections are necessary prior to diagnosing and quantifying presence of residual gas on the basis of separation between density and neutron porosity logs. While presence of clay/shale in an otherwise clean sandstone unit tends to increase the value of the neutron porosity log and to decrease the value of the density porosity log, presence of residual gas will cause exactly the opposite effect. Thus, if the effect of clay is larger than the effect of gas in the two logs, an inexperienced well-log analyst could miss-interpret clay-bearing depth zones saturated with gas as non-productive intervals. Of course, additional information about the same zone should be garnered from other logs, such as mud logs or resistivity logs, for instance.

Chapter 9

Calculation of Porosity

...I am not one and simple, but complex and many...

– Virginia Woolf, *The Waves*.

The calculation of porosity from well logs should be assisted with core laboratory measurements. Density logs are typically used to estimate porosity, although magnetic-resonance logs can also be used for that purpose. In some rare instances, sonic logs can also be used to estimate porosity. The calculation of rock porosity from density logs requires that the density of both solid and fluid components of the rock be known beforehand. This requirement makes it necessary that additional well logs, such as gamma-ray, apparent neutron porosity, and PEF be used in combination with density logs to calculate rock porosity. The specific procedure used to calculate rock porosity from well logs depends on the type of rock (e.g., clastic vs. carbonate rocks) and expected solid/fluid composition. Usage of laboratory measurements of porosity to support the calculation of porosity from well logs is highly recommended in cases where rocks are spatially complex.

9.1 Porosity from Density Logs

First assumption: one type of fluid and one type of rock matrix (grain). Total porosity is then given by the equation

$$\rho_R = \phi \cdot \rho_f + (1 - \phi) \cdot \rho_m \quad (9.1.1)$$

with

$$\rho_f = \begin{cases} 1.0 \text{ gm/cm}^3 & \text{if } [\text{NaCl}] \leq 100,000 \text{ ppm} \\ 1.1 \text{ gm/cm}^3 & \text{if } [\text{NaCl}] > 100,000 \text{ ppm} \\ (0.8 \text{ or } 0.9 \text{ gm/cm}^3) & \text{sometimes in the case of oil-base mud} \\ \leq 0.3 \text{ gm/cm}^3 & \text{in the case of very light oil (e.g., condensate) or gas} \end{cases} \quad (9.1.2)$$

Figure 9.1.1 shows photographs of grains which can potentially give rise to consolidated and cemented clastic rocks. Grains can originate from the “grinding” (mechanical weathering) of volcanic rocks, carbonate rocks, shales, sandstones, or mixed compositions, among others. Grain density, ρ_m , depends on the predominant original grain composition, which has an important impact on the calculation of rock porosity. Likewise, depending on the origin of grain making up clastic rocks, grains can exhibit microporosity, such as in the case of grains originating from shales.

9.1..1 Derivation

The total mass of the rock is given by

$$M_R = M_f + M_m, \quad (9.1.3)$$



(a) Grains originated from volcanic rocks.



(b) Grains originated from carbonate rocks.



(c) Mixed grains originated from sandstones, igneous rocks, metamorphic rocks, and carbonates.

Figure 9.1.1: Photographs of clastic grains originated from (a) volcanic rocks, (b) carbonate rocks, and (c) sandstone, carbonate, igneous, and metamorphic rocks. Clastic rocks can exhibit variable grain composition, which impacts the calculation of grain density and, ultimately, the calculation of porosity.

where M_R , M_f , and M_m are the mass of the rock, of the fluid filling the pore space of the rock, and of the grains (matrix) included in the rock, respectively.

On the other hand, the total volume of the rock is given by

$$V_R = V_f + V_m , \quad (9.1.4)$$

where V_R , V_f , and V_m are the volume of the rock, of the fluid occupying the pore space of the rock, and of the grains (matrix) included in the rock, respectively.

By dividing (9.1.3) by V_R one finds

$$\rho_R = \frac{M_R}{V_R} = \frac{M_f}{V_R} + \frac{M_m}{V_R} . \quad (9.1.5)$$

In addition, by dividing equation (9.1.4) by V_R one obtains

$$1 = \frac{V_f}{V_R} + \frac{V_m}{V_R}. \quad (9.1.6)$$

By recalling that $\rho_m = \frac{M_m}{V_m}$ and $\rho_f = \frac{M_f}{V_f}$, and invoking equation (9.1.6), equation (9.1.5) becomes

$$\rho_R = \underbrace{\rho_f \frac{V_f}{V_R}}_{\phi} + \underbrace{\rho_m \frac{V_m}{V_R}}_{1-\phi}, \quad (9.1.7)$$

where ϕ is total porosity.

Finally,

$$\rho_R = \phi \cdot \rho_f + (1 - \phi) \cdot \rho_m.$$

It then follows that

$$\boxed{\phi = \frac{\rho_R - \rho_m}{\rho_f - \rho_m} = \frac{\rho_m - \rho_R}{\rho_m - \rho_f}}. \quad (9.1.8)$$

Note that $\rho_b = \rho_R$.

9.2 Sensitivity of Calculated Porosity to Errors in Matrix or Fluid Densities

From the previous section, it becomes clear that rock porosity can only be estimated when matrix (solid) and fluid densities are known beforehand. Uncertainties in ρ_m and ρ_f necessarily translate into uncertainty in ϕ . For a given value of nominal porosity, the question arises as to whether a percent error in ρ_m will give rise to a larger percent error in the calculation of porosity than a percent error in ρ_f . To answer this important question, one begins with the relationship

$$\Delta\phi \approx \frac{\partial\phi}{\partial\rho_m}\Delta\rho_m \Rightarrow \frac{\Delta\phi}{\phi} \approx \frac{\partial\phi}{\partial\rho_m} \frac{\Delta\rho_m}{\phi} \Rightarrow \frac{\Delta\phi}{\phi} \approx \frac{\rho_m}{\phi} \frac{\partial\phi}{\partial\rho_m} \left(\frac{\Delta\rho_m}{\rho_m} \right).$$

Similarly,

$$\Delta\phi \approx \frac{\partial\phi}{\partial\rho_f}\Delta\rho_f \Rightarrow \frac{\Delta\phi}{\phi} \approx \frac{\partial\phi}{\partial\rho_f} \frac{\Delta\rho_f}{\phi} \Rightarrow \frac{\Delta\phi}{\phi} \approx \frac{\rho_f}{\phi} \frac{\partial\phi}{\partial\rho_f} \left(\frac{\Delta\rho_f}{\rho_f} \right).$$

From equation 9.1.8 it follows that

$$\frac{\partial\phi}{\partial\rho_m} = \frac{1 - \phi}{\rho_m - \rho_f},$$

whereupon

$$\frac{\Delta\phi}{\phi} \approx \frac{\rho_m}{\rho_m - \rho_f} \left(\frac{1 - \phi}{\phi} \right) \left(\frac{\Delta\rho_m}{\rho_m} \right).$$

For the case of variations of ρ_f one has

$$\frac{\partial\phi}{\partial\rho_f} = \frac{\phi}{\rho_m - \rho_f},$$

which leads to

$$\frac{\Delta\phi}{\phi} \approx \frac{\rho_f}{\rho_m - \rho_f} \left(\frac{\Delta\rho_f}{\rho_f} \right).$$

The above relationships clearly indicate that a nominal percent change in matrix density has a larger percent effect on the calculated porosity than an equal percent change in fluid density. The adverse effect of an erroneous matrix density on the calculated porosity magnifies as porosity decreases.

9.3 Definition of Density Porosity, ϕ_D

Logging companies often report the density log in so-called *Density Porosity* units. This is done by assuming arbitrary but depth-constant fluid and grain densities. Most commonly, the transformation assumes that the fluid is fresh water and that the grain composition is either pure quartz, pure limestone, or pure dolomite.

From equation (9.1.8) it follows that

$$\phi_D = \frac{\rho_R - \rho_m}{\rho_f - \rho_m},$$

where:

$$\rho_f = 1.0 \text{ gm/cm}^3,$$

and

$$\rho_m = \begin{cases} 2.65 \text{ gm/cm}^3 & \text{if the matrix (solid composition) is quartz} \\ 2.71 \text{ gm/cm}^3 & \text{if the matrix is limestone (calcite)} \\ 2.87 \text{ gm/cm}^3 & \text{if the matrix is dolomite} \end{cases}$$

The reason why density porosity is usually preferred to bulk density in the display of density logs is because neutron porosity logs are expressed *only* in water-filled porosity units for either quartz, limestone, or dolomite matrix. If one wishes to *compare* density and neutron porosity logs (which is often done to diagnose presence of gas in the rock's pore space, for instance) the *only* way to do it is to express the density log in the same porosity units as the neutron log (the neutron log is the inflexible one here!), thus why the origin of *density porosity*.

9.4 Estimation of Fluid Density via Core Measurements and Density Logs

Core laboratory measurements of porosity and matrix (solid) density are relatively easy and fast to acquire from core plugs and slabbed core, respectively. Along a depth segment where fluid density can be assumed constant, one can estimate fluid density via linear least-squares regression of the expression

$$\rho_R = \phi \rho_f + (1 - \phi) \rho_m$$

as follows:

$$\min_{\rho_f} \sum_{i=1}^N \{ \rho_R(z_i) - [\phi_i \rho_f + (1 - \phi_i) \rho_m] \}^2,$$

where N is the number of core measurements of porosity (ϕ_i) and matrix density (ρ_m) acquired at depth z_i , and $\rho_R(z_i)$ is the bulk density measured at the same depth with the density log. The larger the value of N the more robust the estimation will be in the presence of noisy core measurements and well logs.

9.5 Porosity From Neutron Logs

This done by comparing the previous result for ϕ_D to neutron porosity ϕ_N and checking which matrix was assumed by the well-logging company to transform count rates (or ratios of count rates) into water-filled porosity units.

The first assumption here relates to one type of matrix $\begin{pmatrix} \text{limestone} \\ \text{dolomite} \\ \text{sandstone} \end{pmatrix}$ and fresh water.

- If ϕ_D and ϕ_N overlap (are equal), then the assumptions made about the type of matrix and type of fluid were correct.

- If $\phi_N < \phi_D$, then one has different types of matrix and/or fluid(s) than those assumed previously.

Specifically, when $\phi_N < \phi_D$ the saturating fluid is lighter than water provided that the rock matrix was properly selected in the calculation of both ϕ_N and ϕ_D . On the other hand, if $\phi_N > \phi_D$ then the rock matrix assumed in the calculation of both ϕ_N and ϕ_D is incorrect.

9.5.a Correct both ϕ_N and ϕ_D for dominant matrix

This correction requires that both neutron and density porosity logs be recalculated with the matrix (grain composition) established with the analysis of density, PEF, neutron, and sonic logs.

9.5.b How many types of solids?

Second assumption: one type of fluid, several types of matrices. The following is an example of correction for the case of siliciclastic sequences containing variable amounts of **dispersed shale**:

$$\rho_R = \phi_s \rho_f + (1 - \phi_s - C_{sh}) \rho_m + C_{sh} \rho_{sh}, \quad (9.5.1)$$

where $C_{sh} = \frac{V_{sh}}{V_{rock}}$ ¹, ϕ_s is non-shale (or sandstone) porosity, and ρ_{sh} is shale density.

9.5.b.1 Derivation

Mass balance:

$$m_R = m_f + m_{sh} + m_m. \quad (9.5.2)$$

Volume balance:

$$V_R = V_f + V_{sh} + V_m. \quad (9.5.3)$$

Divide (9.5.2) by V_R to obtain

$$\rho_R = \frac{m_R}{V_R} = \frac{m_f}{V_R} + \frac{m_{sh}}{V_R} + \frac{m_m}{V_R}. \quad (9.5.4)$$

By dividing equation (9.5.3) by V_R one obtains

$$1 = \frac{V_f}{V_R} + \frac{V_{sh}}{V_R} + \frac{V_m}{V_R}. \quad (9.5.5)$$

By recalling that $\rho_{sh} = \frac{m_{sh}}{V_{sh}}$, $\rho_m = \frac{m_m}{V_m}$ and $\rho_f = \frac{m_f}{V_f}$, and using (9.5.5), equation (9.5.4) can be rewritten as

$$\rho_R = \underbrace{\rho_f}_{\phi_s} \cdot \underbrace{\frac{V_f}{V_R}}_{C_{sh}} + \underbrace{\rho_{sh}}_{C_{sh}} \cdot \underbrace{\frac{V_{sh}}{V_R}}_{1-\phi_s-C_{sh}} + \underbrace{\rho_m}_{1-\phi_s-C_{sh}} \cdot \underbrace{\frac{V_m}{V_R}}_{1-\phi_s-C_{sh}}. \quad (9.5.6)$$

9.5.b.2 Quick corrections

Shale corrections for the case of dispersed-shale systems (grain-coating clay) can be implemented using the following formulae:

$$\phi_D^{(sh)} = \phi_D - C_{sh} \cdot \phi_{D,sh}. \quad (9.5.7)$$

By analogy, for neutron porosity one has

$$\phi_N^{(sh)} = \underbrace{\phi_N}_{\text{Assumption of quartz matrix}} - C_{sh} \cdot \phi_{N,sh}, \quad (9.5.8)$$

¹ $C_{sh} = 1 \Rightarrow \phi_s = 0$

where $\phi_{D,sh}$ and $\phi_{N,sh}$ are the (constant) values of density and neutron porosity logs measured across a pure shale.

Note that ρ_{sh} is found using a depth segment of the log where $C_{sh} = 1$: read ρ_R where $C_{sh} = 1$, then compute ϕ_{sh} using equation (9.5.9):

$$\phi_{D,sh} = \frac{\rho_b, C_{sh}=1 - \rho_m}{\rho_f - \rho_m}. \quad (9.5.9)$$

Similarly, $\phi_{N,sh}$ is found by reading the neutron log at a depth segment where $C_{sh} = 1$ (i.e., at a pure shale).

- If $\phi_D^{(sh)} = \phi_N^{(sh)}$, then the assumption of water as the non-shale saturating fluid is correct (beware of invasion, though).
- If $\phi_D^{(sh)} > \phi_N^{(sh)}$, then we have a fluid that is lighter than water. The difference $|\phi_D^{(sh)} - \phi_N^{(sh)}|$ depends on fluid density (the lighter the fluid the larger the difference) and hydrocarbon saturation (the larger the hydrocarbon saturation the larger the difference). In the presence of invasion, the inferred fluid density will reflect the mixing between mud filtrate and original hydrocarbon; likewise, the difference will depend on the radial length of invasion and residual hydrocarbon saturation. Some logging companies (e.g. Schlumberger) use the ratio $\frac{\phi_N^{(sh)}}{\phi_D^{(sh)}}$ to diagnose the type of fluid (the ratio fluctuates between one for the case of water and zero for the case of pure gas) and its saturation.
- Be aware of environmental corrections (especially those applied to neutron logs): $|\phi_D^{(sh)} - \phi_N^{(sh)}|$ needs to be greater than the applied environmental corrections!

9.5.b.2.1 Derivation of equation (9.5.7):

Using equation (9.5.1), we obtain

$$\phi_D^{(sh)} = \frac{\rho_b - (1 - C_{sh}) \cdot \rho_m - C_{sh} \cdot \rho_{sh}}{\rho_f - \rho_m}, \quad (9.5.10)$$

which can be equivalently expressed as

$$\phi_D^{(sh)} = \underbrace{\frac{\rho_b - \rho_m}{\rho_f - \rho_m}}_{\phi_D} - C_{sh} \cdot \underbrace{\frac{\rho_{sh} - \rho_m}{\rho_f - \rho_m}}_{\phi_{D,sh}}. \quad (9.5.11)$$

9.5.b.3 Case of a shaly (dispersed shale), water-saturated sandstone

For the case of a shaly, water-saturated sandstone, one has

$$\phi_D^{(sh)} = \phi_N^{(sh)}.$$

Explicitly,

$$\phi_D - C_{sh} \cdot \phi_{D,sh} = \phi_N - C_{sh} \cdot \phi_{N,sh}.$$

It follows that

$$C_{sh} = \frac{\phi_N - \phi_D}{\phi_{N,sh} - \phi_{D,sh}}.$$

The preceding formula is often used to assess volumetric concentration of shale in a water-saturated sandstone.

9.6 Assessment of Porosity via Density and Neutron Logs

Non-shale (sandstone) porosity is often calculated with the approximation proposed by Gaymard and Poupon (1968), given by

$$\phi_s^2 \approx \frac{\phi_D^{(sh)2} + \phi_N^{(sh)2}}{2(1 + 0.12S_{rh})^2 \cdot (1 + 0.5PS_{rh})^2},$$

where S_{rh} is residual hydrocarbon saturation and P is $[NaCl]_{ppm}/1,000,000$ (of formation water). It then follows that when S_{rh} is negligible one has

$$\phi_s \approx \sqrt{\frac{\phi_D^{(sh)2} + \phi_N^{(sh)2}}{2}}. \quad (9.6.1)$$

For the particular case in which $\phi_D^{(sh)}$ and $\phi_N^{(sh)}$ are very close, equation (9.6.1) simplifies to

$$\phi_s \approx \frac{\phi_D^{(sh)} + \phi_N^{(sh)}}{2}.$$

The above formulas are widely used approximations of rock porosity based on neutron-density responses.

Note that, as emphasized earlier, the difference $|\phi_N^{(sh)} - \phi_D^{(sh)}|$ is a function of fluid density, hydrocarbon saturation, and porosity and that, in practice, it is also a function of invasion: the deeper the invasion the higher the effect of mud filtrate and the lower the effect of *in situ* (original) fluid.

A more accurate way to calculate porosity is as follows:

- Identify and quantify the solid components of the rock (quantify their volumetric concentrations),
- Assume that water is the saturating fluid,
- Correct both density and neutron porosity logs so that the corrected logs are expressed in porosity units with the solid matrix as calculated above. Let $\phi_D^{(c)}$ and $\phi_N^{(c)}$ be the corrected density and neutron porosity logs, respectively.
- Calculate the ratio of neutron- to density-corrected porosity logs. This ratio should be less or equal to one. It will be one across water-saturated lithology units. The lower the value of this ratio the lighter the saturating fluid and the larger its saturation.
- Calculate an initial value of porosity with the formula

$$\sqrt{\frac{\phi_D^{(c)2} + \phi_N^{(c)2}}{2}}.$$

With this porosity value, via Archie's equations, calculate hydrocarbon saturation, S_H

- The cross-plot of hydrocarbon saturation vs. ratio of neutron- to density-corrected porosity will give a good approximation to hydrocarbon density, ρ_H . With this value, calculate porosity from the formula

$$\rho_R = \phi \cdot [(1 - S_w) \cdot \rho_H + S_w \cdot \rho_w] + (1 - \phi) \cdot \rho_m. \quad (9.6.2)$$

- With the new calculated value of ϕ , recalculate S_w and ρ_H and refine the calculation of ϕ . Stop when the refinements become negligible.
- Alternatively, equation (9.6.2) can be used to calculate hydrocarbon density as follows:

$$\rho_H = \frac{1}{\phi \cdot (1 - S_w)} \cdot [\rho_R - \phi \cdot S_w \cdot \rho_w - (1 - \phi) \cdot \rho_m]$$

9.7 Derivation of Some Important Density/Porosity Formulas

9.7.a Case of laminated shale

In this case, the rock is composed of laminae of “pure” shale and “pure” sandstone (shale is not present in the pore space of sandstone). It follows that

$$V_b = V_s + V_{sh},$$

and

$$M_b = M_s + M_{sh},$$

where V_b and M_b are the volume and mass of the rock, respectively, V_s and M_s are the volume and mass of sandstone, respectively, and V_{sh} and M_{sh} are volume and mass of shale, respectively. It is emphasized that in the above definition (as indicated elsewhere in these notes), the volume and mass of shale include dry clay, water associated with clay, silt, and water included in the pore space between silt grains and clay minerals.

It then follows that

$$\rho_b = \frac{M_b}{V_b} = \frac{M_s}{V_b} + \frac{M_{sh}}{V_b},$$

where ρ_b is rock density. Recall that

$$\rho_{sh} = \frac{M_{sh}}{V_{sh}} \Rightarrow M_{sh} = \rho_{sh} V_{sh},$$

where ρ_{sh} is shale density. Thus,

$$\rho_b = \left(\frac{V_s}{V_b} \right) \rho_s + \left(\frac{V_{sh}}{V_b} \right) \rho_{sh}.$$

Note that

$$V_b = V_s + V_{sh} \Rightarrow 1 = \frac{V_s}{V_b} + \frac{V_{sh}}{V_b} \Rightarrow \frac{V_s}{V_b} = 1 - C_{sh},$$

where $C_{sh} = V_{sh}/V_b$ is volumetric concentration of shale. Finally,

$$\boxed{\rho_b = (1 - C_{sh}) \rho_s + C_{sh} \rho_{sh}}.$$

Consequently,

$$\boxed{\rho_s = \frac{\rho_b - C_{sh} \rho_{sh}}{1 - C_{sh}}}.$$

For the case of total rock porosity, one has

$$\phi_T = \frac{V_f}{V_b}$$

where ϕ_T is total rock porosity and V_f is total fluid volume in the rock, given by

$$V_f = V_{fs} + V_{fsh}$$

where V_{fs} is volume of fluid in the sandstone and V_{fsh} is volume of fluid in the shale. It then follows that

$$\phi_T = \frac{V_{fs}}{V_b} + \frac{V_{fsh}}{V_b}.$$

By definition,

$$\phi_{sh} = \frac{V_{fsh}}{V_{sh}} \Rightarrow V_{fsh} = V_{sh} \phi_{sh} \Rightarrow \frac{V_{fsh}}{V_b} = \frac{V_{sh}}{V_b} \phi_{sh} = C_{sh} \phi_{sh},$$

where V_{sh} and ϕ_{sh} are volume of shale and shale porosity, respectively. Similarly,

$$\phi_s = \frac{V_{fs}}{V_s} \Rightarrow V_{fs} = V_s \phi_s \Rightarrow \frac{V_{fs}}{V_b} = \frac{V_s}{V_b} \phi_s = (1 - C_{sh})\phi_s ,$$

where V_s and ϕ_s are volume of sandstone and sandstone porosity, respectively.

Consequently,

$$\boxed{\phi_T = (1 - C_{sh})\phi_s + C_{sh}\phi_{sh}} ,$$

and

$$\boxed{\phi_s = \frac{\phi_T - C_{sh}\phi_{sh}}{1 - C_{sh}}} .$$

The boxed formulas above represent the density/porosity mixing laws for shale-sandstone laminated systems.

9.7.b Case of dispersed shale (grain-coating clay)

In this specific case, shale resides within the original pore space of “pure” sandstone. The most common example of such a situation is the one of grain-coating shale arising because of diagenesis of grains. One can then express the volume and mass components of the rock as

$$V_b = V_m + V_{fs} + V_{sh} ,$$

and

$$M_b = M_m + M_{fs} + M_{sh} ,$$

where V_m and M_m are the volume and mass, respectively, of the sandstone matrix component, and V_{fs} and M_{fs} are the volume and mass, respectively, of the fluid contained within the non-shale (sandstone) component of the rock.

It then follows that

$$\rho_b = \frac{M_b}{V_b} = \frac{M_m}{V_b} + \frac{M_{fs}}{V_b} + \frac{M_{sh}}{V_b} .$$

By invoking the definitions

$$\rho_m = \frac{M_m}{V_m} ,$$

$$\rho_f = \frac{M_{fs}}{V_{fs}} ,$$

and

$$\rho_{sh} = \frac{M_{sh}}{V_{sh}} ,$$

one obtains

$$\rho_b = \left(\frac{V_m}{V_b} \right) \rho_m + \left(\frac{V_{fs}}{V_b} \right) \rho_f + C_{sh}\rho_{sh} ,$$

where, as usual, $C_{sh} = V_{sh}/V_b$.

To find an explicit expression for V_m/V_b one resorts to the sum of volume components above, to obtain

$$1 = \frac{V_m}{V_b} + \frac{V_{fs}}{V_b} + C_{sh} .$$

At this point, it is pertinent to define

$$\phi_{n-sh} = \frac{V_{fs}}{V_b}$$

as **non-shale porosity**, i.e. the *volumetric fraction of fluid not contained in shale*, whereupon,

$$\frac{V_m}{V_b} = 1 - C_{sh} - \phi_{n-sh}.$$

Thus, the final expression for ρ_b is

$$\boxed{\rho_b = (1 - C_{sh} - \phi_{n-sh}) \rho_m + \phi_{n-sh} \rho_f + C_{sh} \rho_{sh}}.$$

It follows that

$$\boxed{\phi_{n-sh} = \left(\frac{\rho_m - \rho_b}{\rho_m - \rho_f} \right) - C_{sh} \left(\frac{\rho_m - \rho_{sh}}{\rho_m - \rho_f} \right)}.$$

In the case of porosity, one has

$$\phi_T = \frac{V_f}{V_b} = \frac{V_{fs}}{V_b} + \frac{V_{fsh}}{V_b} = \phi_{n-sh} + \frac{V_{fsh}}{V_b}.$$

Recall that, by definition,

$$\phi_{sh} = \frac{V_{fsh}}{V_{sh}} \Rightarrow \frac{V_{fsh}}{V_b} = \left(\frac{V_{sh}}{V_b} \right) \phi_{sh} = C_{sh} \phi_{sh}.$$

Consequently,

$$\boxed{\phi_T = \phi_{n-sh} + C_{sh} \phi_{sh}}.$$

In the above expressions,

$$0 \leq C_{sh} \leq \phi_s,$$

where ϕ_s is the porosity of an idealized shale-free rock and with the same volumetric concentration of grains (matrix) as the original rock (i.e. $\phi_s = \phi_{n-sh}$ when $C_{sh} = 0$ and $\phi_T = \phi_s \cdot \phi_{sh}$ when $C_{sh} = \phi_s$). Such an inequality emphasizes that, unlike in the case of laminated shale, C_{sh} cannot reach the value of 1 in rocks with dispersed shale.

An alternative expression for ρ_b can be obtained by invoking ϕ_s instead of ϕ_{n-sh} : From the expression of volume components, namely,

$$V_b = V_m + V_{fs} + V_{sh} \Rightarrow 1 = \frac{V_m}{V_b} + \frac{V_{fs}}{V_b} + C_{sh}.$$

Making use of the expression

$$\frac{V_m}{V_b} = 1 - \phi_s$$

then yields

$$\frac{V_{fs}}{V_b} = \phi_s - C_{sh}.$$

Therefore,

$$\boxed{\rho_b = (1 - \phi_s) \rho_m + (\phi_s - C_{sh}) \rho_f + C_{sh} \rho_{sh}}.$$

When $C_{sh} = 0$ the above expression simplifies to

$$\rho_b = (1 - \phi_s) \rho_m + \rho_s \rho_f,$$

as expected, while in the case of $C_{sh} = \phi_s$, one obtains

$$\rho_b = (1 - C_{sh}) \rho_m + C_{sh} \rho_{sh} = (1 - \phi_s) \rho_m + \phi_s \rho_{sh}.$$

To derive an equivalent formulation for porosity, one begins with the expression

$$\phi_T = \frac{V_f}{V_b} = \frac{V_{fs}}{V_b} + \frac{V_{fsh}}{V_b} = \phi_s - C_{sh} + C_{sh}\phi_{sh},$$

whereupon

$$\boxed{\phi_T = \phi_s + C_{sh}(\phi_{sh} - 1)},$$

as emphasized by the Thomas-Stieber diagnostic method, in which case $\phi_T = \phi_s$ when $C_{sh} = 0$, and $\phi_T = \phi_s\phi_{sh}$ when $C_{sh} = \phi_s$ (the maximum allowed value for C_{sh} in dispersed-shale rocks).

Chapter 10

Electrical Resistivity, Porosity, and Water Saturation

...Parto del principio de que la reflexión debe preceder a la acción...

– Julio Cortazar, Rayuela.

The quantification of *in situ* water saturation of rocks is traditionally accomplished by estimating porosity and measuring the rock's electrical resistivity. Borehole measurements of electrical resistivity are routinely acquired during and/or after drilling a well using low-frequency induction or galvanic measurement systems. The transformation of rock's porosity and electrical resistivity into water saturation (or water pore volume) is carried out with effective medium theories that include a few adjustable parameters. Petrophysicists have advanced multiple effective medium theories for that purpose which make different assumptions about the rock's solid composition and pore space, and about the electrical properties of the rock's saturating fluids. Let's review the assumptions and implementation of those effective medium theories...

10.1 Introduction

Based on seminal laboratory work by Gus Archie ([Archie, 1942](#)) as well as theoretical work by others, the electrical resistivity of clay-free clastic rocks is governed by porosity, water saturation, and the electrical resistivity of formation water. Such an important relationship permits the calculation of *in situ* hydrocarbon saturation based on knowledge of porosity and electrical resistivity. Borehole measurements of electrical resistivity are routinely acquired by logging companies in order to assess hydrocarbon saturation in porous and permeable formations. Presence of mud-filtrate invasion requires that resistivity measurements be acquired with multiple radial lengths of investigation. The calculation of *in situ* hydrocarbon saturation is commonly performed with the deepest-sensing electrical resistivity log with corrections for bed thickness and invasion whenever necessary.

Electrical conductivity, an intrinsic property of materials, is commonly measured in the units of *Siemens/m* or *mhos · m*. Its reciprocal, electrical resistivity, is measured in *Ohm · m* or $\Omega \cdot m$. Depending on temperature and volumetric concentration of NaCl, the electrical resistivity of water could fluctuate between 0.0001 and 10000 Ohm·m. On the other hand, the electrical resistivity of hydrocarbons, quartz, or calcite is higher than 10^7 Ohm·m. The range of values of electrical resistivity of subsurface materials is so large that is often displayed with a logarithmic scale.

Archie's equations assume that electrical conduction in fluid saturated rocks takes places only within the water-saturated portion of the pore space. Formation water is assumed electrically conductive and grains electrically insulating. For all practical purposes, hydrocarbon are electrically insulating such that the electrical conductivity of oil is indistinguishable from that of gas (electrical resistivity measurements of saturated rocks cannot distinguish between oil- and gas-saturated rocks).

When rocks are subject to a voltage difference, electric flow lines close the circuit of transport of electric charge. At low frequencies (typically below 200 KHz), continuous electric lines can only be enforced through connected pore space with spatially continuous, electrically conductive aqueous phase. Dead-end pores and, in general, non-connected porosity will not contribute to the electrical conductivity of the rock. Portions of the pore space saturated with hydrocarbon will not permit the passage of electric lines and hence will not contribute to the electrical conductivity of the rock. Pores saturated with hydrocarbons will only permit the passage of electric lines if there is a space of continuous aqueous phase in them. In water-saturated rocks, the reason why electrical conductivity is related to porosity is because, when rocks are subject to electrical conduction, electric lines “sweep” the space occupied by pores connected by the aqueous phase. The density and tortuosity of electric lines also conditions the electrical resistivity of rock; the more tortuous the electric lines (the longer their lengths compared to a straight-line length) the higher the resistivity of the rock. Obviously, the tortuosity of electric lines is conditioned by the spatial distribution and continuity of the pore space.

10.2 Assessment of fluid Saturation

The assessment of water saturation of porous and permeable rocks requires specific values of irreducible water saturation, capillary-bound water saturation, and free (movable) water saturation. Electrical resistivity measurements are sensitive to saturation of the topologically continuous aqueous phase in the pore space. Discrimination between irreducible, capillary-bound, and movable water saturation is one of the most significant technical challenges in formation evaluation and requires the integration of electrical resistivity with additional borehole measurements.

Archie's equations (Archie, 1942) are used to estimate water saturation from measurements of electrical resistivity. For the case of 100% water saturation, Archie's first equation is given by (10.2.1):

$$R_0 = R_w \underbrace{\frac{a}{\phi^m}}_F, \quad (10.2.1)$$

where R_0 is the resistivity of the rock fully saturated with water, R_w is the resistivity of formation water, m is the porosity exponent, and a is the Winsauer factor (the original Archie equation did not contain this factor). Both m and a are estimated from rock-core laboratory measurements. In the above equation, F is referred to as **formation factor**, and is a function of grain-size distribution, grain packing, and grain cementation, as these factors impact the efficiency of pore connectivity. The formation factor is a measure of the efficiency of the rock's pore space to conduct electricity when the conduction is not affected by surface effects. Not all the rock's pore space contributes equally to the conduction of electricity; the concentration of electric lines per unit cross section tends to decrease near corners or dead-end conduits. The smaller the formation factor the larger the efficiency of the rock to conduct electricity through its pore space. Along these lines, the factor

$$\frac{1}{\phi^m}$$

is a measure of the *fraction of the rock's total porosity* which contributes to electrical conduction. When $m = 1$ all the available porosity contributes to electrical conduction (this very special situation takes place when the pore space is a distribution of straight capillary tubes of constant cross-section), while for $m > 1$, ϕ^m decreases, whereby only a fraction of the available porosity contributes to electrical conduction (recall that $0 \leq \phi \leq 1 \Rightarrow \phi^m \leq \phi$ for $m > 1$). In the presence of non-connected (isolated) porosity, the rock's formation factor should be written as

$$\frac{1}{(\phi - \phi_{nc})^m},$$

where ϕ_{nc} designates the non-connected (isolated) porosity (also known as percolation threshold porosity). The latter expression for the rock's formation factor is widely used in carbonate rocks, where because of rock genesis and diagenesis often not all the available pore space is interconnected.

For the case of partial hydrocarbon saturation in the rock's pore space, Archie's second equation is given by:

$$R_t = R_w \underbrace{\frac{a}{\phi^m}}_{R_0} \frac{1}{S_w^n}, \quad (10.2.2)$$

where S_w is water saturation and n is the saturation exponent. The ratio

$$\frac{R_t}{R_0} = \frac{1}{S_w^n}$$

is often referred to as the *resistivity index* of the rock. In this context, the saturation exponent, n , governs the efficiency of the pore space occupied by formation water to conduct electricity (recall that hydrocarbons are not electrically conductive). Isolated "packets" of water in the pore space will not contribute to the rock's electrical conduction when the pore volume includes both formation water and hydrocarbon. The spatial distribution of water and hydrocarbon in the pore space is in general controlled by capillary pressure and relative permeability (assuming equilibrium conditions), and depends on the imbibition/drainage history to which the pore space has been subject to. Because of these considerations, the rock's efficiency to conduct electricity in the simultaneous presence of formation water and hydrocarbon is governed by the product ϕS_w . In fact, it has been postulated by some researchers that Archie's equation could be stated in terms of $(\phi S_w)^\ell$, where ℓ is an exponent governed by the efficiency of the rock's water pore volume to conduct electricity.

In terms of electrical conductivity, Archie's general equation is given by

$$\sigma_t = \sigma_w \cdot \left[\frac{\phi^m}{a} \right] \cdot S_w^n,$$

where σ_t is the electrical conductivity of the rock, and σ_w is the electrical conductivity of formation water, with $\sigma_t = 1/R_t$ and $\sigma_w = 1/R_w$.

From the above equations one readily finds that

$$S_w = \left[\frac{R_w}{R_t} \cdot \frac{a}{\phi^m} \right]^{\frac{1}{n}},$$

or, equivalently,

$$S_w = \left[\frac{\sigma_t}{\sigma_w} \cdot \frac{a}{\phi^m} \right]^{\frac{1}{n}}.$$

When calculating S_w , it is important to emphasize that the above formulas do not make a specific distinction between irreducible, capillary-bound, or free (movable) water. The calculation yields the *total* water saturation. A subsequent step of this calculation should include interpretation methods that split the total water saturation into irreducible, capillary-bound, and movable saturations. In cases of non-zero residual hydrocarbon saturation, the calculation of S_w should deliver values smaller than $1 - S_{or}$, where S_{or} is residual hydrocarbon saturation. These considerations are significant in the case of shaly sandstones, where there is a specific distinction between total porosity, non-shale porosity, total water saturation, and clay-bound water saturation.

It is also important to verify the calculations of S_w by inspecting its trends with respect to TVD. For instance, the usual trend in a hydraulically connected reservoir is one in which S_w increases with depth to a maximum at the free oil-water contact. At the highest point in the reservoir, S_w should take the smallest possible value, equal to irreducible water saturation. Repetition of similar trends in different depth segments indicates presence of hydraulic seals (or permeability barriers), which need to be confirmed by fluid-pressure samples. Likewise, trends of S_w with respect to TVD could reflect presence of capillary transition zones. It is important that trends of water saturation with TVD be verified with pressure sampling.

The typical method to calculate the variables a , m , and n in the above expressions is through laboratory measurements of electrical conductivity of rock-core samples. In so doing, it is imperative that rock-core samples be selected to cover a wide-enough range of porosity values. The first step of the measurement process consists of cleaning the core samples of residual oil saturation. Subsequently, the electrical resistivity of the samples is measured at 100% water saturation for several values of salt concentration. Variations of the electrical resistivity of the sample with salt concentration are indicative of non-negligible clay effects and hence of the inadequacy of Archie's equations to relate electrical resistivity and water saturation.

Measurements of electrical conductivity at 100% water saturation are plotted against porosity using a log-log display. If Archie's first equation is valid then such a plot should display a clear linear trend. The corresponding values of a and m are then calculated via least-squares linear regression. It is important to also calculate the error bars of these calculations for subsequent analysis of uncertainty of hydrocarbon-reserves calculations.

The second step of the core-measurement process is a very tedious and delicate one. It consists of subjecting the core samples to partial hydrocarbon saturation under *in situ* grain wettability conditions. Every discrete value of hydrocarbon saturation requires that the sample be properly stabilized under conditions of capillary equilibrium. Depending on the specific petrophysical properties of the sample, such a process may require a few weeks of stabilization per value of hydrocarbon saturation. The electrical conductivity of the rock is measured for each value of hydrocarbon saturation. If Archie's second equation is valid, then a log-log plot of resistivity index and water saturation should display a linear trend. The saturation exponent, n will then be estimated using linear least-squares regression. Several measurement sequences are performed for different values of salt concentration of formation water to diagnose and quantify effects of clay on the rock's electrical resistivity, especially at low values of water saturation. Presence of thin non-conductive films surrounding rock grains (e.g. when rocks are wetted with oil) causes Archie's saturation exponent, n to abnormally increase at low values of water saturation.

The values of a , m , and n should be verified with cross-plots of resistivity and density logs, for instance. In addition, it is important to perform rock classification such that specific sets of Archie's parameters are applied to each of the diagnosed rock classes. One common mistake in well-log analysis is to use the same Archie's parameters across a multitude of non-related sedimentary cycles.

Even though most carbonate rocks do not include granular material (implicitly assumed in Archie's equations), most well-log analysts apply Archie's equation to ascertain their hydrocarbon saturation from electrical resistivity measurements. The electrical resistivity of general carbonate rocks does exhibit trends similar to those of siliciclastic rocks (e.g. electrical resistivity increases with a decrease of porosity, electrical resistivity increases with a decrease of water saturation, etc.) but it is commonly found that the "fitting" parameters a , m , and n included in Archie's equations do not remain constant for a wide range of porosity and water saturation (as it does happen with siliciclastic rocks). Thus, the common practice when evaluating carbonates is to vary those fitting parameters with respect to porosity and hydrocarbon saturation while honoring rock-core capillary pressure measurements (especially irreducible water saturation due to microporosity). Additionally, carbonate rocks often exhibit pore space that is not inter-connected (which does not contribute to electrical conduction) to the remainder of the pore network. In such cases, it is necessary that the value of porosity included in Archie's equations be the value of *inter-connected porosity*.

10.3 Assumptions Implicit in Archie's Equations

Several assumptions need to be honored when using Archie's equations, namely,

1. Eq. (10.2.1):
 - Electrical conduction takes place only through the topologically continuous (connected) pore space occupied by electrically conductive water (grains are assumed electrically insulating; dead-end and isolated pores do not contribute to electrical conduction),
 - It is valid for clean (clay-free) granular media,

- No electrical conduction takes place through the surface of the grains. It is for this very reason that Archie's equation implicitly postulates that the electrical resistivity/conductivity of a rock is not influenced by size (e.g. size of throats or size of pores), as opposed to permeability, which is indeed influenced by size (this condition stems from the non-slip fluid condition on grain walls implicitly assumed in the definition of permeability),
- It remains a good approximation in the presence of clay if R_w is low ($C_w > 30,000 \text{ ppm}$), S_w is relatively large, and the volumetric concentration of clay/shale is low,
- It is valid at low frequencies (at and below the kHz range), wherein dielectric effects are negligible (beware of the fact that LWD resistivity instruments operate at frequencies around 2MHz),
- Inter-connected porosity: the value of porosity included in the equations should not include non-connected porosity, and
- It is not always valid for the case of non-clastic carbonate formations as the relationship between porosity, water saturation, and electrical resistivity may depend on pore texture and other rock factors. Usually, grainstones are one type of carbonate rock where Archie's equation tends to work similarly to the case of clastic formations. It is imperative that the porosity used in Archie's equation be the one corresponding to inter-connected porosity.

2. Equation (10.2.2)

- It becomes unreliable in oil-wet formations at low values of water saturation (presence of non-conductive thin films in general; n varies with water saturation in those cases),
- The spatial distribution of hydrocarbon in the pore space (governed by capillary forces between the wetting and non-wetting fluid phases) influences the saturation exponent, and
- It becomes unreliable when the hydrocarbon saturation is high in the presence of clay/shale.

One can correct equation (10.2.2) for presence of clay using a shaly-sandstone model. Furthermore, one can calculate non-shale porosity in shaly sandstones using the equation

$$\rho_R = \phi [S_w \cdot \rho_w + (1 - S_w) \cdot \rho_H] + (1 - \phi - C_{sh}) \cdot \rho_m + C_{sh} \cdot \rho_{sh} \quad (10.3.1)$$

10.3.a Iteration between porosity and resistivity to improve the calculation of water saturation

The calculation of water saturation via Archie's equation (or from a shaly-sandstone modification of Archie's equation) can be iteratively improved by including the effect of water saturation on the calculation of porosity. This is done as follows: Let S_w be water saturation obtained from

$$S_w = \left[\frac{R_w}{R_t} \frac{a}{\phi^m} \right]^{\frac{1}{n}}.$$

The corresponding value of porosity is given by

$$\rho_R = \phi [S_w \rho_w + (1 - S_w) \rho_H] + (1 - \phi) \rho_m,$$

where ρ_R is rock density, ρ_w is water density, ρ_H is hydrocarbon density, and ρ_m is matrix (solid) density.

It follows that

$$\phi = \frac{\rho_m - \rho_R}{\rho_m - [S_w \rho_w + (1 - S_w) \rho_H]}.$$

The result from this last equation is then substituted back into Archie's equation to recalculate S_w , then substituted back into the calculation of porosity from rock density. This process continues through a few iterations until reaching convergence. Experience shows that the nested iteration between saturation and

porosity usually converges within 5 iterations. Note that the reliability of the above procedure hinges upon the accuracy and reliability of ρ_H , which needs to be specified a-prior or else calculated from other well logs or measured from live fluid samples. The relative improvement of ϕ and S_w through the nested iterations is typically low in high-porosity formations but tends to be as large as 10 or 20% in low-porosity formations depending on the specific petrophysical parameters under consideration.

10.4 Typical Range of Variation of Archie's Parameters a , m , and n

Archie's parameters a , m , and n (actually, the parameter a was introduced by Winsauer, not by Archie's original publication) cannot be inferred from well logs. They need to be ascertained from laboratory core studies that include a set of rock samples with a wide range of porosity. It is also important to recall that by definition the triplet of parameters (a, m, n) remains constant as long as the set of rock samples belong to the same pore-textural class. Thus, careful attention (and verification) should be paid when choosing the rock samples for laboratory studies so that the inferred values of a , m , and n are not affected by pore-textural mixtures.

Another practical point about the triplet (a, m, n) is that their range of variation is not wide unless under abnormal rock conditions. For the case of the porosity exponent, m , effective-medium theory yields a value of 1.5 for a pack of spherical grains suspended in an electrolyte. Some useful guidelines for m are as follows (Schön, 2015):

- Unconsolidated sandstones: $m \approx [1.3, 1.5]$.
- Very slightly cemented sandstones: $m \approx [1.4, 1.5]$.
- Slightly cemented sandstones: $m \approx [1.5, 1.7]$.
- Moderately cemented sandstones: $m \approx [1.8, 1.9]$.
- Highly cemented sandstones: $m \approx [2.0, 2.2]$.

For the case of Archie's saturation exponent, n , Worthington *et al.*'s (1989) survey indicates that $n \approx [1.1, 2.5]$ for sandstones and $n \approx [1.1, 2.4]$ for carbonates. Because the saturation exponent, n , reflects the efficiency of the rock's electrical conduction in the presence of hydrocarbon saturation, one expects $n > m$ in most cases (i.e., the rock's efficiency of electrical conduction is always greater when the rock is fully saturated with formation water than with partial hydrocarbon saturation).

If histograms were to be made of experimental measurements of a , m , and n across a wide variety of Archie-type rocks, the histograms will exhibit sharp peaks at $a \approx 1$, $m \approx 2$, and $n \approx 2$, with relatively small standard deviations. Small/large values of a , m , and n with respect to their global means are uncommon but do take place every once in a while. The important point to remember is that effectively the three parameters do not typically exhibit a wide range of variability.

10.5 Mixing Laws for Archie's Porosity Exponent

In grain laminated sequences (null volumetric concentration of shale), Archie's porosity exponent, m becomes a function of the direction of flow of electrical currents, either perpendicular or parallel to bedding plane. It follows that:

$$m_{\perp} = -\frac{\log \left(\sum_{i=1}^N c_i / \phi_i^{m_i} \right)}{\log \phi},$$

and

$$m_{\parallel} = \frac{\log \left(\sum_{i=1}^N c_i \phi_i^{m_i} \right)}{\log \phi},$$

where

$$\sum_{i=1}^N c_i = 1,$$

$$\phi = \sum_{i=1}^N c_i \phi_i,$$

and

$$R_i = R_w \frac{a}{\phi_i^{m_i}}.$$

10.6 Some Common Abuses of Archie's Equations

Archie's equations emphasize that the value of rock porosity, ϕ , used to calculate water saturation from electrical resistivity measurements be the **inter-connected porosity**, i.e., the fraction of the total porosity which remains inter-connected by the water phase when the rock is 100% water saturated. While in siliciclastic rocks it is usually the case that total porosity is equal to inter-connected porosity, carbonate rocks are notorious for their presence of occluded porosity due to differential dissolution and recrystallization. The "typical" way to bypass this problem when using Archie's equations is to still use total porosity in the expression used to calculate water saturation but let the porosity exponent, m , take larger than normal values in those log segments where total porosity is larger than inter-connected porosity. Values of m as abnormally large as 5 have been reported in the technical literature when implemented such procedure; it is also common to use a variable m depending on total porosity, i.e., $m = m(\phi)$. This is a highly erroneous procedure which can lead to large biases in the calculation of water saturation. It is recommended that differences between total and inter-connected porosity be estimated from well logs and core samples prior to using Archie's equation to calculate water saturation. When doing so the exponent m will take on values closer to 2.

Another common abuse of Archie's equations pertain to shaly rocks, especially in the case of grain-coating clay (often referred to as dispersed shale). It can be shown that shaly rocks concomitantly exhibit both pore conductivity and clay-surface conductivity. Archie's equation does not account for clay-surface conductivity, it only considers the effect of pore conductivity. Surface conductivity originates from the presence of a double layer of electrical charge in the proximity of clay. The relative influence of pore and surface conductivities on the rock's electrical conductivity depends on the electrical conductivity of formation water (electrolyte concentration and temperature), volumetric concentration of clay, and water saturation. In the case of fresh formation water (which is a desirable condition when searching for drinking-water aquifers), surface conduction will dominate pore conduction, thereby rendering Archie's equation useless. Likewise, if water saturation is relatively low (such as in the case of hydrocarbon-bearing rocks at irreducible water saturation conditions), formation water does not need to be fresh to cause the surface conductivity to out-compete pore conductivity, once again rendering Archie's equation inaccurate. Increasing values of clay concentration will only exacerbate the effect of surface conductivity over pore conductivity in the rock's electrical conductivity. An usual but erroneous way to "adjust" Archie's equation in those abnormal conditions is to use total porosity in the expression but *manipulate* the saturation exponent, n . When doing so, it is found that n takes on abnormally low values, close to 1. Not only is the value of n abnormally low under such erroneous practice but it is also found that n needs to be "adjusted" to account for point-by-point variations of water saturation. Rather than arbitrarily manipulating n (as very often done in the analysis of organic shale), the technical solution to this problem is to use a modification of Archie's equation which explicitly and scientifically takes into account the interplay of surface and pore conductivity in the rock's electrical conductivity (e.g., Waxman-Smits, Revil-Cathles, Clavier, etc.)

The case of electrically anisotropic rocks is also conspicuous. This condition occurs when there is a difference between the electrical conductivity of the rock in the directions parallel and perpendicular to bedding plane. Usually, the electrical conductivity parallel to bedding plane is larger than the electrical conductivity perpendicular to bedding plane. Common examples of such a condition are shale laminated sandstones and sandstones exhibiting marked grain-size variations which give rise to variations of irreducible water saturation (e.g., cross-bedded sandstones). The proper way to approach this problem is to “split” the rock’s electrical conductivity into its components parallel and perpendicular to bedding plane, which requires calculations of dip and azimuth. Thereafter, the two perpendicular components are combined with a model of rock electrical conductivity specifically conceived for the case of transversely isotropic electrical conductivity, to interpret electrical conductivity in terms of water saturation. This procedure is customarily used in the interpretation of shale-laminated sandstones to infer sandstone conductivity first, and then use Archie’s equation (or a shaly-sandstone modification of Archie’s equation) to calculate water saturation within the sandstone fraction of rocks. In the case of grain-size laminations, it was shown by Kennedy and Herrick that the components of electrical conductivity parallel and perpendicular to bedding plane need to be associated with separate values of exponents m and n in Archie’s equation to calculate water saturation from electrical conductivity. Another common abuse of Archie’s equation in electrically anisotropic rocks consists of arbitrarily manipulating the saturation exponent, n to calculate water saturation instead of splitting the rock’s electrical conductivity into its parallel- and perpendicular-to-bedding-plane components. This highly erroneous procedure causes n to take on abnormally low values, close to 1, which are not expected in Archie-type rocks. Likewise, this practice invokes a manipulation of n to account for variations in shale or grain-size concentration.

Very recently, Archie’s equation has been used in the analysis of organic shale. Even though organic shale defies several of the assumptions implicit in Archie’s equation, the temptation of a simple power-law relationship is just too great to resist by some formation-evaluation practitioners. Not only are the m and n exponents manipulated in exotic ways but also the value of R_w is adjusted to be inconsistent with values of electrolyte concentration limited by water solubility.

The examples above indicate that even though Archie’s power-law equation is simple, hence attractive to relate porosity, water saturation, and electrical conductivity in porous rocks, care should be exercised to abide by the assumptions implicit in the formula. Arbitrary manipulations of R_w , m , n , and a in Archie’s equation can become too arbitrary and complex (point dependent) to render such practices overly intricate and unreliable. In practice, many rocks do not exhibit Archie-type behavior, hence requiring extensive core studies to infer a physically viable alternative to relate electrical conductivity with other fluid, petrophysical, and textural properties.

10.7 Determination of R_w

There are several possibilities to estimate R_w , namely,

- The SP log,
- The deep resistivity, R_t , measured across a water-saturated sandstone via equation (10.2.1) : $R_w = R_t \frac{\phi^m}{a}$
- Using a Pickett plot $\log(R_t)$ vs. $\log(\phi)$ within a short depth interval that includes the water-saturated sandstone:

$$\log(R_t) = \log(R_w) + \log(a) - m \log(\phi)$$

where $S_w = 1$,

- From fluid samples retrieved with a wireline formation tester, and
- From fluid samples retrieved with a DST (drill-stem test).

To correct R_w for temperature (extrapolate to temperatures other than the one at which R_w was estimated), one uses Arps' formula given by

$$\frac{R_w(T_2)}{R_w(T_1)} = \frac{T_1 + T_0}{T_2 + T_0}, T_0 = \begin{cases} 6.77 & \text{if } T \text{ in } {}^{\circ}\text{F} \\ 21.5 & \text{if } T \text{ in } {}^{\circ}\text{C} \end{cases}, \quad (10.7.1)$$

where T_1 is the temperature at which $R_w(T_1)$ was estimated (or measured) and T_2 is the temperature where $R_w(T_2)$ is desired. Arps' equation assumes water saturated with NaCl. The conversion can also be done with Schlumberger's chart [GEN-9](#), plotted here as Figure 10.7.1. This chart also gives the correspondence between the *NaCl* concentration in *ppm* and the electrical resistivity of the solution. For other aqueous solutions, refer to Schlumberger's chart [GEN-8](#), also plotted here as Figure 10.7.1.

Unit conversions for sodium chloride concentrations can be done using table 10.1¹.

Salt (weight %)	ppm	$mg \cdot L^{-1}$
0.5	5,000	5,020
1	10,000	10,050
2	20,000	20,250
3	30,000	30,700
4	40,000	41,100
5	50,000	52,000
6	60,000	62,500
7	70,000	73,000
8	80,000	84,500
9	90,000	95,000
10	100,000	107,100
11	110,000	118,500
12	120,000	130,300
13	130,000	142,000
14	140,000	154,100
15	150,000	166,500
16	160,000	178,600
17	170,000	191,000
18	180,000	203,700
19	190,000	216,500
20	200,000	229,600
21	210,000	243,000
22	220,000	256,100
23	230,000	270,000
24	240,000	283,300
25	250,000	297,200
26	260,000	311,300

Table 10.1: Equivalent NaCl concentrations.

To convert salt concentration to electrical resistivity, one can use the following formulae at $T_0 = 75 {}^{\circ}\text{F}$

$$[NaCl_{ppm}] \simeq 10^{\frac{3.562 - \log_{10}(R_w_{75} - 0.0123)}{0.955}}, \quad (10.7.2)$$

and

$$R_w_{75} \simeq 0.0123 + \frac{3647.5}{[NaCl_{ppm}]^{0.955}}, \quad (10.7.3)$$

¹Source : [Bourgoyne, Jr. et al. \(2003\)](#) page 52.

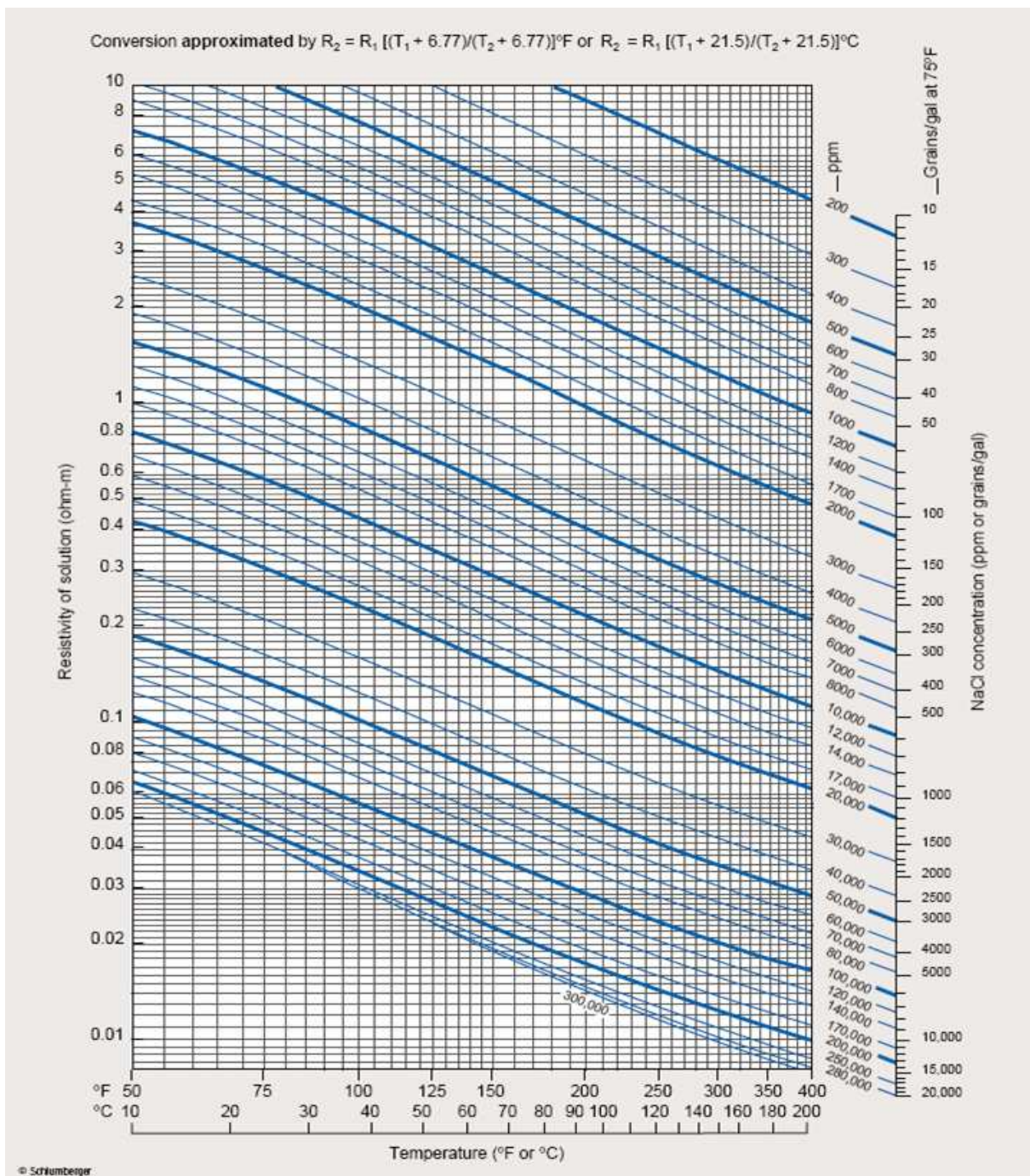


Figure 10.7.1: Conversion chart for NaCl concentration, temperature, and resistivity of aqueous solutions.

where $[NaCl_{ppm}]$ is the concentration of NaCl in ppm. The result can then be corrected for temperature using Arps' equation ((10.7.1)). The combination of both equations when expressed in British measurements units yields

$$R_w \simeq \left(0.0123 + \frac{3647.5}{[NaCl_{ppm}]^{0.955}} \right) \cdot \left(\frac{81.77}{T + 6.77} \right) = \frac{1}{T + 6.77} \cdot \left(1.005771 + \frac{298256.075}{[NaCl_{ppm}]^{0.955}} \right). \quad (10.7.4)$$

The error in the above equation is approximately 2% when the concentration of NaCl is between 500 and 100,000 ppm, and between 2 and 10% when the concentration of NaCl is between 100,000 and 230,000 ppm. It follows that

$$NaCl_{ppm} \approx 10^{1.0471\{3.562 - \log_{10}\left[\left(\frac{T+6.77}{81.77}\right)R_w - 0.0123\right]\}}. \quad (10.7.5)$$

10.8 Electrical Resistivity of Rocks in the Presence of Invasion

Presence of invasion causes the electrical resistivity of formation water to be a function of the radial distance into the invaded formation. This behavior takes place because of salt mixing between mud filtrate and formation water. Near the wellbore, salt concentration will be close to that of mud filtrate, whereas far from the borehole wall the salt concentration will be identical to that of formation water. Such a behavior is also a function of time of invasion and temperature. On account of this phenomenon, in general, Archie's equation can be written as

$$R_t(r, t, T) = R_w(r, t, T) \cdot \left[\frac{a}{\phi^m} \right] \cdot \frac{1}{S_w^n(r, t)},$$

where r is radial distance measured from the borehole wall, t is time of invasion and T is temperature.

We consider two special cases of invasion. For the situation in which invasion takes place with water-base mud one has

$$R_t(T) = R_w(T) \cdot \left[\frac{a}{\phi^m} \right] \cdot \frac{1}{S_w^n}, \quad (10.8.1)$$

for $r \rightarrow \infty$ regardless of time of invasion. Likewise, for $r \rightarrow 0$ at steady-state conditions makes the following definition

$$R_t(r \rightarrow 0, t \rightarrow \infty, T) \equiv R_{xo},$$

in which case, one has

$$R_{xo}(T) = R_{mf}(T) \cdot \left[\frac{a}{\phi^m} \right] \cdot \frac{1}{S_{xo}^n}, \quad (10.8.2)$$

where R_{mf} is the electrical resistivity of mud filtrate at formation temperature and S_{xo} is water saturation in the invaded zone.

For the case of invasion with oil-base mud, the salt concentration in the mud is null, whereupon one has that $S_{xo} = S_w$ and

$$R_{xo}(T) = R_w(T) \cdot \left[\frac{a}{\phi^m} \right] \cdot \frac{1}{S_w^n}. \quad (10.8.3)$$

Shallow-sensing electrical resistivity measurements will respond to R_{xo} whereas deep-sensing measurements will tend to measure R_t . Intermediate-sensing resistivity measurements will respond to rock electrical resistivity values that will be partially influenced by salt mixing and water saturation. Whereas radial variations of S_w are governed by porosity, permeability, relative permeability, and capillary pressure, radial variations of R_w are governed by the process of salt mixing between mud filtrate and formation water. The process of fluid displacement resulting in radial variations of S_w is not governed by the same physical principles governing the radial variations of R_w , as the latter variations are governed by the spatially continuous aqueous phase alone. In some instances, the water saturation front in the radial direction may be "de-phased" from the salt concentration front, thereby giving rise to a so-called electrical resistivity annulus in the radial direction.

10.9. Saturation-Height Analysis: Relationship Between Water Saturation, Capillary Pressure, and Height Above the Free Water-Hydrocarbon Contact

Differences between R_{xo} and R_t attributed to variations of S_w (as opposed to radial variations of the volumetric concentration of salt) can be used to diagnose the ability of the rock formation to displace original fluid. However, care must be exercised when performing such interpretations because the displacement of *in situ* fluids by mud filtrate is also governed by the enforced overbalance pressure exerted by drilling mud.

10.9 Saturation-Height Analysis: Relationship Between Water Saturation, Capillary Pressure, and Height Above the Free Water-Hydrocarbon Contact

There are cases in which the calculation of water saturation obtained from resistivity measurements can be verified against complementary information. One possibility is to examine the calculated values of water saturation against TVD, especially when the well intersects a free water-hydrocarbon contact. In such situations, rock-core capillary pressure measurements can be used to predict the variations of water saturation with height above the free water-hydrocarbon contact. If the depth zone under consideration is hydraulically communicated, water pressure above the free water-hydrocarbon contact is given by

$$\Delta P(z_{TVD}) = P(z_{TVD}) - P(z_{fhw}) = -g(\rho_w - \rho_h)(z_{TVD} - z_{fhw}),$$

where z_{TVD} is the TVD of the depth point under consideration, z_{fhw} is the TVD of the free water-hydrocarbon contact, g is the acceleration of gravity, and ρ_w and ρ_h are the densities of water and hydrocarbon, respectively. If the immiscible fluids that co-exist within the depth interval between z_{TVD} and z_{fhw} (hydrocarbon and water) are in capillary equilibrium and water is the wetting phase of the system, then it follows that

$$\Delta P(z_{TVD}) = P_c(S_w),$$

where P_c is the saturation-dependent capillary pressure. It then follows that

$$z_{TVD} - z_{fhw} = \Delta z_{TVD} = \frac{P_c(S_w)}{g(\rho_w - \rho_h)}.$$

This last equation allows one to predict the value of water saturation expected at a given height above the free water-hydrocarbon contact if the laboratory core measurement of $P_c(S_w)$ is representative of the system. Discrepancies between saturations obtained with resistivity measurements and those obtained with capillary pressure and saturation-height analysis should be examined to discern possible causes.

One way to implement the above procedure is to express capillary pressure in terms of the few parameters that define the petrophysical system. Leverett proposed that capillary pressure be expressed as

$$P_c(S_w) = J(S_w) \cdot \sigma_{hw} \cdot \sqrt{\frac{\phi}{k}},$$

where σ_{hw} is the interfacial tension between water and hydrocarbon, ϕ is porosity, k is permeability, and $J(S_w)$ is the so-called Leverett's J function.

The central idea behind Leverett's formula is that capillary pressure is primarily governed by the porosity-permeability ratio of the system (ratio of storage capacity to flow capacity). The function $J(S_w)$ is intended to capture the variability of capillary pressure with respect to water saturation independently of the porosity-permeability ratio of the system. One way to capture this variability is to express Leverett's J function as

$$J(S_w) = a \cdot (S_w - S_{wi})^b = \frac{P_c(S_w)}{\sigma} \cdot \sqrt{\frac{k}{\phi}},$$

where S_{wi} is irreducible water saturation, and a and b are arbitrary constants obtained from least-squares fitting of the capillary pressure curve measured in the laboratory. Likewise, knowledge of the constants a and

b above permits to “re-scale” the measured capillary pressure curve to obtain that of systems with different porosity-permeability ratios. Conversely, the variations of water saturation as a function of height from the water-hydrocarbon contact (calculated with resistivity measurements) could be fit to Leverett’s J function to estimate the effective porosity-permeability ratio of the entire petrophysical system.

Leverett’s J function and its relationship with capillary pressure is used in well logging to verify the consistency of calculated saturations above a free water-hydrocarbon contact as well as to verify the consistency of the calculated saturations with respect to variations of rock’s porosity and permeability.

The plots displayed in Figure 10.9.1 also show two examples of capillary pressure curves. The end of the curves at $S_w = 1$ can be interpreted as the displacement pressures for the different rocks, i.e. the minimum pressure necessary to initiate drainage. The vertical asymptotes of the curves represent irreducible water saturation. Because fluid pressure in the rock cannot be that high, water saturation cannot take values lower than irreducible water saturation. Rock No. 2 (green curve) is less permeable than Rock No. 1, is also finer grained and has poorer sorting.

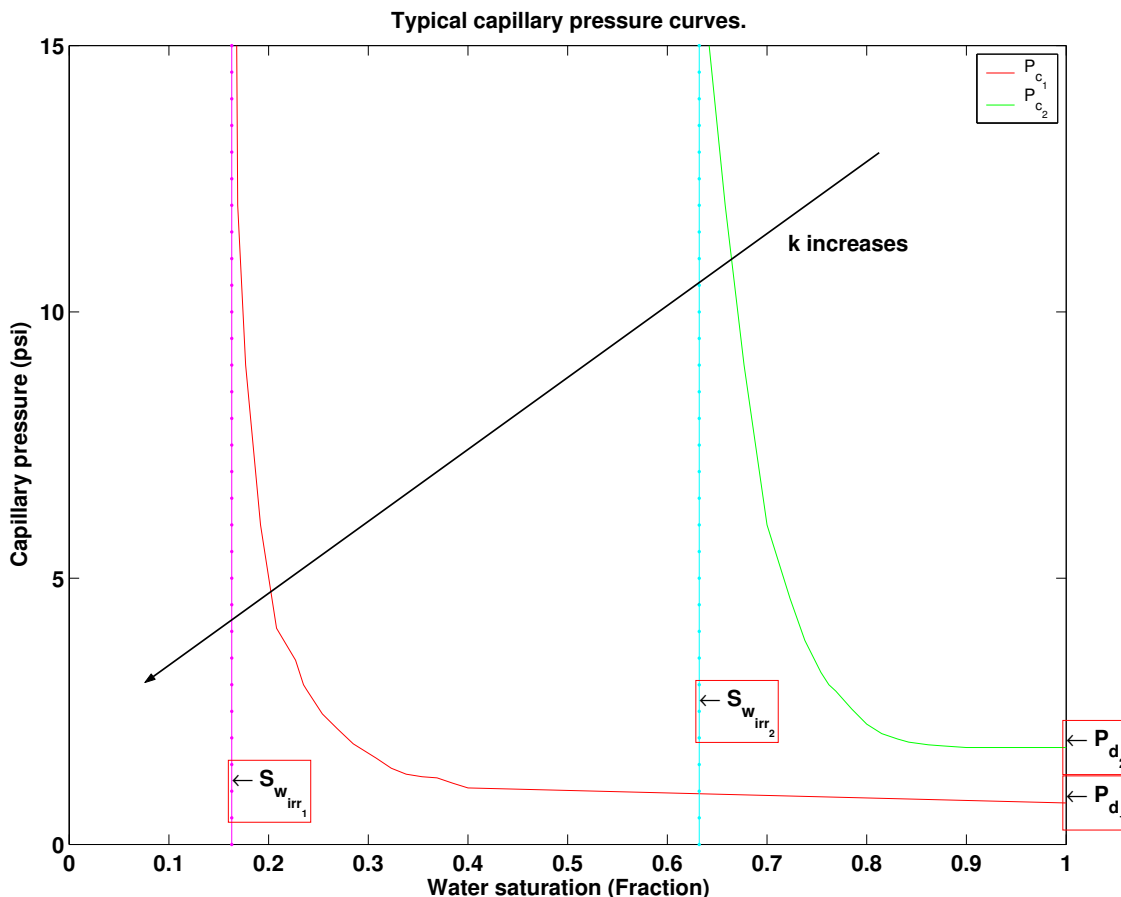


Figure 10.9.1: Two examples of capillary pressure curves.

10.10 Water Saturation is Typically Not Randomly Distributed in Space

Leverett's J function coupled with the concept of rock classes (a rock class in Leverett's sense is a group of rocks that exhibit the same value of k/ϕ), capillary pressure, and presence of a free hydrocarbon-water contact are instructive to understand that **water saturation is not randomly distributed in space** under equilibrium conditions. This is the reason why all calculations of water saturation from well logs need to be verified to satisfy class-by-class capillary equilibrium. Geostatistical interpolations of water saturation between wells should also adhere to this principle.

Non-structured spatial variations of water saturation in reservoirs can only be found in cases where the initial distribution has been artificially modified by water flooding operations, for instance, or by other means of primary and enhanced hydrocarbon recovery.

10.11 Estimation of Fluid Density From Pore-Pressure Measurements

Incidentally, the expression

$$\Delta P(z_{TVD}) = P(z_{TVD}) - P(z_{fhw}) = -g(\rho_w - \rho_h)(z_{TVD} - z_{fhw})$$

above can be used to estimate fluid density from pore-pressure gradients. It follows that

$$\rho_h = \rho_w + \frac{1}{g} \frac{\Delta P(z_{TVD})}{z_{TVD} - z_{fhw}}.$$

The latter equation is widely used for the estimation of fluid density from pore-pressure gradients, where pore pressures are measured with a formation tester.

10.12 Bed-Thickness and Invasion Corrections of Electrical Resistivity Measurements

The calculation of water saturation from electrical resistivity measurements via, for instance, Archie's equations, requires precise knowledge of the rock's electrical resistivity. An important technical issue here is whether resistivity measurements are truly representative of the the electrical resistivity of rocks penetrated by a well.

Resistivity tools measure electric voltages induced at receiver coils (induction devices) or electrical current at contact electrodes (laterolog devices). Such measurements are subsequently transformed into so-called *apparent resistivities* using simple approximations that permit rapid, real-time calculation of resistivity curves for display up-hole. Depending on the geometrical characteristics, physical properties, and frequencies of operation, logging companies make use of specialized algorithms to transform the "raw" voltage measurements into a finite set of resistivity curves with multiple radial lengths of investigation and vertical resolution. In general, such transformations assume infinitely thick, homogeneous, and uninvaded formations. Cases of thin (usually thinner than 4 ft) beds and invaded formations require that apparent resistivity beds be corrected for the effects of bed thickness (also known as "shoulder-bed" corrections) and invasion prior to using them in Archie's equation for the calculation of hydrocarbon saturation. Unaccounted bed-thickness and invasion corrections of resistivity logs could substantially bias the estimation of hydrocarbon reserves.

Logging companies provide charts and correction tables for the effects of both bed thickness and invasion (invasion-correction charts often exhibit the form of a tornado, hence explaining their popular name of "tornado charts"). Also, different resistivity tools (e.g. dual induction and array induction) will have their own set of correction charts. The recommended practice is to always take readings of electrical resistivity at the center of the bed before making the corresponding corrections for bed thickness and invasion.



Figure 10.13.1: Photograph of aeolian Navajo sandstone showing prominent cross-bedding. Grain-size laminations such as those due to cross-bedding in aeolian sandstones give rise to electrical resistivity anisotropy because of the associated variations of irreducible water saturation (Zion National Park, Utah; photograph courtesy of Laura Net).

10.13 Resistivity Anisotropy and Water Saturation

Electrical resistivity measurements acquired in high-angle and horizontal wells may exhibit the effect of electrical anisotropy of thin beds and/or fine laminations penetrated by the well. When these laminations are thinner than the vertical resolution of resistivity measurements then the measurements will be affected by a linear combination of the electrical resistivities parallel and perpendicular to bedding plane. Modern resistivity tools are equipped with multi-component induction sources and multi-component induction sensors to estimate dip and azimuth of layers penetrated by a well in addition to electrical resistivity parallel and perpendicular to bedding plane. The difference between the two values of resistivity can be used to diagnose and quantify presence of thin laminations below the spatial resolution of the measurement.

Figure 10.13.1 shows an outcrop of aeolian Navajo sandstone (Zion National Park, Utah) exhibiting prominent cross-bedding. The grain-size laminations associated with cross-bedded sandstones give rise to electrical resistivity anisotropy because of the corresponding variations of irreducible water saturation in hydrocarbon reservoirs.

Calculation of water saturation from electrical resistivity measurements assumes the use of the rock's electrical resistivity parallel to bedding plane. Thus, to properly calculate hydrocarbon saturation from electrical resistivity measurements acquired in high-angle and horizontal wells it is necessary that the measurements be decomposed into parallel and perpendicular resistivities (or conductivities) to bedding plane.

In laminated systems consisting of alternations of pure sandstone and pure shale, the electrical resistivity of pure sandstone is governed by the equation

$$\frac{1}{R_t} = \frac{C_{sh}}{R_{sh}} + \frac{1 - C_{sh}}{R_s},$$

where R_t is the parallel-to-bedding-plane electrical resistivity, C_{sh} is the volumetric concentration of shale, R_{sh} is the parallel-to-bedding-plane electrical resistivity of pure shale, and R_s is the parallel-to-bedding-plane electrical resistivity of pure sandstone. The above formula, often referred to as the **Poupon equation** is solved for R_s assuming that C_{sh} and R_{sh} are known (while C_{sh} may, of course, be variable with depth, R_{sh} is often assumed constant within the same formation and equal to the electrical resistivity of the closest "pure" shale associated with the rock formation under study). Subsequently, S_w in the sandstone is estimated via Archie's or any shaly-sandstone saturation-resistivity model using the previously calculated value of sandstone porosity (ϕ_s). Accordingly, from the above equation one obtains

$$R_s = (1 - C_{sh}) \frac{R_{sh} R_t}{R_{sh} - C_{sh} R_t},$$

which requires that

$$R_{sh} > C_{sh} R_t.$$

The latter inequality is often not satisfied when (1) the rocks are not laminated, (2) the dip and azimuth are incorrect, (3) C_{sh} is incorrect, and/or (4) R_{sh} is not equal in the shale laminae to that of the assumed "pure" shale.

With the recent commercialization of borehole induction systems capable of measuring dip, azimuth, parallel-to-bedding plane resistivity, R_H , and perpendicular-to-bedding plane resistivity, R_V , it is possible to generalize the above equations to cases where both sandstone and shale end members are both electrically anisotropic. For the case in which both end members are isotropic, one has

$$\frac{1}{R_H} = \frac{C_{sh}}{R_{sh}} + \frac{1 - C_{sh}}{R_s},$$

and

$$R_V = C_{sh} \cdot R_{sh} + (1 - C_{sh}) \cdot R_s,$$

where R_V and R_H are the measured resistivities perpendicular and parallel to bedding plane, respectively. It follows that

$$R_s = \frac{R_V - C_{sh} R_{sh}}{1 - C_{sh}},$$

which requires that

$$R_V > C_{sh} R_{sh}.$$

The above system of equations for R_H and R_V can be solved to calculate both R_{sh} and R_s . Alternatively, when R_{sh} is known, the same system of equations can be used to calculate C_{sh} and R_s .

When the pure-shale end member of the sequence is electrically anisotropic one has

$$\frac{1}{R_H} = \frac{C_{sh}}{R_{shH}} + \frac{1 - C_{sh}}{R_s},$$

and

$$R_V = C_{sh} \cdot R_{shV} + (1 - C_{sh}) \cdot R_s,$$

where R_{shV} and R_{shH} are the perpendicular- and parallel-to-bedding-plane resistivities of shale, respectively. In the latter case, the system of equations could be solved to calculate R_s and R_{shV} .

Finally, in the most general case, where both sandstone and shale end members are electrically anisotropic, one has

$$\frac{1}{R_H} = \frac{C_{sh}}{R_{shH}} + \frac{1 - C_{sh}}{R_{sH}},$$

and

$$R_V = C_{sh} \cdot R_{shV} + (1 - C_{sh}) \cdot R_{sV},$$

where R_{sV} and R_{sH} are the perpendicular- and parallel-to-bedding-plane resistivities of the pure-sandstone end member of the sequence. In the latter case the system of two equations is solved to find R_{sV} and R_{sH} under the assumption that both R_{shV} and R_{shH} are known from measurement acquired across pure shale.

In all of the above cases, R_s is used in connection with either Archie's model or a shaly-sandstone model to estimate hydrocarbon saturation.

10.14 Some Diagnostic Plots

The relationships between porosity, water saturation, and electrical resistivity discussed above are often used to diagnose *in situ* petrophysical conditions, or to calculate petrophysical parameters, from well logs or/and core data. The following are some common examples.

10.14.a Pickett's plot

The log-log plot of electrical resistivity vs. water saturation is often referred to as Pickett's plot. According to Archie's equation,

$$\log(R_t) = \log(R_w) + \log(a) - m \log(\phi) - n \log(S_w).$$

For S_w constant, the above equation indicates that a plot of measurements of $\log(\phi)$ vs. $\log(R_t)$ acquired in co-textural Archie's rocks will trace a straight line with slope equal to $-m$ and ordinate at the origin equal to $\log(R_w) + \log(a) - n \log(S_w)$. For the specific case of 100% water saturation, the ordinate at the origin will be equal to $\log(R_w) + \log(a)$.

Pickett's plot is used to diagnose whether the rocks under consideration belong the same textural family (the plot will then elucidate one single straight line). If that is the case, then for known values of a and m the ordinate at the origin can be used to infer R_w (if the plot is constructed with well logs it is necessary that the samples be constrained to a relatively short depth interval to avoid variations of R_w due to temperature). Also, the dispersivity of the plot (i.e., the plot traces a cloud of points with a strong linear correlation) can be used to diagnose the variability of textural conditions within the set of samples (for instance, due to presence of shale/clay).

In the case of constant porosity, a plot of $\log(S_w)$ vs. $\log(R_t)$ will also tend to elucidate a straight line with slope equal to $-n$ and ordinate at the origin equal to $\log(R_w) + \log(a) - m \log(\phi)$. Such a plot can be used to diagnose whether the set of measurements exhibit a consistent value of n whereas the dispersivity of the "cloud" of points can be used to assess the uniformity of textural properties within the set of samples.

10.14.b Buckle's plot

Buckle's plot is based on the experimental assumption that the water pore volume,

$$\phi \cdot S_w,$$

remains constant and equal to $\phi \cdot S_{wi}$ (where S_{wi} is irreducible water saturation) when rocks belong to the same textural class and are found at conditions of irreducible water saturation. Each textural rock class will then exhibit its own value of $\phi \cdot S_w = c$, whereby a plot of $\log(\phi)$ vs. $\log(S_w)$ will trace a straight line with slope equal to -1 and ordinate at the origin equal to $\log(c)$. If the plot is constructed between ϕ and S_w then it will trace a hyperbola if all the samples belong to same textural class.

Buckle's plot is often used to diagnose whether all sample points belong to a common textural class (they will exhibit a common value of c) and whether all sample points remain at conditions of irreducible water saturation (they will be located along the same straight line with negligible cloud dispersivity).

10.14.c Hingle's plot

Another widely used diagnostic plot is the so-called Hingle plot, which implements Archie's equation written in the form

$$\left(\frac{1}{R_t}\right)^{\frac{1}{m}} = \left(\frac{S_w^n}{aR_w}\right)^{\frac{1}{m}} \phi.$$

The x-axis of the plot is ϕ in linear scale while the y-axis of the plot is $\left(\frac{1}{R_t}\right)^{\frac{1}{m}}$ in logarithmic scale. For a given value of m (usually 2), families of equal S_w values will trace a line with a given slope. This plot is often used in combination with Pickett's plot to ensure consistency in the calculations of S_w and R_w together with the verification of m and n .

10.15 Interpretation for Sandstones with Grain-Coating Clay

Presence of shale in rocks affects the static and dynamic petrophysical properties of their corresponding shale-free members. In addition, presence of shale modifies rock physical properties such as electrical conductivity, acoustic velocity of propagation, shear velocity of propagation, etc. Methods used to quantify the effect of shale on rock physical and petrophysical properties depend on whether the topology of the shale fraction is dispersed (grain-coating), laminated, or structural (or a combination of the three basic types). The case of laminated shale-sandstone system was addressed earlier in these notes. We now concentrate on the specific case of sandstones with grain-coating clay, commonly referred to as dispersed-shale sandstones in the well-logging literature.

Some of the basic equations for interpretation are as follows. In the case of dispersed shale (grain-coating clay), total porosity, ϕ_t is given by

$$\phi_t = \phi_s + C_{sh}\phi_{sh},$$

where ϕ_s is sandstone (non-shale) porosity, C_{sh} is volumetric concentration of shale, and ϕ_{sh} is shale porosity. Bound water saturation is defined as the volumetric fraction of water contained in the shale portion of the rock, and is given by

$$S_b = \frac{V_{shw}}{V_f + V_{shw}} = \frac{V_{shw}}{V_{sh}} \cdot \frac{V_{sh}}{V_f + V_{shw}} = \phi_{sh} \cdot \frac{V_{sh}/V_R}{(V_f + V_{shw})/V_R},$$

where V_{sh} is volume of shale, V_{shw} is volume of water contained in shale, V_f is the total volume of rock fluids, and V_R is the total rock volume. In this context, S_b is not to be confused with irreducible water saturation.

Equivalently,

$$S_b = C_{sh} \cdot \frac{\phi_{sh}}{\phi_t}.$$

Total water saturation, on the other hand, is given by

$$S_w = \frac{V_w + V_{shw}}{V_f + V_{shw}} = \frac{V_w/V_R}{(V_f + V_{shw})/V_R} + S_b = \frac{\frac{V_w}{V_f} \cdot \frac{V_f}{V_R}}{\phi_t} + S_b.$$

Equivalently,

$$S_w = \frac{\phi_s \cdot S_{ws}}{\phi_t} + S_b,$$

where S_{ws} is sandstone (non-shale) water saturation.

It follows that

$$S_{ws} = \frac{S_w - S_b}{1 - S_b}.$$

10.15.a Physical model

The negative surface (hence the importance of surface-to-volume ratio in clays) charge density of clays (due to the prevalent exchange $Si^{4+} \rightarrow Al^{3+}$) gives rise to an electrostatic potential, whereby dipolar water molecules are attracted by clay minerals, thereby generating an immobile thin film of water surrounding them (the hydrated layer). This is the origin of irreducible water in the presence of grain-coating clay. Additionally, the negative surface charge density causes the attraction of cations (e.g., Na^+ and Ca^{2+} surrounded by six water molecules, i.e., hydrated Na^+) present in formation water toward the hydrated layer, to form the so-called Stern layer (a thin layer of adsorbed hydrated cations). Outside the Stern layer, a diffuse cloud of (hydrated) cations is formed whose abnormal concentration (compared to that of water in the pore volume) decreases exponentially away from the Stern layer, often referred to as the diffuse cation cloud. Therefore, the latter phenomenon causes that the volumetric concentration of cations in the vicinity of the Stern layer to increase compared to that of bulk formation water. The combination of the negative surface charge density, the hydrated layer (adsorbed water), the Stern layer, and the diffuse cation cloud is referred as the *electrical double layer of electrical charge, EDL*. When an external electrical current is established through the rock, the electrical double layer is responsible for an enhancement of the rock's electrical conductivity compared to that predicted by Archie's equation, and which is clearly due to surface effects (Archie's conduction is entirely a volumetric effect).

The surface enhancement of rock's electrical conductivity is governed by the following factors:

- salt concentration of formation water, the lower the salt concentration the larger the enhancement,
- temperature,
- surface-to-volume ratio (specific surface) of clay crystals, S/V , the larger the specific surface the larger the enhancement.
- hydrocarbon saturation, the larger the pore volume fraction of hydrocarbon the larger the enhancement, and
- density of negative surface electric charge, the larger the density of negative charge the larger the enhancement.

There are several ways commonly used to describe the electrical conductivity of sandstones with grain-coating clay. The most general description is given by

$$\sigma_R = \sigma_A + X = \frac{\sigma_w \phi^m S_w^n}{a} + X, \quad (10.15.1)$$

where σ_R is the rock's electrical conductivity and σ_A is the rock's electrical conductivity as quantified by Archie's equation. The additive component X above identifies the surface conductivity arising from the presence of grain-coating clay and the equation is motivated by the analogy with a parallel circuit in which part of the current flows through the water pore volume while the remaining one flows through the electrical double later (recall that conductances are additive in a parallel-type circuit). Note also that the additive component X above causes the rock's electrical conductivity to be dependent on size (i.e., size of pores) because it is partially governed by specific surface, which is not the case with Archie's equation. Furthermore, $X = X(C_w, T, S/V, S_H, C_{sh})$.

Another common way used to describe the enhancement of the rock's electrical conduction in the presence of grain-coating clay consists of first expressing the electrical conductivity of formation water as

$$\hat{\sigma}_w = \sigma_w + X, \quad (10.15.2)$$

whereby the rock's electrical conductivity is given by

$$\sigma_R = \hat{\sigma}_w \frac{\phi^m S_w^n}{a} = (\sigma_w + X) \frac{\phi^m S_w^n}{a}.$$

There are several methods commonly used to estimate X as described below. The most common one is to measure the rock's electrical conductivity for multiple values of σ_w , i.e. at different values of water salinity.

10.15.b Waxman-Smits model

We define the Cation Exchange Capacity (CEC) associated with grain-coating clay as a measure of the ability of excess cations to move and diffuse within the Debye length of the electrical double layer. One has:

$$CEC = Q \cdot \rho \cdot \frac{1 - \phi}{\phi}, \quad (10.15.3)$$

where ρ is the density of clay and Q is the concentration of charge per unit pore volume. It follows that

$$\hat{\sigma}_w = \sigma_w + \frac{B \cdot Q}{S_w}, \quad (10.15.4)$$

where B designates the volumetric concentration of charge per liter equivalent and is a function of both σ_w and temperature.

10.15.c Dual-water model

The dual-water model assumes that there are two alternative water pathways for the passage of electrical currents through the pore space: one in the spatial proximity of clays where the spatial density of free charge is abnormally high because of CEC, and another one through the pore water volume with ion-cation concentration equal to that of formation water. The two alternative pathways for electrical conduction function in similar fashion to a parallel circuit of two resistors.

Accordingly, the behavior and relative contribution of the two resistors in parallel is governed by the partial fractions of water saturation ascribed to them:

$$\hat{\sigma}_w = \sigma_b \cdot \underbrace{\frac{S_b}{S_w}}_{\text{Influence of electrical double layer}} + \sigma_w \cdot \underbrace{\left(1 - \frac{S_b}{S_w}\right)}_{\text{Influence of formation water}} \quad (10.15.5)$$

where σ_b is the electrical conductivity in the layer containing the electrical double layer and S_b the water saturation of that layer.

By invoking Archie's equation one obtains

$$\sigma_R = \left[\sigma_b \frac{S_b}{S_w} + \left(1 - \frac{S_b}{S_w}\right) \sigma_w \right] S_w^{n^*} \frac{\phi^{m^*}}{a}, \quad (10.15.6)$$

or

$$\sigma_R = \sigma_w \left[1 + \frac{S_b}{S_w} \left(\frac{\sigma_b}{\sigma_w} - 1 \right) \right] S_w^{n^*} \frac{\phi^{m^*}}{a}, \quad (10.15.7)$$

where m^* and n^* are modified Archie's exponents that account for surface electrical conduction.

Notice that in the above formulas the enhancement of electrical conductivity is explicitly governed by S_w , which requires that if S_w were to be determined from σ_R one would have to solve the modified Archie equation via iterative or nonlinear procedures.

10.15.d Practical implementation of the dual-water model

The following procedure is typically used in the calculation of water saturation in dispersed-shale systems (grain-coating clay) with the dual-water model:

1. Read the resistivities, porosities, gamma ray, and SP values in the sandstone of interest, in a nearby shale, and in a nearby clean sandstone. Correct porosity values to the appropriate matrix if necessary.
2. Calculate C_{sh} using the method described in section 8.2 or the following equations:

•

$$C_{sh}^{ND} = \frac{\phi_N - \phi_D}{\phi_{N,sh} - \phi_{D,sh}}. \quad (10.15.8)$$

•

$$I_{sh}^{GR} = \frac{\gamma - \gamma_{cl}}{\gamma_{sh} - \gamma_{cl}}. \quad (10.15.9)$$

- Convert I_{sh} to C_{sh} using one of the formulas given in section 8.2.

•

$$I_{sh}^{SP} = \frac{SP - SP_{cl}}{SP_{sh} - SP_{cl}}. \quad (10.15.10)$$

- Choose the minimum value. Omit C_{sh}^{ND} if gas is present.

- Correct porosities for shaliness using equations (9.5.7) and (9.5.8). Look for gas indication ($\phi_{N,sh} < \phi_{D,sh}$).
- Calculate non-shale porosity in the shaly sandstone using equation (9.6.1).
- Determine total porosity of the nearby shale:

$$\phi_{sh} = \delta \cdot \phi_{D,sh} + (1 - \delta) \cdot \phi_{N,sh}, \quad (10.15.11)$$

where $\delta \in [0; 1]$ (δ can be estimated from NMR measurements).

- Determine total porosity and the bound-water fraction of the sandstone:

$$\phi_t = \phi_s + C_{sh} \cdot \phi_{sh} \quad (10.15.12)$$

$$S_b = C_{sh} \cdot \frac{\phi_{sh}}{\phi_t} \quad (10.15.13)$$

- Determine the free-water resistivity from a nearby clean (shale-free) sandstone:

$$R_w = R_{cl} \cdot \frac{\phi_{cl}^m}{a} \quad (10.15.14)$$

- Determine bound-water resistivity from a nearby shale:

$$R_b = R_{sh} \cdot \frac{\phi_{sh}^m}{a} \quad (10.15.15)$$

- Determine apparent water resistivity in the shaly sandstone:

$$R_{w,a} = R_t \cdot \frac{\phi_t^m}{a} \quad (10.15.16)$$

- Determine total water saturation corrected for shale¹:

$$S_w = b + \sqrt{b^2 + \frac{R_w}{R_{w,a}}} \quad (10.15.17)$$

where

$$b = \frac{S_b \cdot \left(1 - \frac{R_w}{R_b}\right)}{2}. \quad (10.15.18)$$

¹It is here assumed that $a = 1$, $m = 2$ and $n = 2$. For other values of the coefficients, this becomes slightly more complicated as one has to solve for $S_{w,t}$ iteratively or using a numerical solver.

In the most general case, S_w is obtained by numerically solving the implicit equation

$$S_w^n [\sigma_w] + S_w^{n-1} [S_b (\sigma_b - \sigma_w)] - \sigma_R \frac{a}{\phi_t^m} = 0, \quad (10.15.19)$$

where $\sigma_w = 1/R_w$, $\sigma_b = 1/R_b$, and $\sigma_R = 1/R_t$.

11. Determine non-shale water saturation of the shaly sandstone

$$S_{ws} = \frac{S_w - S_b}{1 - S_b} \quad (10.15.20)$$

12. Determine volumetric fraction of hydrocarbon:

$$\phi_h = \phi \cdot S_h = \phi_t \cdot (1 - S_w) \quad (10.15.21)$$

10.15.e More accurate assessment of ϕ_s using equation (10.3.1)

1. First guess $\phi_1 = \phi_s$ using equation (9.6.1).
2. Compute $S_{w_i} = \sqrt[n]{\frac{R_w}{R_t} \frac{a}{\phi_i^m}}$.
3. Compute $S_{h_i} = 1 - S_{w_i}$ and use Schlumberger's chart [CP-10](#) to assess ρ_{h_i} .
4. Compute ϕ_{i+1} using equation (10.3.1).
5. If $\frac{\phi_{i+1} - \phi_i}{\phi_i}$ is small enough to assess that ϕ_{i+1} is our final value of ϕ_s , then compute $S_{w_{i+1}}$ as the final S_w , else go back to step 2.

In the presence of water-base mud, one can obtain an even more accurate result when using shallow resistivity measurements, so that the depth of investigation of the different tools used¹ for the computations are consistent :

- Compute $S_{xo_i} = \sqrt[n]{\frac{R_w}{R_{xo}} \frac{a}{\Phi_i^m}}$ in step (2).
- Compute $\phi_s = \lim_{i \rightarrow +\infty} \phi_i$ using the preceding steps (2) to (5).
- Now use $S_{w_i} = \sqrt[n]{\frac{R_w}{R_t} \frac{a}{\phi_i^m}}$ to compute S_w and S_h .

Note that $|S_h - S_{xh}|$ is an indicator of the ability of the formation to displace fluids.

10.16 Summary of Resistivity-Porosity-Saturation Formulas for Sandstone with Grain-Coating Clay

Archie with non-shale porosity:

$$\frac{1}{R_t} = \frac{\phi_s^m S_{ws}^n}{a R_w}.$$

Archie with total porosity:

$$\frac{1}{R_t} = \frac{\phi_t^m S_w^n}{a R_w}.$$

¹Do not forget that the density tool has a very shallow depth of investigation

Simandoux:

$$\frac{1}{R_t} = \frac{\phi_s^m S_{ws}^n}{a R_w} + \frac{C_{sh} S_{ws}}{R_{sh}}.$$

Modified Simandoux:

$$\frac{1}{R_t} = \frac{\phi_s^m S_{ws}^n}{a R_w (1 - C_{sh})} + \frac{C_{sh} S_{ws}}{R_{sh}}.$$

Indonesian (Poupon-Leveaux):

$$\frac{1}{\sqrt{R_t}} = \left[\sqrt{\frac{\phi_s^m}{a R_w}} + \frac{C_{sh}^{(1-\frac{C_{sh}}{2})}}{\sqrt{R_{sh}}} \right] S_{ws}^{n/2}.$$

Dual water:

$$\frac{1}{R_t} = \frac{\phi_t^m S_w^n}{a} \cdot \left[\frac{1}{R_w} + \frac{S_b}{S_w} \cdot \left(\frac{1}{R_{wb}} - \frac{1}{R_w} \right) \right].$$

Waxman-Smits:

$$\frac{1}{R_t} = \frac{\phi_t^m S_w^n}{a R_w} \cdot \left(1 + B \cdot Q_v \frac{R_w}{S_w} \right),$$

where:

$$B = \frac{-1.28 + 0.225T - 0.0004059T^2}{1 + R_w^{1.23} (0.045T - 0.27)},$$

$$Q_v = \frac{c_1}{\phi_t} + c_2,$$

T is temperature in degrees Centigrades, and c_1 and c_2 are constants obtained from core measurements; B is expressed in liter/(equivalent Ohm – m). Alternatively,

$$B = \frac{-5.41 + 0.133T - 0.0001253T^2}{1 + R_w^{1.23} (0.025T - 1.07)},$$

for T expressed in degrees Fahrenheit.

Juhasz:

$$\frac{1}{R_t} = \frac{\phi_t^m S_w^n}{a R_w} \cdot \left(1 + B \cdot Q_{vn} \frac{R_w}{S_w} \right),$$

where:

$$Q_{vn} = C_{sh} \frac{\phi_{sh}}{\phi_t}.$$

10.16.a Remark about m and n in shaly-sandstone equations

It is important to note that, in general, the exponents m and n invoked in the above shaly-sandstone equations are not the same as those of the corresponding Archie's equations in shale-free sandstones. Indeed, presence of grain-coating clay also modifies those exponents with respect to the ones of clay-free sandstone. The variables m^* and n^* are commonly used to designate the exponents associated with grain-coating clay. Such exponents should be estimated from core laboratory studies.

**10.16. Summary of Resistivity-Porosity-Saturation Formulas for Sandstone with
August 21, 2023**

Chapter 11

Elastic and Mechanical Properties of Rocks

...It was simply that the mechanical laws found themselves repeated and corroborated in nature...
– Thomas Mann, The Magic Mountain.

11.1 Porosity From Sonic Logs via Wyllie's Equation

The sonic porosity can be assessed using equation (11.1.1), known as Wyllie's equation:

$$\Delta t = \phi_S \cdot \Delta t_f + (1 - \phi_S) \cdot \Delta t_m, \quad (11.1.1)$$

where Δt is the slowness (in $\mu s \cdot ft^{-1}$) given by the first arrival time. This equation assumes that measurements consist of the fastest sonic arrival time. It remains a good approximation in the presence of well consolidated clastics and carbonates, at low porosities ($\phi < 15\%$), when there is no loss of energy due to the shaking of grains. Equation (11.1.1) is often modified to take approximately into account the lack of perfect compaction, as follows:

$$\phi_S = \frac{\Delta t - \Delta t_m}{\Delta t_f - \Delta t_m} \cdot \frac{1}{C_p}, \quad (11.1.2)$$

where C_p is a compaction coefficient¹. Note that the depth of investigation for the head wave is very shallow (less than 1 in) and therefore that the fluid saturating the rock's pore space is, in general, mud filtrate. Often, the sonic velocity of sandstones is lower than the sonic velocity of shales. However, that trend can be reversed because of severe compaction. For the case of clastic rocks, there is depth of burial, z_P , at which shales become plastic :
$$\begin{cases} V_{P_{\text{sands}}} < V_{P_{\text{shales}}} & \text{when } 0 < z < z_P \\ V_{P_{\text{sands}}} > V_{P_{\text{shales}}} & \text{when } z_P < z < z_{max} \end{cases}$$

11.1..1 Using Raymer-Gardner-Hunt's formula

Another possibility to compute the sonic porosity is using equation (11.1.3), known as Raymer-Gardner-Hunt's formula :

$$\frac{1}{\Delta t} = \frac{(1 - \phi)^2}{\Delta t_m} + \frac{\phi}{\Delta t_f}, \quad (11.1.3)$$

which corresponds to :

$$\phi = \frac{2 - \frac{\Delta t_m}{\Delta t_f} - \sqrt{4\Delta t_m \left(\frac{1}{\Delta t} - \frac{1}{\Delta t_f} \right) + \left(\frac{\Delta t_m}{\Delta t_f} \right)^2}}{2}. \quad (11.1.4)$$

¹ According to Bassiouni, $C_p = B_{cp} = \frac{\Delta t_{sh}}{100}$ where Δt_{sh} is the transit time in adjacent shales.

This equation can be simplified as equation (11.1.5) :

$$\phi = C \cdot \frac{\Delta t - \Delta t_m}{\Delta t}, \quad (11.1.5)$$

where C is a constant.

11.1.a Usual values used for the assessment of sonic porosity

The values of ρ_m , ν or Δt used for assessing the porosities are found in table 11.1.6¹ :

Material	ρ_m ($g \cdot cm^{-3}$)	ν ($ft \cdot s^{-1}$)	Δt ($\mu s \cdot ft^{-1}$)
Sandstone	2.65	For (11.1.1) : 18,000	55.5
		For (11.1.3) : 17,850	56
Limestone (Calcite)	2.71	For (11.1.1) : 21,000	47.5
		For (11.1.3) : 20,500	49
Dolomite	2.87	For (11.1.1) : 23,000	43.5
		For (11.1.3) : 22,750	44
Fluid	See (9.1.2)	Water : 5,300 Oil : 4,200	189 238

(11.1.6)

11.2 Biot-Gassmann Fluid Substitution

Using Biot-Gassmann's equations, it is possible to estimate the sonic velocities of a rock with a certain fluid saturation if we know the properties of the rock with another fluid. This theory is valid only at low frequency, i.e., there is no viscous drag of the fluid on the skeleton. It is possible to write the equations in many different ways. We give here a few of these.

11.2..1 First presentation

$$\underbrace{(\rho V_P^2)_{\text{sat}}}_{K_{\text{sat}} + \frac{4}{3}\mu_{\text{sat}}} = \underbrace{K_{\text{dry}} + \frac{4}{3}\mu_{\text{dry}}}_{\text{Dry rock}} + \underbrace{\frac{\left(1 - \frac{K_{\text{dry}}}{K_S}\right)^2}{\left(1 - \Phi - \frac{K_{\text{dry}}}{K_S}\right) \frac{1}{K_S} + \frac{\Phi}{K_{\text{fl}}}}}_{\text{fluid}} \quad (11.2.1)$$

We can write the equation with the convention used in [Mavko et al. \(2003\)](#) :

$$K_P = \frac{\left(1 - \frac{K_{\text{dry}}}{K_S}\right)^2}{\left(1 - \Phi - \frac{K_{\text{dry}}}{K_S}\right) \frac{1}{K_S} + \frac{\Phi}{K_{\text{fl}}}} \quad (11.2.2)$$

with :

¹Source : Bassiouni, [Theory, measurement and interpretation of well logs](#) pages 54 & 56.

Symbol	Meaning	S.I. Unit	Formula unit
V_S	Velocity of shear waves	$m.s^{-1}$	$m.s^{-1}$
V_P	Velocity of compressional waves	$m.s^{-1}$	$m.s^{-1}$
K_S	Bulk modulus of the matrix	$kg.m^{-1}.s^{-2}$	GPa
K_{dry}	Effective bulk modulus of the dry rock	$kg.m^{-1}.s^{-2}$	GPa
K_{sat}	Effective bulk modulus of the saturated rock	$kg.m^{-1}.s^{-2}$	GPa
K_{fl}	Effective bulk modulus of the pore fluid	$kg.m^{-1}.s^{-2}$	GPa
μ_{dry}	Effective shear modulus of the dry rock	$kg.m^{-1}.s^{-2}$	GPa
μ_{sat}	Effective shear modulus of the saturated rock	$kg.m^{-1}.s^{-2}$	GPa
ρ	Density	$kg.m^{-3}$	$g.cm^{-3}$
Φ	Porosity	%	fraction

Moreover,

$$\boxed{\mu_{\text{dry}} = \mu_{\text{sat}} = \rho V_S^2} \quad (11.2.3)$$

We can use to write this formula **Biot's coefficient** defined by :

$$\mathcal{B} = 1 - \frac{K_{\text{dry}}}{K_S}$$

This coefficient has the following property:

$$\underbrace{0 < \mathcal{B}}_{\text{Well-consolidated sediments}} \quad \underbrace{\mathcal{B} \leq 1}_{\text{Unconsolidated sediments and fluids}}$$

11.2.1.1 Wood's formula. In the presence of an homogeneous mixture of fluids, at the wave length scale, the sound velocity is given exactly by equation (11.2.4), known as Wood's formula :

$$V = \sqrt{\frac{K_R}{\rho}} \quad (11.2.4)$$

where $\frac{1}{K_R} = \sum_{i=1}^N \frac{f_i}{K_i}$, $\rho = \sum_{i=1}^N f_i \rho_i$ et f_i , K_i et ρ_i are the volume fractions, bulk moduli and densities of the different phases.

11.2.2 Second presentation

$$\boxed{\frac{K_{\text{sat}}}{K_0 - K_{\text{sat}}} = \frac{K_{\text{dry}}}{K_0 - K_{\text{dry}}} + \frac{K_{fl}}{\Phi(K_0 - K_{fl})}} \quad (11.2.5)$$

Assumptions :

- Homogeneous mineral modulus.
- Statistical isotropy of the pore space.
- Low frequencies, so that the pore pressure is at equilibrium in all the pore space.
- **No assumptions** about pore geometry.

To perform the fluid substitution from fluid 1 to fluid 2 :

$$\boxed{\frac{K_{\text{sat}1}}{K_0 - K_{\text{sat}1}} - \frac{K_{fl1}}{\Phi(K_0 - K_{fl1})} = \frac{K_{\text{sat}2}}{K_0 - K_{\text{sat}2}} - \frac{K_{fl2}}{\Phi(K_0 - K_{fl2})}} \quad (11.2.6)$$

11.2..3 Third presentation

This equation is derived directly from the first presentation...

$$K_{\text{sat}} = K_{\text{dry}} + \frac{\left(1 - \frac{K_{\text{dry}}}{K_0}\right)^2}{\frac{\Phi}{K_{\text{fl}}} + \frac{1-\Phi}{K_0} - \frac{K_{\text{dry}}}{K_0^2}} = \frac{\Phi \left(\frac{1}{K_0} - \frac{1}{K_{\text{fl}}}\right) + \frac{1}{K_0} - \frac{1}{K_{\text{dry}}}}{\frac{\Phi}{K_{\text{dry}}} \left(\frac{1}{K_0} - \frac{1}{K_{\text{fl}}}\right) + \frac{1}{K_0} \left(\frac{1}{K_0} - \frac{1}{K_{\text{dry}}}\right)}$$

One can write $K_\Phi = \frac{\Phi K_0 K_{\text{dry}}}{K_0 - K_{\text{dry}}}$, i.e., $\frac{1}{K_{\text{dry}}} = \frac{1}{K_0} + \frac{\Phi}{K_\Phi}$.

$$K_{\text{sat}} = \frac{1}{\frac{1}{K_0} + \frac{\Phi}{K_\Phi + \frac{K_0 K_{\text{fl}}}{K_0 - K_{\text{fl}}}}} \quad (11.2.7)$$

$$K_{\text{dry}} = \frac{K_{\text{sat}} \left(\frac{\Phi K_0}{K_{\text{fl}}} + 1 - \Phi\right) - K_0}{\frac{\Phi K_0}{K_{\text{fl}}} + \frac{K_{\text{sat}}}{K_0} - 1 - \Phi} \quad (11.2.8)$$

Using M defined by $\frac{1}{M} = \frac{B-\Phi}{K_0} + \frac{\Phi}{K_{\text{fl}}}$, we obtain

$$K_{\text{sat}} = K_{\text{dry}} + B^2 M$$

11.2..4 Reuss presentation

If K_R is defined by $\frac{1}{K_R} = \frac{1}{\frac{\Phi}{K_{\text{fl}}} + \frac{1-\Phi}{K_0}}$, we have :

$$\frac{K_{\text{sat}}}{K_0 - K_{\text{sat}}} = \frac{K_{\text{dry}}}{K_0 - K_{\text{dry}}} + \frac{K_R}{K_0 - K_R}$$

11.2..5 Relationship between the velocities

(Mavko et al. (2003) calls this the VELOCITY FORM of Gassmann's equations.) K_P is defined in equation (11.2.2).

$$\frac{V_{P_{\text{sat}}}^2}{V_{S_{\text{sat}}}^2} = \frac{K_P}{\mu} + \frac{K_{\text{dry}}}{\mu} + \frac{4}{3} \quad (11.2.9)$$

11.2..6 Inverse formula

If we define $x_1 = \frac{K_s}{K_{f1}}$ and $x_2 = \frac{K_{\text{sat}_1}}{K_s}$ (with $K_{\text{sat}_1} = \rho(V_P)^2 - \frac{4}{3}\mu$).

Then :

$$K_{\text{dry}} = \frac{(1-\Phi)K_s x_2 - K_s + \Phi x_1 x_2 K_s}{x_2 + \Phi x_1 - 1 - \Phi} \quad (11.2.10)$$

For a fluid composed of mixed water and "fluid 1" (with bulk modulus K_{f1} and density ρ_{f1}), we have :

$$\frac{1}{K_{f1}} = \frac{S_w}{K_w} + \frac{1-S_w}{K_{f1}} \quad \text{et} \quad \rho_{f1} = S_w \rho_w + (1-S_w) \rho_{f1}$$

11.3 Practical Use of Biot-Gassmann's Equations

In order to perform the fluid substitution, the following steps can be applied :

1. Compute $\mu_{\text{sat}} = \mu_{\text{dry}} = \mu = \rho \cdot V_S^2$.
2. Compute $K_{\text{sat}_1} = \rho \cdot V_P^2 - \frac{4}{3}\mu$.
3. Determine K_S using the assessed lithology, compute x_2 .
4. Compute $K_{f_1} = \frac{1}{\frac{S_w}{K_w} + \frac{1-S_w}{K_{f_1}}}$, then x_1 .
5. Compute K_{dry} as a function of Φ , K_S , x_1 et x_2 (using equation 11.2.10).
6. Using $K_{f_1} = \frac{1}{\frac{S_w}{K_w} + \frac{1-S_w}{K_{f_1}}}$, we get K_{sat_2} as a function of K_{dry} , K_{f_2} , and Φ and K_S that did not change.
7. Compute $\rho_2 = S_w\rho_w + (1 - S_w)\rho_{f_2}$, which will give V_{P_2} and V_{S_2} .

11.4 Slowness-Time Coherence

In order to evaluate the velocities (or slownesses) from the sonic data, a slowness-time coherence algorithm (STC) can be applied. The formula proposed in Kimball (1998) is the following :

$$\rho(\mathcal{S}, T) = \frac{1}{m} \frac{\int_T^{T+T_w} \left| \sum_{n=1}^m s_i [t + \mathcal{S} \cdot (i-1) \cdot \delta] \right|^2 dt}{\sum_{n=1}^m \int_T^{T+T_w} |s_i [t + \mathcal{S} \cdot (i-1) \cdot \delta]|^2 dt} \quad (11.4.1)$$

where \mathcal{S} is the slowness, $s_i(t)$ the filtered time waveform of recorder i at time t (displacement or velocity), m the number of recorders, δ the inter receiver spacing, T_w the length of the time window and T the window starting time. T_w is usually chosen around 2 to 5 cycles of the dominant arrival frequency.

The results are then plotted over a 2-D grid of slowness \mathcal{S} and time T called the slowness-time (ST) plane as contour plot. The more accurate the spots on the plot, the less dispersive the medium. The slowness can then be converted to velocities using the following conversion law :

$$\underbrace{\frac{V}{m \cdot s^{-1}}}_{\mu s \cdot ft^{-1}} = \frac{304,800}{\underbrace{\mathcal{S}}_{\mu s \cdot ft^{-1}}} \quad (11.4.2)$$

11.5 Assessment of Volumetric Concentrations of Mineral Constituents: Linear System Approach

As most of the properties (ρ_b , Δt , PEF, ...) have a linear behavior as functions of the proportions of the different minerals, one can use a linear system to replace the cross-plots. Remember that the cross-plots method, and therefore this one too, can break down in certain conditions (presence of iron triggering a high PEF, presence of gas, ...)

If we assume that the volume of shale has been previously determined (see section 8.2), we then have the matrix equation (11.5.1) :

$$C \times X = D, \quad (11.5.1)$$

with :

- C given by equation (11.5.2) (if ϕ_N is available) or (11.5.3) (if ϕ_N is not available but Δt_S is)¹.

$$C_1 = \begin{pmatrix} \rho_{b\text{quartz}} & \rho_{b\text{limestone}} & \rho_{b\text{dolomite}} & \rho_{\text{fluid}} \\ \phi_{N\text{quartz}} & \phi_{N\text{limestone}} & \phi_{N\text{dolomite}} & \phi_{N\text{fluid}} \\ \Delta t_{\text{quartz}} & \Delta t_{\text{limestone}} & \Delta t_{\text{dolomite}} & \Delta t_{\text{fluid}} \\ PEF_{\text{quartz}} & PEF_{\text{limestone}} & PEF_{\text{dolomite}} & 0 \\ 1 & 1 & 1 & 1 \end{pmatrix} = \begin{pmatrix} 2.65 & 2.71 & 2.87 & 1.0 \\ -0.04 & 0 & 0.02 & 1.0 \\ 53 & 47.6 & 43.5 & 189 \\ 1.81 & 5.08 & 3.14 & 0 \\ 1 & 1 & 1 & 1 \end{pmatrix}, \quad (11.5.2)$$

or

$$C_2 = \begin{pmatrix} \rho_{b\text{quartz}} & \rho_{b\text{limestone}} & \rho_{b\text{dolomite}} & \rho_f \\ \Delta t_{S\text{quartz}} & \Delta t_{S\text{limestone}} & \Delta t_{S\text{dolomite}} & 0 \\ \Delta t_{P\text{quartz}} & \Delta t_{P\text{limestone}} & \Delta t_{P\text{dolomite}} & \Delta t_{P\text{fluid}} \\ PEF_{\text{quartz}} & PEF_{\text{limestone}} & PEF_{\text{dolomite}} & 0 \\ 1 & 1 & 1 & 1 \end{pmatrix} = \begin{pmatrix} 2.65 & 2.71 & 2.87 & 1.0 \\ 74 & 90 & 76 & 0 \\ 53 & 47.6 & 43.5 & 189 \\ 1.81 & 5.08 & 3.14 & 0 \\ 1 & 1 & 1 & 1 \end{pmatrix}. \quad (11.5.3)$$

- $X = \begin{pmatrix} C_{\text{quartz}} \\ C_{\text{limestone}} \\ C_{\text{dolomite}} \\ \phi \end{pmatrix}$.
- $D_1 = \begin{pmatrix} \rho_p^{sh} \\ \phi_N^{sh} \\ \Delta t^{sh} \\ PEF^{sh} \\ 1 - C_{sh} \end{pmatrix}$ (use with C_1) or $D_2 = \begin{pmatrix} \rho_b^{sh} \\ \Delta t_S^{sh} \\ \Delta t_P^{sh} \\ PEF^{sh} \\ 1 - C_{sh} \end{pmatrix}$ (use with C_2).

The MatLab® code used is² :

- If ϕ_N is available :

```
A=[1 1 1 1];
b=1;Aeq=[];Beq=[];
x=ones(length(depth),4);
y=ones(length(depth),4);
for i=1:length(depth)
    d=[rhobc(i) nphic(i) DTC(i) PEFc(i) 1-Ish(i)]';
    x(i,:)=lsqlin(C,d,A,b,Aeq,Beq,zeros(4,1),ones(4,1))';
    y(i,:)=lsqlin(C,d,A,b,Aeq,Beq,0,1)';
end
```

- If Δt_S is available :

```
A=[1 1 1 1];
b=1;Aeq=[];Beq=[];
x=ones(length(depth),4);
y=ones(length(depth),4);
```

¹The matrices filled with values have to be adapted to the case being treated. The values of the properties in matrix D have to be corrected for shale using the method described in section 9.5.b.2. Also, ϕ_N is given in limestone porosity units.

²The c used in the names of the input logs for d meaning the logs have already been corrected for shale.

```
for i=(1:length(depth))
    d=[rhobc(i) DTSc(i) DTC(i) PEFc(i) 1-Ish(i)]';
    x(i,:)=lsqlin(C,d,A,b,Aeq,Beq,zeros(4,1),ones(4,1))';
    y(i,:)=lsqlin(C,d,A,b,Aeq,Beq,0,1)';
end
```

11.5. Assessment of Volumetric Concentrations of Mineral Constituents: Linear System Approach

August 21, 2023

Chapter 12

Estimation of Permeability

...A blade of grass is the journey work of the stars...

– Walt Whitman, Leaves of Grass.

The estimation of permeability is one of the most challenging tasks in formation evaluation. Even though there are general rules to perform the estimation, the specific procedure is highly conditioned by the type of rock and its textural and pore properties. For the case of siliciclastic rocks, the estimation of permeability considers presence of clay and specific types of clay minerals included in the pore space. In the case of carbonate rocks, the estimation of permeability requires knowledge of the pore-size distribution and pore inter-connectivity.

Another degree of complexity in the estimation of permeability comes from the fact that permeability is a tensorial property and hence is sensitive to direction of flow. This property is often unheeded, especially in those cases where permeability is estimated from statistical correlations that involve porosity and irreducible water saturation. Yet another complexity in the estimation of permeability comes from the fact that in porous media saturated with immiscible fluids, the permeability of the rock depends on the type of fluid and its saturation.

Permeability is governed by the degree of interconnectivity and flow capacity of porous media that is subject to fluid pressure gradients. Often, the degree of pore connectivity is measured and described in analogy with the effective permeability of a bundle of capillary tubes.

12.1 Rock classification

One of the first steps in the estimation of permeability of rocks from well logs consists of diagnosing types of rocks (or depth segments of rock formations) that exhibit compatible values of storage and flow capacity. The most common petrophysical grouping, or classification of rocks is performed by invoking their permeability-to-porosity ratio (i.e., k/ϕ). According to this method, rocks that exhibit the same value of k/ϕ belong to the same class. The rational behind this classification is that speed of flow is normalized by the pore volume of fluid available in the rocks: rocks with low porosity can exhibit high permeability, hence behave similarly to rocks with high porosity and low permeability because their production efficiency is equivalent.

12.2 Pore- and Throat-Size Distributions

Pore- and throat-size distributions, together with pore inter-connectivity, govern permeability. Proper assessment of permeability requires specific knowledge of throat radii, their distribution in the pore space, and directional connectivity.

12.2.a Capillary Pressure

If NMR data are unavailable, two main formulae exist for permeability estimation besides the usual Carman-Kozeny equation (equation (12.2.1)¹). They are given as equations (12.2.2) (Tixier-Timur formula) and (12.2.3) (Coates-Dumanoir formula) :

$$k = \alpha \cdot \frac{\phi^\beta}{S_{wi}^\gamma} \quad (12.2.2)$$

with $\alpha = 250$, $\beta = 3$ and $\gamma = 2$ for the equation known as Tixier's (assuming that porosity is given in fraction units and permeability is given in mD) and $\alpha = 100$, $\beta = 2.25$ and $\gamma = 2$ for Timur's.

$$k = \left[\alpha \cdot \frac{\phi^\beta \cdot (1 - S_{wi})}{S_{wi}} \right]^\gamma \quad (12.2.3)$$

S_{wi} being irreducible water saturation. Coates' formula has $\alpha = 100$, $\beta = 2$ and $\gamma = 2$.

If core data are available, the best way to assess permeability is using core data to estimate the coefficient of the general formulae that minimize the error, and then choosing the best match between core data and estimation, i.e. choosing equation (12.2.2) or equation (12.2.3). This gives for the Tixier-Timur model :

$$A \times X = B \quad (12.2.4)$$

$$\text{with } A = \begin{pmatrix} 1 & -\log(\phi_1) & -\log(S_{w,i_1}) \\ 1 & -\log(\phi_2) & -\log(S_{w,i_2}) \\ \vdots & \vdots & \vdots \\ 1 & -\log(\phi_n) & -\log(S_{w,i_n}) \end{pmatrix}, B = \begin{pmatrix} -\log(k_1) \\ -\log(k_2) \\ \vdots \\ -\log(k_n) \end{pmatrix} \text{ and } X = \begin{pmatrix} \log(\alpha) \\ \beta \\ \gamma \end{pmatrix}.$$

Using MatLab[®]'s following procedure sandstone by sandstone, the values of α , β and γ can be found :

X=A\B

This method can be easily transcribed for use with the Coates-Dumanoir formula.

When NMR data are available, permeabilities can be estimated using the following procedure :

1. Estimate the NMR effective porosity using equation (12.2.5)² :

$$(\phi_e)_{NMR} = \int_{T_{2cut-off}}^{T_{2max}} \phi_{nmr} \cdot d \log_{10}(T_2) \quad (12.2.5)$$

2. Estimate the NMR total porosity using equation (12.2.6) :

$$(\phi_t)_{NMR} = \int_{T_{2min}}^{T_{2max}} \phi_{nmr} \cdot d \log_{10}(T_2) \quad (12.2.6)$$

3. Estimate the bulk volume irreducible (BVI) using equation (12.2.7) :

$$\text{BVI} = (\phi_t)_{NMR} - (\phi_e)_{NMR} \quad (12.2.7)$$

¹

$k = A \frac{\phi^\alpha}{(1 - \phi)^\beta} \cdot d^\delta$ (12.2.1)

where A is a constant and d a characteristic length of the grain or pore dimension. (α, β, δ) can usually be chosen as (3, 2, 2).

²The $T_{2cut-off}$ value is usually chosen at 33ms.

4. Permeability can then be estimated using a Coates-Dumanoir formula (equation (12.2.8)) :

$$k_{nmr} = \left(\left(\frac{\overbrace{\phi \cdot 100}^{\phi_e \text{ in p.u.}}}{c} \right)^m \cdot \left(\frac{\phi_e}{\text{BVI}} \right) \right)^n \quad (12.2.8)$$

with usually $c = 10$, $m = 2$ and $n = 2$. If core data are available, they have to be used to find the best values for c , m and n .

12.3 Parallel- and Perpendicular-to-Bedding Plane Permeabilities

We can estimate the horizontal and vertical permeabilities (parallel and perpendicular to bedding plane, respectively) using the electrical analogy. For beds in series, vertical permeability (perpendicular-to-bedding-plane permeability) is given by

$$\frac{1}{k_V} = \frac{\sum_{i=1}^N \frac{h_i}{k_i}}{\sum_{i=1}^N h_i} \quad (12.3.1)$$

while for beds in parallel, horizontal permeability (parallel-to-bedding-plane permeability) is given by

$$k_H = \frac{\sum_{i=1}^N h_i \cdot k_i}{\sum_{i=1}^N h_i} \quad (12.3.2)$$

12.4 Quantification of Uncertainty

We have to give error bounds to the estimation of reserves, as uncertainty can come from a lot of computations in the process :

- Cutoff value for sandstones and shales (based on C_{sh}) : $C_{sh} < C_{\text{cutoff}} \Rightarrow$ sand, otherwise $\begin{cases} \text{shales} \\ \phi = 0, S_H = 0 \end{cases}$
- Estimation of C_{sh} .
- Values of a and m : as a and m vary with the depositional environment, using only one value for the whole section to analyze often gives errors. Thus, we have to give bounds for a and m .
- Estimation of R_w , and influence of temperature.
- Environmental corrections. Example : The PEF, ρ_b , ϕ_N , the gamma ray, ... are all affected by the presence of barite in the mud.
- Interpretation corrections.
- ...

Using ΔC_{sh} , Δa , Δm , Δn , ΔR_w , $\Delta \rho_H$, ..., we can have an estimation of the relative uncertainties $\frac{\Delta S_w}{S_w}$ and $\frac{\Delta \phi}{\phi}$, and therefore also an estimation of $\frac{\Delta \text{Reserves}}{\text{Reserves}}$.

Chapter 13

Formation-Tester Measurements

August 21, 2023

Chapter 14

Rock-Core Measurements

...just because we are not ready for scientific progress does not mean it won't happen...

– Jennifer A. Doudna, A Crack in Creation: Gene Editing and the Unthinkable Power to Control Evolution.

For more information about rock-core measurements, please use Dr. Peters's lecture notes for PGE381L, Advanced Petrophysics.

14.1 Measurements of Porosity

14.2 Measurements of Permeability

The hydraulic permeability of a rock is measured in a permeameter using Darcy's equation. If dry gas is used to minimize the rock-fluid reaction, the results have to be corrected for gas slippage (Klinkenberg effect).

14.3 Relative Permeability

In the case of a multi-phase fluid flow, there are two methods that allow the measurement of relative permeabilities:

- The steady-state method
- The unsteady-state method

14.4 Measurements of Dispersivity

- Scanning device
- Breakthrough curve

14.5 Measurements of Capillary Pressure

- Restored state (porous plate)
- Mercury injection

- Centrifuge
- ~~~~~

Chapter 15

Numerical Simulation of Well Logs

Most well logs can be numerically simulated under specified geometrical and material conditions of well trajectory, borehole size and shape, formation dip and azimuth, formation boundaries and thickness, and formation properties (either physical or petrophysical properties). Additionally, the numerical simulation of well logs needs to take into account the assumed properties of the instrument used to acquire the well logs (e.g. induction vs. laterolog resistivity measurements, LWD vs. wireline measurements, etc.) Nowadays it is possible to rapidly numerically simulate nuclear, sonic, and magnetic resonance logs using the concept of *Spatial Sensitivity Functions* developed by the Joint Industry Research Consortium on Formation Evaluation at the University of Texas at Austin.

The numerical simulation of well logs enables the planning of logging operations by selecting the most appropriate available instrument for specific geometrical, geological, and borehole environmental conditions. It also permits the verification of borehole measurements acquired under adverse and non-trivial geometrical and petrophysical conditions. And, most importantly, it allows the implementation of geophysical inversion techniques for automatic, computer-driven interpretation of well logs by iteratively matching the measured well logs with their numerical simulations in the presence of measurement noise. The latter feature is the basis of automatic well-geosteering processes intended to design well trajectories for maximum and optimal reservoir (subsurface target) coverage.

August 21, 2023

Chapter 16

Pore-Scale Measurements and Calculations

16.1 Other Complementary Field Measurements

In order to check if the values calculated with well logs are correct, field measurements can be acquired when producing the well. An example is the estimation of permeability using type curves.

Bibliography

- Allaud, L. A., & Martin, M. H. (1977). *Schlumberger, The History of a Technique*. New York, New York: John Wiley & Sons, Inc.
- Archie, G. E. (1942). The electrical resistivity log as an aid in determining some reservoir characteristics. *Transactions of the American Institute of Mining, Metallurgical, and Petroleum Engineers*, 146, 54–62.
- Archie, G. E. (1950). Introduction to petrophysics of reservoir rocks. *American Association of Petroleum Geologists Bulletin*, 34(5), 943–961.
- Arps, J. J. (1953). The effect of temperature on the density and electrical resistivity of sodium chloride solutions. *Petroleum Transactions, AIME*, 198, 327–330.
- Bear, J. (1993). 1 - modeling flow and contaminant transport in fractured rocks. In J. Bear, C.-F. Tsang, & G. de Marsily (Eds.) *Flow and Contaminant Transport in Fractured Rock*, (pp. 1 – 37). Oxford: Academic Press.
- URL <http://www.sciencedirect.com/science/article/pii/B978012083980350005X>
- Bigelow, E. (2002). *Introduction to Wireline Log Analysis*. Baker Atlas.
- Bird, R., Lightfoot, E., & Stewart, W. (2002). *Transport Phenomena*. J. Wiley.
URL <https://books.google.com/books?id=wYnRQwAACAAJ>
- Blanke, S. (2015). Petroleum Report Series PR4896: PEP 38264 Caravel-1 Well Completion Report. Tech. rep., New Zealand Petroleum and Minerals (NZP&M), and Ministry of Business, Innovation and Employment (MBIE).
- Bourgoyne, Jr., A., Chenevert, M., Millheim, K., & Young, Jr., F. (2003). *Applied Drilling Engineering*, vol. 2. Society of Petroleum Engineers Textbook Series, Ninth printing ed.
- Bowker, G. C. (1994). *Science on the Run: Information Management and Industrial Geophysics at Schlumberger, 1920-1940*. Cambridge, Massachusetts: The MIT Press.
- Clavier, C., Coates, G., & Dumanoir, J. (1984). Theoretical and experimental bases for the dual-water model for interpretation of shaly sands. *SPE Journal*, 24, Paper SPE-6859-PA(2, April), 153–168.
- Dunstan, A. E., Brooks, B. T., & Illing, V. C. (1938). *The Science of Petroleum : A Comprehensive Treatise of the Principles and Practice of the Production, Refining, Transport and Distribution of Mineral Oil*. London, New York: Oxford University Press. Editors: v. 1-4, A.E. Dunstan ... [et al.]; v. 5, Benjamin T. Brooks and A.E. Dunstan; v. 6, V.C. Illing.
- Hubbert, M. K. (1956). Darcy's law and field equations of the flow of underground fluids. *Petroleum Transactions, AIME*, 207, 222–239.
- Juhasz, I. (1981). Normalized Q_v - the key to shaly sand evaluation using the Waxman-Smits equation in the absence of core data. *SPWLA 22nd Annual Logging Symposium*, (June 23-26).

- Kelly, S., El-Sobky, H., Torres-Verdín, C., & Balhoff, M. T. (2016). Assessing the utility of FIB-SEM images for shale digital rock physics. *Advances in Water Resources*, 95, 302 – 316. Pore scale modeling and experiments. URL <http://www.sciencedirect.com/science/article/pii/S0309170815001360>
- Kimball, C. (1998). Shear slowness measurement by dispersive processing of the borehole flexural mode. *Geophysics*, 63(2), 337–344.
- Kruczek, B. (2015). *Carman-Kozeny Equation*. Berlin, Heidelberg: Springer Berlin Heidelberg. URL https://doi.org/10.1007/978-3-642-40872-4_1995-1
- Leverett, M. C. (1941). Capillary behaviour in porous solids. *Petroleum Transactions, AIME*, 142, 152–169.
- Luthi, S. M. (2001). *Geological Well Logs: Their Use in Reservoir Modeling*. Berlin, Germany: Springer-Verlag.
- Mavko, G., Mukerji, T., & Dvorkin, J. (2003). *The Rock Physics Handbook (Tools for Seismic Analysis in Porous Media)*. Cambridge University Press.
- McPhee, C., Reed, J., & Zubizarreta, I. (2015). *Core Analysis: A Best Practice Guide*. Developments in Petroleum Science, Volume 64. Amsterdam, The Netherlands: Elsevier, second ed.
- Munday, S., Beggs, M., McCarthy, L., & Cozens, N. (2015). Petroleum Report Series PR5185: Reservoir Geology Study, Canterbury Basin PEP 52717. Tech. rep., New Zealand Petroleum and Minerals (NZP&M), and Ministry of Business, Innovation and Employment (MBIE).
- Oristaglio, M., & Dorozychski, A. (2009). *A Sixth Sense: The Life and Science of Henri-Georges Doll*. New York, New York: The Overlook Press.
- Peters, E. J. (2012). *Advanced Petrophysics: Geology, Porosity, Absolute Permeability, Heterogeneity, and Geostatistics*, vol. 1. Austin, Texas: Live Oak Book Company, second ed.
- Poupon, A., Loy, M. E., & Tixier, M. P. (1954). A contribution to electrical log interpretation in shaly sands. *Petroleum Transactions, AIME*, 201, 138–145.
- Schlumberger, A. G. (1982). *The Schlumberger Adventure*. New York: ARCO Publishing, Inc.
- Schön, J. H. (2015). *Physical Properties of Rocks: Fundamentals and Principles of Petrophysics*. Developments in Petroleum Science. Amsterdam, The Netherlands: Elsevier, second ed.
- Timur, A. (1968). An investigation of permeability, porosity, and residual water saturation relationships for sandstone reservoirs. *The Log Analyst, SPWLA*, 9(4), 8–17.
- Tomlin, S., & Herd, B. (2015). Petroleum Report Series PR5184: Endurance 3D Seismic Interpretation Report PEP 52717. Tech. rep., New Zealand Petroleum and Minerals (NZP&M), and Ministry of Business, Innovation and Employment (MBIE).
- VandenBygaart, A., & Protz, R. (1999). The representative elementary area (REA) in studies of quantitative soil micromorphology. *Geoderma*, 89(3), 333 – 346. URL <http://www.sciencedirect.com/science/article/pii/S0016706198000895>
- Waxman, M. H., & Smits, L. J. (1967). Electrical conductivities in oil-bearing shaly sands. *Presented at 42nd Annual Fall Meeting: Society of Petroleum Engineers, Paper SPE1863-A*.
- Waxman, M. H., & Smits, L. J. (1968). Electrical conductivities in oil-bearing shaly sands. *SPE Journal*, 8(2), 107–122.
- Wyllie, M. R. J., Gregory, A. R., & Gardner, L. W. (1956). Elastic wave velocities in heterogeneous and porous media. *Geophysics*, 21(1), 41–70.
- Zinszner, B., & Pellerin, F. M. (2007). *A Geoscientist's Guide to Petrophysics*. Paris, France: Editions Technip.

List of Figures

1.1.1 The discipline of <i>Formation Evaluation</i> “sees” rocks with Physics. This is accomplished by either (a) examining physics phenomena in rocks with an outside excitation source and sensing/measuring the corresponding output, or (b) detecting and measuring physics phenomena spontaneously generated by the rock itself. Examples of Panel (a) are electromagnetic and elastic wave propagation, electrical conduction, nuclear radiation, magnetic resonance, fluid pressure pulsing, electrokinetics, and chemical diffusion. Examples of Panel (b) are spontaneous radioactivity by rock-borne radio-isotopes and electric spontaneous potential. The measurements acquired with both physics methods are subsequently transformed into useful rock properties (e.g., compositional, elastic, and fluid-storage and fluid-flow properties) via so-called effective-medium models.	17
1.1.2 The discipline of <i>Formation Evaluation</i> “transforms” the measured <i>in situ</i> rock physics properties (e.g., electrical conductivity/resistivity, elastic properties, nuclear properties, pressure time decays, magnetic time relaxation, etc.) into rock engineering properties such as porosity, fluid/solid properties, fluid and solid concentrations, and elastic and mechanical properties, for instance, using <i>effective medium</i> models of rock behavior (e.g., Archie’s equation transforms rock electrical resistivity into water saturation).	18
1.1.3 Example of an integrated formation evaluation project: Canterbury Basin, New Zealand. Image panels A, D, E, and G from Munday et al. (2015), image panels B and C from Tomlin & Herd (2015), and image panels F and G from Blanke (2015). Panel A shows whole-core samples; panels B and C are seafloor bathymetry maps; panel D is a seismic amplitude cross-section; panel E are well logs acquired in well K shown in the F seismic amplitude cross-section; panel G is a seismic travel time map (showing the location of well K) next to a geological outcrop analogue. (Montage courtesy of Steve Walkinshaw).	19
1.2.1 Schematic of an electrical surface prospection system: A and B are current injection electrodes while M and N are voltage measuring electrodes (Allaud & Martin, 1977) (Source: Dunstan et al., 1938)	21
1.2.2 Schematic of the borehole instrument invented by Conrad and Marcel Schlumberger to measure electrical resistivity of rock formations: A and B are current injection electrodes while M and N are voltage measuring electrodes (Allaud & Martin, 1977) (Source: Allaud & Martin, 1977)	23
1.2.3 Photograph of one of the earliest systems used to acquire borehole measurements by Schlumberger. The system includes a winch with cable and tensiometer, a printer, and two electrical analogue systems used to acquire electrical resistivity measurements (Allaud & Martin, 1977) (Source: Allaud & Martin, 1977)	24
1.4.1 Outcrop of Quaternary alluvial fans showing the spatial complexity and variability of rocks resulting from sedimentary, diagenetic, and tectonic processes. The variability of rocks impacts the spatial distribution of porosity and permeability, for instance; it also affects larger-scale fluid-transport properties such as hydraulic communication, pressure seals, etc. The <i>contextual</i> geological information of rocks at all scales needs to be assimilated in the interpretation of well logs and core data (Elephant Trees Formation, California; photograph courtesy of Camilo Gelvez).	25

1.5.1 Example of modern well logs acquired in a vertical well. Track 1 is gamma ray, Track 2 is depth below the KB, Track 3 is electrical resistivity, Track 4 is electrical resistivity parallel and perpendicular to bedding plane, Track 5 is high-resolution borehole resistivity image, Track 6 is apparent density-neutron porosities and PEF, Track 7 is compressional- and shear-wave slownesses, and Track 8 is T_2 magnetic resonance distribution.	26
1.5.2 Example of logging-while-drilling (LWD) measurements acquired in a high-angle well. Track 1 is true vertical depth (TVD), Track 2 is the well trajectory, Track 3 is measured depth(MD), Track 4 is gamma ray, Track 5 is electrical resistivity, Track 6 is apparent density-neutron porosities, and Track 7 is high-resolution borehole density image.	27
1.5.3 Photograph of a sandstone-shale clastic sedimentary sequence with faulting blocks (faults in the Honaker Trail Formation, Moab Canyon; photograph courtesy of Peter H. Hennings). Well logs sample but a rather limited spatial segment of the rocks penetrated by a well; it is important to keep the geometrical and geological context in mind when quantifying fluid-transport properties of rocks across large spatial scales.	29
1.6.1 Gamma-ray log acquired in a vertical well plotted over the cross-section of the seismic-derived $\lambda\rho$ product (vertical scale is two-way seismic travel time, ms). Red- and yellow-colored bands on seismic-derived cross-section correspond to gas-saturated sandstones, thereby evidencing their lateral extent away from the well trajectory. Down-dip, the red-to-yellow colors turn green; this is the location of the free gas-water contact. Offshore Western Australia.	29
1.6.2 Well trajectories, seismic amplitude cross-section, and gamma-ray logs acquired along two neighboring wells; vertical scale is two-way seismic travel time (ms). Seismic amplitude data provide 3D geometrical and geological context to the well trajectories and well logs acquired along them. Notice the high degree of correlation between the gamma-ray logs acquired in the two wells. Volve hydrocarbon field, North Sea. (a) Cross-section of post-stack seismic amplitude measurements. (b) Three-dimensional rendering of two well trajectories and seismic reflection surface. (Images courtesy of Valeriia Sobolevskaia).	31
1.9.1 Plots of gamma-ray (green) and resistivity logs (multiple logs in logarithmic scale with blue being the dominant color) acquired in three vertical wells located in neighboring hydrocarbon fields (Lady Nora and Pemberton fields, offshore Western Australia). The high correlation among gamma-ray logs acquired in the three wells enables the identification of common or similar stratigraphic units bearing different fluids. Well-to-well correlation via well logs is the basis of pattern recognition used to identify repetitive or equivalent stratigraphic units across multiple wells.	35
1.10. Example of well logs and core measurements acquired across a mixed carbonate-clastic sedimentary sequence. Track 1 shows gamma-ray and spontaneous potential logs. Track 2 shows depth and formation temperature. Track 3 shows the resistivity logs (shallow-, medium-, and deep-sensing resistivity logs). Track 4 shows the neutron, density, and photo-electric factor (PEF) logs together with core porosity. Track 5 shows the estimated volumetric concentrations of fluid (porosity), shale, quartz, dolomite, and limestone. Tracks 6 and 7 show core permeabilities and core water saturations, respectively.	36
2.1.1 Example of an outcrop of Cretaceous clastic rocks showing lateral variations of sandstone and shale layers resulting from depositional, diagenetic, and tectonic processes. Well logs sample but a very limited spatial segment of rocks encountered along the well trajectory. Quantifying fluid-transport properties of spatially complex rocks requires additional geometrical, geological, and petrophysical information not provided by well logs (Sun River Canyon, Montana; photograph courtesy of Peter H. Hennings).	40
2.1.2 Photograph of a shale outcrop showing finely laminated cycles of fissile layers (Lewis Shale, Colorado). Shales are very finely laminated clastic rocks with negligible permeability because their average grain diameter is $65\ \mu\text{m}$ or smaller. They often serve as pressure seals (fluid flow barriers). Non-fissile shales are often referred to as <i>mudrocks</i> (photograph courtesy of Laura Net).	41

2.1.3 Photograph of a carbonate outcrop showing depositional (precipitation) marine cycles with different thicknesses and porosities; vertical fractures are also present in some of the layers (Cretaceous outcrop, Canyon Lake Dam, Texas). The layers with the largest porosity are those subjected to relatively high differential dissolution and abundance of fossils (photograph courtesy of Jerry Lucia).	42
2.2.1 Thin section of a clastic rock shown variable grain sizes and irregular grain cementation: aeolian sandstone. The storage and fluid-transport properties of clastic rocks are chiefly conditioned by (1) average grain size, (1) grain sorting, (3) grain cementation, (4) grain-size laminations, and (5) presence and concentration of grain-coating or laminated clay/shale. This thin section also includes a few grains with microporosity (photograph courtesy of Laura Net).	43
2.2.2 Photograph of a moldic carbonate rock with voids originated from differential rock dissolution of packets originally occupied by fossils: carbonate rock from the Edwards group, Austin, Texas. Differential rock dissolution due to diagenesis gives rise to pore space. Some of the pore space eventually becomes connected (fluid percolation), thereby enabling the transport of fluid. The latter can in turn accelerate solid dissolution and recrystallization, hence give rise to additional modifications to the storage and fluid-transport properties of the rock.	44
2.2.3 Photograph of a thin section of oolitic limestone showing the pore space in blue (epoxy) (photograph courtesy of Jerry Lucia).	45
2.2.4 The petrophysical and mechanical properties of carbonate rocks can be substantially affected by diagenesis and tectonic deformation (photograph courtesy of Peter H. Hennings).	46
2.3.1 Outcrop of the Monterey formation at Shell Beach (aka Pismo Beach), California. The Monterey formation is composed of chert/porelenite, occasional dolomite, and organic-rich phosphatic shale. The upper light-colored fractured interval is a dolomitized (carbonate) interval overlying organic-rich siliceous (diatoms) shale. Organic richness in the dark shale is 7-10 wt% TOC (total organic content) (photograph courtesy of Quinn Passey).	47
2.3.2 Photograph of the outcrop of an organic shale (organic-rich mudrock) showing presence of finely laminated and very tight layers with abundance of organic material (dark-colored segments; Eagle Ford formation, Del Rio, Texas). These layers are the source rock of clastic gas reservoirs located higher in the sedimentary sequence (photograph courtesy of Rich Aram).	48
3.1.1 Photograph of spatially heterogeneous clastic rocks (slabbed whole core segments) saturated with viscous oil. The high degree of spatial variability of rock properties within relatively short distances causes oil to be present only at a few rock sections that exhibit favorable storage and flow properties. Most petrophysical concepts and the so-called <i>petrophysical models</i> used to quantify rock properties assume spatially homogeneous rocks.	50
3.4.1 Example of well logs and core laboratory measurements acquired in a vertical well across an offshore turbidite sedimentary sequence (Andrew Field, North Sea). Track 1 is gamma ray. Track 2 is depth. Track 3 is electrical resistivity (multiple radial lengths of investigation). Track 4 is density, density correction, apparent neutron porosity, and photo-electric factor (PEF) logs. Track 5 is core porosity. Track 6 is core permeability (mD).	54
3.6.1 Cross-section of the spatial distribution of electric lines (red lines) across a pack of spherical grains (top) and a capillary tube of constant cylindrical section (bottom). Rock porosity is the same in the two cases; lines flow from left to right due to the DC (direct current) electrical potential enforced from left (high electrical potential) to right (low electrical potential). Black lines in the top figure are equipotential lines. The density of electric lines across the capillary tube is uniform while it increases and decreases across constrictions and pores, respectively, in the spherical grain pack. Electrical conduction in both cases is entirely due to body forces because of null electrical conduction on the surface of the grains (diagram courtesy of David Herrick).	56

3.6.2 Cross-section of the spatial distribution of DC electric (left panel) and laminar flow (right panel) lines (red lines) across a pack of spherical grains; lines flow from left to right. Black lines are equipotential lines. The density of flow lines is higher than the density of electric lines at the center of pore throats because the velocity of flow is null at grain boundaries (no-slip condition) and maximum at the center of throats/pores (diagram courtesy of David Herrick).	57
3.7.1 Velocity of single-phase flow across a straight capillary tube of constant circular cross-section of radius R assuming a viscous fluid. The radial distribution of fluid velocity along the tube's circular cross section is illustrated with red shading and exhibits a parabolic shape with maximum value at the tube's axis, decreasing to zero at the tube's boundary (diagram courtesy of David Herrick).	58
3.8.1 Graphical description of the concept of fluid <i>transport efficiency</i> of porous media. The x and y axes describe porosity and transport efficiency, respectively, both varying between 0 and 1. For a given porosity, the most efficient porous media are those constructed with straight capillary tubes of equal-radius circular cross-sections. Transport efficiency decreases as the capillary tubes become tortuous, exhibit non-constant cross-sections, and include non-connected segments (diagram courtesy of David Herrick).	60
3.10. Schematic of the gas-water capillary pressure of a water-wet rock as function of wetting-phase saturation for both imbibition and drainage cycles of fluid displacement (graphic courtesy of Germán Merletti).	62
3.11. If the transport of fluids in rocks is in some ways analogous to the passage of water through a shower head. Hole sizes in a shower head are analogous to throat sizes in rocks. The efficiency of water flow through a shower head is dictated by the velocity and volume of water per unit time transported through the set holes, both of which depend on the applied pressure gradient, the size of holes, and the distribution of hole sizes. Assuming that the total cross section of the shower holes is the same for all the shower heads shown (equal porosity), the most efficient shower head is the one that has the largest and most uniform hole sizes.	63
3.12. Example of spatial scales of analysis, measurement, and quantification of petrophysical properties. The collage of images/photographs illustrates the paradigm a rock sample from an unconventional formation, and emphasizes how the measured/calculated petrophysical property is intimately related to the representative elementary volume (REV). REV diagram adapted from Bear (1993) and VandenBygaart & Protz (1999). Micro-CT images are 11 $\mu\text{m}/\text{voxel}$ and the width of the presented image is approximately 11 mm. The core sample is on the order of centimeters (adapted from Figure 10 of Kelly et al. (2016)).	65
4.2.1 Example of well-log header for a well that was drilled with oil-base mud in the deepwater Gulf of Mexico. The header indicates that the well was logged with a modern triple-combo set of measurements (Schlumberger). Note the maximum depth and temperature reached at the bottom of the well.	69
4.2.2 Example of well-log header for a well that was drilled with water-base mud. The header indicates that the well is located onshore and was logged with a modern triple-combo set of measurements (Halliburton). Note the (1) maximum depth and temperature reached at the bottom of the well, and (2) measurements of electrical resistivity of drilling mud components.	70
4.3.1 Example of mud log comprising rock cuttings descriptions and chromatographic-chemical analyses performed on fluid samples acquired at the surface from the drilling-mud line. The mud log also includes basic drilling measurements which are used to transform the rock cuttings and mud-line measurements from time-of-drilling to depth. Chromatographic measurements can differentiate between thermogenic and biogenic gas (image courtesy of RockWare.)	71

4.3.2 Example of LWD resistivity tool (toroid-based electromagnetic instrument) showing how the transmitter, receivers, electronics, and telemetry are located within the drill pipe while drilling mud flows toward the bit through the center of the pipe. Measurements are acquired in the presence of electrically conductive drill pipe, while the pipe is moving forward and rotating around the wellbore, and when the drill bit is subject to strong vibrations (photograph courtesy of Brian Clark, Schlumberger)	72
4.3.3 Example of wireline logging tools. Some of these tools are designed to work centralized with the borehole and some others require to be pressed against the borehole wall when acquiring measurements. The diameter of the tool determines the maximum size of borehole in which they can operate. Various tools are assembled into a long tool string which is pulled by the wireline cable out of the borehole starting from the bottom (end) of the well. Power and telemetry are delivered/implemented with the wireline cable itself. The cable pulls the tool string at a speed which depends on the type of instruments included in it. Likewise, the cable serves to measure distance along the well trajectory after implementing corrections for cable tension.	73
4.3.4 Comparison of LWD and wireline logs acquired along the same depth interval of a vertical well. LWD logs were acquired during drilling whereas wireline logs were acquired 10 days after drilling. Track 1 is gamma-ray, Track 2 is LWD amplitude resistivities, Track 3 is LWD phase resistivities, Track 4 is wireline Laterolog resistivities, and Track 5 is wireline rock density, apparent neutron porosity, photo-electric factor(PEF), and density correction. Resistivity values are not equal because of (1) mud-filtrate invasion, and (2) instrument used to acquire the measurements. Gas-saturated aeolian sedimentary sequence.	74
4.4.1 Example of two well trajectories, one vertical and one undulated, and their corresponding gamma-ray logs plotted over a cross-section of seismic amplitude data (two-way time converted to depth, m below the bottom of the sea) with formation boundaries and faults. The two well trajectories almost intersect. Well logs are commonly plotted with respect to distance along the well trajectory (measured depth, MD) or true vertical depth(TVD).	75
4.4.2 Photographs of logging truck (or cabin), winch, and cable for onshore (a) and offshore (b) wireline logging operations. The winch includes a cable-length meter and a tensiometer to measure cable tension.	76
4.12. Example of ultrasonic borehole image acquired in a vertical well penetrating the Edwards carbonate formation (Austin, Texas). Track 1 is standard well logs. Track 2 is depth. Track 3 is ultrasonic reflectivity image (light and dark red colors identify high and low ultrasonic reflectivities, respectively. Track 4 is ultrasonic travel time image (dark red color identifies long travel times). Ultrasonic images provide high-resolution descriptions of reflectivity and travel time along the complete borehole surface. This image shows open and closed fractures, and voids resulting from rock collapse, all part of the flow system in the Edwards aquifer.	81
4.12. Comparison of the resolution and radial distance of investigation (aka depth of investigation) of the various commercially available wireline logs. Well-log resolution is a measure of the minimum bed thickness that can be detected with a given logging instrument. Notice that in the context of spatially heterogeneous whole core (as the carbonate whole core shown in the figure), different well logs inherently implement different volumetric averages of the rocks surrounding the well. The figure also shows the typical size of core samples used in laboratory measurements and studies.	82

4.13. Example of resistivity logs numerically calculated to replicate actual field conditions of a vertical well penetrating multiple horizontal layers of various thicknesses and invaded with mud filtrate. Track 1 is depth. Track 2 shows the synthetic earth model (color-coded spatial distribution of electrical resistivity in the vertical and radial directions). Track 3 shows the actual values of electrical resistivity as a function of distance away from the wellbore. Track 4 is wireline induction resistivity. Track 5 is wireline laterolog resistivity. Track 6 is LWD amplitude resistivity. Track 7 is LWD phase resistivity. The deepest- and shallowest-sensing resistivity logs are plotted with red and blue/black lines in each case. Note the difference in “smoothness” between some of the resistivity logs and the original earth-model resistivities. Also note that not all the deepest-sensing resistivity logs are equal among themselves or to the original earth-model resistivities. Discrepancies between actual earth-model resistivities and resistivity logs give rise to errors in the calculation of hydrocarbon saturation, for instance. Numerical simulations performed with UTAPWeLS.	84
4.22. Example of deep-sensing borehole electromagnetic measurements acquired during drilling of a spatially heterogeneous turbidite sedimentary system, North Sea. The upper panel shows standard LWD measurements: density image, apparent density and neutron porosities, electrical resistivity, and gamma-ray logs. The lower panel shows the well trajectory, deep-sensing electrical resistivity (red and blue indicate high and low resistivity, respectively), and interpreted faults. Hydrocarbon-bearing sandstones and shales coincide with the highest and lowest values of resistivity. Note that deep-sensing electrical resistivities on average 15 m away from the well trajectory.	92
5.5.1 Photograph of a wireline formation tester. One of the primary functions of formation testers is to measure pore pressure based on draw-down and build-up pressure transients established with a pump drawing small volumes of fluid from rocks adjacent to the borehole. Formation testers include a pump, a fluid receptacle, and small orifice pressed against the borehole wall through which the pump establishes hydraulic communication with the fluids in the rocks.	99
5.5.2 Example of well logs and pore pressure measurements acquired in a vertical well across an offshore turbidite sedimentary sequence (Andrew Field, North Sea). Track 1 is gamma ray. Track 2 is depth. Track 3 is electrical resistivity (multiple radial lengths of investigation). Track 4 is density, density correction, apparent neutron porosity, and photo-electric factor (PEF) logs. Track 5 is pore pressure (psi). Pore pressure gradients indicate the presence of water, oil, and gas depth zones from the bottom to the top of the well, respectively.	100
6.7.1 (a) Comparison of time decays of NMR transverse relaxation magnetization and (b) their corresponding T_2 distributions for various rock samples (clastics and carbonates) fully saturated with water. All measurements were acquired with a top bench laboratory NMR measurement system (images courtesy of David Medellín).	118
6.7.2 Comparison of time decays of NMR transverse relaxation magnetization and their corresponding T_2 distributions for a Berea sandstone sample before ($S_w = 100\%$) and after centrifuging the sample. The fraction of remnant water after centrifuging the rock sample corresponds to grain- and capillary-bound water, i.e., an approximation of irreducible water saturation. Permeability can be estimated from the difference between the NMR T_2 distributions acquired before and after centrifuging the rock sample. All measurements were acquired with a top bench laboratory NMR measurement system (images courtesy of David Medellín).	119

6.7.3 Comparison of (a) time decays of NMR transverse relaxation magnetization and (b) their corresponding T_2 distributions for a Boise sandstone sample before ($S_w = 100\%$) and after centrifuging the sample. The fraction of remnant water after centrifuging the rock sample corresponds to grain- and capillary-bound water, i.e., an approximation of irreducible water saturation. Permeability can be estimated from the difference between the NMR T_2 distributions acquired before and after centrifuging the rock sample. All measurements were acquired with a top bench laboratory NMR measurement system (images courtesy of David Medellín).	120
6.7.4 Comparison of (a) time decays of NMR transverse relaxation magnetization and (b) their corresponding T_2 distributions for a Berea sandstone sample at full water saturation $S_w = 100\%$ and partial water/oil saturation ($S_w = 41\%$ and $S_{HC} = 59\%$). Partial hydrocarbon saturation causes the NMR transverse relaxation to exhibit superimposed effects due to dominant pore size(s) and fluid type(s). All measurements were acquired with a top bench laboratory NMR measurement system (images courtesy of David Medellín).	122
7.2.1 Photograph of mudcake remaining at the boundary of a cylindrical borehole after several hours of invasion into Navajo sandstone. Invasion experiment conducted with a large block of rock in the laboratory to quantify the effects of water-base drilling mud.	125
7.2.2 X-ray images of Berea sandstone invaded with water- and oil-base drilling mud. Panels a and b correspond to the cases of water- and synthetic oil-base drilling mud, respectively. The color scale describes time after the onset of mud-filtrate invasion. Cylindrical samples of Berea sandstones were subject to injection of drilling mud in the laboratory under the same controlled conditions to compare the relative effects of water- and oil-based mud-filtrate invasion; time-lapse X-ray images were acquired during the process to assess the evolution of mudcake thickness and fluid displacement. Notice that mudcake thickness is larger for the case of water- than oil-base mud-filtrate invasion (images courtesy of Colin Schroeder).	126
7.2.3 Areal and vertical X-ray cross-sections of a Berea sandstone sample (a) before and (b) after water-base mud-filtrate invasion performed in the laboratory. The center of the images is a replica of the borehole and the sample is originally saturated with air. Notice in (b) the formation of mudcake after the onset of invasion and the advancement of the mud-filtrate invasion front into the sample (color-coded density). Because of the petrophysical properties of Berea sandstone (almost unimodal pore/throat size distribution), the fluid-displacement front resulting from invasion (air being displaced by water-base mud filtrate) exhibits a quasi-piston-like behavior (images courtesy of Colin Schroeder).	127
7.2.4 Areal and vertical X-ray cross-sections of a Edwards limestone sample (a) before and (b) after water-base mud-filtrate invasion performed in the laboratory. The center of the images is a replica of the borehole and the sample is originally saturated with air. Notice in (b) the formation of mudcake after the onset of invasion and the advancement of the mud-filtrate invasion front into the sample (color-coded density). Because of the petrophysical properties of the Edwards limestone (non-unimodal and irregular pore/throat size distribution, including vuggy porosity), the fluid-displacement front resulting from invasion (air being displaced by water-base mud filtrate) exhibits an irregular (non-uniform) behavior (images courtesy of Colin Schroeder).	128
8.3.1 White- and ultraviolet-light photographs of whole core of a sandstone-shale laminated rock. Core retrieved from a Miocene turbidite sedimentary system in the deepwater Gulf of Mexico. The ultraviolet-light photograph indicates the sandstone layers in the rock sample are saturated with hydrocarbon.	136
8.3.2 Example of fibrous illite coating the surface of Rotliegend sandstone grains, North Sea (Sample <i>Ill-34</i> : Macaulay Collection; field of view $\approx 30 \mu\text{m}$ wide). Presence of grain-coating clay increases the original surface-to-volume ratio of grains, increases microporosity and irreducible water saturation, thereby decreasing effective porosity and permeability (photograph courtesy of M. Roe, Macaulay Institute).	137

8.4.1 General description of the Thomas-Stieber diagram.	139
9.1.1 Photographs of clastic grains originated from (a) volcanic rocks, (b) carbonate rocks, and (c) sandstone, carbonate, igneous, and metamorphic rocks. Clastic rocks can exhibit variable grain composition, which impacts the calculation of grain density and, ultimately, the calculation of porosity.	144
10.7.1 Conversion chart for NaCl concentration, temperature, and resistivity of aqueous solutions.	164
10.9.1 Two examples of capillary pressure curves.	167
10.13 Photograph of aeolian Navajo sandstone showing prominent cross-bedding. Grain-size laminations such as those due to cross-bedding in aeolian sandstones give rise to electrical resistivity anisotropy because of the associated variations of irreducible water saturation (Zion National Park, Utah; photograph courtesy of Laura Net).	169

Appendices

Appendix A

Summary of Basic Formulas

This appendix summarizes the formulas most commonly used in the interpretation of well logs and core measurements.

A.1 Calculation of Temperature Along the Well Trajectory

Under the assumption of a linear geothermal gradient in the subsurface, one has

$$T(z) = T(z_1) + \frac{T(z_2) - T(z_1)}{z_2 - z_1} (z - z_1), \quad (\text{A.1.1})$$

where:

T = temperature (either $^{\circ}\text{C}$ or $^{\circ}\text{F}$),

z = true vertical depth (TVD) measured with respect to the logging reference point,

z_1 = TVD of the point in the well where the temperature was measured (usually at the surface for onshore wells and at the bottom of the sea for offshore wells), and

z_2 = TVD of a second point in the well where the temperature was measured (usually at the bottom/end of the well).

Note that surface temperatures used in the calculation of borehole temperature via eq. (A.1.1) should be *average* yearly temperatures.

A.2 Correction of Electrical Resistivity for Temperature

The electrical resistivity of aqueous electrolyte solutions varies with temperature when the electrolyte concentration is constant. Based on experimental work, [Arps \(1953\)](#) documented the following formulas for correcting the electrical resistivity of aqueous electrolyte solutions for a change in temperature:

$$R_2 = R_1 \left(\frac{T_1 + 6.77}{T_2 + 6.77} \right) ^{\circ}\text{F}, \text{ and} \quad (\text{A.2.1})$$

$$R_2 = R_1 \left(\frac{T_1 + 21.5}{T_2 + 21.5} \right) ^{\circ}\text{C}, \quad (\text{A.2.2})$$

where:

R_1 = electrical resistivity ($\Omega\cdot\text{m}$) measured at temperature T_1 , and

R_2 = electrical resistivity ($\Omega\cdot\text{m}$) measured at temperature T_2 .

A.3 Electrical Resistivity of Aqueous Solutions

The electrical resistivity of aqueous solutions depends on (1) type of electrolyte(s)(e.g. NaCl, KCl, etc.) present in the solution, (2) electrolyte concentration, and (3) temperature. For the case of electrical resistivity calculations, it is customary to use NaCl as the base case and use conversion factors to calculate the corresponding electrical resistivity for other type of electrolytes. Based on laboratory measurements, there are several approximate formulas that quantify the relationship between concentration of NaCl in aqueous solution, temperature, and electrical resistivity. The most commonly used formula stems from the so-called Baker-Atlas method (Bigelow, 2002), given by:

$$R_w \approx \left[0.0123 + \frac{3647.5}{(NaCl_{ppm})^{0.955}} \right] \left(\frac{81.77}{T + 6.77} \right), \quad (\text{A.3.1})$$

where:

R_w = electrical resistivity of water ($\Omega \cdot \text{m}$),

$NaCl_{ppm}$ = concentration of NaCl in water in ppm, and

T = temperature in $^{\circ}\text{F}$.

A.3.a From Resistivity to Electrolyte Concentration

The inverse of eq. (A.3.1) is used to estimate NaCl concentration in aqueous solution from measurements of electrical resistivity, namely,

$$NaCl_{ppm} \approx 10^{1.0471\{3.562-\log_{10}\left[\left(\frac{T+6.77}{81.77}\right)R_w - 0.0123\right]\}}, \quad (\text{A.3.2})$$

where temperature (T) is given in $^{\circ}\text{F}$ and R_w is given in $\Omega \cdot \text{m}$.

A.4 Calculation of Shale Index

This calculation assumes that the well includes locations for both a pure shale and a shale-free sandstone within the same formation. It also assumes that the properties of the pure shale (i.e., solid constitution, clay minerals, salinity, and porosity)are identical to those of the shale included in a sandstone. By definition,

$$I_{sh}(z) = \frac{\gamma(z) - \gamma_{cl}}{\gamma_{sh} - \gamma_{cl}}, \quad (\text{A.4.1})$$

where:

z = location along the well trajectory,

$I_{sh}(z)$ = shale index at location z ,

$\gamma(z)$ = reading of the gamma-ray log at location z ,

γ_{sh} = reading of the gamma-ray log at the pure-shale location, and

γ_{cl} = reading of the gamma-ray log at a shale-free location.

Notice that $0 \leq I_{sh} \leq 1$, hence eq. (A.4.1) effectively normalizes the gamma-ray log to vary between 0 and 1 (0 for a shale-free rock and 1 for a pure shale). It follows that $I_{sh} = C_{sh}$ in the case of a sandstone-shale laminated sedimentary sequence with shale-free sandstone laminae.

A.4.a Case of a Water-Saturated Sandstone

Very often wells do not include a shale-free sandstone but do include a water-saturated sandstone. If C_{sh} across the water-saturated sandstone is known from independent calculations (i.e., from calculations performed with neutron and density porosity logs), then eq. (A.4.1) can be modified assuming, once again, a linear relationship between I_{sh} and gamma-ray measurements. It follows that

$$I_{sh}(z) = I_{shw} + \frac{1 - I_{shw}}{\gamma_{sh} - \gamma_w} [\gamma(z) - \gamma_w] , \quad (\text{A.4.2})$$

where:

I_{shw} = shale index in the water-saturated sandstone ($0 \leq I_{shw} \leq 1$), and

γ_w = reading of the gamma-ray log in the water-saturated sandstone (same location used for the calculation of I_{shw}).

Notice that both I_{shw} and γ_w are calculations and measurements, respectively, performed/acquired at the same location in the well. Also, note that eq. (A.4.2) still enforces a linear relationship between $\gamma(z)$ and $I_{sh}(z)$, the only difference with respect to eq. (A.4.1) being that the slope of the line is calculated using the point (γ_w, I_{shw}) .

A.5 Spontaneous Electrical Potential (SP) and Water Resistivity

Borehole measurements of Spontaneous Electrical Potential (SP) are often used to calculate the electrical resistivity of formation water. Assuming that the electrokinetic component of borehole SP measurements is negligible, only membrane and diffusion electrical potentials remain, with the sum of the latter two components commonly referred to as *Static Spontaneous Potential*, or *SSP*. A practical approximation of *SSP* is given by

$$SSP \approx -K \log_{10} \left(\frac{C_w}{C_{mf}} \right) , \quad (\text{A.5.1})$$

where:

SSP = static spontaneous electrical potential (mV),

K = temperature-independent constant = 71 mV,

C_w = electrolyte concentration of formation water (NaCl ppm), and

C_{mf} = electrolyte concentration of mud filtrate (NaCl ppm).

The *SSP* is the difference between the SP measured at a water-saturated and shale-free sandstone and the SP of the shale baseline (i.e., the SP measured at the closest pure shale), namely,

$$SSP = SP - SP_{sh} ,$$

where SP_{sh} is the SP measured at the nearby pure shale.

Furthermore, eq. (A.5.1) assumes that both formation water and mud filtrate have the same dominant electrolyte in solution (e.g., NaCl).

From eq. (A.5.1) it follows that

$$C_w = C_{mf} 10^{(-SSP/K)} . \quad (\text{A.5.2})$$

It becomes clear that $SSP < 0$ (negative *SSP*) implies that $C_w > C_{mf}$ (formation water is saltier than mud filtrate), whereas $SSP > 0$ (positive *SSP*) implies that $C_{mf} < C_w$ (mud filtrate is saltier than formation water).

Subsequently, R_w is calculated from C_w via eq. (A.3.1) for a given value of formation temperature, T . Likewise, when R_{mf} (electrical resistivity of mud filtrate) and surface temperature are given (as is often reported in the header of well logs), C_{mf} is calculated via eq. (A.3.1).

Notice that the calculation of R_w from SP above does not require knowledge of either porosity or porosity exponent (m) as Archie's equation does.

A.6 Archie's Equation

Archie's equation (Archie, 1942) quantifies the relationship between porosity, water saturation, and electrical resistivity of porous rocks. It is given by

$$R_t = R_w \left(\frac{a}{\phi^m} \right) \frac{1}{S_w^n}, \quad (\text{A.6.1})$$

where:

R_t = electrical resistivity of a fluid-saturated rock ($\Omega \cdot \text{m}$),

R_w = electrical resistivity of formation water ($\Omega \cdot \text{m}$),

ϕ = porosity,

S_w = water saturation,

a = Winsauer coefficient,

m = porosity exponent, and

n = saturation exponent.

In terms of electrical conductivity, Archie's equation is written as

$$\sigma_t = \sigma_w \left(\frac{\phi^m}{a} \right) S_w^n, \quad (\text{A.6.2})$$

where:

σ_t = electrical conductivity of a fluid-saturated rock (S/m), and

σ_w = electrical conductivity of formation water (S/m).

Archie's equation assumes that the solid components of the rock are perfect electrical insulators, whereby electrical conduction through a rock can only be established through the portion of the pore space that is interconnected and filled with electrically conductive formation water. Further, Archie's equation neglects surface conduction effects similar to those associated with grain-coating clay minerals, and it assumes that the rock is isotropic. Note that the original Archie equation did not include the Winsauer's coefficient, a , which was later included by Winsauer himself. Lastly, note that Archie's equation indicates that the electrical resistivity of rocks is insensitive to grain or pore sizes.

The so-called formation factor included in Archie's equation, $F = a/\phi^m$ (or its inverse, ϕ^m/a), quantifies the fraction of the pore space that effectively contributes to electrical conduction; the larger the value of m the smaller the fraction of total porosity, ϕ , that contributes to electrical conduction (recall that $m > 1$ by definition, and $\phi < 1$, whereby $\phi^m \leq \phi$). When $m = 1$ the entire pore space contributes to electrical conduction (e.g., the entire pore space is contained in straight and parallel capillary tubes), which results in the most efficient type of electrical conduction through the rock. However, as the pore space deforms away from a bundle of parallel and straight capillary tubes the efficiency of conduction decreases, with the consequence that not all

the available pore space contributes to electrical conduction. The value $m \approx 2$ is commonly associated with well sorted and well cemented clastic rocks.

It is emphasized that ϕ in Archie's equation denotes *total porosity*. This designation explicitly assumes that the rock's pore space remains topologically connected by the water phase. If the latter is not correct, i.e., a fraction of the pore space occludes the water phase, then rather than arbitrarily increasing m , ϕ in Archie's should be replaced by $\phi - \phi_p$, where ϕ_p is the so-called *percolation threshold porosity*, which is the minimum porosity for which the water phase remains topologically connected through the rock's pore space. It is often not possible to assume that a and m remain constant for a wide range of ϕ . However, when a and m do remain constant for some range of ϕ it is said that the rocks belong to the same *electrical rock class*.

Note that Archie's equation indicates that the electrical resistivity of saturated rocks is independent of the rock's pore/throat sizes. This behavior is due to the fact that Archie's equation describes electrical conduction as a net volumetric effect, i.e., surface effects are not included in Archie's model of rock electrical conduction. By contrast, hydraulic permeability does depend on pore/throat sizes because the phenomenon of fluid transport in porous rocks involves both volume and surface (friction) forces.

A.7 Relationship Between Rock Density and Porosity

Porosity is not directly measured with well logs but calculated from measurements of rock (bulk) density. The relationship between rock density and porosity is given by

$$\rho_b = \phi \rho_f + (1 - \phi) \rho_m , \quad (\text{A.7.1})$$

where:

ρ_b = rock density (also known as *bulk* density) (gm/cm^3),

ϕ = porosity,

ρ_f = density of the fluid occupying the rock's pore space (gm/cm^3), and

ρ_m = density of the solid (non-fluid) component of the rock (gm/cm^3).

From eq. (A.7.1) it follows that

$$\phi = \frac{\rho_b - \rho_m}{\rho_f - \rho_m} = \frac{\rho_m - \rho_b}{\rho_m - \rho_f} . \quad (\text{A.7.2})$$

Likewise, from eq. (A.7.1) it follows that

$$\rho_f = \frac{1}{\phi} [\rho_b - (1 - \phi)\rho_m] . \quad (\text{A.7.3})$$

Note that the calculation of porosity from rock density requires precise knowledge of both fluid density and density of the solid rock composition (matrix density). Independent measurements and/or information are required to estimate fluid and matrix densities prior to calculating rock porosity.

A.8 Rock Density and Porosity of Rocks with Laminated Shale

Shale-free clastic rocks interspersed with laminae of shale are often referred to as *sandstone-shale laminated rocks*; that is, such clastic rocks are composed of alternations of clean (clay free) sandstone and pure shale. However, in the more general case, sandstone-shale laminated rocks could be formed by the alternation of laminae of sandstone with grain-coating clay minerals and laminae of pure shale. In all cases, the laminae of pure shale are assumed impermeable.

For the case when (1) all shale laminae in the rock exhibit the same constitution (i.e, the laminae of shale have the same grain and clay mineral composition and the same porosity and fluid type) and (2) all sandstone laminae in the rock exhibit the same solid composition, porosity, and saturating fluid, the relationship between rock density and porosity is given by

$$\rho_b = (1 - C_{sh}) \rho_s + C_{sh} \rho_{sh}, \quad (\text{A.8.1})$$

where:

ρ_b = rock density (also known as *bulk* density) (gm/cm^3),

ρ_s = sandstone density (gm/cm^3),

ρ_{sh} = shale density (gm/cm^3), and

C_{sh} = volumetric concentration of shale ($0 \leq C_{sh} \leq 1$).

It is customary to refer to $(1 - C_{sh})$ as *net-to-gross* in sandstone-shale laminated systems. Also, $C_{sh} = I_{sh}$ in sandstone-shale laminated systems.

Likewise,

$$\phi = (1 - C_{sh}) \phi_s + C_{sh} \phi_{sh}, \quad (\text{A.8.2})$$

where:

ϕ = rock porosity,

ϕ_s = sandstone porosity, and

ϕ_{sh} = shale porosity.

It follows that

$$\phi_s = \frac{\phi - C_{sh} \phi_{sh}}{1 - C_{sh}}. \quad (\text{A.8.3})$$

The latter equation enables the calculation of the porosity of individual sandstone laminae from the previously estimated total rock porosity. Notice that ϕ_s could be larger or smaller than ϕ depending on whether ϕ_{sh} is smaller or larger than ϕ_s , respectively.

A.9 Rock Density and Porosity of Rocks with Grain-Coating Clay

Clastic rocks with grain-coating clay minerals are often referred to as *dispersed-shale clastic rocks*. Under such conditions, the term “shale” is used to designate the component of the rock that is comprised by grain-coating clay minerals and their associated irreducible water saturation (micro-porosity). There are two limiting states of the rock: one in which grain-coating clay minerals are negligible and one in which the original pore space is completely occupied by grain-coating clay minerals. The latter state causes the rock to exhibit negligible permeability.

It follows that

$$\rho_b = \phi_s \rho_f + (1 - \phi_s - C_{sh}) \rho_m + C_{sh} \rho_{sh}, \quad (\text{A.9.1})$$

where:

ρ_b = rock density (also known as *bulk* density) (gm/cm^3),

ϕ_s = non-shale porosity,

ρ_f = density of the fluid occupying the rock's non-shale porosity (gm/cm^3), and

ρ_m = density of the solid (non-fluid) component of the rock that does not include clay minerals (gm/cm^3),

ρ_{sh} = shale density (gm/cm^3), and

C_{sh} = volumetric concentration of shale ($0 \leq C_{sh} \leq \phi_s$).

In the above equation, ϕ_s designates the *ideal* (and largest possible) rock porosity when grain-coating clay is negligible (i.e., when $C_{sh} = 0$). Consequently, the maximum possible value of C_{sh} is ϕ_s . Likewise, ρ_m designates the density of grains when the rock is free of grain-coating clay minerals (i.e., when the rock exhibits its *ideal* state).

The total rock porosity is then given by

$$\phi = \phi_s + C_{sh}(\phi_{sh} - 1) , \quad (\text{A.9.2})$$

where:

ϕ = rock porosity, and

ϕ_{sh} = shale porosity.

From eq. (A.9.1) one obtains

$$\phi_s = \frac{\rho_m - \rho_b}{\rho_m - \rho_f} - C_{sh} \left(\frac{\rho_m - \rho_{sh}}{\rho_m - \rho_f} \right) , \quad (\text{A.9.3})$$

Likewise,

$$\phi_f = \frac{1}{\phi_s} [\rho_b - (1 - \phi_s - C_{sh}) \rho_m - C_{sh} \rho_{sh}] . \quad (\text{A.9.4})$$

A.10 Fluid Density and Saturations

For fluid saturating the rock pore space and consisting of water and hydrocarbon, one has

$$\rho_f = S_w \rho_w + (1 - S_w) \rho_H , \quad (\text{A.10.1})$$

where:

ρ_f = density of the fluid occupying the rock's pore space (gm/cm^3),

ρ_w = density of water (depends on salt concentration, gm/cm^3),

ρ_H = density of hydrocarbon (gm/cm^3), and

S_w = water saturation.

It follows that

$$\rho_H = \frac{\rho_f - S_w \rho_w}{1 - S_w} . \quad (\text{A.10.2})$$

For the case of water, oil, and gas co-existing in the pore space as immiscible fluid phases, one has

$$\rho_f = S_w \rho_w + S_o \rho_o + (1 - S_w - S_o) \rho_g , \quad (\text{A.10.3})$$

where:

ρ_o = density of oil (gm/cm^3),

ρ_g = density of gas (gm/cm^3),

ρ_H = density of hydrocarbon (gm/cm^3), and

S_o = oil saturation.

Notice that the above densities are assumed at *in situ* conditions of pressure and temperature. Miscibility of oil and gas may occur below the so-called bubble point. Also,

$$S_w + S_o + S_g = 1.$$

A.11 Density-Neutron Porosity Corrections for Shaly Sandstones

One of the methods widely used for the calculation of sandstone porosity in sandstone-shale rock systems consists of first correcting both density and neutron porosity logs for presence of shale. This correction assumes that the type of shale distribution is known beforehand, i.e., laminated shale or grain-coating clay (aka dispersed shale), and that a previous step has been taken to calculate volumetric concentration of shale, C_{sh} .

The procedures and equations below also assume that both density and neutron porosity logs are expressed with the dominant solid (matrix, grain) composition for sandstones (e.g., quartz).

A.11.a Case of Sandstone-Shale Laminated Rocks

In this case, the rock is composed of juxtaposed laminae of shale and sandstone where the properties of the individual laminae of shale or sandstone are constant. Furthermore, sandstone laminae are assumed to exhibit negligible concentration of grain-coating clay minerals. All properties of the pure-shale laminae in the rock are assumed identical to those of the pre-defined pure shale in the sedimentary sequence.

Let us first assume that both density and neutron porosity logs can be calculated with a solid composition equal to the dominant solid composition of sandstone laminae. Most commonly, both density and neutron porosity logs are expressed assuming that quartz is the dominant solid (matrix) composition (which is the case in siliciclastic rocks).

It follows that

$$\phi_D^\circledcirc = \frac{\phi_D - C_{sh}\phi_{D,sh}}{1 - C_{sh}}, \quad (\text{A.11.1})$$

and

$$\phi_N^\circledcirc = \frac{\phi_N - C_{sh}\phi_{N,sh}}{1 - C_{sh}}, \quad (\text{A.11.2})$$

where:

ϕ_D = density porosity expressed in dominant matrix,

ϕ_N = neutron porosity expressed in dominant matrix,

$\phi_{D,sh}$ = density porosity measured at the pure shale in the sedimentary sequence,

$\phi_{N,sh}$ = neutron porosity measured at the pure shale in the sedimentary sequence,

ϕ_D^\circledcirc = density porosity corrected for shale laminae,

ϕ_N^\circledcirc = neutron porosity corrected for shale laminae, and

C_{sh} = volumetric concentration of shale ($0 \leq C_{sh} \leq \phi_s$).

It is found that

$$\phi_D^\circledcirc = \phi_N^\circledcirc$$

when the dominant saturating fluid is water,

$$\phi_N^\circledcirc < \phi_D^\circledcirc$$

when the dominant saturating fluid is lighter than water (e.g., hydrocarbon), and

$$\phi_N^{\circ} > \phi_D^{\circ}$$

when the assumed dominant matrix to calculate ϕ_D and ϕ_N is incorrect, C_{sh} is incorrect, or the sandstone laminae are not shale free.

When $\phi_N^{\circ} \leq \phi_D^{\circ}$ the following approximation holds:

$$\phi_s \approx \sqrt{\frac{(\phi_D^{\circ})^2 + (\phi_N^{\circ})^2}{2}}, \quad (\text{A.11.3})$$

where:

ϕ_s = porosity of shale-free sandstone laminae in the rock.

Finally, the pore volume of mobile fluids is given by

$$\phi_s (1 - C_{sh}).$$

A.11.b Case of Rocks with Grain-Coating Clay Minerals

Sandstones with grain-coating clay minerals are often referred to as “dispersed-shale sandstones” or “sandstones with dispersed shale.” These are clastic rocks which originated in sedimentary environments where mud was not actively mixed with larger grains (such as in the case of sandstone-shale laminated rocks). Instead, clay minerals arise because of the diagenetic alteration of the original grains due to changes in temperature, pressure (e.g., compaction), and fluid composition with respect to those at pre-burial conditions. *Authigenic clay* is the name often used to refer to this type of clay minerals. For instance, presence of feldspar in the original grains promotes the generation of chlorite (a common clay mineral) surrounding the grains. In turn, such a condition promotes the generation of microporosity where the space between clay crystals is overtaken by immobile (irreducible) water which is part of the total porosity but not of the fraction of porosity that contains fluid that is readily movable when applying a pressure gradient.

Note that the generation of clay crystals surrounding the original grains is different from the process of compaction and cementation of grains. Grain cementation occurs because of the precipitation of solid materials contained in the fluids filling and circulating through the rock’s pore space, such as silica, calcite, etc. Both grain cementation and authigenic clay minerals cause a reduction of porosity and permeability with respect to original conditions.

When assessing the petrophysical properties of grain-coating clay rocks, one considers two extreme cases: one in which the rocks is free of clay minerals (i.e., the rock is a clean sandstone; effectively, an ideal condition) and another when the original rock porosity is completely overtaken by clay minerals (and their associated microporosity), at which point the rock becomes impermeable. Under these conditions, volumetric concentration of shale (C_{sh}) is defined as the fraction of the rock’s volume occupied by grain-coating clay minerals and their associated microporosity. Non-shale porosity (ϕ_{n-sh}) is then defined as the remaining porosity which allows free transit of fluids. Furthermore, all the properties of the grain-coating clay mineral fraction of the rock (including their microporosity) are assumed to be identical to those of the pre-defined pure shale in the same sedimentary sequence.

It follows that

$$\phi_D^{\circ} = \phi_D - C_{sh}\phi_{D,sh}, \quad (\text{A.11.4})$$

and

$$\phi_N^{\circ} = \phi_N - C_{sh}\phi_{N,sh}, \quad (\text{A.11.5})$$

where:

ϕ_D = density porosity expressed in dominant matrix,

ϕ_N = neutron porosity expressed in dominant matrix,

$\phi_{D,sh}$ = density porosity measured at the pure shale in the sedimentary sequence,

$\phi_{N,sh}$ = neutron porosity measured at the pure shale in the sedimentary sequence,

ϕ_D^{\circledC} = density porosity corrected for grain-coating clay,

ϕ_N^{\circledC} = neutron porosity corrected for grain-coating clay, and

C_{sh} = volumetric concentration of shale.

Notice that

$$0 \leq C_{sh} \leq \phi_s,$$

where:

$\phi_{hi,s}$ = rock porosity in the ideal state when $C_{sh} = 0$, i.e., in the absence of grain-coating clay minerals.

It is found that

$$\phi_D^{\circledC} = \phi_N^{\circledC}$$

when the dominant saturating fluid is water,

$$\phi_N^{\circledC} < \phi_D^{\circledC}$$

when the dominant saturating fluid is lighter than water (e.g., hydrocarbon), and

$$\phi_N^{\circledC} > \phi_D^{\circledC}$$

when the assumed dominant matrix to calculate ϕ_D and ϕ_N is incorrect or C_{sh} is incorrect.

When $\phi_N^{\circledC} \leq \phi_D^{\circledC}$ the following approximation holds:

$$\phi_{n-sh} \approx \sqrt{\frac{(\phi_D^{\circledC})^2 + (\phi_N^{\circledC})^2}{2}}, \quad (\text{A.11.6})$$

where:

ϕ_{n-sh} = porosity with mobile fluids.

Finally, the pore volume of mobile fluids is given by

$$\phi_{n-sh}.$$

A.11.c Case of Rocks with Laminated Shale and Grain-Coating Clay Minerals

This highly common condition occurs when a sandstone-shale laminated rock is subject to diagenesis whereby grain-coating clay minerals arise in the originally shale-free laminae of sandstone. To calculate non-shale porosity (ϕ_{n-sh}), one first calculates the volumetric concentration of laminated shale, C_{sh-lam} , and calculates ϕ_D^{\circledC} and ϕ_N^{\circledC} based on eqs. (A.11.1) and (A.11.2), respectively. If the sandstone is water saturated then $\phi_N^{\circledC} > \phi_D^{\circledC}$ will signal the presence of grain-coating clay minerals in the sandstone laminae. Next, one calculates $C_{sh-disp}$, i.e., the volumetric concentration of grain-coating clay minerals (and their associated microporosity) in the sandstone laminae. Equations (A.11.4) and (A.11.5) are then invoked to calculate the corrected density and neutron porosity logs from the previously laminated-shale corrected density and neutron porosity logs, respectively, and eq. (A.11.6) is finally used to calculate the non-shale porosity, ϕ_{n-sh} of the laminae of shale.

The pore volume of mobile fluids is then given by

$$\phi_{n-sh} (1 - C_{sh-lam}).$$

A.12 Volumetric Calculation of Shale from Density and Neutron Porosity Logs in a Water-Saturated Sandstone

For the cases of either sandstone-shale laminated rocks or sandstones with grain-coating clay minerals, the corrected density and neutron porosity logs, ϕ_D° and ϕ_N° , respectively, obtained following eqs. (A.11.1) and (A.11.2), or (A.11.4) and (A.11.5), respectively, one has

$$\phi_D^{\circ} = \phi_N^{\circ}$$

in a water-saturated sandstone. It then follows that

$$\phi_D - C_{sh}\phi_{D,sh} = \phi_N - C_{sh}\phi_{N,sh},$$

whereupon,

$$C_{sh} = \frac{\phi_N - \phi_D}{\phi_{N,sh} - \phi_{D,sh}}. \quad (\text{A.12.1})$$

Notice that $\phi_{N,sh} > \phi_{D,sh}$ while in non-shale free, water saturated sandstone, $\phi_N > \phi_D$ and $\phi_{N,sh} - \phi_{D,sh} > \phi_N - \phi_D$, whereby $C_{sh} \leq 1$, as expected.

Equation (A.12.1) can be used to diagnose whether a water-saturated sandstone is free of shale or not; if C_{sh} is not negligible in the water-saturated sandstone ($\phi_N > \phi_D$ in the water-saturated sandstone) then a correlation between C_{sh} and γ (gamma-ray log) in the water-saturated sandstone can be established to calculate C_{sh} from γ elsewhere (i.e., in a hydrocarbon-saturated sandstone). Likewise eq.(A.12.1) can be used to calculate I_{shw} , which is required in eq. (A.4.2).

A.13 Electrical Resistivity of Sandstone-Shale Laminated Rocks

Sandstone-shale laminated rocks exhibit anisotropy in direction-dependent physical properties such as electrical resistivity (electrical conductivity), permeability, and velocity of propagation of elastic waves, among others. Depending on the properties of the individual laminae of shale and sandstone included in the laminated rock system, the latter can exhibit various types and degrees of effective anisotropy (e.g., transverse isotropy, vertical transverse isotropy, orthorhombic anisotropy, etc.) For the analysis of direction-dependent physical properties, it is important to first define the principal axis of symmetry for the system and subsequently define the type of anisotropy. In the case of layers perpendicular to the borehole trajectory (e.g., horizontal layers penetrated by a vertical borehole), the vertical axis constitutes the main axis of symmetry of the rock system. The simplest type of anisotropy for such a system is the so-called *Transverse Isotropy*, or TI, where directional properties only vary in the vertical and horizontal directions (regardless of azimuth around the borehole). In the case of layers dipping at an angle with respect to the borehole direction, the principal TI directions are defined as *parallel and perpendicular to bedding plane*. This is the most common anisotropic condition encountered in the subsurface.

For the case of a vertical axis of symmetry and horizontal layers, the electrical resistivity tensor of TI rocks is given by

$$\overline{\overline{R}} = \begin{bmatrix} R_h & 0 & 0 \\ 0 & R_h & 0 \\ 0 & 0 & R_v \end{bmatrix}, \quad (\text{A.13.1})$$

where R_h and R_v are horizontal and vertical resistivities, respectively.

In the more general case of TI rocks, one can write

$$\overline{\overline{R}} = \begin{bmatrix} R_{\parallel} & 0 & 0 \\ 0 & R_{\parallel} & 0 \\ 0 & 0 & R_{\perp} \end{bmatrix}, \quad (\text{A.13.2})$$

where R_{\parallel} and R_{\perp} are parallel- and perpendicular-to-bedding-plane resistivities, respectively.

For the case of sandstone-shale laminated rock systems, it follows that

$$\frac{1}{R_{\parallel}} = \frac{1 - C_{sh}}{R_s} + \frac{C_{sh}}{R_{sh}}, \quad (\text{A.13.3})$$

and

$$R_{\perp} = (1 - C_{sh}) R_s + C_{sh} R_{sh}, \quad (\text{A.13.4})$$

where:

C_{sh} = volumetric concentration of shale,

R_{\parallel} = electrical resistivity of the rock parallel to bedding plane ($\Omega \cdot \text{m}$),

R_{\perp} = electrical resistivity of the rock perpendicular to bedding plane ($\Omega \cdot \text{m}$),

R_s = electrical resistivity of the sandstone fraction of the rock, and

R_{sh} = electrical resistivity of the shale fraction of the rock ($\Omega \cdot \text{m}$).

In the above equation, R_{sh} should be read at the closest pure shale that most closely resembles the constitution of shale laminae included in the rock. When the objective is to calculate hydrocarbon saturation in the sandstone fraction of the rock system it is necessary to first calculate R_s from the above equations. Typically, one only has access to R_{\parallel} from standard commercial borehole resistivity measurements (induction or laterolog measurements) acquired in vertical wells penetrating quasi-horizontal layers. In the latter case, eq. (A.13.3) gives rise to the following solution for R_s originally introduced by [Poupon et al. \(1954\)](#):

$$R_s = (1 - C_{sh}) \frac{R_{sh} R_{\parallel}}{R_{sh} - C_{sh} R_{\parallel}}. \quad (\text{A.13.5})$$

Next, hydrocarbon saturation is calculated from R_s via Archie's equation, where porosity is equal to sandstone porosity, ϕ_s .

Notice that eq. (A.13.5) requires that

$$R_{sh} > C_{sh} R_{\parallel} \implies 0 \leq C_{sh} < \frac{R_{sh}}{R_{\parallel}} \leq 1.$$

The above condition is often not met when layer dip is not negligible, C_{sh} was not calculated correctly, or R_{sh} is not correct (i.e., the resistivity reading at the closest pure shale is different from that of shale laminae included in the rock). Likewise, notice from eq. (A.13.5) that the calculation of R_s is not necessary when $C_{sh} \rightarrow 1$ (the sandstone fraction of the rock becomes negligible).

Modern tri-axial borehole induction tools enable the estimation of dip and azimuth of layers relative to the well trajectory (borehole axis). Upon determination of layer dip and azimuth, the measurements can be aligned (rotated) to coincide with the directions parallel and perpendicular to bedding plane. At that point, if rock anisotropy is TI then the measurement provides both R_{\parallel} and R_{\perp} . From eq. (A.13.4) one independently obtains that

$$R_s = \frac{R_{\perp} - C_{sh} R_{sh}}{1 - C_{sh}}. \quad (\text{A.13.6})$$

This latter formula requires that

$$R_{\perp} \geq C_{sh} R_{sh} \implies 0 \leq C_{sh} < \frac{R_{\perp}}{R_{sh}} \leq 1.$$

Similar to eq. (A.13.5), the above condition is often not met when layer dip is not negligible, C_{sh} was not calculated correctly, or R_{sh} is not correct. Notice also from eq. (A.13.6) that the calculation of R_s is not necessary when $C_{sh} \rightarrow 1$ (the sandstone fraction of the rock becomes negligible).

When both R_{\parallel} and R_{\perp} are available then eqs. (A.13.3) and (A.13.4) can be solved simultaneously to estimate either R_s and C_{sh} (assuming that R_{sh} is known) or R_s and R_{sh} (assuming that C_{sh} is known), with the latter option being the most practical one because shale laminae may exhibit variable composition. Likewise, in the presence of noisy measurements it is best to simultaneously solve eqs. (A.13.3) and (A.13.4) via least-squares minimization subject to positivity (in the case of R_s and R_{sh}) and/or value-range constraints (in the case of C_{sh}).

If the common case where shales are intrinsically transverse isotropic, eqs. (A.13.3) and (A.13.4) are rewritten as

$$\frac{1}{R_{\parallel}} = \frac{1 - C_{sh}}{R_s} + \frac{C_{sh}}{R_{sh\parallel}}, \quad (\text{A.13.7})$$

and

$$R_{\perp} = (1 - C_{sh}) R_s + C_{sh} R_{sh\perp}, \quad (\text{A.13.8})$$

where:

$R_{sh\parallel}$ = parallel-to-bedding-plane electrical resistivity of shale ($\Omega \cdot \text{m}$), and

$R_{sh\perp}$ = perpendicular-to-bedding-plane electrical resistivity of shale ($\Omega \cdot \text{m}$).

Both $R_{sh\parallel}$ and $R_{sh\perp}$ are measured directly across the closest pure shale. The assumption is made that the principal directions of intrinsic shale anisotropy are the same as those of the sandstone-shale laminated sequence. Equations (A.13.7) and (A.13.8) are then simultaneously solved to calculate R_s and C_{sh} .

Finally, in the case of sandstone-shale laminated sequences in which sandstone laminae are intrinsically anisotropic because, for instance, of grain-size laminations due to cross-bedding, eqs. (A.13.3) and (A.13.4) are rewritten as

$$\frac{1}{R_{\parallel}} = \frac{1 - C_{sh}}{R_{s\parallel}} + \frac{C_{sh}}{R_{sh\parallel}}, \quad (\text{A.13.9})$$

and

$$R_{\perp} = (1 - C_{sh}) R_{s\perp} + C_{sh} R_{sh\perp}, \quad (\text{A.13.10})$$

where:

$R_{s\parallel}$ = parallel-to-bedding-plane electrical resistivity of sandstone laminae ($\Omega \cdot \text{m}$), and

$R_{s\perp}$ = perpendicular-to-bedding-plane electrical resistivity of sandstone laminae ($\Omega \cdot \text{m}$).

The above equations need to be solved separately to calculate $R_{s\parallel}$ and $R_{s\perp}$.

A.14 Electrical Resistivity of Rocks with Grain-Coating Clay Minerals

The presence of grain-coating clay minerals causes non-negligible grain-surface electrical conduction effects that are not accounted for in Archie's equation (A.6.2) (quartz grains also exhibit surface conduction effects because of their net negative surface electrical charge but the corresponding effect is negligible for all practical purposes compared to that of grain-coating clay minerals).

The standard way to account for surface electrical conduction effects in Archie's equation is to describe the effective conduction in the aqueous electrolyte of the rock as a parallel circuit between (1) aqueous conduction near the surface of grain-coating clay minerals, and (2) volumetric conduction in the remainder of the water pore volume.

A.14.a Waxman-Smits Conduction Model

There are several formulations available to describe such parallel-circuit model of electrolyte conduction, with the first one advanced by [Waxman & Smits \(1967, 1968\)](#) using electrochemical concepts of cation exchange, given by

$$\sigma_t = \hat{\sigma}_w \left(\frac{\phi^{\hat{m}}}{\hat{a}} \right) S_w^{\hat{n}}, \quad (\text{A.14.1})$$

and

$$\hat{\sigma}_w = \sigma_w + \sigma_x(\sigma_w, T, S_w, Q_v) = \sigma_w \left[1 + \frac{\sigma_x(\sigma_w, T, S_w, Q_v)}{\sigma_w} \right], \quad (\text{A.14.2})$$

where:

σ_t = electrical conductivity of the rock (S/m) = $1/R_t$,

σ_w = electrical conductivity of formation water (S/m) = $1/R_w$,

ϕ = porosity of the rock (total porosity),

S_w = water saturation (total water saturation),

$\hat{\sigma}_w$ = modified (effective) electrical conductivity of formation water (because of surface conduction effects associated with grain-coating clay minerals) (S/m),

σ_x = electrical conductivity of formation water due to surface conduction effects associated with grain-coating clay minerals (S/m),

\hat{m} = modified porosity exponent (because of surface conduction effects associated with grain-coating clay minerals),

\hat{n} = modified saturation exponent (because of surface conduction effects associated with grain-coating clay minerals),

\hat{a} = modified Winsauer coefficient (because of surface conduction effects associated with grain-coating clay minerals),

T = temperature ($^{\circ}\text{F}$), and

Q_V = cation exchange capacity (CEC) per unit pore volume (meq/mL).

The specific functional relationship for σ_x introduced by [Waxman & Smits \(1968\)](#) is written as

$$\sigma_x = \frac{BQ_v}{S_w}, \quad (\text{A.14.3})$$

where:

$$B = \frac{-5.41 + 0.133T - 0.0001253T^2}{1 + R_w^{1.23}(0.025T - 1.07)} \quad (\text{A.14.4})$$

for T given in $^{\circ}\text{F}$ and R_w in $\Omega \cdot \text{m}$. In the above equations, Q_v is a function of the specific type of clay mineral(s) coating the grains *and* its volumetric concentration in the pore space (including its associated microporosity). The type of clay mineral impacts the specific surface (surface-to-volume ratio) available for electrical conduction effects as well as the surface density of electric charge responsible for the generation of the so-called electrical double layer (EDL). The relationship between Q_v and CEC is given by [\(Waxman & Smits, 1968\)](#):

$$Q_v = \text{CEC} \left(\frac{1 - \phi}{\phi} \right) \rho_g,$$

where ρ_g is grain density (gm/cm^3).

However, measuring Q_v (or CEC) in the laboratory involves multiple technical challenges (McPhee et al., 2015), which limit the practical implementation of the above equations. Several alternative models have been introduced to overcome these challenges.

Note that the implementation of eqs. (A.14.1), (A.14.2), and (A.14.3) to evaluate S_w from measurements of R_t (or σ_t) does not allow an explicit solution such as in Archie's equation given that σ_x is also a function of S_w . A simple numerical way to overcome this difficulty is the use of nested iterations, where an initial value of S_w obtained from Archie's equation is used to calculate σ_x , whereupon a new value of S_w is calculated to update the calculation of σ_x , and so on. Convergence is typically achieved within a few nested iterations. Parenthetically, the reason why there is no explicit mathematical solution for S_w with the Waxman-Smits equation is because surface electrical conduction effects due to grain-coating clay minerals amplify in the presence of hydrocarbon in the pore space (as described by eq. A.14.3), and this amplification is not known *a-priori*.

A.14.b Juhasz's Modification of the Waxman-Smits Conduction Model

Juhaz (Juhasz, 1981) developed a practical approximation to bypass the need of measuring Q_v in the laboratory when implementing the Waxman-Smits method to calculate S_w . This approximation presupposes the availability of water saturated sandstones with various volumetric concentrations of grain-coating clay in the same sedimentary sequence where hydrocarbon-bearing sandstones exist. It also assumes that the types of clay minerals are constant across the clastic sedimentary sequence; only their volumetric concentrations vary from sandstone to sandstone. Juhaz uses the values of electrical resistivity measured in the water saturation sandstones to normalize them with respect to volumetric concentration of grain-coating clay. Further, he posits that a fraction of the pore volume of water, S_b , is responsible for surface electrical conduction which is proportional to the volumetric concentration of grain-coating clay

$$\sigma_x = \frac{BQ_v}{S_w} \approx B \frac{S_b}{S_w}, \quad (\text{A.14.5})$$

where

$$S_b = C_{sh} \frac{\phi_{sh}}{\phi},$$

and ϕ_{sh} is shale porosity. Notice that, as emphasized before, $C_{sh} \leq \phi_s$, where ϕ_s is the porosity of the idealized case when $C_{sh} = 0$. Likewise, the assumption is made that the microporosity associated with the grain-coating clay is the same as that encountered in the closest pure shale, i.e., ϕ_{sh} .

Consequently, from eqs. (A.14.1), (A.14.2), and (A.14.5), it follows that

$$\sigma_t = \sigma_w \left(1 + \frac{B}{\sigma_w S_w} C_{sh} \frac{\phi_{sh}}{\phi} \right) \left(\frac{\phi^m}{\hat{a}} \right) S_w^{\hat{n}}, \quad (\text{A.14.6})$$

or, equivalently,

$$\frac{1}{R_t} = \frac{1}{R_w} \left(1 + \frac{BR_w}{S_w} C_{sh} \frac{\phi_{sh}}{\phi} \right) \left(\frac{\phi^m}{\hat{a}} \right) S_w^{\hat{n}}.$$

A.14.c Dual-Water Approximation of the Electrical Surface Conduction Model

Proposed by Clavier et al. (1984), the dual-water model of electrical surface conduction approximates the relative effects of surface and pore volume electrical conduction with an equivalent parallel electrical circuit. The parallel circuit partitions the bulk volume of water into the fractions occupied by the volume of water subject to surface electrical conduction (in the proximity of grain-coating clay minerals) and the remaining pore volume subject to Archie-type electrical conduction. It follows that

$$\hat{\sigma}_w = \sigma_w \left(1 - \frac{S_b}{S_w} \right) + \sigma_b \frac{S_b}{S_w} = \sigma_w \left[1 + \frac{S_b}{S_w} \left(\frac{\sigma_b}{\sigma_w} - 1 \right) \right], \quad (\text{A.14.7})$$

with

$$S_b = C_{sh} \frac{\phi_{sh}}{\phi},$$

where:

σ_b = electrical conductivity of the fraction of the pore volume in the proximity of grain-coating clay minerals (S/m), and

S_b = fraction of the pore volume of water supporting surface electrical conduction.

The final expressions for rock electrical conductivity is given by

$$\sigma_t = \sigma_w \left[1 + \frac{1}{\sigma_w S_w} (\sigma_b - \sigma_w) C_{sh} \frac{\phi_{sh}}{\phi} \right] \left(\frac{\phi^{\hat{m}}}{\hat{a}} \right) S_w^{\hat{n}}, \quad (\text{A.14.8})$$

or, equivalently,

$$\frac{1}{R_t} = \frac{1}{R_w} \left[1 + \frac{1}{S_w} \left(\frac{R_w - R_b}{R_b} \right) C_{sh} \frac{\phi_{sh}}{\phi} \right] \left(\frac{\phi^{\hat{m}}}{\hat{a}} \right) S_w^{\hat{n}},$$

where $R_b = 1/\sigma_b$.

A.15 Sonic Porosity

The calculation of sonic porosity assumes that the acoustic time of flight through a rock is the sum of the separate acoustic times of flight through the fluid and solid components of the rock. This approximation is due to Wyllie et al. (1956), and is given by

$$\Delta t_b \approx \phi_{sonic} \Delta t_f + (1 - \phi_{sonic}) \Delta t_m, \quad (\text{A.15.1})$$

where:

ϕ_{sonic} = sonic porosity (Wyllie porosity),

Δt_b = sonic slowness of the rock ($\mu\text{sec}/\text{ft}$), and

Δt_f = sonic slowness of the fluid component of the rock ($\mu\text{sec}/\text{ft}$), and

Δt_m = sonic slowness of the solid (matrix) component of the rock ($\mu\text{sec}/\text{ft}$).

Sonic slowness if inversely proportional to sonic velocity. It follows that

$$\phi_{sonic} \approx \frac{\Delta t_b - \Delta t_m}{\Delta t_f - \Delta t_m}. \quad (\text{A.15.2})$$

Sonic porosity as calculated above typically approaches actual rock porosity in homogeneous, well consolidated and cemented sandstones; the lower the porosity the more accurate the approximation. However, sonic porosity departs substantially from the actual rock porosity in unconsolidated, fractured, anisotropic, and high-porosity rocks. Significant differences may also arise in the case of rocks with large variations in pore sizes, such as in vuggy carbonates, for instance. Often, the discrepancy between sonic porosity and actual porosity is used to detect abnormal rock conditions, i.e., spatially heterogeneous and anisotropic rocks. Without verification and/or calibration, sonic porosity should be never be used in place of porosity calculations performed with density logs.

A.15.a Sonic Porosity Corrected for Compaction Effects

Several attempts have been made to correct the Wyllie time-of-flight, sonic porosity formula (eq. A.15.2) for compaction effects in unconsolidated rocks. The most common correction procedure is written as

$$\phi_{sonic} \approx \frac{1}{C_p} \frac{\Delta t_b - \Delta t_m}{\Delta t_f - \Delta t_m}. \quad (\text{A.15.3})$$

where C_p is the so-called *sonic compaction coefficient*. Typically $1 < C_p \leq 3$; calibration between density porosity and sonic porosity in water-saturated sandstones is necessary to estimate C_p .

A.16 Calculation of Permeability

There are multiple possibilities for calculating rock permeability from porosity and other petrophysical properties. The calculation of permeability exclusively from porosity is invalid because, by definition, porosity is size-independent, i.e., it is a ratio of volumes which does not keep track of pore or grain sizes. Permeability, on the other hand, is size-dependent because it is partially governed by surface forces.

One of the most widely used formulas for calculating permeability was advanced by Timur (Timur, 1968) and is given by

$$k = \alpha \frac{\phi^\beta}{S_{wi}^\gamma} \quad (\text{A.16.1})$$

or its variant,

$$k = \alpha \phi^\beta \left(\frac{1 - S_{wi}}{S_{wi}} \right)^\gamma \quad (\text{A.16.2})$$

where S_{wi} is irreducible water saturation. The above formulas assume that water is the grain-wetting fluid phase. Note that S_{wi} is size dependent because it is directly related to surface forces: it quantifies the (1) pore volume of water which is attached to grains or clay minerals in the form of wetting thin films, (2) funicular/pendular-ring distributions of water in the pore space, and (3) the volume of other forms of capillary-trapped water. As such, S_{wi} in Timur's equations "normalizes" total porosity into *effective porosity*, i.e., the fraction of the available rock porosity that allows fluid transport. The lower the value of S_{wi} the larger the rock permeability. Conversely, as $S_{wi} \rightarrow 1$ the rock becomes impermeable, such as in the case of shales, where all the water included in the pore space is immobile.

The difference between eq. (A.16.1) and eq. (A.16.2) is that eq. (A.16.2) exhibits the expected behavior for permeability as $S_{wi} \rightarrow 1$, i.e., $k \rightarrow 0$, while eq. (A.16.1) does not. Also, note that the constancy of variables α , β , and γ in eqs. (A.16.1) and (A.16.2) for a wide range of values of porosity and irreducible water saturation implicitly defines the concept of *rock class*: a given petrophysical rock class includes all the rocks whose storage and flow properties are governed by Timur's equations and for which α , β , and γ are constant. In practice, however, α , β , and γ tend to be constant only within narrow value-range intervals for ϕ and S_{wi} .

The implementation of eqs. (A.16.1) and (A.16.2) in practice is technically challenging because either the rocks under examination need to be at conditions of irreducible water saturation or an independent measurement of S_{wi} is necessary, such as magnetic resonance.

Appendix B

Nomenclature

The following are acronyms commonly used in Formation Evaluation

TVD True Vertical Depth

MD Measured Depth

BS Bit Size

KB Kelly Bushing

GL Ground Level

BHT Bottom-Hole Temperature

LWD Logging While Drilling

MWD Measurements While Drilling

SP Spontaneous Potential

SSP Static Spontaneous Potential

WL Wireline

MICP Mercury Intrusion Capillary Pressure

NMR Nuclear Magnetic Resonance

PTA Pressure Transient Analysis

1D One Dimensional

2D Two Dimensional

3D Three Dimensional

TI Transverse Isotropy

VTI Vertical Transverse Isotropy

EM Electromagnetic

REV Representative Elementary Volume

SEM Scanning Electron Microscope

FIB Focused Ion Beam

BIB Broad Ion Beam

CT Computerized Tomography

TOC Total Organic Content

Appendix C

Key to Well-Log Compendium

August 21, 2023

About the Author



Carlos Torres-Verdín completed his BSc degree in Engineering Geophysics at the National Polytechnic Institute of Mexico. He holds a MSc degree in Electrical Engineering from The University of Texas at Austin (1985), and a PhD degree in Engineering Geoscience from the University of California, Berkeley (1991). From 1982 to 1983 he worked for the Mexican Petroleum Institute as Development Engineer. From 1991 to 1997 he worked as Research Scientist for Schlumberger-Doll Research in Ridgefield, Connecticut, USA. From 1997 to 1999 he held the positions of Reservoir Specialist and Product Champion (Special Projects) while working for the Vice Presidency of Engineering and Technology of the oil company YPF S.A., in Buenos Aires, Argentina. Since August 1999 he has been with the Hildebrand Department of Petroleum and Geosystems Engineering of The University of Texas at Austin, where he currently holds the position of Professor. He teaches undergraduate and graduate courses formation evaluation, well logging, integrated reservoir characterization, inverse theory, and computer programming. Dr. Torres-Verdín is founder and director of the Joint Industry Research Consortium on Formation Evaluation at the University of Texas at

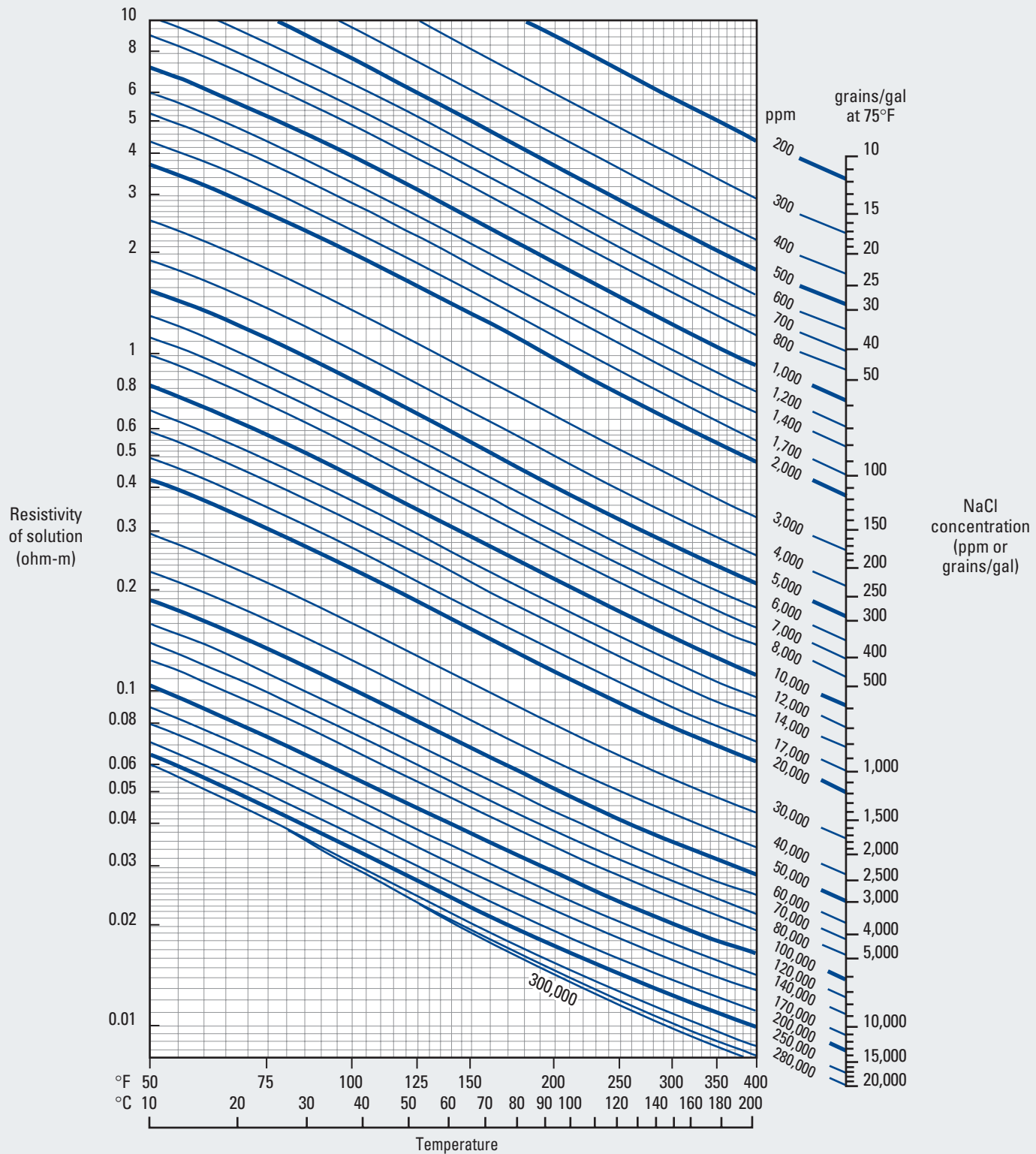
Austin, which has been in operation since 2000 and is currently sponsored by 20 companies. His research work has been sponsored by the US Department of Energy, US National Science Foundation, American Chemical Society, Texas Water Development Board, Afren, Anadarko, Apache, Aramco, Baker-Hughes, BG, BHP Billiton, BP, Chevron, ConocoPhillips, COSL, Det Norske, ENI, Equinor, ExxonMobil, Halliburton, Hess, Maersk, Marathon Oil Company, Mexican Institute for Petroleum, Nexen, ONGC, OXY, Petrobras, PTT Exploration and Production, Repsol, RWE, Schlumberger, Shell, Southwestern Energy, TOTAL, Weatherford, Wintershall, and Woodside Petroleum Limited, among others. He has published more than 250 articles in refereed technical journals, over 250 articles in refereed international conferences, two book chapters, and is co-author of one book. Dr. Torres-Verdín is co-inventor of 7 US patents. He has served as Invited Editor for *Radio Science*, Associate Editor for the *Journal of Electromagnetic Waves and Applications*, Technical Editor for *SPE Journal* (Society of Petroleum Engineers, SPE), Associate Editor for *Interpretation* (Society of Exploration Geophysicists, SEG), Editor of *Petrophysics* (Society of Petrophysicists and Well Log Analysts, SPWLA), Chairman of the Editorial Board of the periodical *The Leading Edge* (published by the SEG), and Assistant Editor for *Geophysics* (SEG). Dr. Torres-Verdín is a member of the research committee of the SEG, was a member of the technical committee of the SPWLA during two 3-year terms, and was VP of Publications of the SPWLA for 2 one-year terms and VP of Technology for the SPWLA for a one-year term. He received the 2020 Virgil Kauffman Gold Medal from the SEG, the 2019 Anthony F. Lucas Gold Medal from the SPE, the 2017 Honorary Membership from the SEG, the 2017 Conrad Schlumberger Award from the EAGE (European Association of Geoscientists and Engineers), is a Distinguished Member of the SPE (2015), received the 2014 Gold Medal for Technical Achievement Award

from the SPWLA, the 2008 Formation Evaluation Award from the SPE, the 2006 Distinguished Technical Achievement Award from the SPWLA, is recipient of the 2003, 2004, 2006, and 2007 Best Paper Awards by *Petrophysics*, of the 2020 Best Paper Award in the *Geophysics* by the SEG, of two Honorable Mentions for the Best Paper Category in *Geophysics* by the SEG in 2015 and 2020, is recipient of the 2006 and 2014 Best Presentation Awards and the 2007 Best Poster Awards by the SPWLA, and was Distinguished Technical Speaker during 2006-2007, 2013-2014, and 2016-2017 for the SPWLA. Dr. Torres-Verdín is a Provost Teaching Fellow at UT Austin, recipient of the Texas Ten Award 2018 (annual list of the 10 most inspiring UT Austin professors, nominated by alumni and selected by the Alcalde magazine, published by the Texas Exes), Lockheed Martin Aeronautics Company Award for Excellence in Engineering Teaching by the Cockrell School of Engineering, University of Texas Austin (2017), of the Engineering Foundation Award by the College of Engineering of the University of Texas at Austin (2001), the 2001-2002 Departmental Teaching Award by the Department of Petroleum and Geosystems Engineering (University of Texas at Austin), the Deans Fellowship by the College of Engineering of the University of Texas at Austin (Spring 2002), and was named Outstanding Faculty in the Department of Petroleum and Geosystems Engineering and recognized with the Faculty Appreciation Award by the UT Student Engineering Council of the University of Texas at Austin (2010). Currently, he holds the Brian James Jennings Memorial Endowed Chair in Petroleum and Geosystems Engineering and the Zarrow Centennial Professorship in Petroleum Engineering. He has supervised 42 PhD and 47 Master's students at UT Austin. Dr. Torres-Verdín has conducted numerous training courses for oil companies in the areas of petrophysics, formation evaluation, well logging, geophysical inversion, seismic amplitude inversion, reservoir characterization, and geostatistics. He has completed 21 officially certified marathons (including Boston 2007) with a P.R. of 3 hours and 18 minutes, and 16 officially certified half marathons (approximately 420 unofficial half marathons) with a P.R. of 1 hour and 24 minutes, is an avid bicyclist, and a consummate fanatic of the outdoors. He currently serves as District 3 Director of the Hays Trinity Groundwater Conservation District (HTGCD) in Hays County, TX.

Resistivity of NaCl Water Solutions

Gen-6
(former Gen-9)

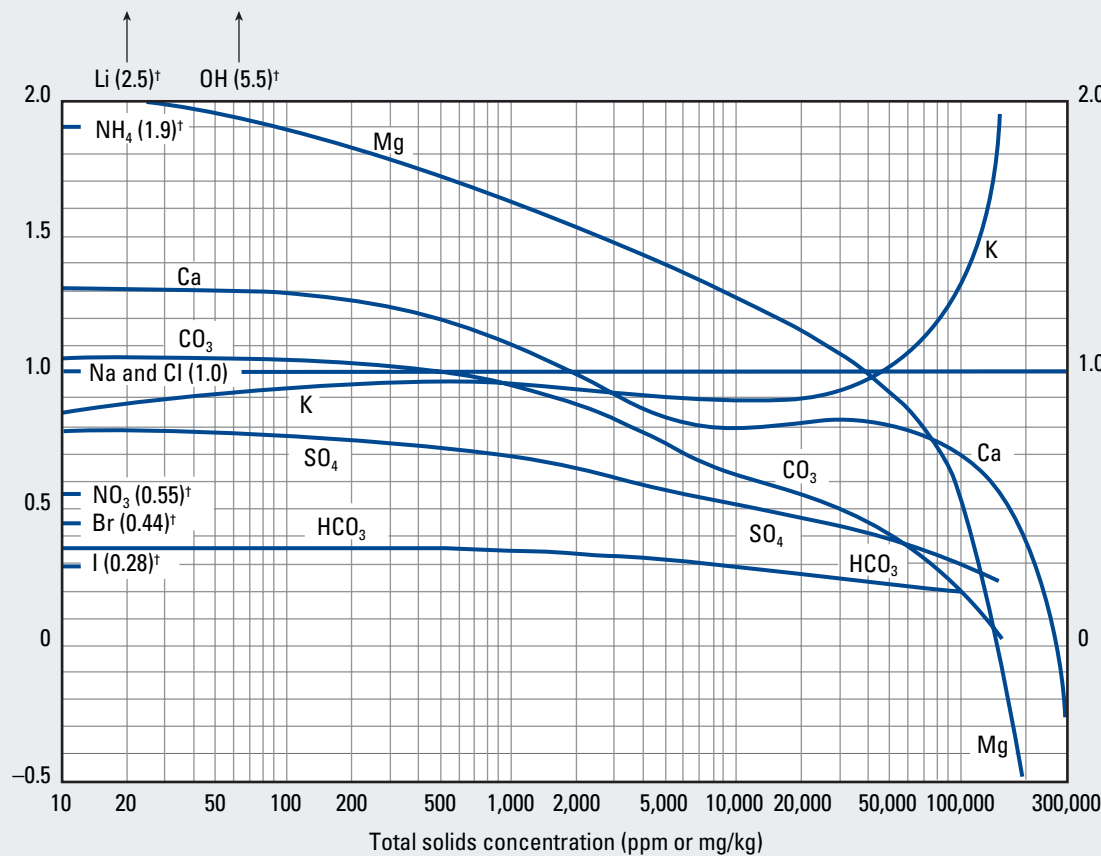
Gen

Conversion approximated by $R_2 = R_1 [(T_1 + 6.77)/(T_2 + 6.77)]^{\circ}\text{F}$ or $R_2 = R_1 [(T_1 + 21.5)/(T_2 + 21.5)]^{\circ}\text{C}$ 

Equivalent NaCl Salinity of Salts

Gen-4
(former Gen-8)

Gen



† Multipliers that do not vary appreciably for low concentrations (less than about 10,000 ppm) are shown at the left margin of the chart

© Schlumberger

Purpose

This chart is used to approximate the parts-per-million (ppm) concentration of a sodium chloride (NaCl) solution for which the total solids concentration of the solution is known. Once the equivalent concentration of the solution is known, the resistivity of the solution for a given temperature can be estimated with Chart Gen-6.

Description

The x-axis of the semilog chart is scaled in total solids concentration and the y-axis is the weighting multiplier. The curve set represents the various multipliers for the solids typically in formation water.

Example

Given: Formation water sample with solids concentrations of calcium (Ca) = 460 ppm, sulfate (SO_4) = 1,400 ppm, and $\text{Na} + \text{Cl}$ = 19,000 ppm. Total solids concentration = $460 + 1,400 + 19,000 = 20,860$ ppm.

Find:

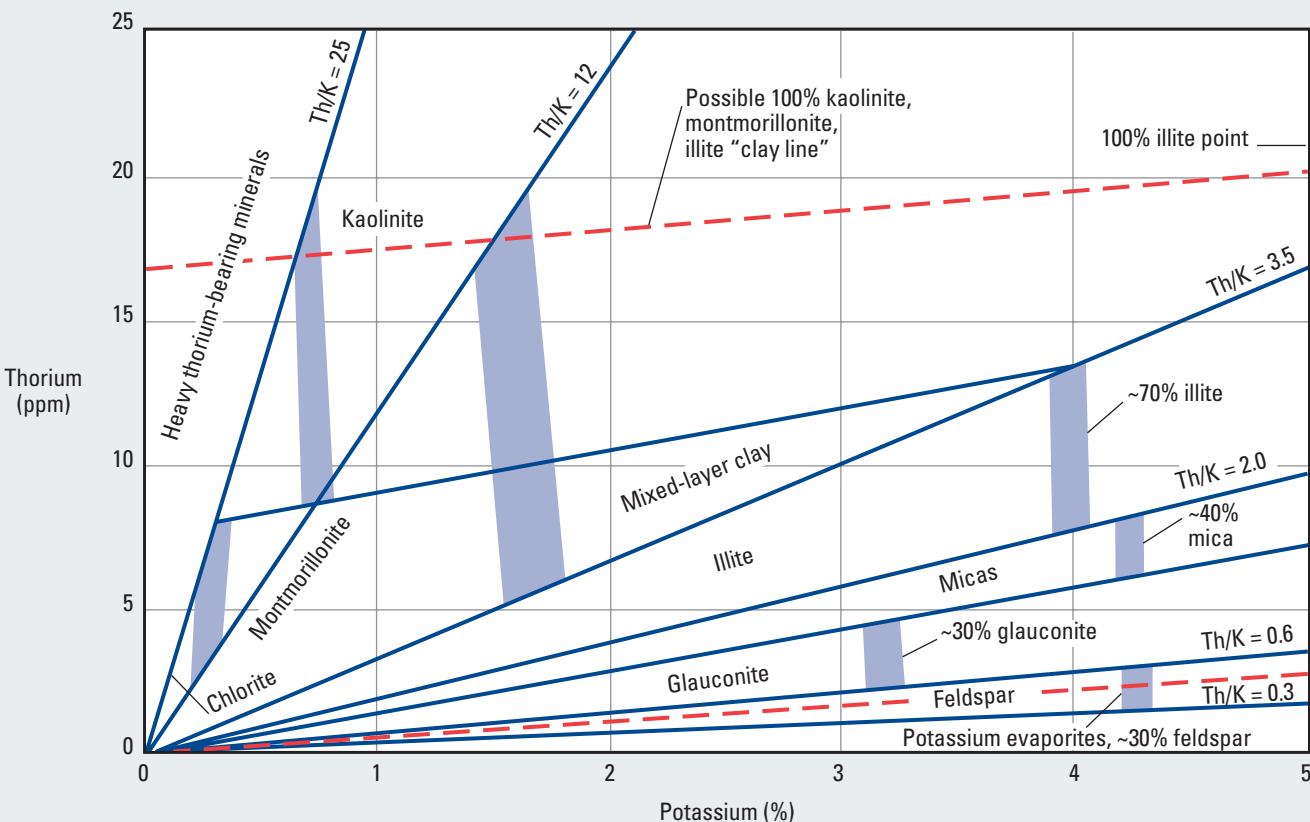
Equivalent NaCl solution in ppm.

Answer: Enter the x-axis at 20,860 ppm and read the multiplier value for each of the solids curves from the y-axis: $\text{Ca} = 0.81$, $\text{SO}_4 = 0.45$, and $\text{NaCl} = 1.0$. Multiply each concentration by its multiplier:

$$(460 \times 0.81) + (1,400 \times 0.45) + (19,000 \times 1.0) = 20,000 \text{ ppm.}$$

NGS* Natural Gamma Ray Spectrometry Tool

Mineral Identification—Open Hole

Lith-2
(former CP-19)

*Mark of Schlumberger
© Schlumberger

Lith

Purpose

This chart is used to determine the type of minerals in a shale formation from concentrations measured by the NGS Natural Gamma Ray Spectrometry tool.

Description

Entering the chart with the values of thorium and potassium locates the intersection point used to determine the type of radioactive minerals that compose the majority of the clay in the formation.

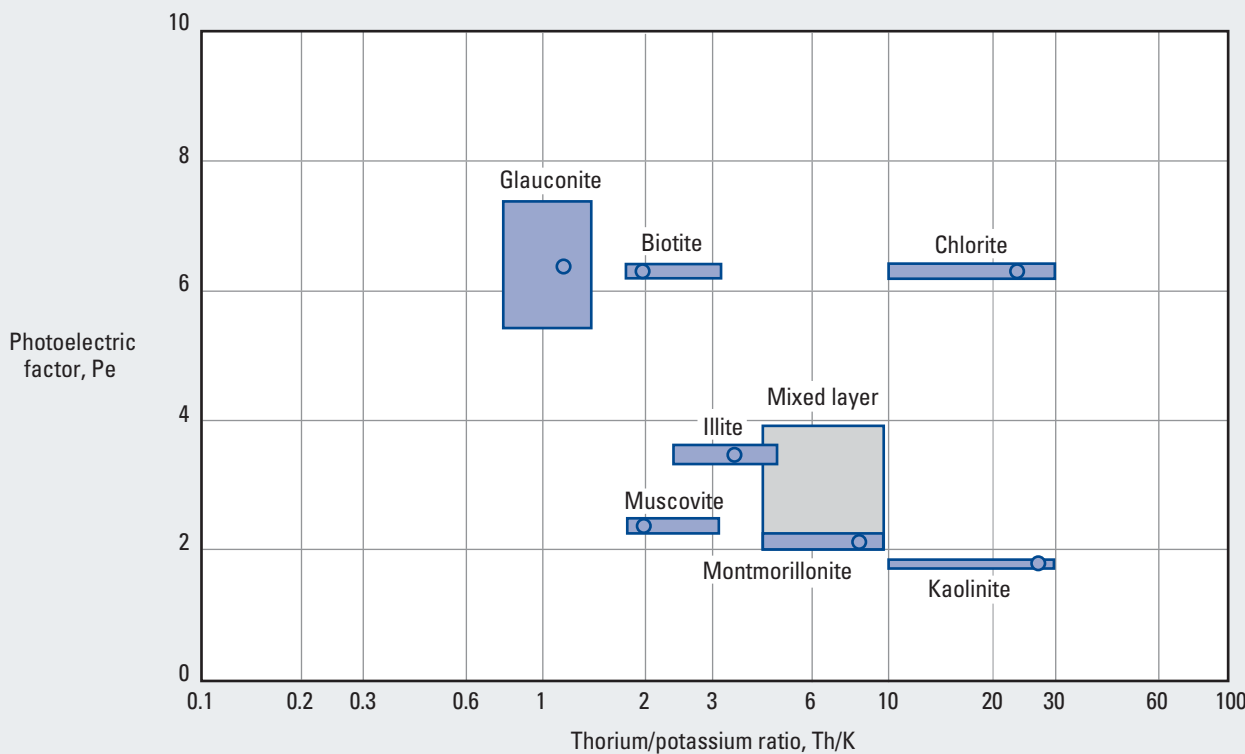
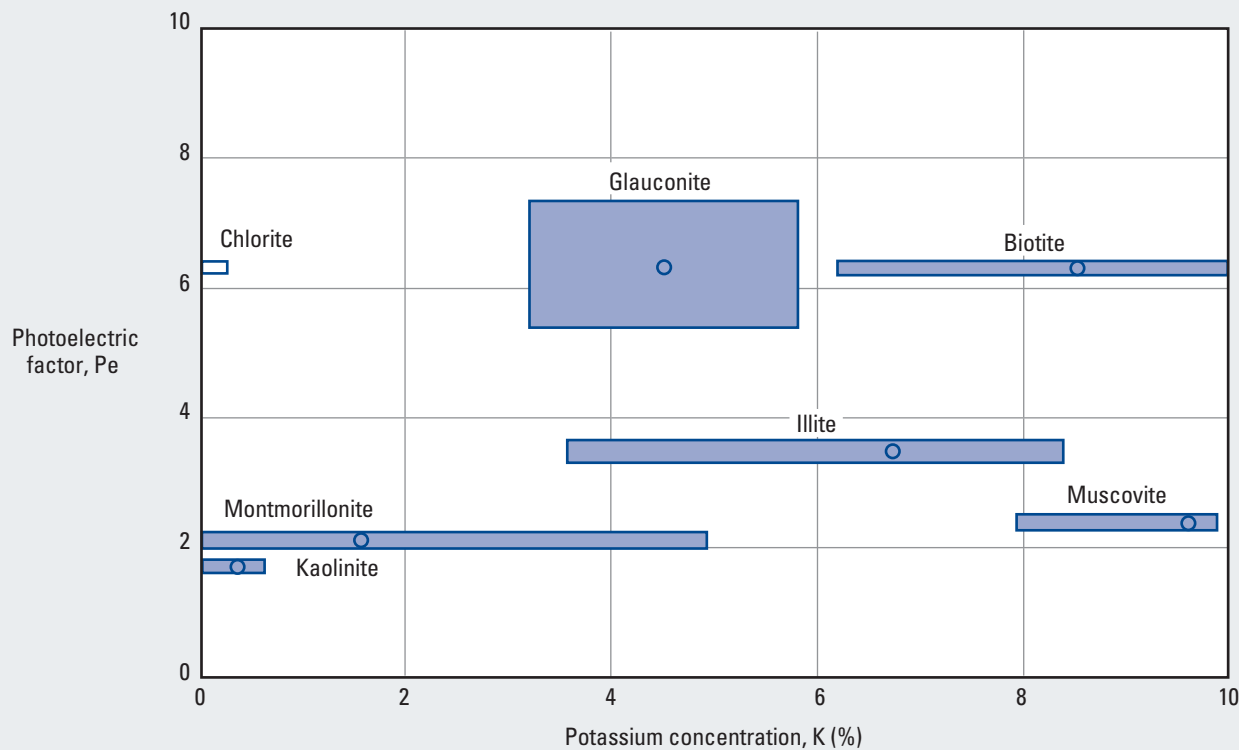
A sandstone reservoir with varying amounts of shaliness and illite as the principal clay mineral usually plots in the illite segment of the chart with Th/K between 2.0 and 3.5. Less shaly parts of the reservoir plot closer to the origin, and shaly parts plot closer to the 70% illite area.

Density and NGS* Natural Gamma Ray Spectrometry Tool

Mineral Identification—Open Hole

Lith-1

(former CP-18)

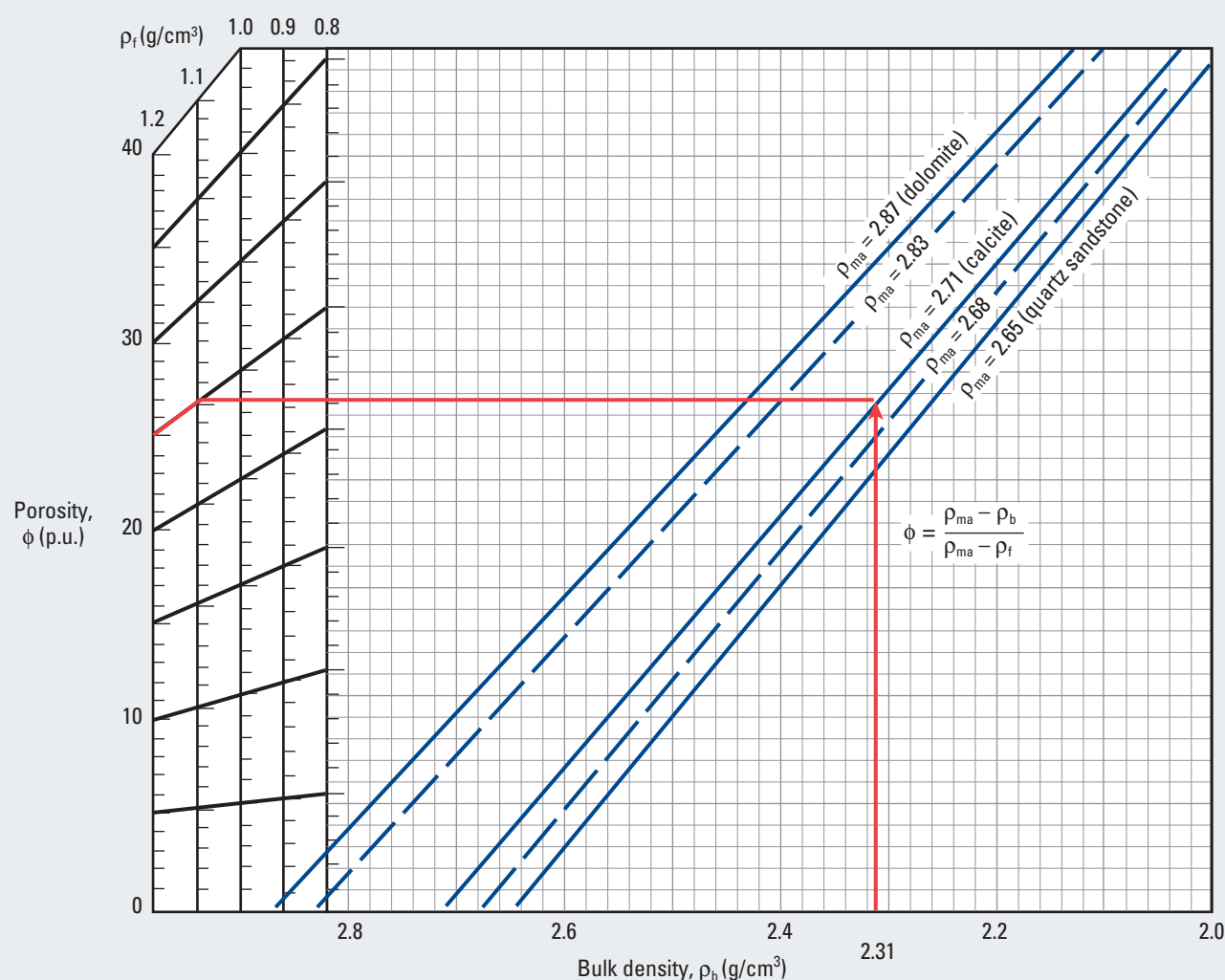


Density Tool

Porosity Determination—Open Hole

Por-3

(former Por-5)



*Mark of Schlumberger
© Schlumberger

Purpose

This chart is used to convert grain density (g/cm^3) to density porosity.

Description

Values of log-derived bulk density (ρ_b) corrected for borehole size, matrix density of the formation (ρ_{ma}), and fluid density (ρ_f) are used to determine the density porosity (ϕ_D) of the logged formation. The ρ_f is the density of the fluid saturating the rock immediately surrounding the borehole—usually mud filtrate.

Enter the borehole-corrected value of ρ_b on the x-axis and move vertically to intersect the appropriate matrix density curve. From the intersection point move horizontally to the fluid density line. Follow the porosity trend line to the porosity scale to read the formation

porosity as determined by the density tool. This porosity in combination with CNL* Compensated Neutron Log, sonic, or both values of porosity can help determine the rock type of the formation.

Example

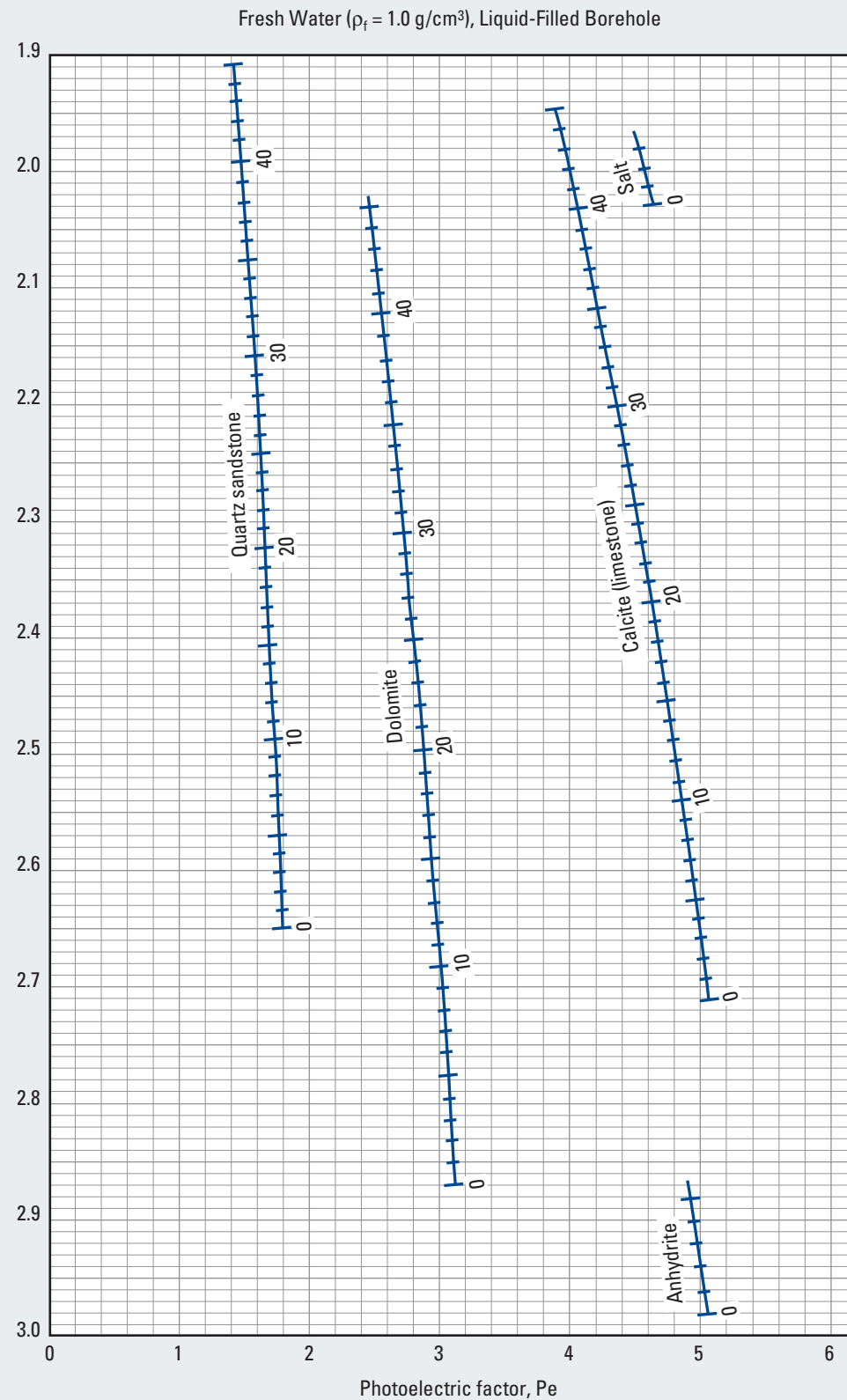
Given: $\rho_b = 2.31 \text{ g}/\text{cm}^3$ (log reading corrected for borehole effect), $\rho_{ma} = 2.71 \text{ g}/\text{cm}^3$ (calcite mineral), and $\rho_f = 1.1 \text{ g}/\text{cm}^3$ (salt mud).

Find: Density porosity.

Answer: $\phi_D = 25 \text{ p.u.}$

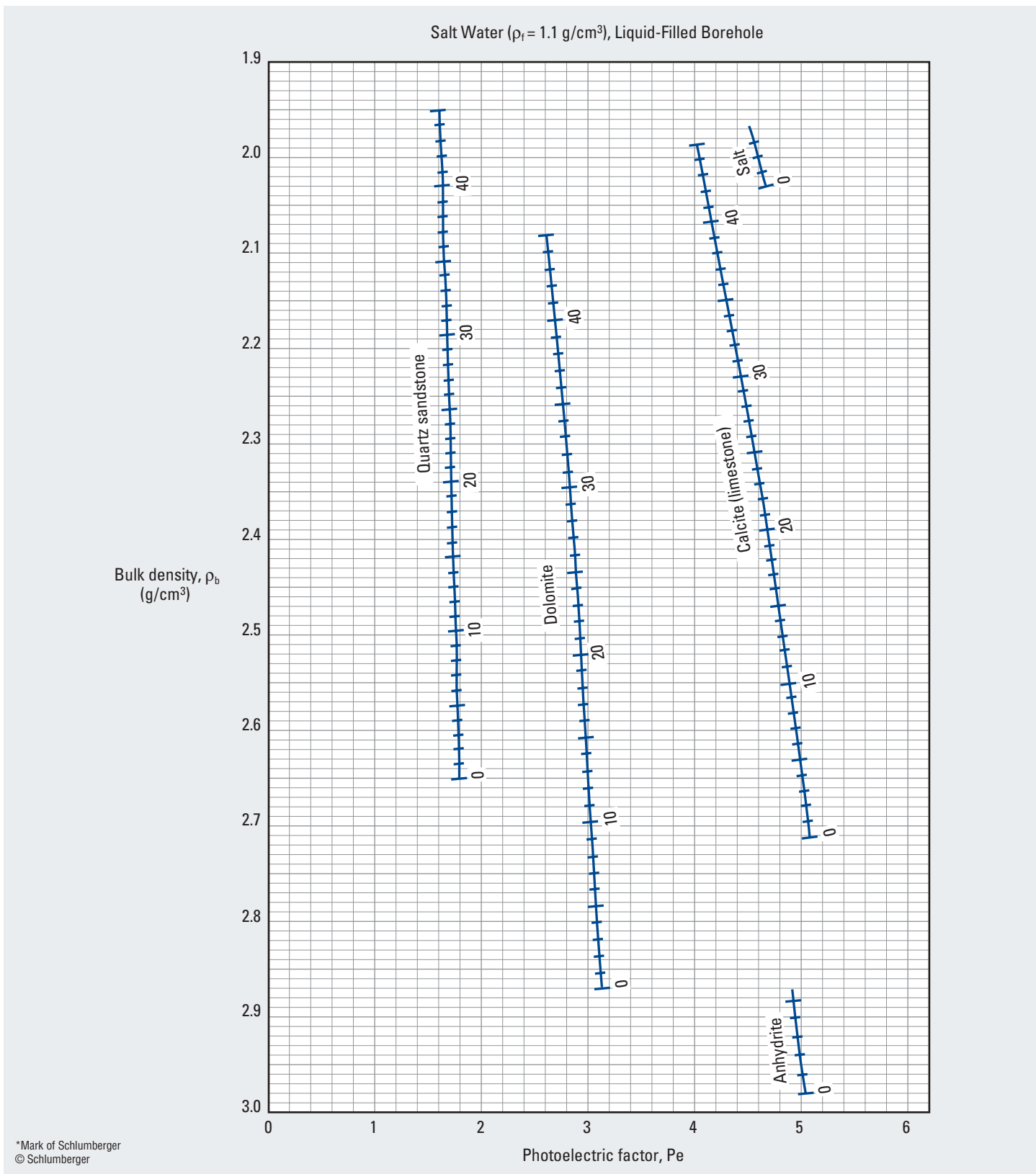
Platform Express* Three-Detector Lithology Density Tool

Porosity and Lithology—Open Hole

Lith-3
(former CP-16)

Platform Express® Three-Detector Lithology Density Tool

Porosity and Lithology—Open Hole

Lith-4
(former CP-17)

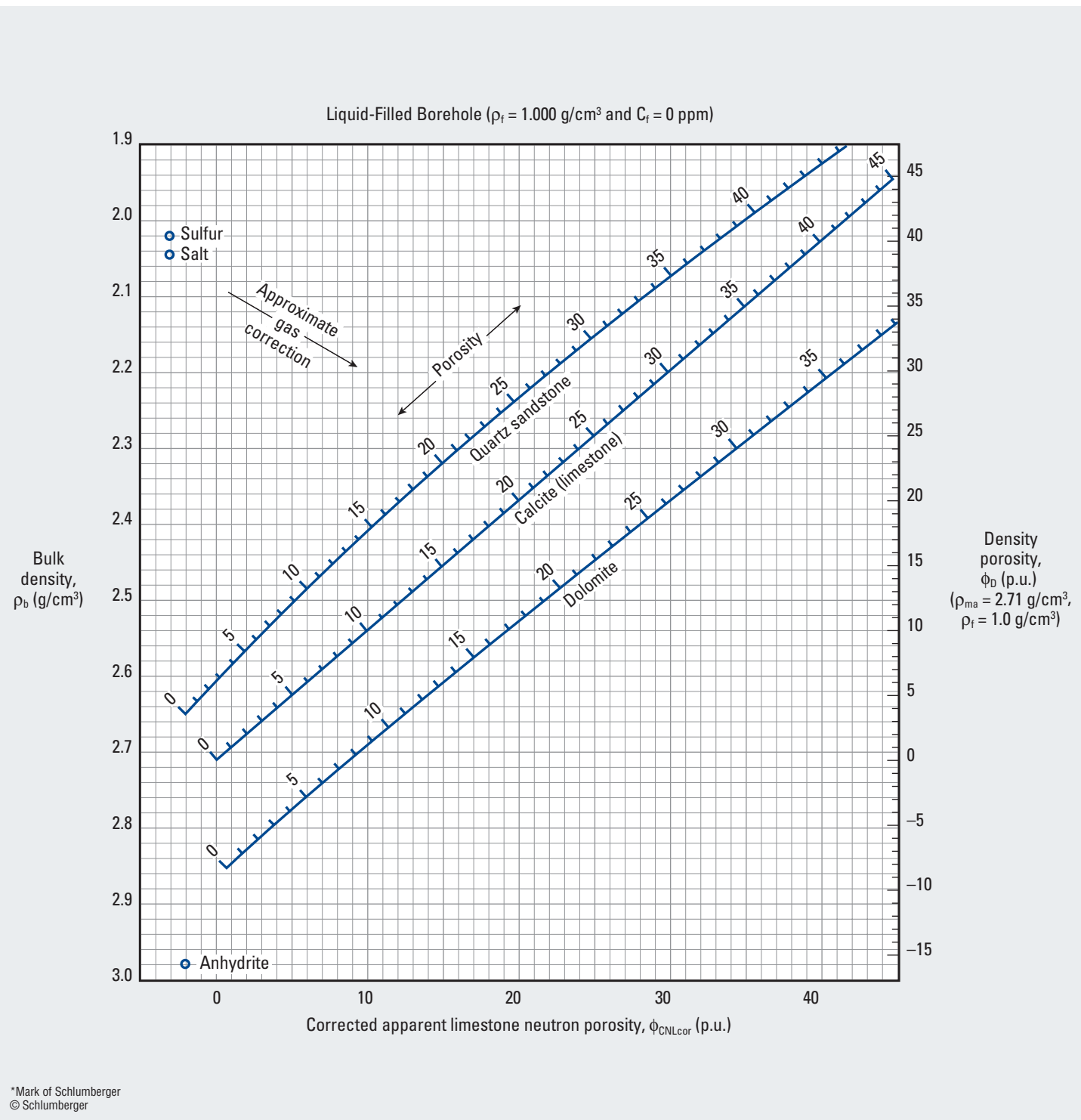
This chart is used similarly to Chart Lith-3 for lithology and porosity determination with values of photoelectric factor (Pe) and

bulk density (ρ_b) from the Platform Express TLD tool in saltwater borehole fluid.

**CNL* Compensated Neutron Log and Litho-Density* Tool
(fresh water in invaded zone)**

Porosity and Lithology—Open Hole

Por-11
(former CP-1e)



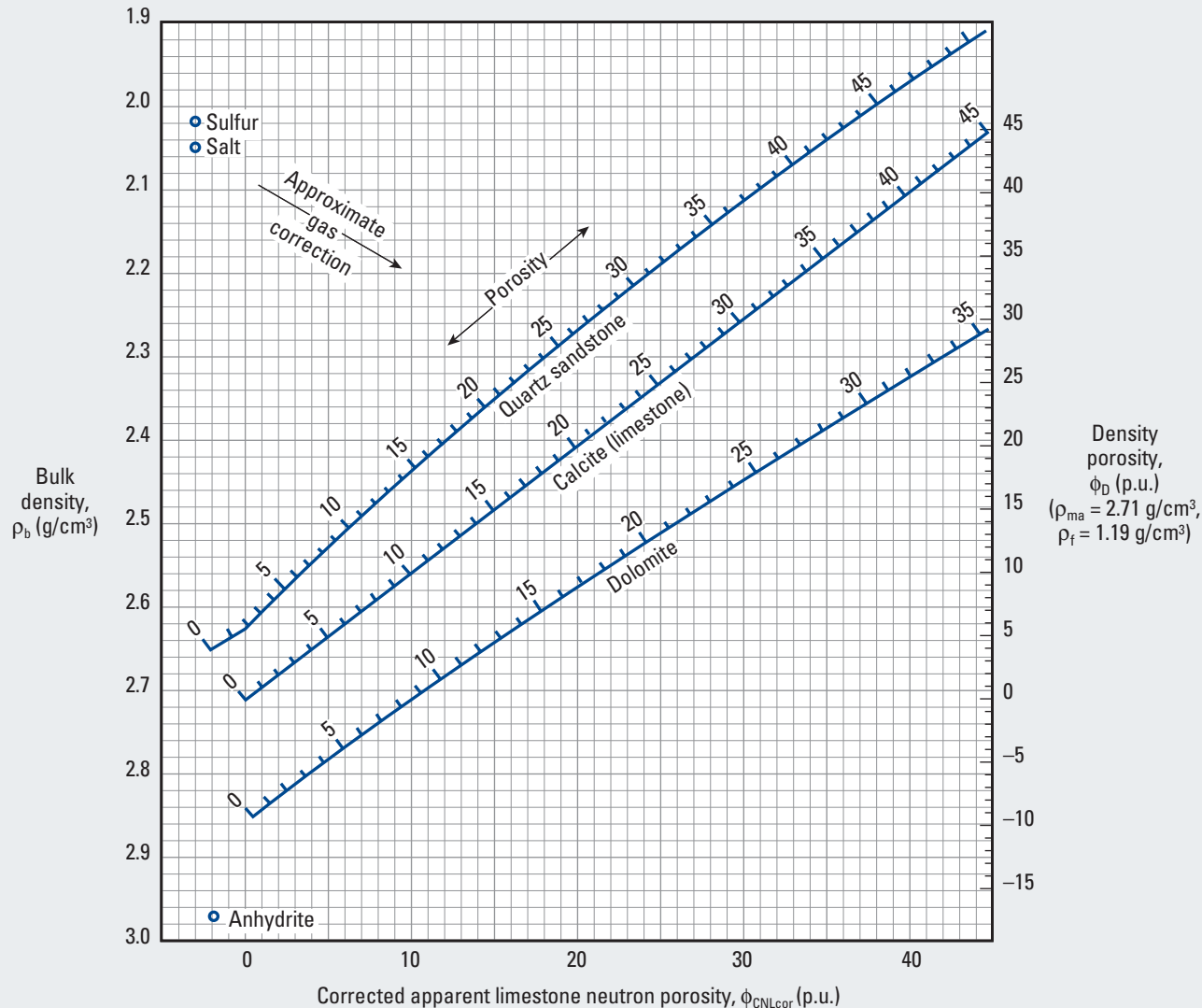
*Mark of Schlumberger
© Schlumberger

CNL* Compensated Neutron Log and Litho-Density* Tool (salt water in invaded zone)

Porosity and Lithology—Open Hole

Por-12
(former CP-11)

Liquid-filled borehole ($\rho_f = 1.190 \text{ g/cm}^3$ and $C_f = 250,000 \text{ ppm}$)



*Mark of Schlumberger
© Schlumberger

Por

Purpose

This chart is used similarly to Chart Por-11 with CNL Compensated Neutron Log and Litho-Density values to approximate the lithology and determine the crossplot porosity in the saltwater-invaded zone.

Example

Given: Corrected apparent neutron limestone porosity = 16.5 p.u. and bulk density = 2.38 g/cm³.

Find: Crossplot porosity and lithology.

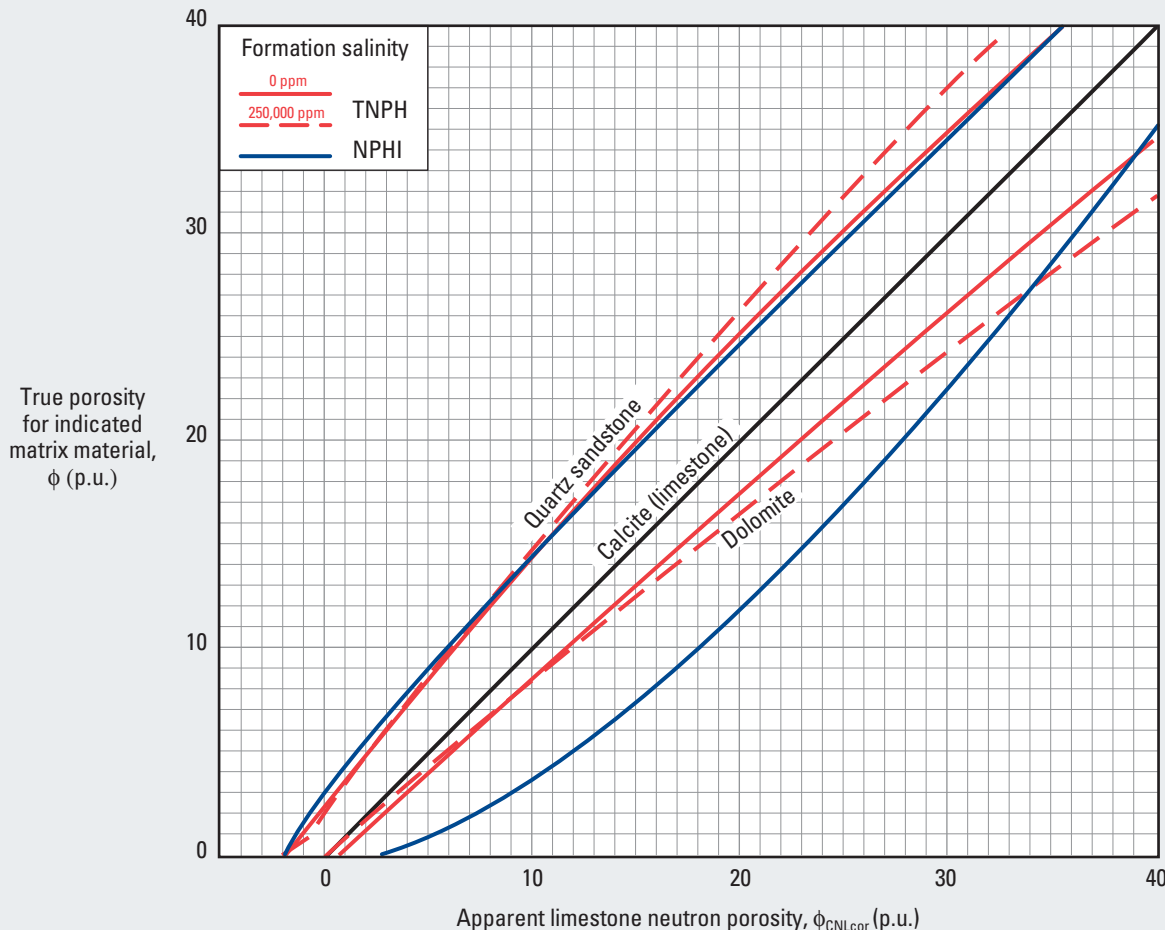
Answer: Crossplot porosity = 20 p.u. The lithology is approximately 55% quartz and 45% limestone.

Thermal Neutron Tool

Porosity Equivalence—Open Hole

Por-5

(former Por-13b)



*Mark of Schlumberger
© Schlumberger

Purpose

This chart is used to convert CNL* Compensated Neutron Log porosity curves (TNPH or NPHI) from one lithology to another. It can also be used to obtain the apparent limestone porosity (used for the various crossplot porosity charts) from a log recorded in sandstone or dolomite porosity units.

Description

To determine the porosity of either quartz sandstone or dolomite enter the chart with the either the TNPH or NPHI corrected apparent limestone neutron porosity (ϕ_{CNLcor}) on the x-axis. Move vertically to intersect the appropriate curve and read the porosity for quartz sandstone or dolomite on the y-axis. The chart has a built-in salinity correction for TNPH values.

NPHI	Thermal neutron porosity (ratio method)
NPOR	Neutron porosity (environmentally corrected and enhanced vertical resolution processed)
TNPH	Thermal neutron porosity (environmentally corrected)

Example

Given: Quartz sandstone formation, TNPH = 18 p.u. (apparent limestone neutron porosity), and formation salinity = 250,000 ppm.

Find: Porosity in sandstone.

Answer: From the TNPH porosity reading of 18 p.u. on the x-axis, project a vertical line to intersect the quartz sandstone dashed red curve. From the y-axis, the porosity of the sandstone is 24 p.u.

Por

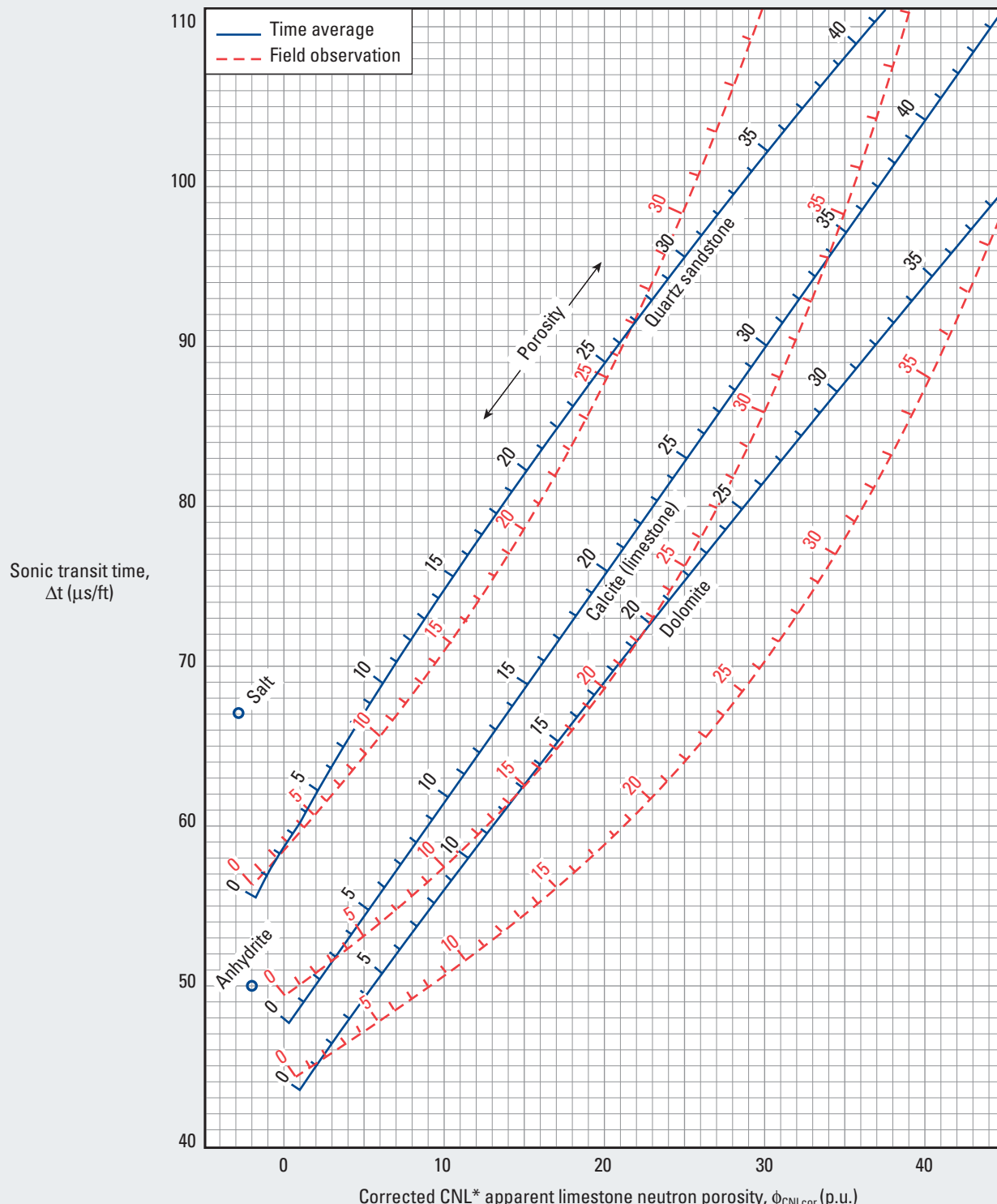
Sonic and Thermal Neutron Crossplot

Porosity and Lithology—Open Hole, Freshwater Invaded

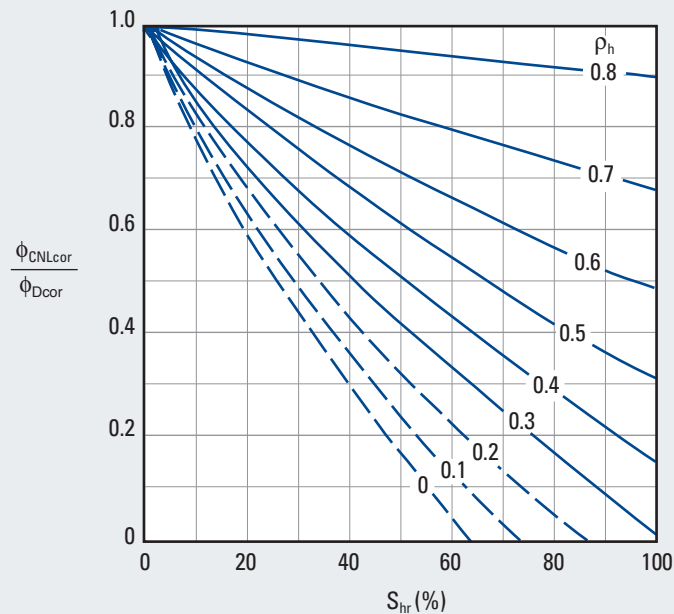
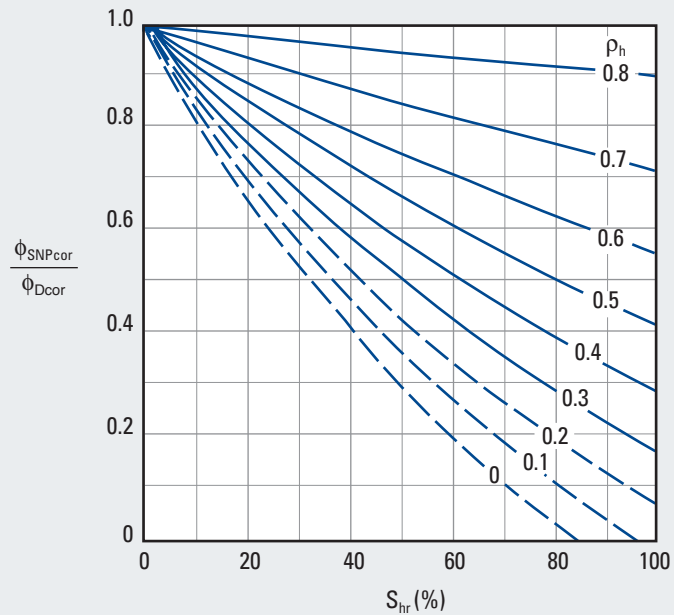
Por-20

(customary, former CP-2c)

$$t_f = 190 \mu\text{s}/\text{ft} \text{ and } C_f = 0 \text{ ppm}$$



Hydrocarbon Density Estimation

Por-27
(former CP-10)

*Mark of Schlumberger
© Schlumberger

Purpose

This chart is used to estimate the hydrocarbon density (ρ_h) within a formation from corrected neutron and density porosity values.

Description

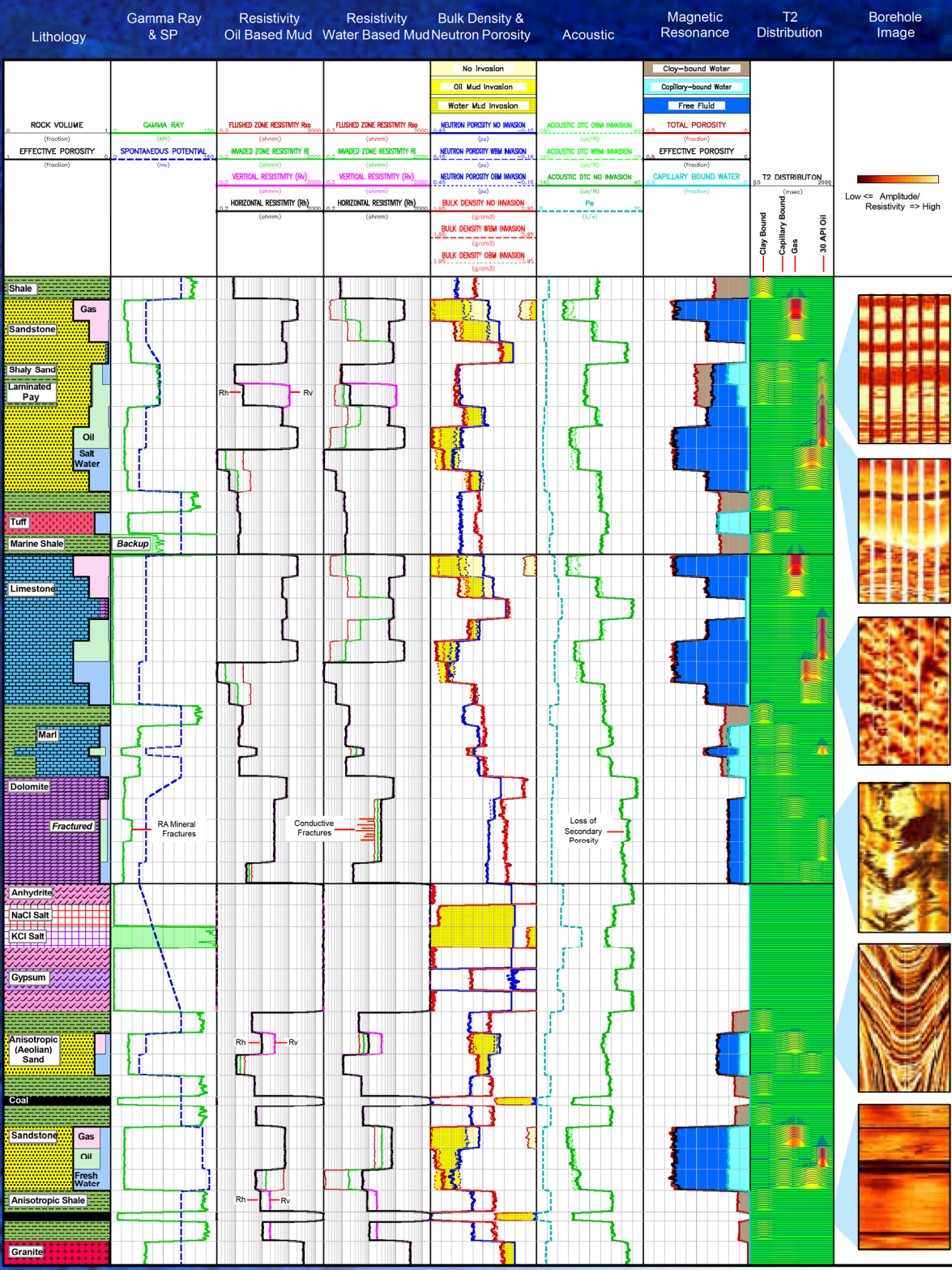
Enter the ratio of the sidewall neutron porosity (SNP) or CNL* Compensated Neutron Log neutron porosity and density porosity corrected for lithology and environmental effects (ϕ_{SNPcor} or $\phi_{CNLcor}/\phi_{Dcor}$, respectively) on the y-axis and the

hydrocarbon saturation on the x-axis. The intersection point of the two values defines the density of the hydrocarbon.

Example

Given: Corrected CNL porosity = 15 p.u., corrected density porosity = 25 p.u., and $S_{hr} = 30\%$ (residual hydrocarbon).
 Find: Hydrocarbon density.
 Answer: Porosity ratio = 15/25 = 0.6. $\rho_h = 0.29 \text{ g/cm}^3$.

Atlas of Log Responses



The Changing Face of Formation Evaluation

www.bakerhughesdirect.com
formationevaluation@bakerhughes.com

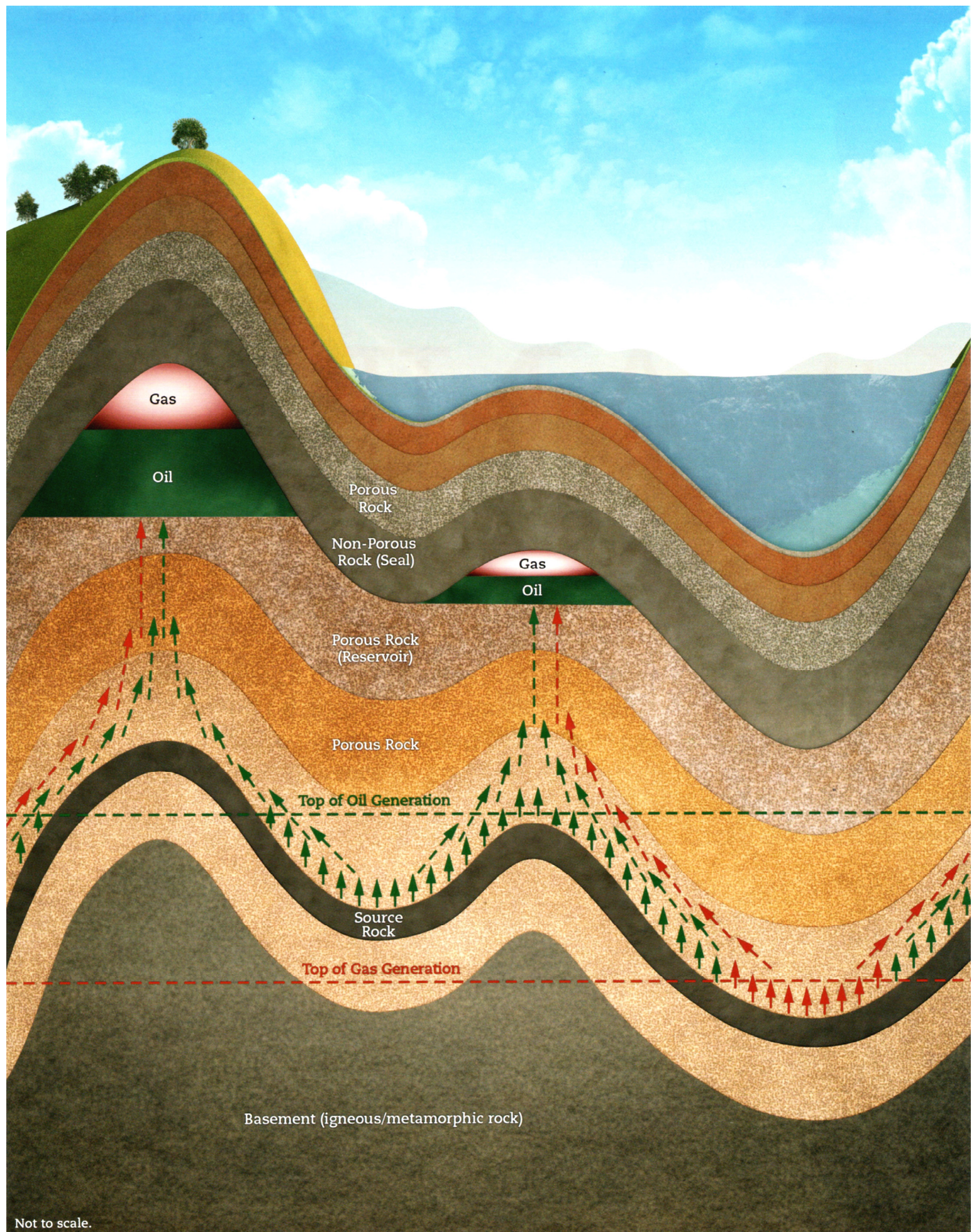
We cannot, and we do not guarantee the accuracy or correctness of any information on this chart. We shall not be liable or responsible for any loss, cost, damage or expense whatsoever arising or resulting by the customer relying upon this information.

Lithology	GR	Density	Neutron	Acoustic	Resistivity	PE
Sandstone	Low (dilute salt)	2.65	-4	53	High	1.81
Limestone	Low	2.71	0	47.5	High	5.08
Shale	High	2.2-2.7 (water content)	High (water content)	50-150 (water content)	Low (water content)	1.0
Dolomite	Low (dilute salt)	2.67	+4	43	High	3.14
Anhydrite	V.Low	2.68	-1	50	V.High	5.06
Salt	Low (dilute salt)	2.53 (salt & temp)	-3 (salt & temp)	57 (salt & temp)	V.High	4.65
Water	0	1.11 (salt & temp)	100	180-190 (salt & temp)	0 - infinite (salt & temp)	0.36 (salt & temp)
Oil	0	0.86 (salt & temp)	20-100 (salt & temp)	215-240 (salt & temp)	V.High	Low
Gas	0	0.2-0.5 (pressure)	10-50 (salt & temp)	>1000	V.High	Low



Baker Atlas
INTEQ
FORMATION EVALUATION

© 2002 Baker Hughes Incorporated
All rights reserved



Not to scale.

BASIC WELL LOGGING FORMULAE

Temperature Calculation Assuming a Linear Geothermal Gradient

$$T(z) = T(z_1) + \frac{T(z_2) - T(z_1)}{z_2 - z_1} (z - z_1)$$

where:

T = temperature (either °C or °F),

z = true vertical depth (TVD) measured with respect to the logging reference point,

z_1 = TVD of a point in at which the temperature was measured (usually the at the surface), and

z_2 = TVD of a second point at which the temperature was measured (usually at the bottom of the well).

Shale/Clay Index Based on Gamma-Ray Log

$$I_{sh} = \frac{GR - GR_{cn}}{GR_{sh} - GR_{cn}}$$

where:

I_{sh} = shale index,

GR = gamma-ray reading in the depth zone of interest,

GR_{cn} = gamma-ray reading in a depth zone which is considered clean (shale/clay free),

also referred to as GR_{min} , and

GR_{sh} = gamma-ray reading in a “pure” shale depth zone, also referred to as GR_{max} .

Shale/Clay Index Based on Gamma-Ray Log Across a Water-Saturated Sandstone

$$I_{sh} = I_{shw} + \frac{1 - I_{shw}}{GR_{sh} - GR_w} (GR - GR_w)$$

where:

I_{sh} = shale index,

I_{shw} = shale index in the water-saturated sandstone ($I_{shw} \leq 1$),

GR = gamma-ray reading in the depth zone of interest,

GR_w = gamma-ray reading in the water-saturated sandstone ($GR_w \leq GR_{sh}$), and

GR_{sh} = gamma-ray reading in a “pure” shale depth zone, also referred to as GR_{max} .

Spontaneous Electrical Potential

$$SSP \approx -K \times \log_{10} \left(\frac{C_w}{C_{mf}} \right)$$

where:

- SSP = Static spontaneous electrical potential in mV,
- C_{mf} = salt concentration of mud filtrate in NaCl ppm,
- C_w = salt concentration of connate water in NaCl ppm, and
- K is a temperature-independent constant = 71 mV.

Conversion of Electrical Resistivity due to Temperature Change

$$R_2 = R_1 \left(\frac{T_1 + 6.77}{T_2 + 6.77} \right) \text{ deg } F$$

or

$$R_2 = R_1 \left(\frac{T_1 + 21.5}{T_2 + 21.5} \right) \text{ deg } C$$

where:

- R_1 = electrical resistivity (Ohm-m) measured at temperature T_1 , and
- R_2 = corresponding electrical resistivity (Ohm-m) at temperature T_2 .

Conversion of Salt Concentration to Electrical Resistivity of Water Diluted with NaCl

$$R_w \approx \left(0.0123 + \frac{3647.5}{[NaCl_{ppm}]^{0.955}} \right) \left(\frac{81.77}{T + 6.77} \right)$$

where:

- R_w = Electrical resistivity of water in $\Omega \text{ m}$ (Ohm-m),
- $NaCl_{ppm}$ = salt (NaCl) concentration of water in ppm, and
- T = temperature in $^{\circ}\text{F}$.

The error of the above equation is approximately 2% when the concentration of NaCl is between 500 and 100,000 ppm, and between 2 – 10% when the concentration of NaCl is between 100,000 and 230,000 ppm.

It follows that

$$\left[NaCl_{ppm} \right] \approx 10^{\frac{3.562 - \log_{10} \left[\left(\frac{T+6.77}{81.77} \right) \cdot R_w - 0.0123 \right]}{0.955}}$$

Archie's Equation

$$R_t \approx R_w \left[\frac{a}{\phi^m} \right] \frac{1}{S_w^n}$$

where:

R_t = electrical resistivity of a fluid-saturated porous rock,

R_w = electrical resistivity of the water contained in the rock's pore space,

ϕ = interconnected porosity,

S_w = water saturation,

a = Winsauer's multiplier,

m = porosity exponent, and

n = saturation exponent.

General Relationship between Bulk Density and Porosity

$$\rho_b = \phi \rho_f + (1 - \phi) \rho_m$$

where:

ρ_b = bulk density of the rock (aka rock's density),

ρ_f = density of the fluid occupying the rock's pore space,

ϕ = total porosity, and

ρ_m = density of the matrix (solid component) contained in the rock.

Alternatively, one can write

$$\phi = \frac{\rho_b - \rho_m}{\rho_f - \rho_m} = \frac{\rho_m - \rho_b}{\rho_m - \rho_f} .$$

Likewise,

$$\rho_f = \frac{1}{\phi} [\rho_b - (1 - \phi) \rho_m]$$

General Relationship between Bulk Density and Non-Shale (Sandstone) Porosity for the Case of Shaly Sands with **Laminated** Shale

$$\rho_b = (1 - C_{sh}) \rho_s + C_{sh} \rho_{sh}$$

where:

ρ_b = bulk density of the rock (aka rock's density),

C_{sh} = volumetric concentration of shale,

ρ_s = sandstone density, and

ρ_{sh} = shale density (includes shale porosity, silt, dry clay, and water).

Likewise,

$$\phi_t = (1 - C_{sh}) \phi_s + C_{sh} \phi_{sh}$$

where:

ϕ_t = total rock porosity,

C_{sh} = volumetric concentration of shale,

ϕ_s = porosity of the sand fraction, and

ϕ_{sh} = shale porosity.

It follows that

$$\phi_s = \frac{\phi_t - C_{sh} \phi_{sh}}{1 - C_{sh}}$$

General Relationship between Bulk Density and Non-Shale (Sandstone) Porosity for the Case of Shaly Sandstone with **Dispersed** (Grain-Coating) Shale

$$\rho_b = \phi_s \rho_f + (1 - \phi_s - C_{sh}) \rho_m + C_{sh} \rho_{sh}$$

where:

ρ_b = bulk density of the rock (aka rock's density),

ρ_f = density of the fluid occupying the rock's pore space,

ϕ_s = non-shale (sandstone) porosity,

C_{sh} = volumetric concentration of shale,

ρ_m = grain density (for reference, density of quartz = 2.65 gm/cm³), and

ρ_{sh} = shale density (includes shale porosity, silt, dry clay, and water).

Alternatively, one can write

$$\phi_s = \frac{\rho_m - \rho_b}{\rho_m - \rho_f} - C_{sh} \frac{\rho_m - \rho_{sh}}{\rho_m - \rho_f}.$$

Likewise,

$$\rho_f = \frac{1}{\phi_s} [\rho_b - (1 - \phi_s - C_{sh}) \rho_m - C_{sh} \rho_{sh}]$$

Additionally,

$$\phi_T = \phi_s + C_{sh} \phi_{sh},$$

where:

ϕ_T = total porosity,

ϕ_{sh} = shale porosity, and

ϕ_s = sandstone (non-shale) porosity.

Fluid Density and Saturation

For the case of water and hydrocarbon, one has

$$\rho_f = S_w \rho_w + (1 - S_w) \rho_H$$

where:

ρ_f = density of the fluid occupying the rock's pore space,

ρ_w = density of water (depends on salt concentration),

ρ_H = density of hydrocarbon, and

S_w = water saturation.

It follows that

$$\rho_H = \frac{\rho_f - S_w \rho_w}{1 - S_w}$$

For the case of water, gas, and oil, one has

$$\rho_f = S_w \rho_w + S_o \rho_o + (1 - S_w - S_o) \rho_g$$

where:

ρ_f = density of the fluid occupying the rock's pore space,

ρ_w = density of water (depends on salt concentration),

ρ_o = density of oil,

ρ_g = density of gas,

S_w = water saturation, and

S_o = oil saturation.

Density-Neutron Porosity Corrections for Shaly Sandstone (case of **laminated shale**)

$$\phi_D^\circ = \frac{\phi_D - C_{sh} \phi_{D,sh}}{1 - C_{sh}},$$

where:

ϕ_D = density (apparent) porosity expressed in water-filled sandstone porosity units,

$\phi_{D,sh}$ = density (apparent) porosity of “pure shale” expressed in water-filled sandstone porosity units,

C_{sh} = volumetric concentration of shale, and

ϕ_D° = shale-corrected density porosity expressed in water-filled sandstone porosity units.

$$\phi_N^\circ = \frac{\phi_N - C_{sh} \phi_{N,sh}}{1 - C_{sh}},$$

where:

ϕ_N = neutron (apparent) porosity expressed in water-filled sandstone porosity units,

$\phi_{N,sh}$ = neutron (apparent) porosity of “pure shale” expressed in water-filled sandstone porosity units,

C_{sh} = volumetric concentration of shale, and

ϕ_N° = shale-corrected neutron porosity expressed in water-filled sandstone porosity units.

It follows that

$$\phi_s \approx \sqrt{\frac{(\phi_D^\circ)^2 + (\phi_N^\circ)^2}{2}}$$

where:

ϕ_s = sandstone porosity.

Density-Neutron Porosity Corrections for Shaly Sandstone (case of dispersed shale)

$$\phi_D^\circ = \phi_D - C_{sh} \phi_{D,sh},$$

where:

ϕ_D = density (apparent) porosity expressed in water-filled sandstone porosity units,

$\phi_{D,sh}$ = density (apparent) porosity of “pure shale” expressed in water-filled sandstone porosity units,

C_{sh} = volumetric concentration of shale (by definition, lower than non-shale porosity in this case), and

ϕ_D° = shale-corrected density porosity expressed in water-filled sandstone porosity units.

$$\phi_N^\circ = \phi_N - C_{sh} \phi_{N,sh},$$

where:

ϕ_N = neutron (apparent) porosity expressed in water-filled sandstone porosity units,

$\phi_{N,sh}$ = neutron (apparent) porosity of “pure shale” expressed in water-filled sandstone porosity units,

C_{sh} = volumetric concentration of shale (by definition, lower than non-shale porosity in this case), and

ϕ_N° = shale-corrected neutron porosity expressed in water-filled sandstone porosity units.

It follows that

$$\phi_s \approx \sqrt{\frac{(\phi_D^\circ)^2 + (\phi_N^\circ)^2}{2}}$$

where:

ϕ_s = non-shale (sandstone) porosity.

Density-Neutron Calculation of Volumetric Concentration of Shale in a Water-Bearing Sandstone

$$C_{sh} = \frac{\phi_N - \phi_D}{\phi_{N,sh} - \phi_{D,sh}},$$

where:

C_{sh} = volumetric concentration of shale,

ϕ_D = density (apparent) porosity expressed in water-filled sandstone porosity units,

$\phi_{D,sh}$ = density (apparent) porosity of “pure shale” expressed in water-filled sandstone porosity units,

ϕ_N = neutron (apparent) porosity expressed in water-filled sandstone porosity units, and

$\phi_{N,sh}$ = neutron (apparent) porosity of “pure shale” expressed in water-filled sandstone porosity units.

Relationship Between Rock Resistivity and Sandstone Resistivity in Laminated Shale-Sandstone Systems (Case of Isotropic Sandstone and Shale)

$$\frac{1}{R_{||}} = \frac{1 - C_{sh}}{R_s} + \frac{C_{sh}}{R_{sh}}$$

where:

C_{sh} = volumetric concentration of shale,

$R_{||}$ = electrical resistivity of the rock parallel to bedding plane,

R_s = electrical resistivity of the sandstone fraction of the rock, and

R_{sh} = electrical resistivity of the shale fraction of the rock.

$$R_{\perp} = (1 - C_{sh}) R_s + C_{sh} R_{sh}$$

where:

R_{\perp} = electrical resistivity of the rock perpendicular to bedding plane.

Wyllie's Relationship and Sonic Porosity

$$\Delta t_b \approx \phi_{sonic} \Delta t_f + (1 - \phi_{sonic}) \Delta t_m$$

where:

Δt_b = bulk sonic slowness (aka rock's sonic slowness) [$\mu\text{s}/\text{ft}$],

Δt_f = sonic slowness of the fluid occupying the rock's pore space [$\mu\text{s}/\text{ft}$],

ϕ_{sonic} = sonic porosity (aka Wyllie's porosity), and

Δt_m = sonic slowness of the matrix (solid component) contained in the rock [$\mu\text{s}/\text{ft}$].

Alternatively,

$$\phi_{sonic} = \frac{\Delta t_b - \Delta t_m}{\Delta t_f - \Delta t_m}.$$

Timur-Tixier Equation

$$k \approx \alpha \phi^\beta \left(\frac{1 - S_{wirr}}{S_{wirr}} \right)^\gamma$$

where:

k = permeability,

ϕ = total porosity, and

S_{wirr} = irreducible water saturation.

Electrical Resistivity of Dispersed (Grain-Coating Clay) Shaly Sandstone

$$\frac{1}{R_t} \approx \frac{1}{R_w} \left[1 + B R_w \frac{S_b}{S_w} \right] \left[\frac{\phi^{m^*}}{a^*} \right] S_w^{n^*},$$

where:

$$S_b = C_{sh} \frac{\phi_{sh}}{\phi},$$

$$B = \frac{-5.41 + 0.133 T - 0.0001253 T^2}{1 + R_w^{1.23} (0.025 T - 1.07)},$$

and

R_t = electrical resistivity of the sandstone with grain-coating clay,

R_w = electrical resistivity of the water contained in the rock's pore space,

ϕ = interconnected porosity,

ϕ_{sh} = shale porosity,

C_{sh} = volumetric concentration of shale ($C_{sh} < \phi$),

S_w = water saturation,

a^* = modified Winsauer's multiplier,

m^* = modified porosity exponent,

n^* = modified saturation exponent, and

T = temperature in °F.